Software Architecture for Capturing Clinical Information in Hadron Therapy and the Design of an Ion Beam for Radiobiology

Daniel Abler
Wolfson College, Oxford

Thesis submitted in fulfillment of the requirements
for the degree of
Doctor of Philosophy at the University of Oxford

Trinity Term, 2013

Abstract

Hadron Therapy (HT) exploits properties of ion radiation to gain therapeutic advantages over existing photon-based forms of external radiation therapy. However, its relative superiority and cost-effectiveness have not been proven for all clinical situations. Establishing a robust evidence base for the development of best treatment practices is one of the major challenges for the field. This thesis investigates two research infrastructures for building this essential evidence.

First, the thesis develops main components of a metadata-driven software architecture for the collection of clinical information and its analysis. This architecture acknowledges the diversity in the domain and supports data interoperability by sharing information models. Their compliance to common metamodels guarantees that primary data and analysis results can be interpreted outside of the immediate production context. This is a fundamental necessity for all aspects of the evidence creation process. A metamodel of data capture forms is developed with unique properties to support data collection and documentation in this architecture. The architecture's potential to support complex analysis processes is demonstrated with the help of a novel metamodel for Markov model based simulations, as used for the synthesis of evidence in health-economic assessments. The application of both metamodels is illustrated on the example of HT.

Since the biological effect of particle radiation is a major source of uncertainty in HT, in its second part, this thesis undertakes first investigations towards a new research facility for bio-medical experiments with ion beams. It examines the feasibility of upgrading LEIR, an existing accelerator at the European Organisation for Nuclear Research (CERN), with a new slow extraction and investigates transport of the extracted beam to future experiments. Possible configurations for the slow-resonant extraction process are identified, and designs for horizontal and vertical beam transport lines developed. The results of these studies indicate future research directions towards a new ion beam facility for biomedical research.

Acknowledgements

Numerous people have contributed to and helped me completing this thesis through their support and advice, both personal and technical. I would like to express my sincere gratitude to all of them.

First, I would like to thank my thesis advisors in Oxford, as well as my supervisors at CERN where I carried out most of my research. Their support and advice made these years a very rich and instructive experience. I would like to express my deepest gratitude to Ken Peach for his guidance and support. His availability and encouragements were a great motivation throughout my doctoral studies. I wish to thank Jim Davies for co-supervising my thesis, for sharing his inspiring ideas and accompanying my progress. I am particularly grateful to Manjit Dosanjh, for her continued support during my time at CERN, as Marie-Curie fellow in the Particle Training Network for European Radiotherapy (PARTNER) programme and beyond, and for the opportunities she gave me to explore my interests and to expand my skills. I also would like to thank Christian Carli for sharing his expertise and his experience with the LEIR synchrotron, as well as for his technical guidance on the accelerator studies towards its upgrade.

I wish to extend my special thanks to my colleagues and collaborators in the different groups and projects.

Numerous discussions with Steve Harris and Charles Crichton, during my first year in Oxford and on subsequent visits, fundamentally shaped my understanding of the aspects of cancer research informatics that are addressed in this thesis. Together with Andrew Tsui, they patiently answered my novice questions and helped me overcome many of the technical challenges that I encountered. I also wish to thank James Welch for introducing me to a domain-specific-language development framework which, although abandoned at a more advanced stage of my research, accelerated my progress.

I have greatly benefited from Ulrich Dorda's technical advice and discussions regarding slow extraction from medical synchrotrons, and I am grateful that I could build my analysis tools on his self-developed accelerator library. I wish to thank Giulio Magrin for his availability to discuss transfer lines and beam delivery for a new ion-beam research facility, and for his suggestions towards its design. My special thanks goes to Adriano Garonna for two years of collaboration in which we complemented and cross-checked our understanding of the slow extraction process from LEIR. I very much enjoyed our discussions and learned a lot during this time.

I would like to acknowledge my colleagues at the Particle Therapy Cancer Research institute (PTCRi), Claire Timlin, Tracy Underwood, Dan Warren and Wilson Puthenparampil, who warmly welcomed me and made my stay in Oxford an especially enjoyable and productive experience. Also, I wish to thank Bleddyn Jones for teaching me the basics of radiobiology and sharing some of his insights into the clinical aspects of radiotherapy.

I feel very advantaged having been part of the PARTNER network during my doctoral studies. Without its remarkable people and diverse training programme, I could not have developed such a wide perspective on the field of HT. In particular, I wish to acknowledge my fellow PARTNER colleagues at CERN: Till Tobias Böhlen, as well as Faustin Laurentiu Roman and Vassiliki Kanellopoulos with whom I developed a prototype data-sharing platform for HT in the frame of PARTNER.

Since the experiences gained over the course of that project are reflected in parts of this thesis, I wish to extend my thanks to the team of medical doctors and researchers who supported the PARTNER platform through their clinical advice and technical expertise. I am particular grateful to Ramona Mayer and Rajesh Jena whose clinical experience and believe in the benefits of such an infrastructure were important sources of information and motivation throughout the project. Rajesh Jena's suggestions for a platform use-case motivated the HT research scenario that is employed to demonstrate the practical application of the information architecture proposed here. In this context, I also wish to acknowledge Manuela Cirilli and my colleagues in CERN IT, in particular Andrea Valassi and Alessandro Di Girolamo, whose expertise and hands-on attitude was essential for the project's completion. I would like to thank Jamie Shiers and Markus Schulz, as well as Massimo Lamanna and Julia Andreeva for hosting me in their section and group, respectively.

I wish to thank Audrey Ballantine, Helen Dixon-Altaber, Joelma Tolomeo and Sue Geddes for their administrative assistance within and across CERN and the Physics department of the University of Oxford.

While working on this thesis, I received financial support through the EU FP7 programmes Particle Training Network for European Radiotherapy (PARTNER) (215840) and Union for Light Ion Centres in Europe (ULICE) (228436) which I also wish to acknowledge.

On a more personal note, I would like to thank my friends for sharing their time and moral support when most needed. Their friendship and all their help were greatly appreciated. I wish to acknowledge my friends from Wolfson College, particularly the 2009 group from 'M block' ground-floor whose superior kitchen facilities always provided a good excuse for enjoying great company, as well as my former 'colocataires' in St. Genis who received me on short-term trips to CERN and when I returned from Oxford.

I would like to express my deepest gratitude to my family and to my parents for their unconditional love, support and encouragement. They gave me the freedom, but also the confidence and security, to explore new opportunities and to persue the ones that most interested me.

Finally, I would like to thank Giannina for accompanying me on this journey with her love and support, also in the sometimes difficult moments of thesis research and writing. I look forward to our next project!

Contents

List of Figures viii

List of Tables xi

1. Introduction 1
- 1.1. Hadron Therapy . . . 1
  - 1.1.1. Cancer . . . 1
  - 1.1.2. Photon-based Radiation Therapy vs. Hadron Therapy . . . 2
    - 1.1.2.1. Physical Dose Distribution . . . 2
    - 1.1.2.2. Biological Effect . . . 3
    - 1.1.2.3. Rationale for Hadron Therapy . . . 4
  - 1.1.3. Current situation . . . 4
  - 1.1.4. Challenges . . . 4
- 1.2. Nature of Evidence for new Cancer Therapies . . . 5
  - 1.2.1. 'Evidence' in Evidence-based Medicine . . . 5
  - 1.2.2. The Hadron Therapy Case . . . 6

2. Evidence for Hadron Therapy 7
- 2.1. Derivation of Clinical Evidence . . . 7
  - 2.1.1. Meta-analysis of Clinical Studies . . . 7
    - 2.1.1.1. Data Quality . . . 8
    - 2.1.1.2. Clinical Research Data Collection . . . 9
  - 2.1.2. Modelling and Simulation . . . 10
  - 2.1.3. Contribution . . . 11
- 2.2. Facilities for Radiobiological Research . . . 12
  - 2.2.1. Contribution . . . 13

3. Software Architecture for Capturing Clinical Information 14
- 3.1. Concepts and Related Work . . . 14
  - 3.1.1. Interoperability . . . 14
  - 3.1.2. Conceptual Modelling of Information Systems . . . 15
    - 3.1.2.1. Meta-modelling . . . 15
  - 3.1.3. (Meta-)Models for Interoperability . . . 16
    - 3.1.3.1. ISO/IEC 11179 - Metadata Registries . . . 17
    - 3.1.3.2. ISO/IEC 19763 - Metamodel Framework for Interoperability 19
  - 3.1.4. Model-driven Architecture . . . 19
- 3.2. Architecture for the Derivation of Clinical Evidence . . . 20
  - 3.2.1. Architecture . . . 21
  - 3.2.2. Distinctive Features . . . 22

3.3. Methods, Systems and Standards . . . 24
3.3.1. Clinical Data Capture and Documentation . . . 24
3.3.1.1. Selected Systems, Technologies and Standards . . . 24
3.3.1.2. Identification and Logical Structure . . . 26
3.3.1.3. Entry Constraints . . . 28
3.3.1.4. Process and Presentation Constraints . . . 30
3.3.1.5. Summary . . . 32
3.3.2. Secondary Analysis Processes . . . 33
3.3.2.1. Decision Analytic Models in Health Care . . . 33
3.3.2.2. Markov Models . . . 34

4. Metamodels for Clinical Data Capture and Analysis 36
4.1. Metamodel for Form-based Data Capture . . . 36
4.1.1. Requirements for Forms-Metamodel . . . 36
4.1.2. Forms-Metamodel - Structural Model . . . 37
4.1.2.1. Form Element . . . 37
4.1.2.2. Interaction Element . . . 38
4.1.2.3. Simple Structure and Simple Response Type . . . 39
4.1.2.4. Composed Structure . . . 40
4.1.2.5. Structure in Composition . . . 41
4.1.2.6. Constraints . . . 42
4.1.2.7. Prepopulation Assignment . . . 43
4.1.2.8. Expression Language . . . 44
4.1.2.9. Annotation . . . 44
4.1.2.10. Form Properties and Presentation . . . 46
4.1.3. Forms-Metamodel - Behavioural Model . . . 46
4.1.3.1. SimpleStructure State Machine . . . 48
4.1.3.2. ComposedStructure State Machine . . . 48
4.1.3.3. Composition State Machine . . . 49
4.1.3.4. State Machine Composition . . . 49
4.1.4. Forms-Metamodel - Behavioural Composition . . . 49
4.1.4.1. Sequential Composition . . . 51
4.1.4.2. Parallel Composition . . . 53
4.1.4.3. Choice Composition . . . 53
4.1.5. Model Implementation and Validation . . . 55
4.1.5.1. Example Forms-Metamodel Instance . . . 55
4.1.5.2. Common Transformation Steps . . . 57
4.1.5.3. OpenClinica . . . 59
4.1.5.4. ISO 19763-13 . . . 63
4.1.6. Summary . . . 73
4.2. Metamodel for Markov Model-based Simulations . . . 74
4.2.1. Metamodels . . . 74
4.2.2. Computational Model and Outputs . . . 77
4.2.2.1. Markov Model . . . 77
4.2.2.2. Chained Markov Models . . . 82
4.2.2.3. Markov Model Simulation . . . 83

4.2.2.4. Simulation-based Health-Economic Assessment 84
4.2.3. Validation 85
4.2.3.1. Specification of Health-Economic Modelling Studies . . . 85
4.2.3.2. Reporting Requirements 88
4.2.3.3. Suggestions for Improvements 89
4.2.4. Summary 89
4.3. Application to Hadron Therapy 90
4.3.1. Research Case 90
4.3.2. Usage of Forms-Metamodel for Data Capture 92
4.3.2.1. Creation of Form Specifications from Form Fragments . 93
4.3.2.2. Generation of Data Capture System 94
4.3.3. Metadata-based Data Selection for Analysis 97
4.3.3.1. Clinical Study as Context for Data Capture 97
4.3.3.2. Selection of Data Sources and Interoperability 99
4.3.3.3. Pre-coordination of Data Collection across Studies . . . 101
4.3.4. Analysis 102
4.3.4.1. Analysis of Primary Data 102
4.3.4.2. Analysis of Derived Data 103
4.3.5. Summary 104
4.4. Conclusion 104

5. Design of Ion Beam for Radiobiology 106
5.1. Ion Beam Facility at LEIR 106
5.1.1. Requirements for Ion Beam Facility 106
5.1.2. LEIR 108
5.1.3. Local Constraints 110
5.1.3.1. Location and Space Availability 110
5.1.3.2. Ion Species 110
5.1.3.3. Extraction Method 111
5.1.3.4. Extraction Energies 111
5.2. Accelerator Physics Concepts 112
5.2.1. Linear Particle Motion 112
5.2.1.1. Magnetic Fields 113
5.2.1.2. Hill's Equation and Twiss Functions 113
5.2.1.3. Dispersion and Chromaticity 115
5.2.1.4. Particle Transport 117
5.2.2. Resonances 117
5.2.2.1. Third-order Resonance 118
5.2.3. Third-order Resonant Extraction 122
5.2.3.1. Description of Extraction Process 122
5.2.3.2. Resonance-driving Mechanisms 122
5.2.3.3. Spiral Step and Kick across Electrostatic Septum 124
5.2.3.4. Virtual Sextupole 124
5.2.3.5. Geometric Considerations 125
5.2.3.6. Hardt Condition 126

5.3. Slow Extraction Study (Transverse Aspects) . . . 127
5.3.1. LEIR-specific Constraints . . . 128
5.3.1.1. Lattice Parameters and selected Beams . . . 128
5.3.1.2. New Extraction Septa . . . 132
5.3.2. Resonance Configuration in LEIR . . . 134
5.3.2.1. Spiral Step Size . . . 134
5.3.2.2. Quadrant and Angle of Extraction Separatrix . . . 135
5.3.2.3. Phase and Strength of Resonance-driving (virtual) Sextupole . . . 135
5.3.2.4. Fulfilling Hardt-Condition . . . 136
5.3.2.5. Sextupole Configuration . . . 136
5.3.3. Particle Tracking Study . . . 138
5.3.3.1. Tools and Tracking Procedure . . . 138
5.3.3.2. Particle Tracking - Momentum Selection . . . 146
5.3.3.3. Particle Tracking - Tune Selection . . . 156
5.3.3.4. Characteristics of Extracted Beams . . . 160
5.3.4. Summary & Discussion . . . 163
5.3.4.1. Amplitude-dependent Detuning . . . 163
5.3.4.2. Extraction Configurations . . . 164
5.3.4.3. Placement of Downstream Septa . . . 167
5.3.4.4. Conclusion . . . 168
5.4. Design of Beam Transfer lines . . . 169
5.4.1. Design Criteria and Constraints . . . 169
5.4.1.1. Space Constraints for Beam Transfer Lines . . . 170
5.4.1.2. Start Parameters for Beam Transfer Line . . . 170
5.4.1.3. Reshaping Slow Extracted Beam . . . 173
5.4.1.4. Uniform Dose Distribution across Sample . . . 175
5.4.1.5. Beam Envelopes and Apertures . . . 176
5.4.2. Beamlines . . . 177
5.4.2.1. Extraction Line and Common Horizontal Bend . . . 178
5.4.2.2. Vertical Transfer Line . . . 181
5.4.2.3. Horizontal Transfer Line . . . 182
5.4.2.4. Quadrupole Properties . . . 184
5.4.3. Summary & Discussion . . . 188
5.4.3.1. Design Parameters and Effect of Random Errors . . . 188
5.4.3.2. Future Upgrade Options . . . 189
5.4.3.3. Conclusion . . . 189
5.5. Conclusion . . . 190

6. Summary & Conclusion **192**
6.1. Software Architecture for Capturing Clinical Information . . . 192
6.2. Design of Ion Beam for Radiobiology . . . 193

A. Appendix Software Architecture **195**
A.1. Forms-Metamodel Definition and Model Mappings . . . 195
A.2. Markov-Metamodel Definition . . . 218

B. Appendix Accelerator Study **221**
B.1. Detailed Tracking Results 221

List of Figures

1.1. Schematic of depth-dose distribution of photon beams vs. spread-out Bragg peak (SOPB). . . . 3

3.1. General MOF Metadata Architecture. . . . 16
3.2. Data description metamodel in ISO/IEC 11179-3:2013. . . . 18
3.3. Model-driven Architecture. . . . 20
3.4. Evidence creation and derivation process in evidence-based medicine. . . . 21
3.5. Architecture for capturing clinical information. . . . 23
3.6. Markov model example structure and time evolution. . . . 34

4.1. Forms-Metamodel metaclass diagram: *FormElement* inheritance. . . . 38
4.2. *EnumeratedResponseType* example: 'Likert items'. . . . 39
4.3. Forms-Metamodel metaclass diagram: *InteractionElement*, *SimpleResponseType*. . . . 40
4.4. Forms-Metamodel metaclass diagram: StructureComposition and example. 41
4.5. Forms-Metamodel metaclass diagram: *Structure* - *InteractionElement* . . . 42
4.6. Forms-Metamodel metaclass diagram: *Constraint* . . . 43
4.7. Forms-Metamodel metaclass diagram: LocalPrepopulationAssignment . . . 44
4.8. Forms-Metamodel metaclass diagram: *BooleanExpression* . . . 45
4.9. Forms-Metamodel metaclass diagram: *Annotation* . . . 45
4.10. Form example: semantically dependent questions. . . . 46
4.11. Forms-Metamodel metaclass diagram: Form . . . 47
4.12. Form example: control flow with 'go-to' statements. . . . 47
4.13. Forms-Metamodel statemachine: *SimpleStructureStateMachine* . . . 49
4.14. Forms-Metamodel statemachine: *ComposedStructureStateMachine* . . . 50
4.15. Forms-Metamodel statemachine: *CompositionStateMachine* . . . 51
4.16. Forms-Metamodel statemachine: composition types. . . . 52
4.17. Form example: `sequential` composition. . . . 53
4.18. Form example: `parallel` composition. . . . 53
4.19. Form example: `choice` composition. . . . 54
4.20. Example Forms-Metamodel instance. . . . 56
4.21. Forms-Metamodel-Template metaclass diagram: StructureComposition and example. . . . 58
4.22. Example Forms-Metamodel-Template instance. . . . 60
4.23. OpenClinica forms metamodel metaclass diagram. . . . 61
4.24. ISO/IEC 19763-13 metaclass diagram: Form_Design and Form_Design_Element 63
4.25. ISO/IEC 19763-13 metaclass diagram: Form_Design_Element - Text_Element. 64
4.26. ISO/IEC 19763-13 metaclass diagram: *Input_Field* - Text_Element. . . . 65
4.27. Forms-Metamodel metaclass diagram: modified inheritance hierarchy. . . . 66

4.28. Forms-Metamodel metaclass diagram: extended Enumerated_Response_Type. 70
4.29. Form example: 'exclusive choice' options from predefined answer sets. . . 71
4.30. Form example: 'fill-in' fields as 'exclusive' and 'non-exclusive' choice options from predefined answer sets. 71
4.31. Form example: 'hidden' questions. 72
4.32. Markov model metaclass diagram: *MarkovModelComponent* inheritance and relations. 76
4.33. Markov model simulation metaclass diagram: *Value*. 77
4.34. Markov model simulation metaclass diagram: *MarkovModelSimulationComponent* inheritance and relations. 78
4.35. Computation algorithm for the evaluation of Markov model simulations. . 79
4.36. Metamodel for Estimates used in Markov models. 83
4.37. Metamodel of usage context of Markov model simulation. 84
4.38. General Markov models for investigation of adverse events after RT. . . . 91
4.39. Form example: Question group for evaluation of adverse events. 92
4.40. Derivation of Fields from CDEs and annotation of form components. . . . 93
4.41. Usage of Forms-Metamodel for data interoperability in clinical studies. . 95
4.42. *XForms* implementation of adverse event reporting group. 96
4.43. Metaclass diagram: relation between form specification and submitted data. 97
4.44. Metaclass diagram: example 'application context model' for clinical studies. 98

5.1. LINAC3 and LEIR in LHC injection chain. 109
5.2. Current and proposed beam cycle of LEIR. 109
5.3. LEIR and South Hall. 110
5.4. Curvilinear coordinate system. 113
5.5. Characteristics of linear particle motion in real and normalised phase-space. 115
5.6. Separatrix of third order resonance motion at resonance-driving sextupole. 121
5.7. Steinbach diagram (stable configuration). 121
5.8. Schematic illustration of separatrix at resonance-driving sextupole. 121
5.9. Steinbach diagram (extration mechanisms). 123
5.10. Spiral Step and Spiral Kick across ES. 123
5.11. Comparison of fulfilled and unfulfilled Hardt condition. 127
5.12. LEIR lattice. 129
5.13. Optical functions at resonance (LEIR-like, LEAR-like). 130
5.14. Proposed septa for extraction from SS30. 132
5.15. Phase positions of sextupoles in LEIR. 137
5.16. Steinbach diagram for *momentum selection*. 142
5.17. Steinbach diagrams for *tune selection*. 143
5.18. Steinbach diagrams for *tune selection*: changing $\delta p/p_0$ at constant $\delta\widetilde{Q}$. . . 143
5.19. Phase-space plot *C1-M-BR-1*: extraction geometry at ES. 148
5.20. Spiral step size versus particle tune distance $\delta\widetilde{Q}$ (*C1*, momentum selection). 149
5.21. Selected orbit corrections in Low Energy Ion Ring (LEIR) 149
5.22. Particle losses at ES due to amplitude of orbit correction. 150
5.23. Particles at MS with well adjusted orbit correction (*C1-M-BR-3*). 151
5.24. Horizontal positions of extracted particles between ES and MS (*C1*). . . 152
5.25. Phase-space plots *C1-M-AR-1* at electrostatic ejection septum (ES). . . . 152

5.26. Separatrix orientations at ES for different extraction angles φ (analytic). 154
5.27. Phase-space plots *C2-M-BR-1* and *C4-M-BR-1* at ES 154
5.28. Phase-space plots *C4-ABE-BR-1* at ES and magnetic ejection septum (MS).158
5.29. Phase-space plots *C4-ABE-AR-1* at ES and MS. 159
5.30. Spiral step width in function of tune distance $\widetilde{\delta Q}$. 159
5.31. Horizontal positions of extracted particles between ES and MS. 160
5.32. Phase-space plots *C5-ABE-BR-1* at ES and MS. 161
5.33. Extracted beam segments at ES. 161
5.34. Maximum stable particle amplitudes $\propto \sqrt{\epsilon}$ versus tune distance $\widetilde{\delta Q}$. . . . 164
5.35. Unfilled ellipse approach. 171
5.36. Initial D and D' from extracted beam. 171
5.37. Thickness of scatter foil and adjustment of beta functions. 175
5.38. Required rms half-width vs. accepted I/I_0. 175
5.39. Survey plots of proposed beamlines. 179
5.40. Extraction line from LEIR and common horizontal bending line. 181
5.41. Optical functions in vertical beamline. 183
5.42. Optical functions in horizontal beamline, pencil beam. 185
5.43. Optical functions in horizontal beamline, broad beam. 186

List of Tables

3.1. Selected frameworks, systems and standards for electronic data capture. . 25
3.2. Comparison of form-related metamodels and frameworks: Identification and logical structure. 27
3.3. Comparison of form-related metamodels and frameworks: Data constraints. 29
3.4. Comparison of form-related metamodels and frameworks: Process and presentation constraints. 31

4.1. Completion and validation requirements at form submission. 50
4.2. Restrictions on form CompositionComponent siblings. 54
4.3. Mapping ISO:List_Item:*guarded_element* to FM:StructureComposition. . . . 68

5.1. Beam requirements for hadron therapy research. 107
5.2. Values for $\Delta\mu$ and α in dependence of S and $\widetilde{\delta Q}$. 126
5.3. Lattice Parameters for LEIR- and Low Energy Anti-proton Ring (LEAR)-like configurations. 131
5.4. Beam parameters at injection and extraction energies. 131
5.5. Integrated strength limits of sextupole families in LEIR. 131
5.6. Horizontal positions for new septa. 133
5.7. Properties of possible extraction septa for LEIR. 134
5.8. β_x, d_x and $\Delta\mu$ for sextupole magnets XFLS and PFW. 136
5.9. Resonance configuration parameters from analytic estimates. 139
5.10. Comparison of resonance-driving options and their simulation. 140
5.11. Resonance configurations for tracking (momentum selection). 146
5.12. Sextupole coefficients for tracking configurations. 155
5.13. Resonance configurations for tracking (tune selection). 156
5.14. Requirements and constraints for low and high energy extraction. 165
5.15. Extraction parameters and gap at MS for configurations *C4* and *C5*. . . 166
5.16. Courant-Snyder parameters of extracted beam segments from tracking. . 173
5.17. Start parameters for beam transport lines. 173
5.18. Matching constraints for beam transport lines. 177
5.19. Properties of beamline dipole magnets. 180
5.20. Beam functions in target plane for vertical beamline. 184
5.21. Beam functions in target plane for horizontal beamline. 185
5.22. Maximum quadrupole gradients and beam envelopes in beamlines. 187

A.1. Forms-Metamodel metaclasses. 196
A.2. Forms-Metamodel ENUMERATION types. 202
A.3. Mapping of selected elements from ISO/IEC 11179-3 to Forms-Metamodel. 204
A.4. Mapping between Forms-Metamodel and Forms-Metamodel-Template . . 206

A.5. Mapping between Forms-Metamodel-Template and OpenClinica forms metamodel. 208
A.6. Mapping between Forms-Metamodel-Template and ISO/IEC 19763-13:2013. 211
A.7. Proposed changes to Forms-Metamodel metaclasses. 216
A.8. Proposed changes to ISO/IEC 19763-13:2013 metaclasses. 217
A.9. Markov model and Markov model simulation metaclasses. 219

B.1. Detailed particle tracking results for extraction configurations. 222

1. Introduction

This chapter provides the contextual background for the remainder of the thesis. After a brief introduction into the principles of Hadron Therapy and its current situation and remaining challenges in Section 1.1[1], Section 1.2 discusses the kind of evidence expected for the introduction of new cancer therapies.

1.1. Hadron Therapy

Hadron Therapy (HT) is a form of external beam radiation therapy using beams of hadrons for cancer treatment. This technique dates back to 1946 when Robert Wilson suggested the radiological use of accelerated protons and other hadrons [6]. While other types of ionising radiation, such as gamma rays, electrons and neutrons, had been used for radiation therapy before, heavier charged particles could not be accelerated to sufficiently high energies for medical applications. With the invention of the cyclotron by Ernest Lawrence [7] and the construction of a sufficiently powerful accelerator, the 184-inch synchro-cyclotron [8] at the *Lawrence Berkeley Laboratory*, such energies became attainable. Already 1954, first patients were treated with proton beams, and from 1957 with beans of helium ions. Other groups followed this example.

1.1.1. Cancer

Cancer, in general terms, is a condition of uncontrolled cell proliferation due to 'abnormal' functioning of cellular control mechanisms. On the cellular level, cancerous cells have been characterised by a set of distinct capabilities that distinguishes them from 'normal' cells [12, 13]. They may form *tumours*, invade nearby organs, and spread to other parts of the body forming secondary cancer *metastases*. Worldwide, about 12.7 million new cases of cancer and 7.8 million cancer deaths occurred in 2008 [14]. With improved control over other health conditions and an over-all increasing life expectancy, deaths from cancer are expected to rise to over 13 million per year by 2030 [15]. In Europe, cancer accounted for 28% of all deaths in 2010, making it the second leading cause of mortality, after diseases of the circulatory system [16]. Radiation therapy is used in about 50% of patient treatments with curative outcome. In about 60% of those, radiation therapy is the only treatment, while the others are cured by a combination of radiation therapy with surgery and chemotherapy [17]. Overall cancer-related costs, including treatment, informal care and losses in productivity, were estimated to 124 billion Euros per year [18] in the European Union.

[1] Further historical and technical information can be found for example in [1–5].

1.1.2. Photon-based Radiation Therapy vs. Hadron Therapy

Radiation therapy uses ionising radiation to 'kill' tumour cells. This biological effect results from a series of physical, physico-chemical, and finally biological mechanisms that are triggered by the energy deposition of radiation on its transit through a medium. The *absorbed dose*, corresponding to the deposition of a certain amount of energy [*Joule* (J)], per unit of mass of the medium [kg], is measured in *Gray* (Gy). Generally, cellular damage increases with absorbed dose, however, the biological effect depends on characteristics of the radiation and the biological system. The *equivalent dose*, expressed in *Sievert* (Sv), relates to the absorbed dose by a radiation weighting factor.

Both, tumour and healthy cells are affected by ionising radiation. All developments in radiation therapy therefore aim at improving the *therapeutic ratio*, the relative damage caused in tumour tissue compared to the damage in adjacent healthy tissue, in order to achieve high tumour control at low normal tissue complication probability. The two main strategies employed are *a*) optimisation of beam paths through critical anatomical structures, in order to minimise the dose to healthy tissue, and *b*) splitting the total required dose for tumour eradication into multiple smaller dose fractions, delivered over several days or weeks. The latter approach, *fractionation*, exploits differences in the cell cycles and damage repair mechanisms between tumour and 'normal' cells that make tumour cells more susceptible to radiation damage. Nevertheless, normal tissue complication often limits the maximum doses that can be given in clinical practice.

1.1.2.1. Physical Dose Distribution

To optimise the therapeutic ratio, the depth-dose relationship has to be considered. Figure 1.1 shows the relative dose deposited by different kinds of radiation in function of penetration depth into the tissue.

Most external radiation therapy techniques are based on high-energy photons, typically between 6 MV to 20 MV, produced by clinical linear accelerators. In this energy range, the photon-tissue interaction is dominated by Compton scattering, whereby the incident photons transfer energy to electrons in the medium. The number of scattered electrons decreases with depth, which results in continuously decreasing dose with depth, as indicated by the black line in Fig. 1.1. The position of the initial peak corresponds to the range of secondary electrons in the medium. Regardless of the location of the tumour, a significant proportion of the delivered dose is absorbed by healthy tissue before and behind the target. Conventional radiation therapy focused on optimising fractionation schemes in order to achieve sufficiently good therapeutic ratio despite this dose-depth dependency. Modern forms of radiation therapy attempt to improve the therapeutic ratio by shaping the irradiation field to the tumour target and spreading the dose over multiple entry channels. While latter approach allows reducing the dose given to a particular organ at risk, it does not reduce the total integrated dose to surrounding healthy tissue.

The blue curves in Fig. 1.1 illustrate the dose-depth dependency for charged hadrons of different energies. These particles interact continuously with orbital electrons of the absorber atoms through the Coulomb force, mainly via inelastic scattering. In this process, energy is transferred to the electrons and the incident particles are slowed down. The amount of energy lost per distance travelled is inversely proportional to the square

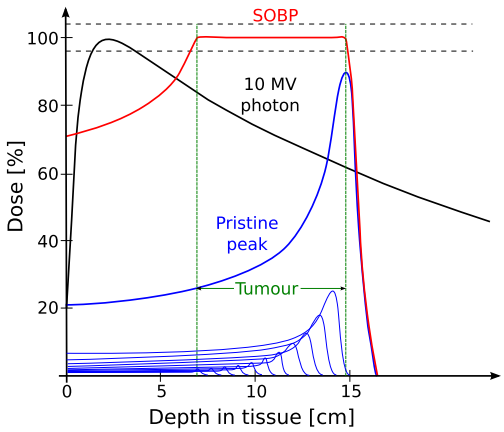

Figure 1.1.: Schematic of depth-dose distribution of photon beam (black), single Bragg Peak (blue), and spread-out Bragg peak (SOPB) (red) constituted of multiple Bragg Peaks. Only little dose is deposited beyond the distal fall-off edge of the SOPB. (adapted from [19])

of the particles' velocity. As the particles slow down towards the end of their range in the medium, energy loss increases. The resulting characteristic shape is called *Bragg Peak*. Its position in depth increases with particle energy.

R. Wilson realised [6] that superposition of multiple Bragg Peaks, corresponding to particles with different energies, would allow the full volume of a tumour to be covered with high ionisation density. The resulting *spread-out Bragg peak (SOPB)* is illustrated by a red line in Fig. 1.1.

In terms of physical dose distribution, HT therefore offers clear advantages compared to photon therapies: *a*) the well-defined range in tissue guarantees that only little dose is given to healthy tissues beyond the target, and *b*) the relative dose deposited in the proximal region of the SOPB is lower than for photons.

1.1.2.2. Biological Effect

The biological effect of ionising radiation depends on the kind of molecular damage it causes. It is measured by the *Radiobiological Effectiveness (RBE)*, which compares the doses of a reference and of a test radiation needed to achieve the same biological effect. RBE depends on radiation quality (type of radiation and energy), dose and dose rate, number of fractions, and the biological system and endpoint.

The Linear Energy Transfer (LET), the energy absorbed by the medium per unit length, provides a measure for radiation quality. High LET radiation, such as heavy charged particles or slow protons, causes a high proportion of irreparable DNA damage, whereas low-LET radiation, such as photons or fast protons, induces DNA damage mainly as secondary effect, resulting from the creation of oxygen radicals. The effectiveness of low-LET radiation therefore increases with the partial pressure of oxygen in the tissue. Many tumour tissues are deprived of oxygen, *hypoxic*, and their sensitivity to low-LET radiation is therefore often reduced, leading to a low therapeutic ratio.

Two theoretical advantages of HT over photon-based therapies result from this. By using ions for tumour treatment *a*) the RBE in the target region, where LET is highest, could be increased, with *b*) the biological effect being independent from oxygenation levels.

1.1.2.3. Rationale for Hadron Therapy

The rationale for HT is based on the assumption that the aspects discussed before, improved dose distribution and preferable radiobiological characteristics, manifest in better clinical outcomes. Benefits are expected in localised tumours close to critical organs and in radio-resistant tumours. Due to an overall dose-sparing effect compared to photon treatments, HT is also expected to reduce late side effects in paediatric cancer patients, such as impairment of organ function or secondary cancers. While 'better clinical outcome' is typically associated to higher tumour control and reduced treatment-related morbidity, the dose sparing potential of HT may also result in reduction of treatment side-effects that are not clinically relevant but affect patients' quality of life.

1.1.3. Current situation

At the time of writing, 41 HT centres are operational worldwide, 16 of which started treating their first patients within the last 4 years. Further 41 centres are planned to be built, of which 25 aim for patient treatment by 2018 [20]. While most of the operating centres exclusively provide protons, 7 centres also treat patients with carbon ions. Five of them are located in Japan, two are based in Europe, where a further one will become operational by 2015.

Clinical experience has been collected with almost 110 000 patients treated by HT [20]. The vast majority of patients, 90 000, was treated with protons and almost 10 000 patients with carbon ions, most of them in Japan. Despite this experience and the large number of operational and planned centres, HT is still subject of intensive study.

1.1.4. Challenges

While the physics of HT is well-understood, challenges remain in the delivery of the treatment [21, 22]. These include improved and new imaging techniques for tumour localisation and quality assurance, better calibration of treatment planning with regard to the range of particles in tissues, and advances in active beam delivery techniques regarding the treatment of moving organs. Cheaper and more compact accelerators might be decisive in achieving wider availability of HT. The same applies for rotating gantries for 'heavy'-ion beam delivery, if these prove to be clinically needed.

Most clinical experience has been gained with protons and carbon ions, however, interest in the use of other types of hadrons for medical applications also exists and patients have been treated with neutrons, helium and neon ions, as well as pions.

The use of other ions, heavier than protons but lighter than carbon ions, is motivated by *a*) better conforming lateral dose deposition due to reduced lateral scattering compared to protons, *b*) higher RBE in the Bragg Peak compared to protons, and at the same time lower RBE in the entrance region compared to carbon ions, as well as *c*) more rapid dose fall-off at the distal edge of the Bragg Peak compared to carbon ions due to reduced nuclear fragmentation. According to those criteria, optimal ions are expected to be found between helium and carbon [23].

Despite the experience with carbon ion treatment, inaccuracy in the estimates of RBE still represents the main source of dose uncertainty in therapy [21]. Most RBE estimates for lighter ions date back to radiobiological experiments performed in the early years of HT. Also beyond systematic studies of RBE for different cell lines, radiation types and energies, further in-vitro and in-vivo radiobiological research is needed [21].
Probably the most important challenge for HT at the moment lies in the identification of clinical situations in which its theoretical advantages do translate into improved clinical outcomes compared to other treatment strategies. Multiple reviews of photon and particle radiation therapy literature, mainly based on protons, such as [25–36], investigated this question in order to derive guidelines for future best treatment practice. Many of these studies failed to draw definite conclusions on the relative superiority of HT compared to modern photon techniques due to insufficient clinical evidence and the lack of data. Such findings gave rise to an ongoing debate in the field about the kind of evidence that is necessary and appropriate for the introduction of new health technologies for individualised cancer treatments. The following section summarises this debate in the context of Evidence-Based Medicine.

1.2. Nature of Evidence for new Cancer Therapies

1.2.1. 'Evidence' in Evidence-based Medicine

Modern medicine is based in the paradigm of *Evidence-Based Medicine (EBM)* which is defined as 'the conscientious, explicit, and judicious use of current best evidence in making decisions about the care of individual patients' [37]. *Evidence-based health care* extends the approach of evidence-based decision making from individual patients to the delivery of health service, including decisions about the acceptance and support for new health technologies, treatment guidelines and reimbursement policies. Due to finite resources, such decisions need to be based on 'comparative analysis of alternative courses of action in terms of their costs and consequences' [38], evaluated in terms of objective and subjective outcome measures.

The Cochrane Collaboration's definition of evidence-based health care understands *best current evidence* as 'up-to date information from relevant, valid research about the effects of different forms of health care' [39], comprising a potentially very large body of evidence, with different levels of applicability to decision making. Quality levels had been introduced for assessing and grading the available body of clinical evidence, based on the methodology of its underlying studies. While different grading approaches exist [40], evidence created from *Randomised Controlled Trials (RCTs)* is commonly considered the gold-standard in evidence-based medicine, providing the highest quality level evidence for clinical effectiveness. Observational studies are considered lower clinical evidence, followed by case-series studies and expert opinion. Study participants in RCTs are selected according to eligibility criteria and then randomly assigned to one of several treatment arms in order to minimise potential biases on the estimated treatment effect [41, 42]. In order for randomisation to be ethically acceptable, *equipoise*, that is the existence of a 'genuine uncertainty' within the expert medical community over the preferred treatment [43], is required. RCTs have been introduced as a successful methodology for

the evaluation of clinical utility of pharmaceutical interventions. However, it is disputed whether RCTs are always required for an intervention to be accepted in the frame of EBM [44], and whether RCTs constitute the best and only method for evaluating the utility for other kinds of health technologies [45]. Possible issues with RCTs relate to the lack of *external validity* [46] and to difficulties in randomisation and follow up of patients over long periods of time when multiple complex endpoints are to be studied [47]. Latter is particularly relevant for forms of personalised medicine where treatments are specifically targeted to the genetic characteristics or physiology of every individual patient.

1.2.2. The Hadron Therapy Case

Radiotherapy is such a form of personalised medicine. Indeed, the question of the need and appropriateness of RCTs as primary evidence for novel radiotherapy technologies and techniques is subject of debate in the field of HT. It was triggered by criticism brought forward in several review articles [29, 33, 34] regarding the lack of evidence from RCTs and the large amount of data that would be required to justify the implementation of particle therapy in clinical practice. The debate is centred around the interpretation of equipoise and the prior information that is accepted to count towards the judgement over the existence of equipoise.

Arguments against the need for RCTs [45, 48, 49] are based on the well-studied physical characteristics of charged particle radiation, Section 1.1.2, and existing clinical experience with photons: *a*) Treatment planning studies showed that particle therapy results in a significant improvement in the target conformity of the dose distribution and a two- to three-fold reduction of the integrated dose given to surrounding normal tissues compared to photons. Further, *b*) from clinical experience it is known that the tissue response to protons in the therapeutic energy range is similar to the one of photons and *c*) that the level of dose to tissue (normal or cancerous) correlates with the level of damage inflicted to the tissue. From these points it is argued that, in most cases, proton therapy is inherently superior to photon therapy, and therefore RCTs between photon and particle therapy are not required and even not appropriate in most situations due to a *lack* of equipoise. This judgement about (non-)existence of equipoise is based on a weighted consideration of *all available evidence* [49], including evidence not obtained from clinical studies.

Arguments for the need of RCTs [50–53], on the other hand, exclusively accept *clinical evidence* as basis for determining the existence of equipoise: Given the lack of measurable clinical superiority [29, 33, 34], clinical equipoise is fulfilled and therefore randomised controlled trials are required to ensure that patients only receive treatments with measurable benefits. Inferences drawn from technological experience, basic science experiments and proven models alone are deemed insufficient for the introduction of a new treatment modality or health care technology, and systematic *clinical testing* is considered essential before new technologies can be widely accepted.

In this situation, decision algorithms, such as [54, 55], may provide a pragmatic approach for determining the additional clinical evidence required for the introduction of novel health technologies by making use of modelling approaches to synthesise different kinds of available evidence and to predict the potential clinical benefit and cost effectiveness of these technologies.

2. Evidence for Hadron Therapy

Despite its relatively long history and the accumulated experience, Hadron Therapy (HT) is still considered an 'experimental technique' by many. A recent review article identifies 'the historic failure to leverage the collection and sharing of anonymised data' [25] as the *core problem* for the field of HT, leading to a lack of clinical evidence. Additionally, HT suffers from uncertainties in the Radiobiological Effectiveness of ion beams, particularly for ions heavier than protons. The vision of individualised treatments that use the 'optimum ion' for a given treatment situation requires further research into the effect that irradiation with different ion species has on relevant cells and tissues.

This thesis investigates two areas of research that are less studied in the context of HT, but essential for the future of the field.

The first topic relates to the creation process of 'clinical evidence'. Section 2.1 introduces aspects of this process and identifies shortcomings related to the collection and re-use of clinical information. Informatics-driven solutions are proposed in Chapter 3, and elaborated in Chapter 4.

The second topic responds to the need for additional research into the radiobiology of charged particle beams. Section 2.2 outlines current developments in the biomedical research community towards a new research facility dedicated to such experiments. Chapter 5 presents first results of a feasibility study for the establishment of a new ion beam at the European Organisation for Nuclear Research (CERN).

Finally, Chapter 6 summarises results obtained from both studies and draws conclusions on their impact on evidence creation for and beyond HT.

2.1. Derivation of Clinical Evidence

Requirements for the synthesis and analysis of existing clinical evidence and its efficient use in medical decision making are the subject of this section. Section 2.1.1 introduces the concept of meta-analysis and derives requirements on clinical data collection in order for the collected data to optimally support the analysis process. Quality and completeness of the collected data, Section 2.1.1.1, are hereby of particular importance. Section 2.1.1.2 outlines how the practice of clinical research data capture may affect these characteristics of the collected data. The role of modelling and simulation approaches for the synthesis of evidence and the prediction of potential clinical benefits of new technologies is introduced in Section 2.1.2. Section 2.1.3 summarises the contribution of Chapter 3 and 4.

2.1.1. Meta-analysis of Clinical Studies

Meta-analysis represents 'the statistical analysis of a large collection of analysis results from individual studies for the purpose of integrating the findings' [56]. Among the

potential advantages of meta-analyses are improvement in precision of the estimated treatment effect and the ability to provide answers to questions that were not posed by the individual studies [57].

Instead of extracting data from study publications, meta-analysis on Individual Patient Data (IPD) involves 'the central collection, validation, and reanalysis of raw data from all clinical trials worldwide that have addressed a common research question with data obtained from those responsible for the original trials' [58]. Compared to meta-analyses based on published aggregate data, IPD-based analyses provide methodological advantages [59], among them the ability to carry out survival or other time-to-event analyses and to verify and correct the data. The greater statistical power of IPD-based analyses compared to the original studies may allow patient subgroups to be identified and treatment effects on these subgroups to be analysed. Also, IPD-based analyses provide an opportunity to update the individual trial analysis by including additional long-term follow-up data. This form of research is particularly important for areas of health care which require large-scale randomised evidence due to small differences in outcome between the treatment options [60].

In cancer-related research, the power of this technique had been demonstrated in the analysis of individual patient data from more than 37000 women enrolled in randomised trials for the breast cancer drug Tamoxifen [61]: The findings allowed identification of the subset of the population responsive to the drug, and indicated the optimum period of treatment. However, such efforts are labour-intense [62] and not always successful because relevant studies need to be identified, data be requested from the trial managers and be reconciled into a common format that is appropriate for the purpose of the analysis.

Often, the manual work required for identification of suitable data and its integration may be prohibitive. The cost of data integration is linked to the amount of readily available computable information and provides the basis for automatic processing. However, as discussed in the following Section 2.1.1.1, availability of such information is often limited.

Furthermore, its availability alone is not sufficient for observations from different studies to be combined in a common analysis scenario, if the observations themselves are not 'interoperable'. Coordination of data collection across studies, Section 2.1.1.2, may prevent incommensurable data sets from being collected.

2.1.1.1. Data Quality

The challenge for the integration of clinical data is not its volume, but its complexity. In general, such complexity arises from the need to describe the data in its originating context, along with information about its prior use and trust levels [63].

Three data dimensions contributing to the complexity of clinical data were identified [64]: *Intra-facility* and *cross-facility* dimensions account for the different types of information acquired by systems *within* a single institution and the necessity of sharing data *across* institutions for providing continuity of care or for research purposes. Over *time*, and with advances in medical knowledge, clinical practice will change within institutions and across institutions.

Further to these three dimensions, clinical data is collected for different *purposes*, each posing distinct requirements on the representation and information content of the collected data. While data that is primarily collected for the purpose of patient treatment

typically represents information in an unstructured, narrative form, research use demands a more structured representation, amendable to computer processing. In general, the *contextual nature* of medical information [65] requires the collected information to be clearly identified and to be distinguished from assumptions linked to the context of data production. The wider the context in which data should be correctly interpreted, the more such contextual information is required.

The degree to which contextual information is accessible, directly affects the usefulness and usability of the data. The *interpretability* of data is one of several dimensions of *data quality*. It describes the extent to which data provides sufficient contextual information so that its 'fitness' for a specific purpose can be determined. Other dimensions comprise *accuracy*, the degree to which data corresponds to its intended interpretation, and *completeness*, the extent to which data collected is complete [66].

Research naturally requires data to be considered in different contexts and from different perspectives. This is only possible if the data adheres to high quality standards. Insufficient data quality, may render the use of data outside of its immediate collection context impossible [67]. The quality of data is limited by the methods and processes employed during its collection.

2.1.1.2. Clinical Research Data Collection

Data collection in clinical research involves the collection of *data items* needed for investigating the research hypothesis. The majority of such data items are collected from questions arranged in Case Report Forms (CRFs). Answers to these questions may comprise information about patient demographics, baseline variables, diagnosis, treatment, and follow up, partly acquired by transcribing values from other clinical information systems or external sources onto the CRFs, partly collected in treatment encounters between doctor and patient directly, or possibly submitted by the patient himself.

CRFs were historically based on paper-forms that had to be completed at the study sites and then be transcribed either centrally, or at each study site individually, into data-bases. The process of manual transcription is error prone, reducing the accuracy of the final data set, and time and labour consuming, resulting in significant delay between primary data capture and first possibility for data validation and consistency checks. With upcoming web-based technologies in the 1990, primary Electronic Data Capture (EDC) was expected to overcome the drawbacks of paper-based data collection, in particular to eliminate transcription errors and provide possibilities for immediate data validation and user feedback [68]. The use of EDC has slowly but steadily increased since, promising higher data-integrity and savings in cost and time [69].

Data capture instruments, in particular 'forms', in the health care context are directly exposed to the different dimensions of clinical data [64], so that their design and documentation can have a substantial impact on the quality of the collected data and its suitability for interoperation in research scenarios.

Before data capture takes place, aspects of form design and behaviour need to be harmonised to ensure that interoperable data is collected. Ideally, agreement on data formats, the main observables and their clinical coding would be reached prior to data collection. Data standards were introduced for the documentation of collected data,

to increase data quality, and to speed up the clinical research process and reduce its cost. Agreement on the definition of research variables and re-use of suitable questions and expected value domains are recognised means of facilitating interoperability in clinical research data capture: ISO/IEC 11179, a meta-standard defining the information provided by 'data elements', is introduced in Section 3.1.3.1; an overview of current research data standards in the clinical domain is provided in [70]. The degree to which such pre-coordination is realised has direct implication on the kind of data collected. However, loosely coupled participating study centres will have difficulties reaching a high level of prior coordination. Particularly in the context of long-term observational studies, the requirements for data interoperability may not be clear from the outset.

The central role of forms in the clinical and research data collection process is widely recognised, and system providers often are required to demonstrate that data capture requirements have been faithfully transcribed into an information system. Besides implementation and design, forms and design requirements also have a documentation role. During and after data capture, inspecting the form by which data has been collected may help clarifying the meaning of the data items themselves, stored for example in a data base schema.

Also beyond the re-use of single data elements, CRF re-use is known to facilitate data sharing and to improve the ability to aggregate data [71]. Libraries of CRFs are valuable knowledge repositories, however, standards and tool support for building an 'intelligent' digital library [72] of CRFs remain missing.

Despite the ubiquity of forms in clinical data capture, and indeed many business processes, standardisation efforts are limited to domain-specific solutions. While standards on the data component level are relatively advanced, few standardisation efforts encompassing whole forms or parts of forms exist. In particular, standards were found to be missing for CRF-wide processes and workflows, workflows for CRF sections, as well as for data collection and validation [73].

2.1.2. Modelling and Simulation

The role of modelling and simulation in Evidence-Based Medicine (EBM) is illustrated on the example of health-economic appraisals that inform 'decision making' by establishing and comparing estimates for benefits and costs related to alternative treatment options. Different kinds of economic evaluations can be distinguished by the way in which they measure treatment 'outcomes': in natural units, such as 'lives' or 'life years', in measures of subjective treatment utility, such as *Quality-Adjusted Life Years (QALYs)*, or in monetary terms. Any analysis that computes the ratio of costs to benefits, that is cost per 'life year' or per QALY saved, is referred to as *Cost-Effectiveness Analysis (CEA)* in the following. The underlying assumption of CEA is that for any given level of resource availability, society or the decision maker aims to maximise health benefit [74]. The primary outcome of a CEA is the Incremetal Cost-Effectiveness Ratio (ICER): the differences in expected costs of two interventions divided by the difference in the expected outcome measure, 'life years' or QALYs gained. The value of the computed ICER relative to a threshold value, the so-called Willingness-To-Pay (WTP) may then be used as indicator for or against the funding of a new health technology.

Expected cost and outcome estimates required for this computation are inferred from

clinical evidence. An 'ideal' single source of evidence does typically not exist, because Randomised Controlled Trials (RCTs) may not have been undertaken, and because RCT data is of limited use for economic evaluations [75]. Even if RCTs exist, they may not provide all the data required. For example, long-term data on beneficial and adverse effects are often needed for evaluating new treatment modalities, but difficult to obtain due to the limited duration of clinical studies. When relevant data is not available, decision-analytic modeling provides an analytic framework for the synthesis of evidence. It also allows intermediate clinical endpoints to be extrapolated beyond the duration of a particular study [76]. Current cost-effectiveness and future research priorities can thus be established, and the uncertainty surrounding these results be assessed [77].

This approach to decision making commonly informs treatment guidelines in cancer care. Markov model-based simulations were used, for example, by the National Institute for Health and Clinical Excellence (NICE) to evaluate the cost-effectiveness of different hormonal therapies for specific forms of early breast cancer [78] and of different screening approaches [79].

A review of cost-effectiveness studies for HT [31] also identified Markov models as the most commonly used modelling approach for the assessment of cost-effectiveness in this field: Four [80–83] out of five published studies chose Markov modelling as methodology for assessing the health-economic impact of HT. Since then further studies have been conducted [84, 85].

By definition, the validity of results obtained from modelling simulations is constrained by the underlying assumptions, including decisions regarding the model structure, as well as model input parameters. Transferability of cost-effectiveness results depends on methodological factors, characteristics of the health care systems and population [86]. Drummond et al. [87] first showed that a common decision-analytic model can account for local differences when country-specific data is applied. Evidence suggests that costing data in particular, and, in some instances, baseline risk are country-specific, whereas treatment effects are considered more generalisable. The question of transferability of resource use and utility data, however, remains open [88].

In order for results of modelling studies to be correctly interpreted, transparent and accessible reporting of the assumptions on which model structure and input parameter estimates are based is vital [89]. This 'can be a major task' [90], since all data 'manipulations' related to model structure and input parameters need to be reported. The amount of information required for scrutinising health-economic evaluations poses challenges for peer review [91], particularly given the large variability in methods and quality of reporting [92, 93].

It was suggested [91] that 'changes in electronic publication' might provide a solution to this problem by placing 'data and assumptions ... on a journal's web site', together with 'all the necessary information to reproduce the study findings'. However, no general mechanisms exist for 'warehousing' economic evaluation data [94].

2.1.3. Contribution

Chapter 3 proposes a model-driven approach to data capture and analysis in medicine. This approach is further explored in Chapter 4 for the case of form-captured medical data and in the context of evidence-based decision making for HT, as introduced in the

previous Section 1.2 and 2.1. Its aim is to provide the means for automatically resolving questions of data interoperability for a given analysis purpose, and for improving the level of data interoperability in a domain.

First, an information architecture for supporting the collection of form-captured medical information and the subsequent evidence-creation process is proposed in Section 3.2. After reviewing common methods, and existing systems and standards in Section 3.3, Chapter 4 sets out to develop suitable metamodels as main components of this architecture:

Given the lack of comprehensive standards for form-based data capture [70, 73], Section 4.1 develops an information metamodel for data capture forms which distinguishes itself from other existing standards by providing sufficient expressiveness to support both the generation of data collection artifacts, as well as the documentation of collected data. The proposed metamodel is validated against standards for form generation and against a recent ISO-standard development for form documentation [95]. A novel property of the metamodel is its compositionality, allowing the creation of new data capture instruments from existing fragments, each of which may serve for the collection of a specific, possibly compound, clinical information. As part of the proposed architecture, the model has the potential to decrease the level of expert knowledge required for the creation of data capturing instruments, to decrease implementation efforts, and to increase the quality of collected data and thus its suitability and availability for future re-use.

Section 4.2 develops a metamodel for Markov model-based CEAs in health care, addressing the difficulties in reporting, exchanging and re-using components of such simulations, as outlined in Section 2.1.2. The metamodel is sufficiently expressive to describe data input and modelling assumptions, as they are commonly used in Markov model simulation studies in this context. With the computation algorithm provided in Section 4.2.2, it may serve as basis for an open-source software package for the evaluation of Markov model-based simulations for health-economic assessments in, but not limited to, HT. Its wider adaption has the potential to increase the transparency of economic evaluations in health care and to facilitate their reproduction and verification as components of these Markov model simulations could be reused and study results be transferred into other contexts more easily.

Section 4.3 presents the methodology of application of the developed metamodels within the proposed architecture. In particular, it identifies situations in which the question of interoperability of data collected across multiple studies can be resolved automatically based on contextual metadata available in the system. It further proposes how the Forms-Metamodel might be used for pre-coordination of data collection instruments so that data collected across studies can be guaranteed to suffice the interoperability requirements for future joint analyses.

2.2. Facilities for Radiobiological Research

Despite the increased availability of clinical ion beams in Europe, beam-time for pre-clinical radiation biology, chemistry and physics studies at these centres is likely to remain limited due to their focus on clinical use and related quality assurance. However, such studies will be needed for improving the understanding of radiobiology, and basic nuclear and applied physics for medical applications.

Suitable beams, with a variety of ion species and beam characteristics, could be provided by nuclear physics research centres. A survey among these centres showed, however, that their overall availability of beam-time for biomedical experiments is limited to approximately 1000 h/y [96]. This figure includes beam-time reserved for internal research, as well as beam-time available to external researchers through access agreements.

In response to strong interest in ion beams from the bio-medical community, and given the limited beam-time availability, a feasibility study for the creation of a dedicated research facility based on the Low Energy Ion Ring (LEIR) at CERN was initiated [97]. Interest was confirmed in a subsequent community meeting [98–100], and research priorities were identified [100]: In particular, *a*) the need for systematic experiments of the Radiobiological Effectiveness of different Linear Energy Transfer conditions on a large number of human cell lines, and *b*) studies on the effect of drugs, nanoparticles or other bio-modifiers in combination with ion beam exposure.

The rationale for upgrading the existing LEIR is based on the technical and co-ordinational expertise of CERN and expected savings in the cost for infrastructure and maintenance: LEIR has very similar characteristics to HT accelerators, so that its use as 'medical accelerator' has already been proposed in the past [101, 102]. As part of the heavy-ion injection chain of the Large Hadron Collider (LHC), it will be maintained, but not be used to full capacity. Furthermore, an adjacent storage hall provides space for dedicated infrastructure, such as beamlines, experimental endstations and laboratories.

2.2.1. Contribution

Chapter 5 presents investigations in the frame of this feasibility study.

The main requirements for a bio-medical research facility in the context of HT, and constraints imposed by the existing infrastructure, are established in Section 5.1. Section 5.3 investigates resonance configurations for slow extraction based on available infrastructure in and constraints imposed by LEIR. Since LEIR continues to be used for heavy ion accumulation in LHC, any modifications must be compatible with this primary role. The results of this study provide first estimates of extracted beam properties and their dependence on the extraction 'driving' mechanism.

Based on these results, beam transport lines towards the selected site for future biomedical experiments are designed. No infrastructure for these parts of the facility exists at the moment. In order to minimise delays and up-front investment, a staged implementation approach may therefore be envisaged in which an initially minimalistic, but extensible and functional design, is refined successively. Linear-optic designs for such an approach are presented in Section 5.4. The design covers a common beam transport line to the adjacent experimental area and two separate lines for 'horizontal' and 'vertical' delivery of ion beams. Attainable beam characteristics from this setup are investigated in order to inform future design decisions.

Both studies identify areas of future research towards a biomedical facility at LEIR.

3. Software Architecture for Capturing Clinical Information

Medical information, collected in the course of clinical studies, represents the primary evidence for Evidence-Based Medicine. Through analysis, this information becomes part of the evidence base that informs decision making. This chapter adopts an information and processing perspective of the clinical evidence creation process and proposes an information architecture to support it.

The concepts necessary for the remainder of this chapter are summarised in Section 3.1. Section 3.2 outlines the proposed software architecture and introduces the role of the architecture components that are developed in Chapter 4. Relevant methods for their development, as well as existing systems and standards, are reviewed in Section 3.3.

3.1. Concepts and Related Work

Section 3.1.1 introduces semantic interoperability and its characteristics and significance for information system design. Section 3.1.2 provides a brief introduction into conceptual and 'meta'-modelling, followed by an exemplified description of metamodels for interoperability. Section 3.1.4 outlines the main concepts of Model-Driven Architecture.

3.1.1. Interoperability

Interoperability generally refers to the ability of a (computer or software) system to 'exchange and make use of information' [103].

Meta-analysis, as described in Section 2.1.1, can only succeed if the available data *interoperates*. This includes two aspects: *a*) The data must be *interoperable*: Data items must have the same, or at least sufficiently close, 'meaning' so that they can be used for a joint analysis purpose. Consider the example of 'blood-pressure measurements' where a variety of factors, such as measurement methods and position, may significantly influence the measured values [104]. Depending on the analysis scenario, all those measurements must have been taken under sufficiently similar conditions for their corresponding data to interoperate. *b*) The data can be identified as being interoperable: This depends on the amount and quality of information that is available about the data, so-called *metadata*. For the example of blood-pressure measurements: A minimum level of additional information about the circumstances of measurement is needed in order to investigate and assert interoperability of the measured values for the given analysis scenario. Clearly, if this is not possible, or practical, then collection of interoperable data is of little use.

In the context of information systems, the ability to correctly interpret exchanged information, clinical data in this case, is referred to as *semantic interoperability*. The

ability to interpret the meaning of data based on its metadata, implies that the meaning of the metadata itself must be well understood. The following section outlines how this is achieved in information systems.

3.1.2. Conceptual Modelling of Information Systems

Conceptual modelling is the activity of eliciting the general knowledge within a domain [105]. Any domain, for the purpose of information systems, consists of *objects* and *relationships* between them. In a process called *classification*, these individual objects can be classified into *concepts* based on their common and distinguishing properties. The inverse process, the creation of an *instance* from a concept, is called *instantiation*. Both processes allow knowledge about a given domain to be structured into two levels: the concept level, describing the properties of all instances of the concept, and the instance level, providing additional information about specific instances.

The set of concepts used in a particular domain constitutes a *conceptualisation* of that domain. For a system to operate in a domain, prior conceptualisation of that domain is necessary. This conceptualisation may be made explicit and is then called an *ontology* or a *conceptual schema*, or *model* of that domain.

Conceptual schemas can be expressed in logical languages, such as first order logic, or in specialised modelling languages, such as the Unified Modeling Language (UML). UML is a language for specifying, documenting and visualising the static and dynamic aspects of software systems. The Object Management Group (OMG) adapted UML 1.1 as a standard in 1997, its current version is 2.4.1 [106]. The following notation for UML model characteristics is used throughout the remainder of this chapter: Metaclass, *Abstract Metaclass*, *attribute*, *relation*, `simple data type`, `ENUMERATION`, `CLASS TYPE`.

Returning to the question of interoperability: A conceptual schema for the metadata related to some data item defines the information that may be available for its interpretation. It can be represented in the form of an UML class diagram, or of another modelling language.

Computing services can then be defined in terms of the elements of this metadata model, so that they can base their actions on the specific metadata instances associated to a particular data item.

3.1.2.1. Meta-modelling

A modelling language, such as UML, defines rules for the creation of models, regarding their well-formedness and possibly their relations to other models. It thus provides a conceptualisation of the 'domain of models'. A model that represents knowledge about the 'domain of models' is called a *metamodel*.

Various such metamodelling frameworks exist. Among the best known is the Meta Object Facility (MOF) [107], a *metadata architecture* developed by the OMG, see Fig. 3.1:

The highest level in this architecture (*M3*) corresponds to universal modelling languages, and is represented by MOF. It corresponds to a meta-metamodel and provides the abstract syntax in which other modelling systems can be specified. The metamodel layer (*M2*) contains modelling languages, such as UML. The *M1* layer contains models

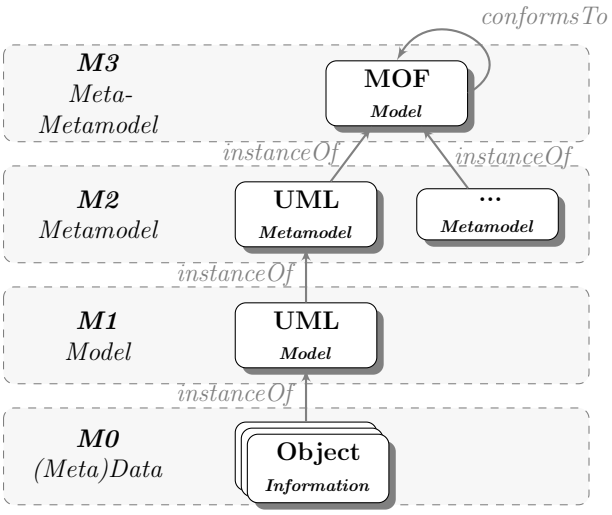

Figure 3.1.: Four-level metadata architecture as defined by MOF [107].

that were created in one of the modelling languages for a particular application. They describe the information in the *M0* data layer.

The naming of the MOF model layer (*M3*) assumes the existence of a total of four levels. However, MOF does not prescribe four fixed levels and any number of intermediate 'metalayers' can be handled. In this view, the metadata associated to a data item is part of the *M0* layer, its metadata schema is part of the *M1* layer.

The metadata architecture is not linked to a particular modelling language or technology. For example, the 'metadata record' describing some data item could be represented as a document in the Extended Markup Language (XML). In that case, an XML-schema document would provide its *M1* model, and the language definition of XML-schema would represent the *M2* level. This shows that *metadata* is *data* about other data, and may be described and managed as such. *M0* objects are therefore called *data* in the following. Their schema (*M1*) may be referred to as *metadata*.

3.1.3. (Meta-)Models for Interoperability

The view of data provided by the metadata architecture allows comparing different approaches for achieving data interoperability [108].

A common approach to achieve interoperability among multiple parties is the creation of a *shared conceptualisation* (*M1*) of a particular domain of interest. Physical integration (data warehousing), and virtual integration through a 'global schema' or through a global ontology are examples of this approach. It requires agreement to be reached on the important concepts in the domain, including their attributes and data types used for recording. A central authority will maintain this conceptualisation, and all participating parties are required to adopt it. However, adherence to one single conceptualisation may be difficult due to varios reasons: In larger, relatively independent communities no such central authority may exist. In research, *the* conceptualisation frequently needs to fit multiple disciplines and continues evolving as science in the field advances. A recent example of this approach in cancer research is given by [109] where a 'master ontology'

was devised for the integration of clinical and genomic data.

An alternative method, based on the idea of metamodelling, approaches interoperability by standardisation on the metamodel (*M2*) level. This does not mean that the level of general modelling languages, such as UML in Fig. 3.1, is removed. Rather, an additional layer is introduced in the metadata architecture to provide suitable abstractions for the respective domain. This layer represents a *domain-specific* metamodel that can be expressed in a general-purpose modelling language. Like other metamodels, this domain-specific metamodel provides a language for models. Users can define their own conceptualisation of the domain that they wish to represent, *user-models* (*M1*), in terms of this metamodel. Since all such models are based on the same language constructs, defined by the domain-specific metamodel, these user-models are structurally interoperable. If the user-model can be interpreted, so can the data objects that conform to it. Semantic data interoperability in this approach can be achieved through re-use of user-models: If data is collected against identical conceptualisations of the domain, it can be expected to interoperate. Since user-models can be interpreted through their common domain-specific metamodel, differences in user-models - and their implications on data interoperability - can be examined.

In order for this approach to work efficiently, the metamodel that a user-model conforms to must be known, and user-models must be identifiable and accessible. Standardisation approaches towards this goal are relevant to the architecture proposed in Section 3.2 and therefore explained in the following.

3.1.3.1. ISO/IEC 11179 - Metadata Registries

ISO/IEC 11179 [110] is an international standard for the representation of metadata in a *metadata registry*. A Metadata Registry (MDR) is a database for metadata with registration functionality, such as the ability to submit and maintain metadata and to monitor its quality, provenance and aspects of its identification.

In the view of the metadata architecture introduced before, such metadata can be regarded as a user-model that defines the characteristics of a *data element* recorded elsewhere. Data elements represent the 'fundamental units of data an organization manages' [110]. The data description package in part 3 of ISO/IEC 11179 [111] provides a metamodel for describing these data elements. Figure 3.2 introduces selected components of this metamodel which are described in the following. More details can be found in the documentation of the standard [111].

A Data_Element in ISO/IEC 11179-3 is defined by an association between Data_Element_Concept, specifying its *meaning*, and *Value_Domain*, specifying its representation *domain*. Instances of the Concept metaclass represent *concepts*. As seen before, such concepts form part of the conceptualisation of a domain and can be described in modelling languages. Instances of Data_Element_Concept maintain information about concepts and their relation to data elements. A data element concept may be associated to an instance of Object_Class and of Property. Instances of Object_Class are concepts that represent a set of ideas, abstractions or things in the real world. Instances of Property are concepts that correspond to features which may be used to distinguish individual objects from each other. An object class 'person' and a property 'height' could thus be associated to the data element concept 'person height'. Instances of subclasses of *Conceptual_Domain*

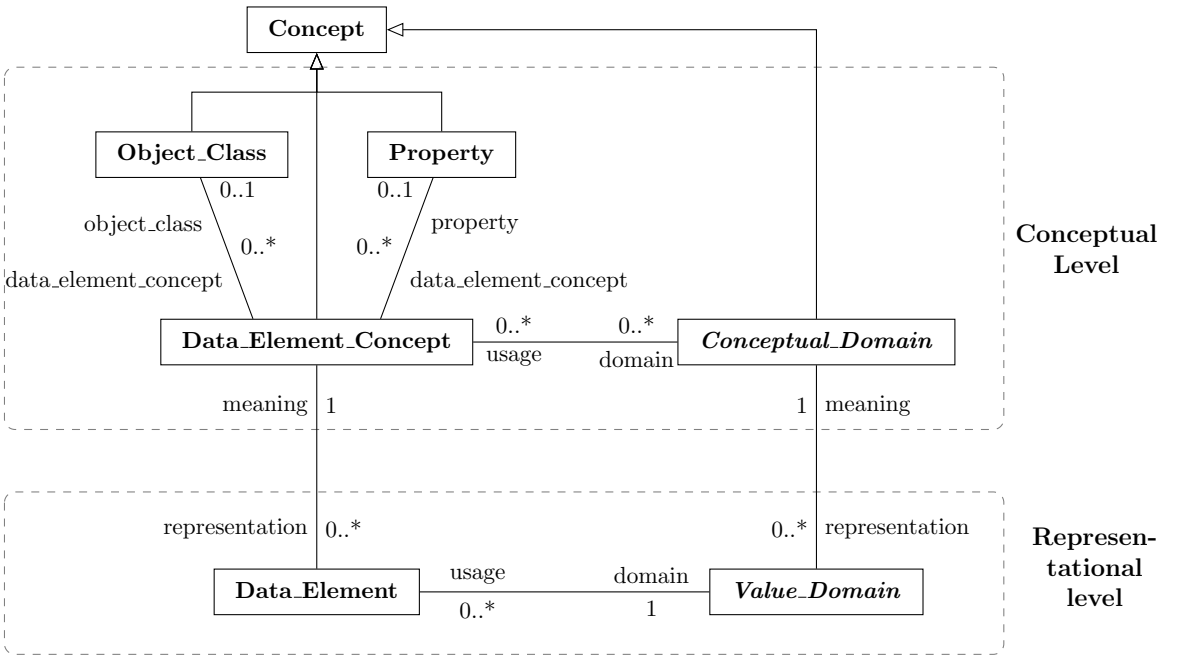

Figure 3.2.: The data description metamodel region in ISO/IEC 11179-3:2013 is divided into *conceptual level*, or semantic level, and a *representational level*, describing the information artifacts. (Adapted from [111].)

model sets of value meanings, such as 'countries' or 'spoken languages'. *Value_Domain* corresponds to the representation of such a set of value meanings. 'Spoken languages' could be represented for example by two distinct value domains using full names or three letter codes. Both, *Conceptual_Domain* and *Value_Domain* have further subtypes that define sets of value meanings.

Different representations of a data element concept are described through the use of different data elements. These representations may differ for example in their name or the value domains they use. Data elements can be grouped by their data element concepts which themselves are grouped by a common object class and by high-level concepts. The conceptual level thus helps distinguishing structural differences among data elements from semantic differences, and it allows identification of semantically equivalent elements.

Data elements can be registered in a MDR as *administered items*. As such they will be uniquely identifiable and can be made publicly available with the intent to encourage their reuse and thus to decrease data heterogeneity within a domain. Since all possible data elements are based on the same metamodel, any persisting heterogeneity can be analysed.

ISO/IEC 11179 is not concerned with the storage of metadata or data, and does not define an implementation of its standard. Implementations of ISO/IEC 11179-3, however, were developed and have been used in the field of cancer research, most prominently *cgMDR*[1] developed in the frame of the *CancerGrid* [112] project, and *caDSR*[2] of the *caBIG* [113] project.

Instances of the Concept metaclass in ISO/IEC 11179 may be drawn from any domain

[1] `https://wiki.nci.nih.gov/display/caDSR/cgMDR`
[2] `https://wiki.nci.nih.gov/display/caDSR/caDSR+Wiki`

conceptualisation, for example from domain vocabularies or ontologies, such as the National Cancer Institute (NCI) *Thesaurus*[3], and be served through vocabulary services, such as the NCI *EVS*[4].

The conceptual level in Fig. 3.2 may also be regarded as *one specific* approach to modelling the meaning of a data element. A more generic approach is proposed in [114]. Based on the observation that the meaning of a data element is largely determined by the specific context in which it is used, [114] suggests to simplify the conceptual layer of ISO/IEC 11179: Data elements and value domains only obtain their meaning through their use in models; any 'user-model' (*M1*, as discussed in the context of metadata architecture) may therefore represent the semantic metadata that defines a data element.

To maintain interoperability, such user-models need to be registered and be accessible in a way similar to data elements in ISO/IEC 11179. ISO/IEC 19763 will provide a framework for this.

3.1.3.2. ISO/IEC 19763 - Metamodel Framework for Interoperability

ISO/IEC 19763 [115] is a multipart standard towards a *Metamodel Framework for Interoperability* and defines a set of metamodels that allow common types of user-models to be registered. It includes a core model that defines common concepts used across the other metamodels. Metamodels for the registration of ontologies, process models, services, role definitions, information models and forms are being developed.

A registered user-model in ISO/IEC 19763 will be identifiable in the same way as an 'administered item' in ISO/IEC 11179. Mappings are foreseen that allow 'semantic equivalence' or 'semantic similarity' to be asserted between registered user-models and their components. ISO/IEC 19763 aims at facilitating interoperability by exposing the information models that describe the meaning of the data to be shared. The format of these information models is standardised through their metamodels.

Part 13 of this standard deals with the development of a metamodel for the registration of data capture forms. Although the development of this and other parts of ISO/IEC 19763 is still on-going, part 13 will be covered in detail in Section 4.1.5.4, and will serve as validation reference for the form metamodel developed in Section 4.1.

3.1.4. Model-driven Architecture

The information provided by *models* may be used not only to document the meaning of data, but also to automate the creation of software artifacts.

The Model-Driven Architecture (MDA) [116, 117] is a set of standards proposed by OMG for Model-Driven Engineering (MDE), a software development methodology that exploits conceptual models for all aspects of software design. The two main stages of the software development process in MDA are explained in the following [118]: First, a Platform Independent Model (PIM) of a system is created. This model is independent of any implementation technology and should be designed to best support a particular purpose. In the next step, the PIM is transformed into one or multiple Platform Specific Models (PSMs), tailored to specific implementation technologies. Alignment between

[3] `http://ncit.nci.nih.gov/`
[4] `http://evs.nci.nih.gov/`

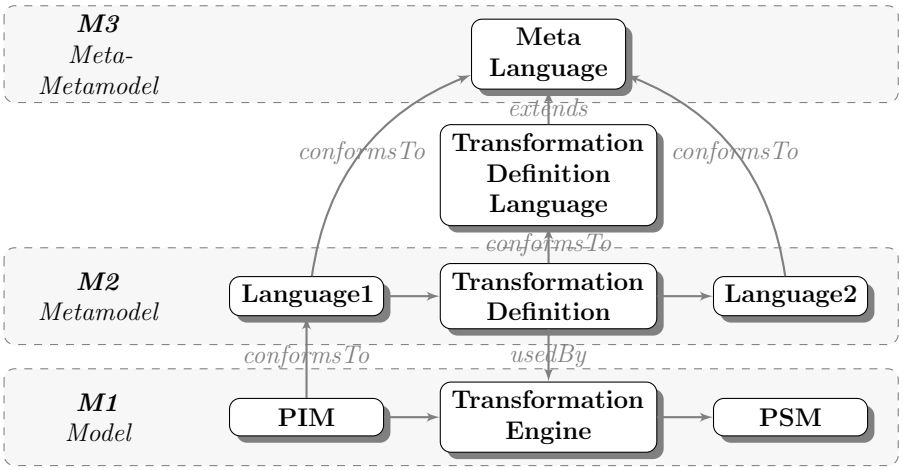

Figure 3.3.: Model-Driven Architecture (MDA).

the concepts of the PSM and the implementation technology then allows for automatic code generation. This process is illustrated in the *M1* layer in Fig. 3.3.

Generation of PSMs from a given PIM represents the most complex step in the transformation process; it is often subdivided into a sequence of intermediate transformation steps and models that are successively more closely aligned with the target platform. The MDA approach thus attempts to separate the business logic from the intricacies of the target platform, with the aim of reducing the accidental complexity of the system and to facilitate portability to new technologies, maintenance and interoperability of system components.

Many approaches to 'model-transformation' exist [119]. In general it is a process, in which a *source model* (*M1*) is transformed into a *target model* (*M1*) that conform to different metamodels (*M2*). A *transformation definition* relates concepts of source and target metamodel. This definition is then interpreted by a *transformation engine* that reads the source model, executes the transformation definition and writes the target model. The transformation definition requires a language that uses the same language constructs as source and target metamodels. Once a transformation definition between two metamodels is established, any user-model that conforms to the source metamodel can be transformed into an instance of the target metamodel.

3.2. Architecture for the Derivation of Clinical Evidence

Following a conceptual view of the 'evidence derivation process' in Evidence-Based Medicine (EBM), Section 3.2.1 describes the main characteristics of the proposed architecture. Its distinguishing features are summarised in Section 3.2.2.

Figure 3.4 shows data and processing aspects of the evidence derivation process introduced in Section 2.1: It distinguishes between 'Data Collection & Primary Analysis' of clinical studies, and 'Secondary Analysis' of the evidence produced by these studies. Secondary analysis hereby comprises statistical analyses of the *results* of clinical studies, in form of 'meta-analysis', or analyses of the *primary data* collected in medical studies in the form of 'Individual Patient Data (IPD) meta-analysis'. The 'estimates' obtained

from these analyses may be used as input parameters to 'modelling simulation' studies which allow the *synthesis of evidence* from different sources. A software architecture supporting this process requires services for data capture and analysis routines, including retrieval of primary 'data' or derived data 'estimates'.

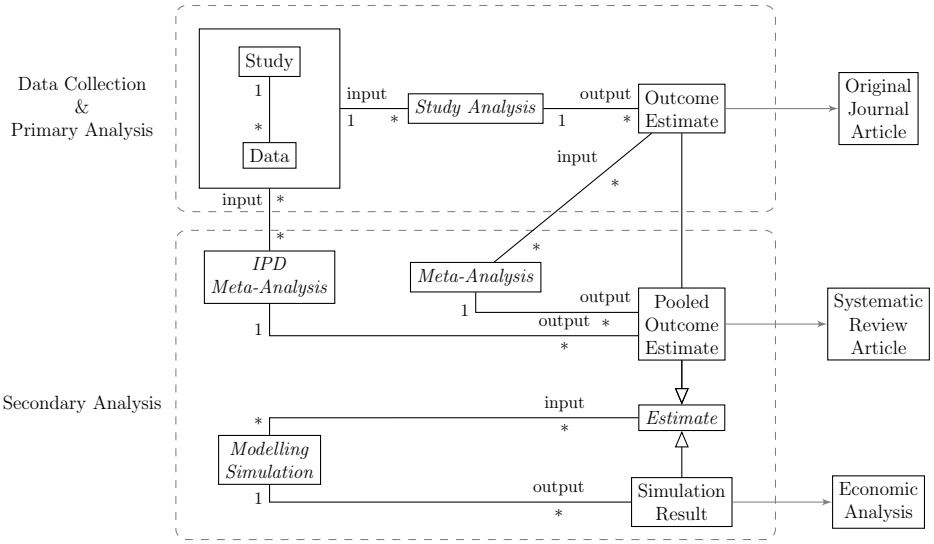

Figure 3.4.: Information and processing view of the evidence creation and derivation process in Evidence-Based Medicine (EBM).

3.2.1. Architecture

As described in Chapter 1 for Hadron Therapy (HT), data capture and subsequent derivation of evidence in medicine often requires international collaboration and thus encompasses multilingual contributions from distinct organisational entities. Despite this heterogeneity, collected information needs to be synthesised in order to provide sufficient evidence to inform treatment and health care decisions. This is only possible if collected and derived data interoperate. Section 2.1 identified some of the steps and difficulties in the processes of meta-analysis and subsequent modelling studies.

The approach of meta-modelling, Section 3.1.2.1, provides a pragmatic solution to this problem because it recognises the existence of multiple perspectives throughout the evidence creation process. Instead of standardising on *what* observations are allowed to be made, it defines *how* these observations are to be documented.

The medical research domain is well-suited for this approach: Most steps in the process shown in Fig. 3.4 are well-established and their conduct and publication are guided by protocols and best practise recommendations. Examples include the CONSORT statement [120, 121] for the reporting of randomised trials, the Cochrane Handbook [57] for the conduct of systematic reviews, or CHEERS [94, 122] for reporting of economic evaluations. Such guidelines can be formalised as metamodels.

User-models, as their conforming instances, may not only serve as documentation, but may also be used for the creation of software artifacts. The advantages of a model-driven approach for the generation of data capture and other software artifacts in the clinical domain were shown in [123–125] on the example of clinical trial design. By

providing study-specific instantiations of a CONSORT metamodel, the development effort of trial-related informatics services could be reduced substantially, as could the cost of validation.

The proposed architecture combines a metamodel-based interoperability framework, Section 3.1.3.2, with MDA, Section 3.1.4. Figure 3.5 shows its most important components: *a*) metamodels that provide the language for user-model definition; *b*) a *model registry* for the registration of user-models, their maintenance and identification; *c*) a model repository for the physical storage of user-models; *d*) model transformations that derive the required software artifacts from user-models stored in the registry; *e*) a repository for those artifacts; and *f*) a repository for data produced by those artifacts.

All aspects of the evidence-derivation process in this architecture are expressed through user-models, conforming to selected metamodels: Clinical studies, the data capture instruments used in these studies, and analysis procedures acting on collected data. These user-models are registered in a model registry that conforms to a model registration standard, such as ISO/IEC 19763, Section 3.1.3.2. Models within the registry are uniquely identified and versioned and may be classified or reference each other. Once a suitable transformation definition and engine has been created for a given metamodel, software artifacts can be generated automatically from any of its instances. The resulting artifacts, such as data capture services, are characterised by their corresponding user-model, and the transformation definition and engine used for their generation, Section 3.1.4.

The information provided by models, interpreted through their metamodels, provides rich metadata that may inform the further usage of model artifacts and the data that they produce: Both data capture and analysis services lead to the creation of new raw or derived data whose meaning is defined through their creation context.

The model-driven approach allows the 'annotation process' of this resulting data to be automated. Any process in Fig. 3.4, as well as the data created by it, is thus be documented by computable metadata, so that error-prone and costly manual post-hoc annotation can be avoided.

3.2.2. Distinctive Features

The architecture differs from most interoperability architectures in the clinical research domain in that it defines data semantics in terms of user-models. It proposes to document every aspect of data creation by discoverable and accessible user-models that conform to different metamodels. These metamodels represent distinct aspects of the clinical research domain in which the architecture operates. Different aspects of data semantics may thus be documented, and assessed, separately:

Assuming, interoperability of 'adverse event data' collected over the course of different clinical studies is intended to be assessed: Interoperability will not only depend on the way the observations were made and reported in each study, but also on the context in which they were collected (type of study, time of observation relative to treatment, who reported it) and the purpose for which they are required to interoperate (the information and granularity of information needed to perform a joint analysis). Correctly specifying this level of detail in terms of the ISO/IEC 11179 conceptual model becomes difficult. The information expressed by Common Data Elements (CDEs) in ISO/IEC 11179-based interoperability frameworks, such as in [113, 123], is therefore often insufficient to

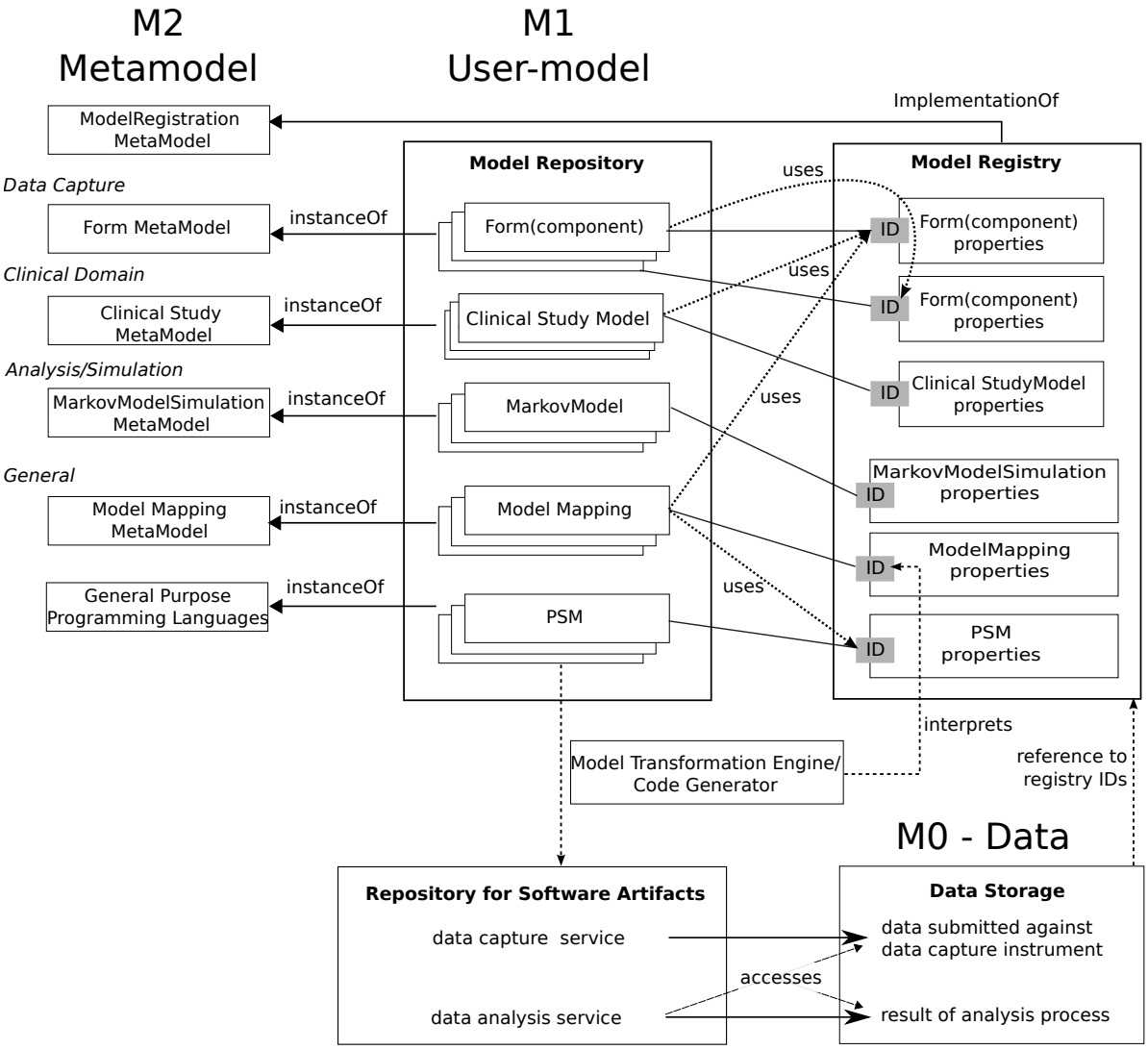

Figure 3.5.: Architecture for capturing clinical information.

Metamodels provide the language for user-models that are relevant to the clinical research domain. User-models are created by domain experts and registered in a model registry that exposes administrative information about these models through their unique ID and tracks model changes. The models themselves are stored in a model repository and can be accessed through the model registry. Models may link to other registered models: For example, a clinical study model may use a particular user-model for data capture that defines the data capture requirements for this study. Model transformation from a PIM, such as a user-model describing a data capture form, to its PSM in a particular target technology, can be defined and registered in the model registry. These transformations are enacted by model transformation engines and may subsequently be serialised into code. Software artifacts resulting from this process are stored in a further repository. New data may be created by some artifacts, for example services for data capture or analysis. The semantics of this data is defined by the user-models and transformation processes that led to their creation. Each user-model can be interpreted through its respective metamodel.

determine whether data is interoperable.

On the other hand, all contextual information can be specified in terms of usage contexts, described through distinct models: data collection, clinical studies, and the types of analyses. Different aspects of data semantics can thus be specified separately and only relevant aspects of the available information may be considered for a given task: If compatible clinical contexts for an interoperability scenario have been identified, data interoperability can be discussed in terms of the data collection instruments that were used in these contexts, on the level of single questions, groups of questions, or forms.

The proposed architecture is not limited to the domain of medical research. In particular the need for interoperability of data collected in distributed and heterogeneous environments is ubiquitous. Adaption to different domains corresponds to the modification of existing, or the introduction of alternative, metamodels that support the domain context. Certain metamodels, such as the Forms-Metamodel, may be suited for many domains, whereas others, such as the metamodel of clinical studies, are clearly domain-specific.

Sufficiently expressive metamodels for the clinical research domain are needed to realise this architecture. In preparation for Chapter 4, current technologies and standards for clinical data capture and analysis processes are therefore reviewed in the following Section 3.3.

3.3. Methods, Systems and Standards for Clinical Data Capture and Analysis

The development of domain metamodels requires familiarity with the relevant domain concepts. This section reviews systems and technologies for electronic data capture, Section 3.3.1, and introduces Markov model-based health-economic assessments as a form of secondary analysis processes, Section 3.3.2.

3.3.1. Clinical Data Capture and Documentation

Since 'forms' are widely used for data capture, a large number of systems, technologies and standards exists to support this process. Common abstractions for data capture forms and their usage patterns across domains are analysed in this section by comparing multiple existing systems, technologies and standards, Section 3.3.1.1. Particular attention is paid to abstractions related to *identification* and *logical structure* of forms and form components, Section 3.3.1.2, *data constraints*, Section 3.3.1.3, as well as *process* or *presentation constraints*, Section 3.3.1.4. The findings of this review are summarised, and gaps in the models identified in Section 3.3.1.5.

3.3.1.1. Selected Systems, Technologies and Standards

The artifacts listed in Table 3.1 span a wide range of abstraction levels related to form design and data capture: from programming frameworks supporting the implementation of data capturing systems, to configurable data collection and management solutions that

require minimum programming skills. An overview of selected historic form languages has been given in [126].

	Name	Version	Domain
Data interchange standards	CDISC ODM [127]	1.3.1	Archive and interchange standard for data and metadata in clinical research.
	DDI [128]	3.1	Social science data interchange.
Questionnaire interchange standards	queXML [129]	1.3.9	Questionnaire definition interchange.
	eDCI [130]		HL7 message specification development for transmission of Case Report Form (CRF) data.
Clinical data capture and data management systems	OpenClinica [131]	3.1.3	Clinical study management.
	RedCAP [132]		Research electronic data capture.
	CancerGrid [123]		Model-driven framework for data collection in clinical studies.
	caBIG Form Builder [133]	4.0.3	Model-driven framework for data collection in clinical studies.
Survey tools, general purpose data collection and analysis frameworks	SPSS Data Collection [134]	feature list	Data collection for survey and market research, data analysis.
	Survey Gizmo [135]	feature list	Data collection for online surveys.
	Lime Survey [136]	1.92	Data collection for online surveys.
	Survey Monkey [137]	feature list	Data collection for online surveys.
	Google Forms [138]		Data collection for online surveys.
	Group Complete [139]	feature list	Data collection with mobile devices.
Web form development	Xforms [140]	1.1	Standard for web forms.
	Django [141]		Library for forms in Django web framework.

Table 3.1.: Selected frameworks, systems and standards for electronic data capture.

Web-form Development Frameworks for the design of forms and data capture systems provide form-specific abstractions such as question types, presentation widgets and validation constraints in the framework language with the aim to facilitate the development of form-based data capturing systems. They provide facilities for binding data entry fields to 'data-objects', such as database tables, XML or JSON. The presentation of forms relies on existing web-technologies like HTML[5] and CSS. Examples of this category include web development frameworks such as the Python-based *Django* [141], the Java-based *Spring* [143], *OpenXava* [144], *Apache Struts* [145] or commercial solutions such as *Oracle Forms* [146]. *XForms* [140] and *InfoPath* [147] follow a document-centric approach based on XML technologies. Both use XPath to bind data from form controls, such as a 'text entry field', into an explicitly provided instance of XML. An XML schema of the instance model enables *XForms* to perform basic validation of data and to provide appropriate form controls corresponding to the data type.

All these technologies are targeted at programmers and system designers involved in the implementation of data capturing systems. In order to be used by domain experts, these systems need to afford a higher level of abstraction.

Survey Tools A large variety of – frequently web-based – data collection frameworks aims to provide easy-to-configure tools for the creation of customised data collection services. These frameworks use internal form metamodels to guide the creation of forms, and to store and exchange form specifications across instances of the framework. Examples include general-purpose 'survey' tools, such as *Google Forms* [138], *Survey Monkey* [137], *Lime Survey* [136], *Survey Gizmo* [135], *Group Complete* [139]. They provide functionality to define and manage online questionnaires, oversee the data collection process and frequently also allow for statistical analysis of the resulting responses to different degrees

[5] *HTML* itself (in current version 5 [142] or earlier) is not included in this review because it is mainly concerned with presentational aspects of forms.

of sophistication. In most of the reviewed cases, the underlying form metamodel was not directly accessible, so that its characteristics could not always be separated from features of the application framework.

Domain-specific Data Capture Tools: Clinical Study Management Systems Besides the previous general purpose systems, domain-specific tools support data capture and management in particular domains. Examples for the domain of clinical research data capture include the open source software for web-based clinical trial support *OpenClinica* [131] and the *REDCap* [148] study management system [132]. These systems use form metamodels for specification and subsequent generation and deployment of data input forms. In both systems, these are based on spreadsheets with entries in different columns representing question text, answer range, value constraints and navigation rules. This approach offers a straight-forward solution for the specification of forms and their interchange across instances of the same study management framework.

The UK CancerGrid [123] project and the US NCI caBIG [113], focus on the re-use of common data elements for bio-medical studies to promote data interoperability across studies. Both use form models for the generation of electronic CRFs.

Questionnaire Interchange Standards *queXML* [129] provides an XML-schema based model for the design and interchange of questionnaires. *eDCI* [130] represents a former development of an Health Level 7 (HL7) message specification for transmitting definitions of data collection instruments. It aims to be closely aligned to the Clinical Data Standards Consortium's Operational Data Model (CDISC-ODM).

Data Interchange Standards Data interchange standards, such as the CDISC-ODM [127] for medical study data, or the Data Documentation Initiative (DDI) [128] for archiving social science data [149], contain form metamodels for the purpose of documentation and interchange of study data and metadata.

A detailed overview of the form-related characteristics of these selected tools and standards is provided in the following sections.

3.3.1.2. Identification and Logical Structure

The reviewed tools and standards cover different scopes, from a single form or questionnaire to whole studies, comprising multiple data capture instruments (e.g. *CDISC-ODM* or *DDI*). Abstractions related to aspects of *identification and logical structure* of forms are summarised in Table 3.2.

Structure hierarchy defines the logical structure of the data capture process supported by the respective metamodel. Most metamodels differentiate three distinct hierarchy levels, corresponding to an entire *form*, a *group* of questions and a single *question*. Every model structure must be uniquely identifiable within the structure hierarchy of the model. In most cases, the identifier is part of the form metamodel. The *identifier scope*, within which an identifier must be unique, therefore corresponds to the highest level 'container' for model structures. Changes to form components may be traced by

Name	Structure hierarchy	Identifier scope	Versioning	Repeat	Annotation	Reuse
CDISC ODM	Study, StudyEvent, Form, ItemGroup, Item	ODM file (multiple studies)	at Study level	✔	–	n.a.
DDI	StudyUnit, DataCollection, QuestionScheme, MultipleQuestionItem, QuestionItem	StudyUnit	at every level	–	✔	n.a.
queXML	Questionnaire, Section, Question, SubQuestion	Questionnaire	–	–	–	n.a.
eDCI	Instrument, Section, Group, Item	DciDefinition, Instrument	–	✔	✔	n.a.
openClinica	CRF, Section (subsection), Group, Item	Form[a]/ Study[b]	at CRF level	✔	–	✔ [d](also CDISC-ODM)
RedCAP	Form, Section, Question	Form	–	–	–	✔ [d]
CancerGrid	Form, FormModel, Control (Section, Table), Variable	Form	all levels[c]	✔	–	✔ [d]
caBIG Form Builder	Module, CDE	NCI caDSR	all levels[c]	–	–	✔ [d, e]
SPSS Data Collection	Survey, QuestionGroup, Item	?	?	?	?	?
Survey Gizmo	Survey, Section(?), question	Survey	–	?	–	✔ [e]
Lime Survey	Survey, QuestionGroup, Question	Survey	–	–	–	✔ [d](also queXML)
Survey Monkey	Survey, Page, Question	Survey	–	–	–	✔ [e]
Google Forms	Form, SectionHeader, Question	Form	–	–	–	?
Group Complete	Form, Group, Question	Form	–	✔	–	?
Xforms	model, instances; controls: container (group, switch, repeat), input	Form	–	✔	–	–
Django	Form, field	?	–	–	–	–

[a] In form metamodel.
[b] In application framework.
[c] External as administered item in metadata registry.
[d] Import and export of form definitions in propriatory standard.
[e] Question library.

Table 3.2.: Identification and logical structure.
Non-existing features are marked '-', '?' indicates missing information.

versioning attributes on some level of the model hierarchy, as in *OpenClinica*, *CDISC-ODM*, or *DDI*. *CancerGrid* or *caBIG* use an external metadata registry for the versioning of form artifacts.

Structure annotation denotes a facility for linking information to form structures. Such information may help guiding the interpretation of data collected against a given structure. Examples of such links are internal links across structures, external links to concepts in an ontology that could serve for structure classification, or links to audio-visual information clarifying the structure's data capture intent. Only *DDI* and *eDCI* provide a mechanism for similar functionality as part of their form metamodel.

Form structures may be *reused* by means of an import/export functionality for form model serialisations from application frameworks or by an online question library. Such reuse is typically limited to other instances of the same software or framework and to either full forms or single question items. Sharing of form fragments, such as a single form section is possible in the NCI Form Builder, but is uncommon otherwise.

Some structures may be identified as *repeating*, thus providing information about the appropriate presentation of the structure and its behaviour in a data capturing workflow.

3.3.1.3. Entry Constraints

Entry constraints imposed as validation rules on the level of the data collection instrument can guide user interaction and can increase data accuracy. In combination with a notion of submission – the possibility to 'sign-off' a completed form – such constraints become universal properties of any data set corresponding to the submitted form.

Table 3.3 compares the reviewed form systems with regard to various aspects of data entry constraints. The table adopts a wide interpretation of such constraints, including explicit 'semantic' constraints, such as a textual specification of the data that is intended to be collected, as well as constraints on the range or patterns of data values. Constraints are classified according to the structure type and the data component to which they can be bound. The expected value domain of 'simple structures', such as 'fields', that record the response to single questions, is typically defined in terms of a *data type*, such as `string` or `boolean`, possibly extended by an *unit*, or in terms of an *enumeration*. This information is used for input validation and to guide the presentation of the structure, i.e. for rendering an appropriate data input field. Further constraints on the field level comprise *range* checks for numeric value domains, or pattern checks via *regular expressions* for string-based value domains, respectively. Enumerated value domains can be constrained by the number of selectable alternatives (*selection multiplicity*) and possibly by the specification of a single *exclusive response*.

Many tools define 'question type' as abstraction that combines implicit information about the value domain and data entry constraints, such as 'single-select' field, as well as about the presentation of the form control, such as 'slider widget' for selecting numeric value from a constrained value domain, see Section 3.3.1.4.

The values entered against different data components on the form – the answers to different questions – may be related. *Functional constraints* across the values of data components can express these relations. For example, consistency may be required between the response to an 'age' question and the time difference between the person's year of birth and the date of form completion. Information given in previous questions

Name	Question / Field						across Fields		Structures				
	Data type	**Enumeration**	**Unit**	**Range** (numeric)	**Selection multiplicity** (enumerated)	**Exclusive response** (enumerated)	**Regular expression** (text)	**Prepopulation** (fixed/function)	**Functional**	**Mandatory**	**Text. definition**	**Multilanguage support**	**Generic expression language**	**Exception handling**
CDISC ODM	✓	✓	✓	✓	?	–	expr.l.	✓/?	expr.l.	✓	✓	✓	✓	✓
DDI	✓	✓	–	✓	–	–	✓	?/?	?	–	✓	✓	?	–
queXML	✓ [a]	✓ [a]	–	✓	–	–	–	–	–	–	✓	–	–	–
eDCI	✓	✓	–	✓	–	–	?	–	?	✓	✓	✓	?	✓
openClinica	✓	✓	✓	✓	–	–	✓	✓/?	?	✓	✓	–	✓	✓
RedCAP	?	✓	–	–	–	–	–	–	–	✓	✓	–	?	–
CancerGrid	✓	✓	✓	–	–	–	–	–	–	–	✓	?	–	–
caBIG Form Builder	✓	✓	✓	–	–	–	–	✓/–	–	✓	✓	?	–	–
SPSS Data Collection	✓ [b]	✓	–	?	✓ [b]	✓	?	✓/?	?	?	✓	✓	✓	✓
Survey Gizmo	✓ [b]	✓	–	?	✓ [b]	?	✓	✓/?	?	✓	✓	?	✓	✓
Lime Survey	✓ [b]	✓	–	✓	✓	✓	✓	✓/✓	✓	✓	✓	✓	✓	–
Survey Monkey	✓ [b]	✓	–	–	–	–	–	?	?	✓	✓	✓	?	✓
Google Forms	✓ [b]	✓	–	–	–	–	–	–	–	✓	✓	–	–	–
Group Complete	✓ [b]	✓	–	?	?	?	✓	✓/?	?	✓	✓	✓	✓	?
Xforms	✓	✓	–	Xpath	Xpath	Xpath	Xpath	✓/✓	✓	✓	✓	–	✓	✓
Django	✓ [b]	✓	–	expr.l.	expr.l.	expr.l.	expr.l.	✓/?	expr.l.	✓	✓	?	✓	✓

[a] Free or fixed response with analogue or discrete scale.
[b] Specification of 'question type', e.g. text field, multiline text field, numeric, single-select, multi-select etc.

Table 3.3.: Data Constraints
Non-existing features are marked '-', '?' indicates missing information.

or from external sources may also be used to *pre-populate* data components. Once the 'date of birth' of a person is known, there is no need to prompt for the person's 'age at form completion'.

Some entry constraints or validation rules are not restricted to simple data components. Constraints referring to the existence or the intended meaning of a form structure can be applied to all structure types: Data components may be *mandatory* or optional and their intended meaning and semantic answer domain may be specified by a *textual definition*. It is often possible to impose further constraints by means of a *generic expression language* which provides access to a structure's data component and to comparison operators. In order to maximise completeness and correctness of collected data, the form user must be notified if validation fails. Many tools provide mechanisms for *exception handling*, allowing the specification of notification messages to guide user interaction.

3.3.1.4. Process and Presentation Constraints

The responses to questions and thus the interpretation of the data collected by a form may be influenced by the presentation of the form and – conversely – the presentation of a form may have great impact on its usability and the quality of the data that it will collect. Table 3.4 summarises aspects of *process and presentation constraints* that may affect the behaviour and appearance of a form.

Form-based data capture always assumes data to be collected in a certain order, usually given by the order in which questions appear on the form. Additional 'routing logic' is required to guide the user through the questionnaire and to prevent the collection of unnecessary or contradicting data. Such *control flow* statements are typically expressed either as 'skip-logic', rendering a specific element irrelevant subject to a boolean condition, or as 'go-to' statements, directing the user to another form element. By deactivating form components that have been rendered irrelevant by earlier answers, the control flow has direct implications on the presentation of data collection instruments. Furthermore, it affects validation logic, since deactivated form components must not contribute to a form's validation behaviour.

Question piping is a specific kind of presentation logic, found among survey tools. It allows the modification of question text subject to previous user responses.

Submission of a form or of parts of a form represents a special event in the data capturing process: By submitting a form, the submitter confirms the correctness of the answers given. Any data constraints imposed as 'guards' on the submission process become data properties in case of successful submission. Some form systems allow 'behaviours' to be associated with the submission of a form (*submission settings*), such as the possibility to review the data entered, or to specify whether data constraints should be enacted as hard constraints (*guards*), denying submission in case of failure, or as soft constraints, informing the user about invalid data entries but accepting submission.

The *order of questions* on the form is typically specified in the form definition: explicitly by numbering form structures or by the order in which form elements appear in the form definition. Most survey tools also allow for *randomisation of question order*, some also for randomisation of response options in enumerated value domains.

Several systems allow the definition of additional text fields for user guidance, placed before or after an structure input field (*pre/after text*).

	Logic		Submission	Presentation					
Name	**control flow**	**piping**	**settings**	**question order**	**order randomisation**	**pre text / after text**	**simple structure rendering**	**composed structure rendering**	**other formatting**
CDISC ODM	skip	–	–	explicit	?	–	n.a.	–	–
DDI	–	–	–	?	–	?	n.a.	–	–
queXML	go-to	–	–	–	–	–	response type	–	rotate matrix, position of directives, indenting of directives
eDCI	go-to	–	–	explicit	–	–	–	–	–
openClinica	?	–	–	explicit	–	✔	response type	–	column number, response layout (vertical, horizontal), width
RedCAP	skip	–	–	?	–	–	response type	–	–
CancerGrid	go-to	–	–	from order	–	–	–	–	–
caBIG Form Builder	–	–	–	from order	–	–	–	–	–
SPSS Data Collection Author Professional	go-to	✔	?	?	✔ [a, b]	– [c]	question type	✔	html formatting of questions and responses
Survey Gizmo	skip, go-to	✔	?	from order	✔ [a, b]	?	question type	✔ [d]	text formatting, orientation of labels and options, remove question numbers, branding features
Lime Survey	skip	✔	✔	from order	✔ [b]	✔	question type	✔ [d]	hide hints, css styles
Survey Monkey	skip	✔	–	from order	✔ [a, b]	– [c]	question type	✔ [d]	size and placement options for question elements, themes
Google Forms	–	–	–	–	–	–	question type	–	–
Group Complete	?	?	?	?	–	?	question type	–	?
Xforms 1.1	skip	–	✔	–	–	–	field type & data type	–	css stylesheet
Django	–	–	✔	–	–	–	field types & widget	–	html, css

[a] Randomisation of question order.
[b] Randomisation of response options from enumerated value domain.
[c] No dedicated abstractions but possible via html or other formatting.
[d] Special composed structure 'question types', such as 'other... please specify', tables, matrix, dual scale.

Table 3.4.: Process and Presentation Constraints.
Non-existing features are marked '-', '?' indicates missing information.

Correct *rendering* of *simple structures* in a way to support the data collection intent of the respective form control is usually determined by predefined 'question type', such as 'checkbox', 'radio', 'multi-select', etc. in the case of *OpenClinica*. If no 'question type' abstraction is available, suitable rendering may be inferred from the data type.

In addition to presentation information for simple structures, most survey tools provide 'question types' corresponding to *composed structures*. These imply specific control flow and validation logic, as well as control rendering: For example an enumerated value domain may be extended by an answer 'other...please specify:' together with an additional free-text entry field, or multiple questions that share the same simple response type may be rendered as matrices.

3.3.1.5. Summary

The foregoing review indicates various differences in form metamodels, depending on their application domain and their role in data capture processes.

Frameworks for web-form development provide abstractions required for the graphical presentation of forms, means for binding data-objects to form controls, and for imposing constraints on data input via a framework specific expression language. The possibility to exchange form specifications among these tools is limited due to differences in form conceptualisations, serialisation and the tight coupling of form elements to 'data-objects'. Facilities for coordinating interoperable data collection such as shared data element definitions are beyond the scope of these standards.

General purpose survey tools provide a range of pre-defined question types to ease creation of complex survey questions. They do not support versioning of form structures, nor are form specifications portable across applications - with the exception of the open-source tool *Lime Survey* that allows the export of form descriptions in the *queXml* standard. None of the systems in this category supports shared data semantics in the form of shareable CDEs.

Frameworks for clinical data capture provide specification templates for structure and presentation of forms, supporting simple data constraints and control flow as the basis for form generation and deployment. However, none of them is suited for expressing all data and process constraints that can be imposed by the corresponding software framework. While its form models cannot directly be re-used in other study management systems, *OpenClinica* allows the export of study data in the CDISC-ODM [127] standard. Despite the efforts of the clinical informatics community to achieve interoperability by harmonising clinical reporting through shared CDEs, the form metamodels of these study management frameworks do not support unique global identifiers, nor references to external standards that would permit creating such links. *CancerGrid* and *caBIG Forms Builder* on the other hand allow for the description of a form as a collection of CDEs. However, both models provide only little process and presentation information and do not allow consistency constraints to be specified. As a consequence, these form models are not suited for documenting the results of more complex data capture processes. Instead, documentation of data capture instruments and collected data is attempted by using separate standards.

Standards for documentation and exchange of study data and metadata are well-suited to express form structure and content, as well as the role of a form within a study. They

support unique identifiers within the scope of an Operational Data Model (ODM) or DDI file, as well as the versioning of study artifacts. Since they are focused on the post-hoc documentation of forms, they lack features required for the generation of complex data capturing forms and their retrospective interpretation.

Clearly, the use of separate standards for generation of data capture artifacts and the documentation of the collected data is disadvantageous: For researchers, detailed documentation of their study data represents additional workload from which they are unlikely to draw direct benefits for their own work. Further, manual post-hoc documentation is error-prone and likely to be inaccurate.

Using a single model for the generation of study artifacts as well as their documentation constitutes a more reliable approach: Since documentation does not require additional manual intervention, accurate description of the actual data capture instrument is ensured. This lack of a comprehensive standard for 'forms' is addressed in Chapter 4 by developing a metamodel for data capture forms.

3.3.2. Secondary Analysis Processes

As indicated in Fig. 3.4, secondary analysis processes play an important role in the evidence creation process. This section focuses on the role of decision-analytic modelling for health-economic assessments of new medical technologies, Section 3.3.2.1. Section 3.3.2.2 provides the necessary background information about Markov models for the development of suitable metamodels in Chapter 4.

3.3.2.1. Decision Analytic Models for Economic Analyses in Health Care

A brief overview of common modelling techniques for the economic evaluation of health technologies is given in the following. Further details can be found in [150, 151].

All relevant modelling techniques represent the natural history of a disease, common treatment interventions and their effects as 'health-states' or decision nodes. They can be characterised along multiple dimensions, such as *a*) the object to be modelled (*cohort* versus *individual*), *b*) whether interaction between objects is allowed, *c*) the treatment of time (untimed versus timed, discrete versus continuous time), and the *d*) evaluation method (*deterministic* versus *stochastic*).

'Cohort models' account for different population attributes, such as different ages, disease stages, or other risk factors, by creating a dedicated 'health-state' for any relevant combination of those factors. This causes the dimensionality of the simulation to rise exponentially with the number of relevant attribute combinations. 'Individual-level' simulations overcome this problem. Fixed values are used as model parameters in 'deterministic' evaluation, yielding an average population estimate. For the 'stochastic evaluation' of models, values are drawn from the distributions that describe the input parameters so that the variability of simulation outcomes can be assessed.

The choice of the most suitable modelling approach for a given health economic evaluation depends on the disease to be modelled, the relationship between input parameters, the output measures required by the decision maker, as well as practical considerations, such as the availability of data [150]. An algorithm for making this choice is proposed in [151].

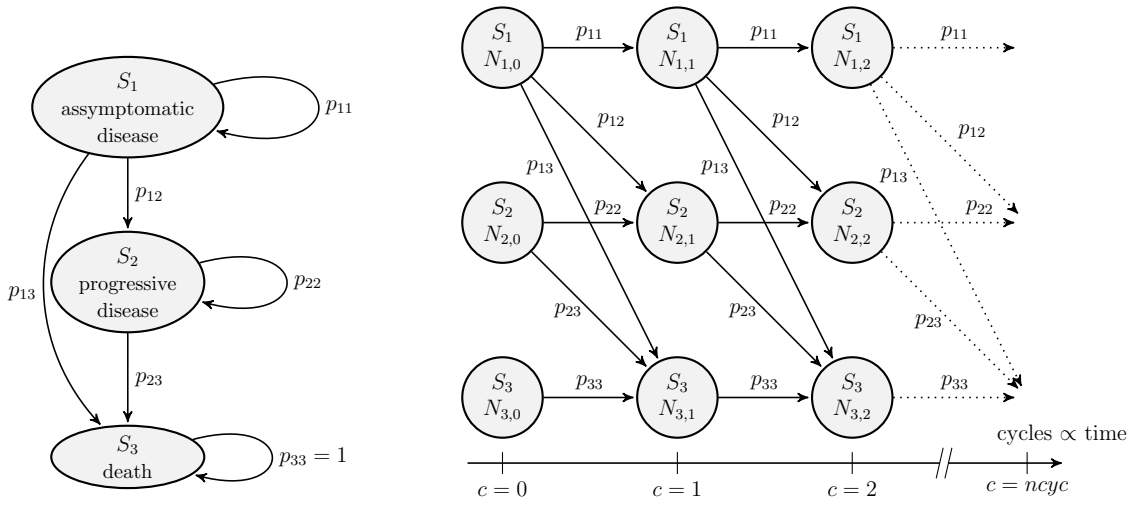

(a) Markov model structure, example adapted from [153].

(b) Evolution of state occupation $N_i(t)$ in discrete time steps ('Markov cycles').

Figure 3.6.: Markov model structure with 'health states' S_i and transition probabilities p_{ij} (a), and its time evolution (b).

Decision trees and *state transition models* are well-suited model structures when only a small number of population attributes needs to be considered and no interactions between members of this population are required. Decision tree models represent alternatives as chance nodes in a tree like structure. Any path through the decision tree represents one possible sequence of events. However, recurring events are not easily represented in decision trees. In such cases, state transition models, such as Markov models, provide a more efficient representation.

3.3.2.2. Markov Models

The main characteristics of Markov models and cohort-based Markov model simulations are summarised in this section, in preparation for the development of a suitable metamodel in Section 4.2.1. More detailed introductions to Markov models and their use for health-economic assessment can be found in the literature, for example in [152, 153].

Markov models are often used to describe the disease progress of chronic diseases. The natural history of the disease is represented by a finite number of discrete and mutually exclusive health states that are connected by transitions, corresponding to clinically important events. Figure 3.6a shows a simple Markov model with three states S_1, S_2 and S_3, representing different disease stages. Transitions from state S_i into state S_j are indicated by arrows and may occur with transition probability p_{ij}.

Depending on the modelled disease, some transitions may not be possible. For instance, after having entered the 'progressive disease' state S_2 in example Fig. 3.6a, a patient cannot return to the 'asymptomatic disease' state S_1, $p_{21} = 0$. States that only allow transitions to themselves, such as the 'death' state in Fig. 3.6a with $p_{33} = 1$, are called 'absorbing states'.

Most Markov models are discrete-time models, in which transition probabilities are evaluated in fixed time intervals, so-called 'Markov cycles'. The length of the cycle time

Δt has to be chosen to represent clinically meaningful time intervals. At the end of each cycle, transition probabilities are applied to the population of each state and transitions may occur.

As a result of these transitions, the state occupation $N_{i,cyc}$, that is the number of persons or the cohort proportion occupying a state S_i at some cycle *cyc*, changes from cycle to cycle, Fig. 3.6b. A Markov model simulation terminates either after a fixed number of cycles or when a termination condition is fulfilled, for example when the whole simulation population is found in the absorbing state.

In health economic evaluations, 'outcome' measures, typically 'cost' and 'utility', are associated to states and transitions in order to account for resource use over the course of a treatment and the gain or loss of overall life-time, or of life-quality as perceived by the patient. The outcomes of a particular treatment strategy can then be estimated by following the course of a fictitious patient cohort through the model.

Two different types of Markov models are distinguished by the form of their transition probabilities [153]: In *Markov-chain models*, transition probabilities between states are constant over time. These models can be evaluated using matrix algebra. The assumption of constant transition probabilities, however, is often too restrictive for health care related models. For example, the all-cause-mortality is known to be best described by an exponential age dependency. So-called *Semi-Markov models* allow for this time dependency to be taken into account by updating the transition matrix in every cycle. Most Markov models employed in health care economics are of this type [151].

Markov processes satisfy the 'Markov property' which requires the future state of the system to exclusively depend on its current state, not on its past. The probability for a transition between two states must therefore be independent of the states that a certain part of the patient population has experienced in previous cycles. This restriction does not reflect medical reality where those dependencies do exist, for example in the form of short deterministic disease episodes after the occurrence of a certain clinical event. 'Transient states', states that may only be occupied during one single cycle, and sequences of transient states, so-called 'tunnel states', represent common workarounds to these limitations.

Health-economic assessments are typically implemented in, often proprietary, special purpose software packages, spread-sheeting applications, or high-level programming languages [150, online companion]. Despite the extensive body of literature on the use of Markov models for decision-analytic modelling in health care, no common standard for the exchange of modelling assumptions exists. Such metamodels are developed in Chapter 4.

4. Metamodels for Clinical Data Capture and Analysis

Informed by the review of relevant concepts, existing systems and standards for clinical data capture and analysis in Section 3.3, suitable metamodels are proposed in this chapter. First, a metamodel for Data Capture Instrument is developed in Section 4.1. Section 4.2 then defines a metamodel for Markov model-based simulations that form part of a specific type of secondary analysis processes. A methodology for the usage of these metamodels within the proposed information architecture, Chapter 3, is introduced in Section 4.3. Section 4.4 concludes on the suitability of the developed metamodels to support evidence creation processes in this architecture.

4.1. Metamodel for Form-based Data Capture

The development of a form metamodel (a Platform Independent Model (PIM) for forms) is motivated by the advantages of Model-Driven Architecture (MDA), Section 3.1.4, such as the possibility to derive generators into multiple target platforms: Data capture instruments as well as documentation can be directly generated from form specifications, instances of a form metamodel. Furthermore, a well-designed formal specification of forms can help increase the level of interoperability in distributed data capture scenarios: By supporting reuse of reporting fragments and by providing means for the coordination of data capture, it facilitates the collection of commensurate data-sets.

Section 4.1.1 summarises properties of the metamodel that are required to fulfill these needs. The *Forms-Metamodel* developed in Section 4.1.2 is optimised towards the modular design of forms from shareable and reusable components. It specifies the properties of these components, such as textual information, response types and constraints, and allows some of those to be further constrained or augmented in the context of larger data capture fragments. The data collected against a form component are characterised by the component's (composite) response type, defined by composition rules and constraints among its substructures. Section 4.1.3 and 4.1.4 discuss behavioural aspects of the Forms-Metamodel, as well as the composition of its components. Its suitability to support general form design is demonstrated in Section 4.1.5 by comparison to an existing data capture framework [131] and to ISO/IEC 19763-13:2013 [95], a proposed standard for the registration of forms. Section 4.1.6 concludes on the developed Forms-Metamodel.

4.1.1. Requirements for Forms-Metamodel

The minimum set of features of the Forms-Metamodel is defined by the anticipated usages of form specifications, namely *a*) generation of data collection artifacts, and

b) documentation of collected data.

As identified from the metamodels review in Section 3.3, generation of data collection artifacts requires:

Form components as the structure types relevant for the design of data capture forms, such as 'field' or 'form'.

Response Types and Constraints associated to the different form components. Constraints may refer to a single form component or may involve multiple form components.

Presentation attributes defining the appearance of form components and of their (possibly constrained) response types.

Process constraints defining the order and relevance of form components.

Automatic generation of data documentation additionally requires mechanisms that provide:

Unique identification and versioning of form components and forms, permitting collected data to be traced back to the specifications employed in their collection.

Semantic definition of form components, defining their meaning through textual specifications, links to other form components or to ontology concepts. Linkage to additional metadata can clarify the 'semantic context' in which a form or form component was used and which may be important for the interpretation of the collected data.

These properties can be modelled either explicitly as part of the Forms-Metamodel or be inherited from existing standards for metadata registration, such as ISO/IEC 11179.

In order to support the collection of interoperable data from clinical studies, the Forms-Metamodel requires a *composition mechanism* that allows data capture forms to be assembled from existing form fragments. Each of those fragments may itself serve for the collection of specific, possibly compound, clinical information.

4.1.2. Forms-Metamodel - Structural Model

The metaclasses of the Forms-Metamodel are introduced in this section and listed in Table A.1 in Appendix A. Enumeration types that are not included in the following metaclass diagrams are summarised in Table A.2.

4.1.2.1. Form Element

The Forms-Metamodel distinguishes between three types of *FormElement* specialisations, all of which represent reusable components of form design, Fig. 4.1: *Structure*, *SimpleResponseType* and UnitOfMeasure. *FormElement*, and metaclasses inheriting from it, are derived from *NamedItem* and *IdentifiedItem*. Their instances are thus uniquely identifiable by their *globalID*, named (*name*) and provide a textual *definition*, as well

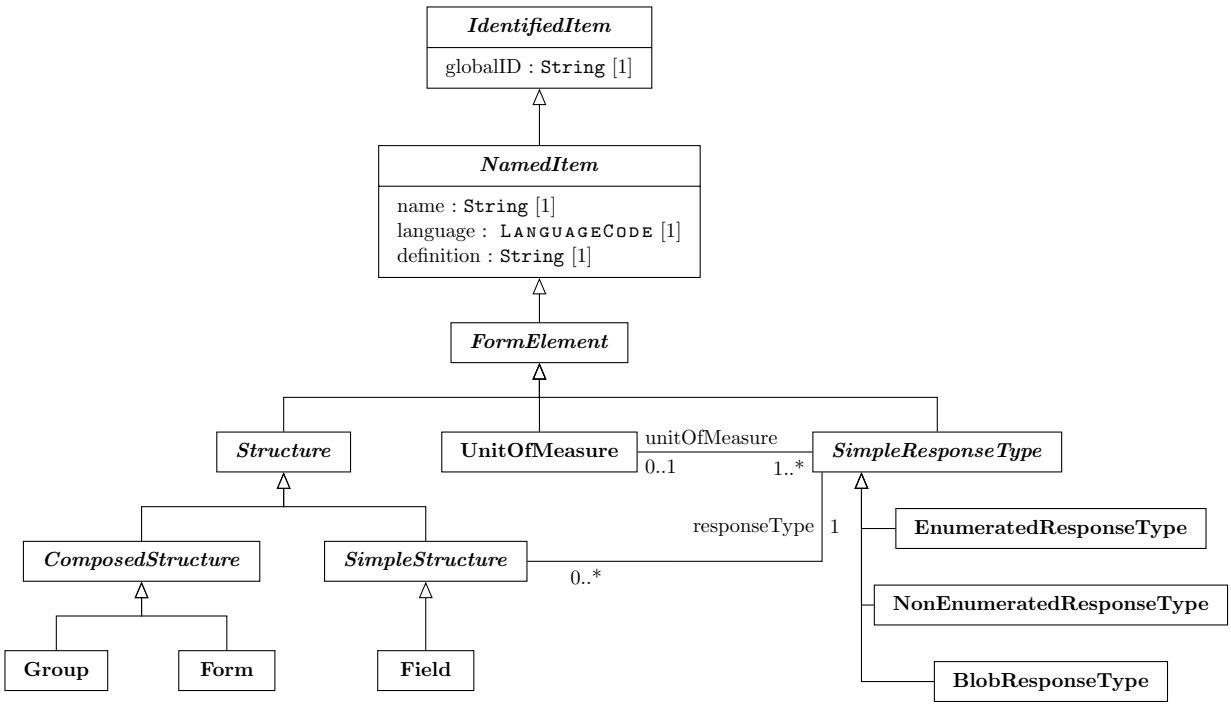

Figure 4.1.: *FormElement* metaclass, inheritance and specialisations.

as information about their *language*. Any *IdentifiedItem* may be registered and administered by a registration authority. To account for this process, *FormElement*s may inherit properties of additional derivation types, such as ISO/IEC 11179-3:2012 metaclasses *Registered_Item* (ISO/IEC 11179-3:2012, 8.1.2.1) and *Administered_Item* (ISO/IEC 11179-3:2012, 8.1.2.2). The registration authority may also provide a model for versioning that guarantees modifications of existing instances to result in the creation of new identifiers, so that modified models can be distinguished from their ancestors.

All reviewed form models feature at least three different types of form-related structures, corresponding to the 'form' itself, 'sections' on the form, and 'question fields'. The Forms-Metamodel adopts this view and defines *Structure* as the fundamental building block of forms. It classifies *Structure* into *ComposedStructure*, Group and Form, which may aggregate other *Structure* components, and into *SimpleStructure*, namely Field.

4.1.2.2. Interaction Element

Every form contains information elements, such as 'questions', 'section titles' or 'instructions' that guide users in the process of form completion. The Forms-Metamodel supports the specification of such information via its *InteractionElement* metaclass, Fig. 4.3a. It assumes that TextElement and MediaElement may be used for any information purpose depending on the requirements of the specific form specification. A 'question', for example, will typically be specified by the *text* attribute of a TextElement. However, if the form specification is intended to support data capture among illiterate participants, a graphical representation of the 'question' may be needed - and can be specified by MediaElement. In such cases, textual and other information elements (audio, figures) may be used in conjunction, in order to increase the accessibility of a form for a wider

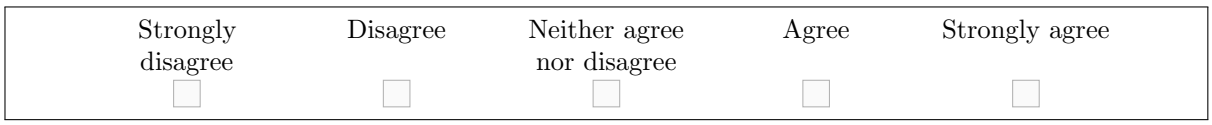

Figure 4.2.: Example of EnumeratedResponseType where order of EnumeratedResponseTypeComponents is significant, *Likert items*.

group of users, see [154] for an example from e-governement. The intended role of a MediaElement can then be documented via its *explanationText* attribute. Figure 4.5 details all possible relations between *Structure* and StructureInComposition metaclasses and *InteractionElement*.

4.1.2.3. Simple Structure and Simple Response Type

A *SimpleStructure*, a Field, corresponds to a single question for the collection of one data item. This data item is represented by a *SimpleResponseType* that characterises its properties.

The meaning of the data item collected by a single Field may be described by a Data_Element (ISO/IEC 11179-3:2012, 11.5.2.1). Its representation on a form, *SimpleResponseType*, therefore has been chosen to be closely aligned to Value_Domain (ISO/IEC 11179-3:2012, 11.3.2.5) and its Unit_Of_Measure (ISO/IEC 11179-3:2012, 11.4.3.1), Table A.3.

Three distinct kinds of *SimpleResponseType* are provided by the Forms-Metamodel: NonEnumeratedResponseType, EnumeratedResponseType, or BlobResponseType, Fig. 4.3b.

Every *SimpleResponseType* represents values of some *dataType*, as specified by Datatype (ISO/IEC 11179-3:2012, 11.3.2.9). Additionally, a UnitOfMeasure may be associated to a *SimpleResponseType* in order to further characterise its permissible values. User guidance with regard to the correct use of a given *SimpleResponseType* may be provided via optional *instruction* components.

Field elements with NonEnumeratedResponseType correspond to questions without predefined answer choices, similar to Described_Value_Domain (ISO/IEC 11179-3:2012, 11.3.2.8) for a Data_Element (ISO/IEC 11179-3:2012, 11.5.2.1).

An EnumeratedResponseType defines multiple answer choices as EnumeratedResponseTypeComponent elements. Each *component* is characterised by a *valueCode*, interpreted as being of type *dataType*, a textual *valueDefinition*, and one or more *valueDisplay* components that specify the answer choice information available for the user. In some cases, the order in which available answer choices are presented to the user is of importance. EnumeratedResponseTypes for rating, such as the *Likert items* shown in Fig. 4.2, require the order of their answer choices to be maintained. This dependency can be specified via the *ordered* attribute. EnumeratedResponseType is closely related to Enumerated_Value_Domain (ISO/IEC 11179-3:2012, 11.3.2.6) and EnumeratedResponseTypeComponent to Permissible_Value (ISO/IEC 11179-3:2012, 11.3.2.7).

A BlobResponseType expects data of binary *dataType* and of some *mimeType*, such as 'text'. It is only available for digital data collection forms.

The kind of *SimpleResponseType* and its *dataType* may inform the presentation of the

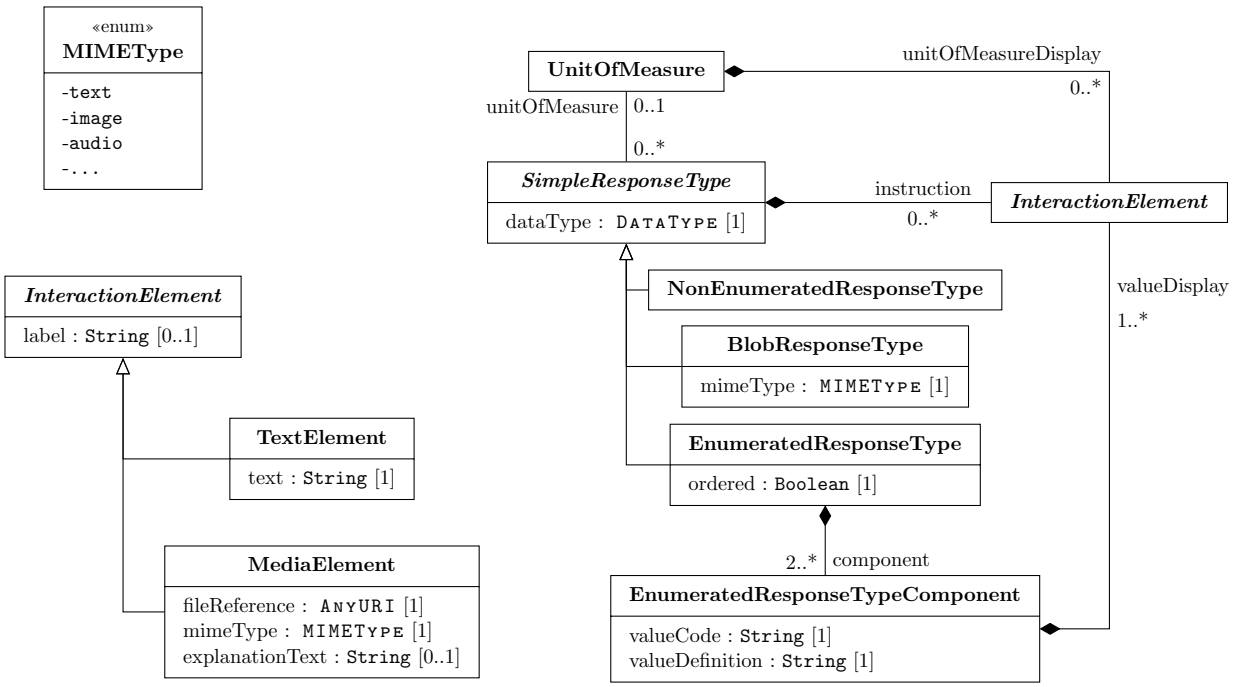

(a) Forms-Metamodel *InteractionElement*.

(b) Forms-Metamodel *SimpleResponseType*

Figure 4.3.: Forms-Metamodel metaclasses *InteractionElement* (a) and *SimpleResponseType* (b).

corresponding 'input field' on a form. For example, an instance of NonEnumeratedResponseType with *dataType* = `date` may be rendered as a date-selection field; an instance of EnumeratedResponseType may be chosen to be represented by a selection form control, such as a 'drop-down' list or 'radio-buttons'.

4.1.2.4. Composed Structure

ComposedStructure, Group and Form, may enclose multiple Field or Group components by means of a StructureComposition, Fig. 4.4a. Inclusion of a *Structure* in the context of another *Structure* adds contextual information about its usage for a specific data collection purpose. Every StructureComposition *composes* two or more *CompositionComponent*s, that is either another StructureComposition or a StructureInComposition, according to a *compositionType* indicating `SEQUENTIAL`, `PARALLEL` or `CHOICE` composition. These *compositionType*s affect completion order of the *ComposedStructure* and determine its validation logic and presentation, as will be explained in Section 4.1.4.

Figure 4.4b illustrates the nested composition of *CompositionComponent*s. Every StructureInComposition element references an existing *Structure*, a Field or Group, and represents a 'form component in context' against which data can be collected. Any existing *Structure* may be used in multiple contexts. A *ComposedStructure* thus extends the context of its enclosed StructureInComposition elements and defines the scope for their interaction. StructureInComposition elements must be uniquely identifiable within this scope via their *localID* attribute.

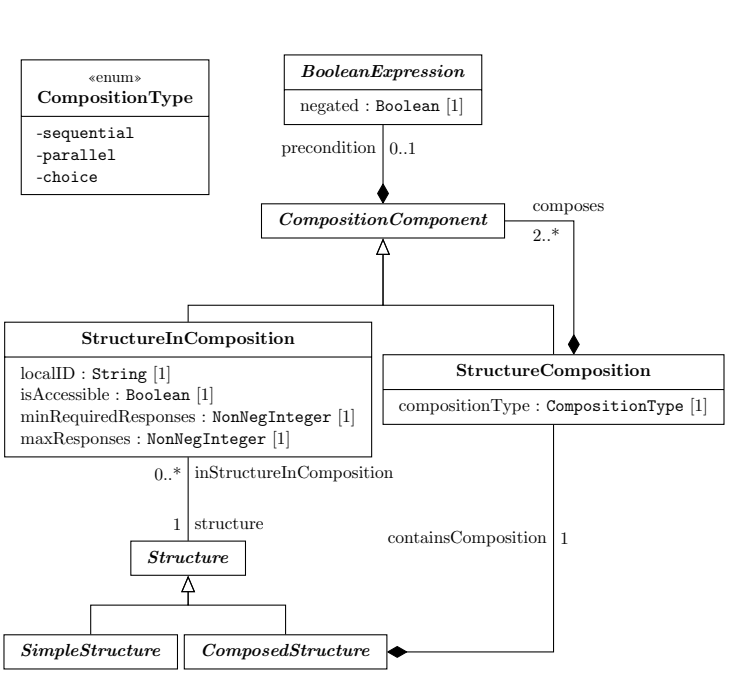

(a) Forms-Metamodel *ComposedStructure* and StructureComposition

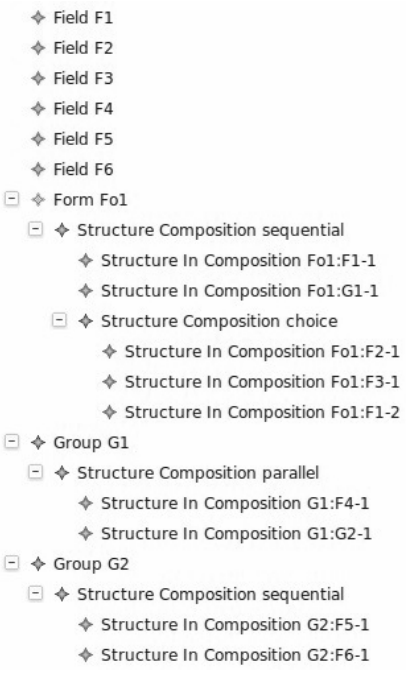

(b) StructureComposition instance.

Figure 4.4.: StructureComposition metamodel (a) and model instance (b).

When Group elements are included in another Group, such as *G2* in *G1* in Fig. 4.4b, or a Form, *G1* in *Fo1*, their *direct scope* contains ComposedStructure elements which themselves compose multiple sub-structures. The *total scope* of a ComposedStructure comprises all StructureInComposition elements (Field, Group) in its direct scope, including their substructures (in case of Group elements).

The maximum set of data items that can be collected against a *ComposedStructure* is defined by the StructureInComposition elements (Field) in its total scope.

4.1.2.5. Structure in Composition

Included as StructureInComposition elements in the context of a ComposedStructure, Field or Group structures acquire additional properties. The *localID* attribute provides an unique identification of the StructureInComposition in the direct scope of its superstructure. Their usage context may require StructureInComposition elements to be 'repeating' with a certain number of *minRequiredResponses* or *maxResponses*. Possible references to *InteractionElement* are shown in Fig. 4.5. EntryConstraint and ConsistencyConstraint, Fig. 4.6, as well as *Annotation*, Fig. 4.9, and *LocalPrepopulationAssignment*, Fig. 4.7, may be associated to StructureInComposition elements as context-dependent specifications of the referenced *Structure* elements.

A StructureInComposition element with its *isAccessible* attribute set to `false` will be hidden from the user.

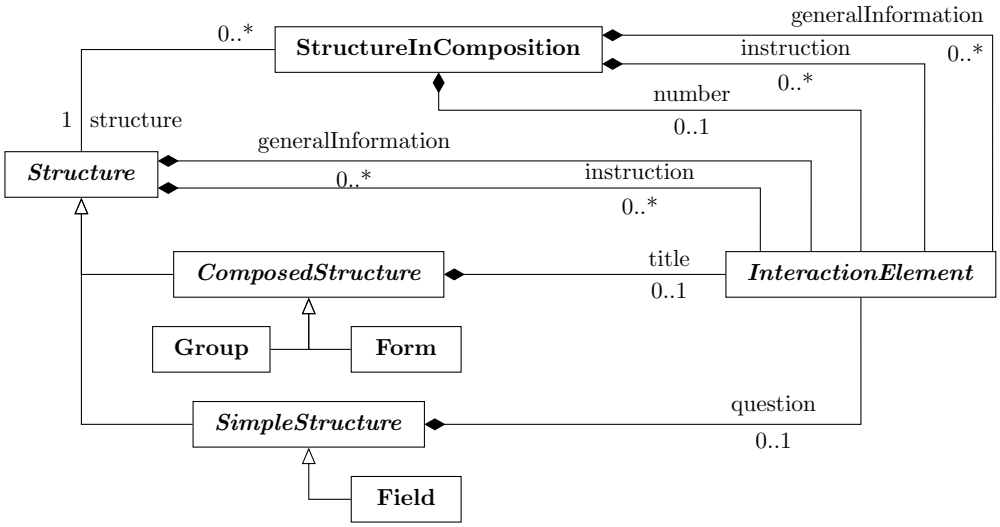

Figure 4.5.: Relations between metaclasses *Structure*, StructureInComposition and *InteractionElement*.

4.1.2.6. Constraints

Every *Structure* has a notion of 'validation', expressing whether a response is in agreement with the structure's 'response type'. The *SimpleResponseType* of SimpleStructures may additionally be refined by EntryConstraints, Fig. 4.6. Most reviewed form-related systems provide three types of constraints, either directly as constraint-abstraction in the model or through the choice of a specific form-control: ValueRangeConstraint for restricting the acceptable range of a numeric value domain, PatternConstraint for restricting data input to a well-defined string format, and SelectionMultiplicityConstraint for defining the number of items that may be selected from a discrete value domain. While ValueRangeConstraint and PatternConstraint only apply to *SimpleStructure*s with NonEnumeratedResponseType, SelectionMultiplicityConstraint only applies to EnumeratedResponseType. BlobResponseType may have a dedicated *EntryConstraint* to limit the maximum size of the data file.

Additionally, *ComposedStructure* elements may require certain constraints to hold across their included substructures. The *constraint* expression in such a ConsistencyConstraint, Fig. 4.6, is expressed by means of a *BooleanExpression* built from boolean and relational operators, numeric values and variables. A suitable expression language is introduced in Fig. 4.8.

ConsistencyConstraint and *EntryConstraint* may also be subject to another relevance condition that can be expressed through an optional *precondition* inherited from their common generalisation *Constraint* metaclass. Completion flow and structure validation resulting from these constraints are discussed in Section 4.1.3 and Section 4.1.4.

Constraints can be included at two distinct levels: directly on the respective *Structure* element, making the constraints an intrinsic property of a shareable data capture fragment, or as a context-specific modification to an existing *Structure* element within a StructureInComposition.

The Forms-Metamodel intends to restrict context-specific modifications on StructureInComposition elements to those that *narrow* the acceptable entry values within the limits

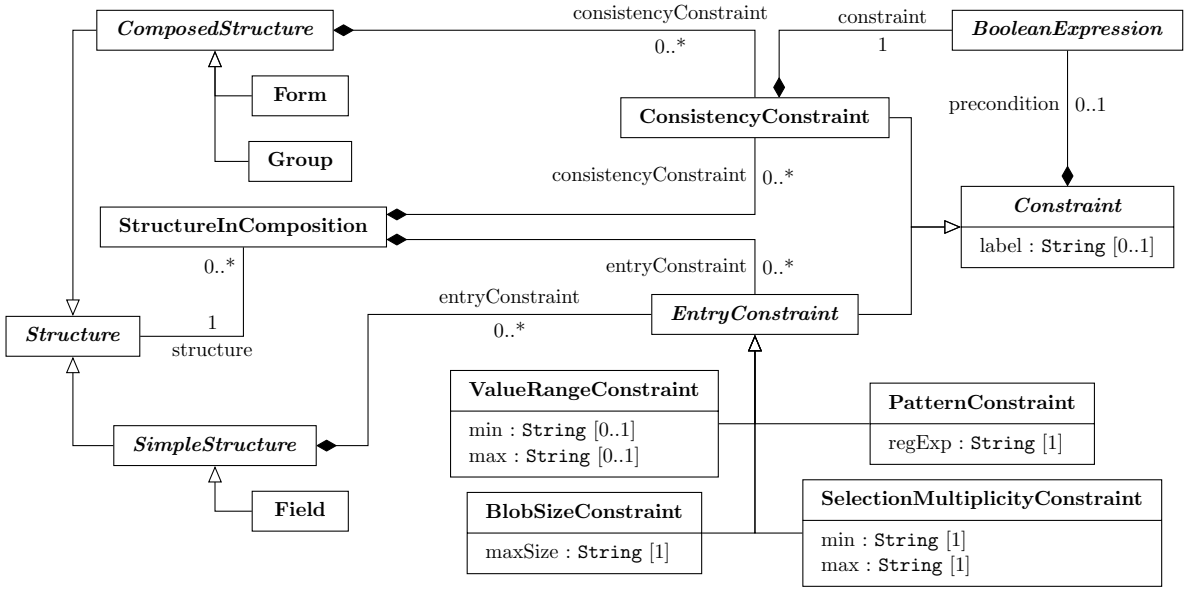

Figure 4.6.: Form Model *EntryConstraint* and *ConsistencyConstraint*

defined by the *Structure* element. For example, the permitted value range for a Field recording the *height of a person* may need to be additionally constrained for the use of this field in another context, in which data about the *height of young children* are collected.

Conflicting requirements on ValueRangeConstraint, SelectionMultiplicityConstraint and FileSizeConstraint can easily be prevented by means of additional rules on the level of StructureInComposition. For other constraints (PatternConstraint, MIMEtypeConstraint, ConsistencyConstraint), correct usage is more difficult to enforce.

4.1.2.7. Prepopulation Assignment

Within a given context, *SimpleStructure* elements may be pre-populated with default values via a *LocalPrepopulationAssignment* with the aim to increase data accuracy or to reduce the time needed for form completion. Simple default values, such as a default selection from an enumerated value domain (*no*) or a default date (*today*), as well as fields pre-populated with external information or information obtained or derived from previous data input (the *age of a person* based on the person's *date of birth* and *today's date*) are examples of pre-population.

Pre-populated values can be accepted or changed by the user, unless the required *value-Locked* attribute is set to prevent user modification. Every LocalPrepopulationAssignment refers to an *assignmentTarget* corresponding to the StructureInComposition element (Field) that is to be pre-populated. Its pre-population value is defined as *assignmentExpression*, based on the *Expression* part of the expression language, Fig. 4.8. Similar to constraints, also pre-population may be subject to a *precondition*.

LocalPrepopulationAssignment can be specified against any *ComposedStructure* or any StructureInComposition that references a *ComposedStructure*. The scope of *assignment-Target*, as well as variables involved in *precondition* and *assignmentExpression*, is limited to the scope of the *ComposedStructure* that defines the LocalPrepopulationAssignment.

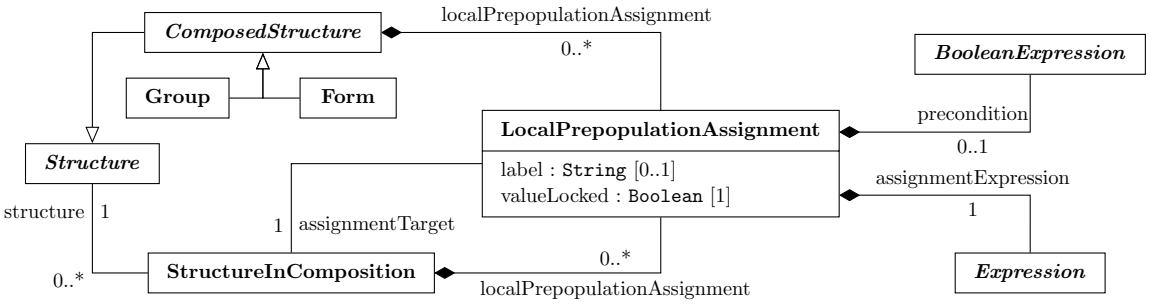

Figure 4.7.: Forms-Metamodel LocalPrepopulationAssignment

4.1.2.8. Expression Language

The Forms-Metamodel defines an expression language, Fig. 4.8, which is used in the specification of *precondition*, *constraint* and *assignmentExpression*.

A *BooleanExpression* can be constructed as BooleanCombination of other *BooleanExpression* specifications, such as SimpleBooleanExpression or Relation. Any *BooleanExpression* may be *negated*. A Relation compares two *Expression*s, *lhsExpression* and *rhsExpression*, by mathematical comparators of `ComparatorType` resulting in a boolean return value. Every *Expression* may consist of a *SimpleExpression*, such as a Constant provided at form design-time, or an ExternalValue or Variable provided at form run-time. *SimpleExpression*s can be combined in ExpressionCombinations by means of standard mathematical operators of `ExpressionCombinatorType`.

The 'value' of a Variable corresponds to the data entered against a specific StructureInComposition element during form run-time. The scope of the *structureInCompositionReference* is limited to StructureInComposition elements in the total scope of the *Structure* or StructureInComposition element that defines the *Expression*.

In order to ensure availability and unambiguousness of the Variable value at run-time, only non-repeating and mandatory ($minRequiredResponse$=$maxResponse$=1) StructureInComposition elements can be referenced. These StructureInComposition elements must refer to a Field *Structure*.

4.1.2.9. Annotation

Every *Structure* can be complemented by information about its relation to other objects via an *Annotation*, Fig. 4.9.

StructureAnnotation allows specification of the relationship to other *Structure* elements. A newly created *Structure* may, for example, use this facility to indicate that it is `derivedFrom` another *Structure*, and represents a `narrower` meaning. ExternalAnnotation allows a *Structure* to be linked to any 'external' resource by its fully qualified name; for example a concept from a published ontology may thus be associated to a *Structure*. The purpose of LocalAnnotation is to clarify the semantic relationship among substructures within the context of a *ComposedStructure*. For example, the notion that a question `depends` on another question, such as *Q2* on *Q1* in Fig. 4.10, can thus be made explicit.

The scope of *localAnnotationSubject* and *localAnnotationObject* references is limited to StructureInComposition elements within the total scope of the owning *ComposedStructure*.

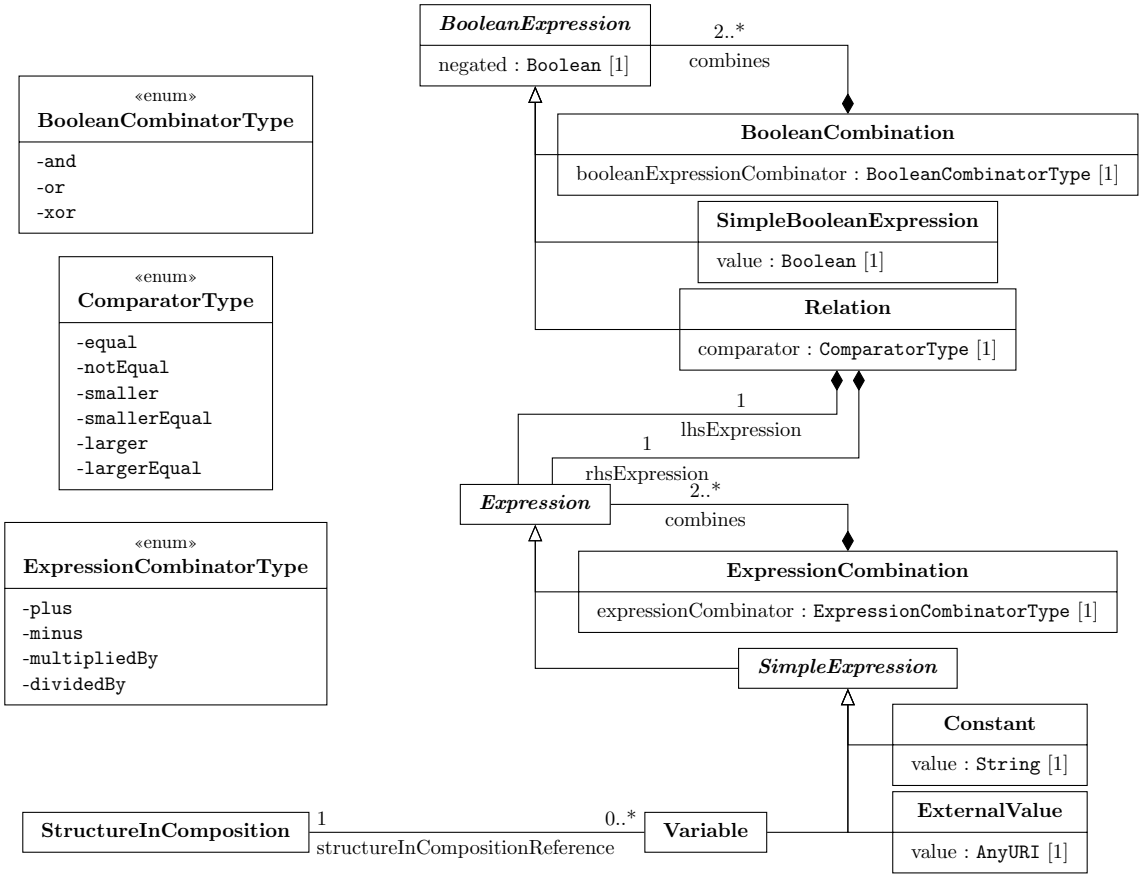

Figure 4.8.: Forms-Metamodel expression language *BooleanExpression*

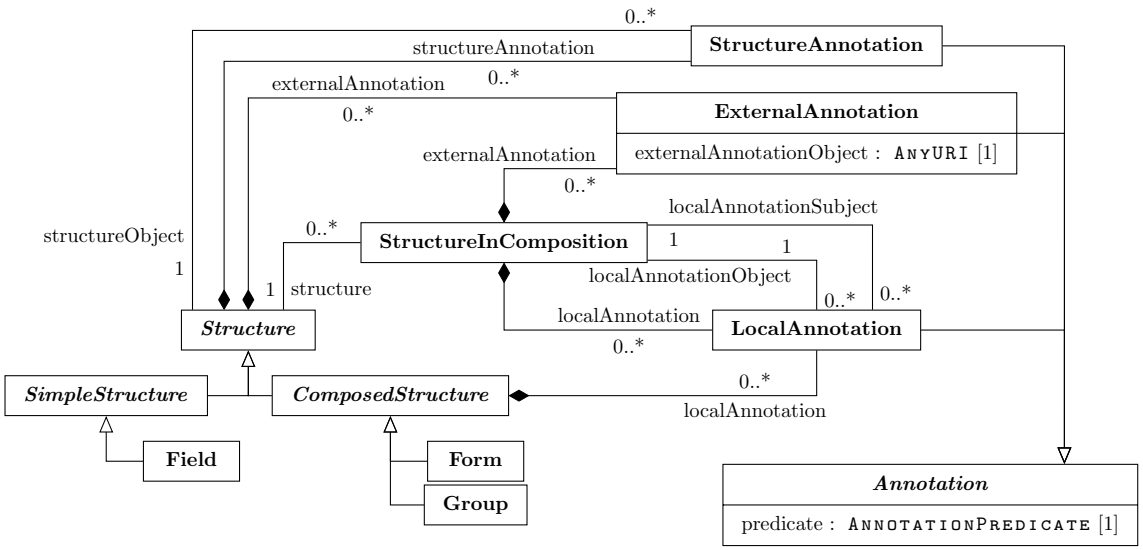

Figure 4.9.: Forms-Metamodel *Annotation* metaclass.

Figure 4.10.: The meaning of question *Q2* depends on the question text of the preceding question *Q1*.

4.1.2.10. Form Properties and Presentation

Field and Group elements are accessed and completed through a Form, Fig. 4.11, which provides the larger context for a given data capture process and allows for the collected data to be submitted. SubmissionProperties define aspects of form submission such as the level of enforcement of validation and completion constraints.

Group elements contained within the nested hierarchy of a Form may fulfill a particular structuring purpose, such as dividing the form into 'sections' and 'subsections'. In order to facilitate reuse of *Structure* components, this distinction is modelled on the Form level: LogicalHierarchy allows an *hierachyLevel* to be assigned to selected StructureInComposition elements.

Similarly, presentation aspects are modelled as properties of a Form rather than properties of its constituents in order to guarantee coherent presentation on the Form level. The Forms-Metamodel provides two mechanisms to link *Presentation* information to form components: SimplePresentation specifies the presentation of StructureInComposition elements and their 'input fields' (InputFieldPresentation), such as the *selectorType*, or the presentation of form control flow concepts ('irrelevance' and 'repeating').

Alternatively, existing 'layout' languages, such as Cascading Style Sheets (CSS), may be used in StylesheetPresentation to provide a more detailed specification of form presentation aspects.

The degree to which a specified *Presentation* can be realised, depends on the *preferredAccessMode* for which the form specification was created. For example, 'hiding' of *inactive* form components can only be accomplished in combination with `visualDigitalAccessmodeType`.

4.1.3. Forms-Metamodel - Behavioural Model

In addition to the structural properties introduced in Section 4.1.2, forms show dynamic behaviour that depends on information available at form run-time. 'Behaviour' with regard to form design comprises the accessibility of form elements and their expected completion order, as well as the validation of their corresponding data components.

Control flow specifications help designing comprehensive forms, while at the same time avoiding the collection of unnecessary data items, thus reducing the time required for form completion and improving the accuracy of the resulting data. So-called 'skip-logic' is frequently used to determine if additional questions are necessary, and 'go-to' statements may be used to instruct the user where to continue form completion, see Fig. 4.12 for an example.

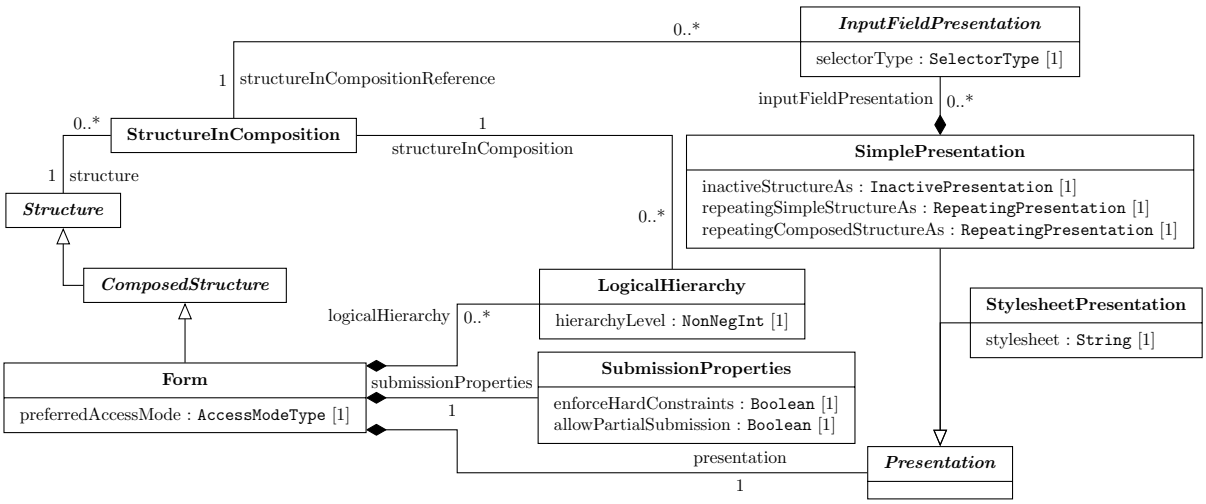

Figure 4.11.: Form Model Form metaclass.

Q1 **Do you smoke?**

☐ Yes *If 'No', please continue with*

☐ No *question Q5.*

Figure 4.12.: Simple control flow with 'go-to' statement.

The Forms-Metamodel allows such conditional relevance of form components to be expressed by an optional *precondition* for every CompositionComponent within a *Structure-Composition*, Fig. 4.4a. Every StructureComposition with its *compositionType* represents the control flow specification for a *ComposedStructure* element. Different numbers of variables - and indeed different variables - may be collected against different *realisations* of the same control flow. Each of these realisations imposes different criteria on the *completeness* and *validity* of the form and thus results in the collection of data sets with distinct properties.

The Forms-Metamodel uses three types of *states* to describe form behaviour:

Relevance state expresses whether a StructureInComposition component is considered relevant in a given data capture context. By default, all StructureInComposition elements are *active*. However, if a *precondition* is specified, the corresponding form component will remain *inactive* until the *precondition* is fulfilled.

Completeness state indicates whether an *active* form component has been *completed* as specified by its *minRequiredResponses* attribute. A composed form component is considered *completed* when all its 'relevant' components are in the *completed* state.

Validity state summarises the correctness of responses with regard to formal validation constraints, namely *SimpleResponseType*, *EntryConstraint* and ConsistencyConstraint. When an *active* form component is *completed*, it may enter the *valid* state if all such constraints are fulfilled.

Form behaviour is modelled by *hierarchical state machines* [106]. Differences between the state machines associated to *SimpleStructure*, *ComposedStructure* elements, and *StructureComposition* components are detailed in the following.

4.1.3.1. SimpleStructure State Machine

A *SimpleStructure state machine* is associated to Fields that participate as StructureInComposition elements in a StructureComposition. Figure 4.13 illustrates its state hierarchy. If the StructureInComposition *precondition* is fulfilled (or trivial), the *Structure* enters the *active* state and accepts data input. As the 'relevance' of a form component depends upon data entry into other components on the form, this initial choice needs to be re-evaluated every time the form receives data (*trgGlobalDataInput*). In its *inactive* state, the form component will show the behaviour specified in its Form *Presentation*, such as hiding the corresponding form control from the user. In its *active* state, the form component's data component might initially be *empty*. This state has to be verified upon any user interaction with the form component (*trgLocalDataInput*). Once the entered data suffices the StructureInComposition:*minRequiredResponses* constraint, the component is considered *completed*. Subject to *entryConstraint*, the component reaches either the *valid* or *invalid* state. *trgSubmit* is an external event, triggered by the user upon form submission. Depending on its current state, this event may allow a form component to reach its *final* state, which corresponds to 'valid completion' of this form component. An *inactive* form component that is not relevant to the data capturing process does not impose further validation constraints and therefore can directly progress into the *final* state. If the form component is *active*, the final state may be reached in distinct ways, depending on the setting of Form:*submissionProperties*, Table 4.1:

Case ① (SubmissionProperties:*enforceHardConstraints* = TRUE and SubmissionProperties:*allowPartialSubmission* = FALSE) represents the most stringent validation case, corresponding to the transitions indicated in Fig. 4.13. Optional form components may be left *empty*, in which case no further validation constraints apply. Once data has been entered against a form component, control completion requires this component to satisfy further validation constraints in order to progress into the *valid* state. If these are not satisfied, the component will remain in its *invalid* state.

In case ②, no completeness check occurs, but completed structures are required to fulfil validation constraints. Case ③ requires completion of all form components but not their validation. In case ④, the form can be submitted in any completion state and without fulfilling the validation constraints.

trgLocalDataInput corresponds to any user action that changes the data component of the current structure. Likewise, *trgGlobalDataInput* represents an user action that changes the data component of any of the form components on the current form. *trgSubmit* is associated to form submission by the user.

4.1.3.2. ComposedStructure State Machine

A *ComposedStructure state machine* differs from *SimpleStructure state machine* in that its successful completion depends on its substructures and their composition, as illustrated in Fig. 4.14 by an additional hierarchical *Composition state machine*. Once this state

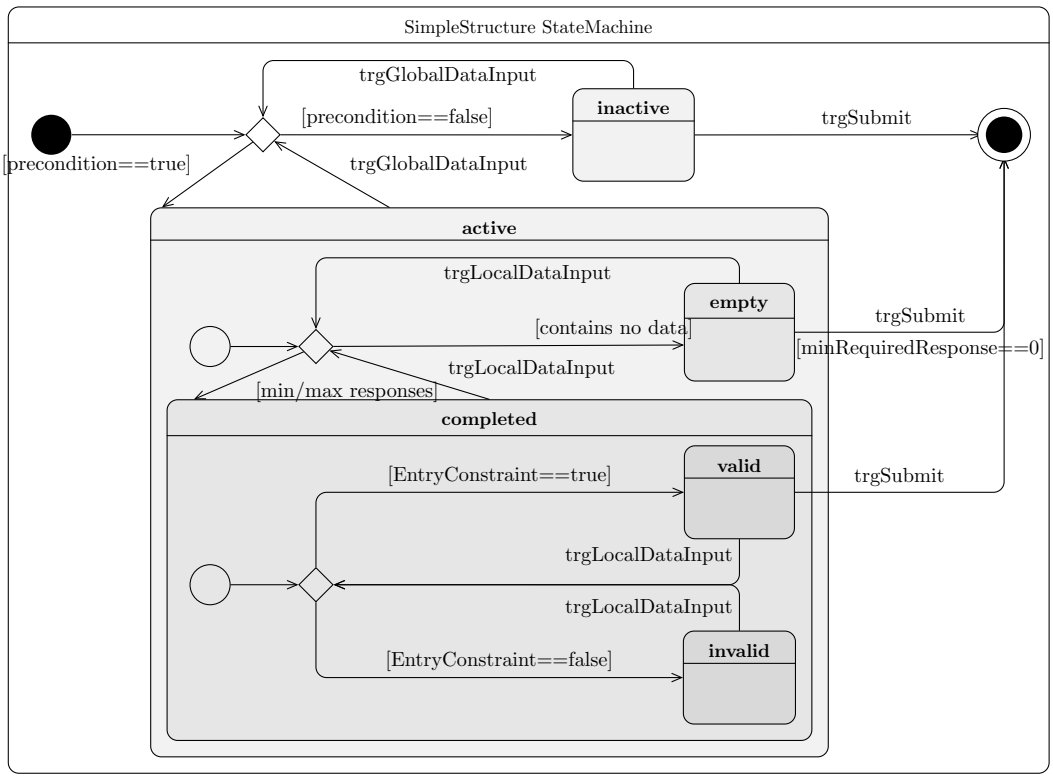

Figure 4.13.: *SimpleStructure state machine.*

machine has completed, ConsistencyConstraints across the composed substructures remain to be evaluated for the *ComposedStructure state machine* to reach its *valid* state.

4.1.3.3. Composition State Machine

Every StructureComposition represents part of a control flow and may be (de-)activated subject to a *precondition*. Its *Composition state machine* therefore distinguishes between *active* and *inactive* state, Fig. 4.15. The behaviour of the composition depends on the *compositionType* and its *CompositionComponent*s. It is modelled by a *StateMachineComposition state machine*, Fig. 4.16. Whenever the *StateMachineComposition* of an *active* StructureComposition terminates, the *Composition state machine* also terminates.

4.1.3.4. State Machine Composition

StateMachineComposition, Fig. 4.16, makes use of the transition and termination rules of state machines to model the validation behaviour of different types of StructureCompositions, Figure 4.4. The effect of different *compositionType*s on the behaviour of *ComposedStructure*s is detailed in the following Section 4.1.4.

4.1.4. Forms-Metamodel - Behavioural Composition

Assembly of forms from multiple independent data capture fragments requires the resulting composition to show well-defined behaviour that can be predicted from the

	Hard [a] **constraint**	**Partial** [b] **submission**	**Submission requirements**	**Termination transitions**
①	Y	N	*complete* & *valid*	
	SimpleStructureStateMachine			*empty* → *final* [minRequiredResponses==0] *valid* → *final*
	ComposedStructureStateMachine			*valid* → *final*
	CompositionStateMachine			*StateMachineComposition* → *final*
②	Y	Y	*valid*	
	SimpleStructureStateMachine			*empty* → *final* *valid* → *final*
	ComposedStructureStateMachine			*valid* → *final*
	CompositionStateMachine			*StateMachineComposition* → *final*
③	N	N	*complete*	
	SimpleStructureStateMachine			*empty* → *final* [minRequiredResponses == 0] *completed* → *final*
	ComposedStructureStateMachine			*CompositionStateMachine* → *final*
	CompositionStateMachine			*StateMachineComposition* → *final*
④	N	Y	–	
	SimpleStructureStateMachine			*active* → *final*
	ComposedStructureStateMachine			*active* → *final*
	CompositionStateMachine			*active* → *final*

[a] Corresponding to SubmissionProperties:*enforceHardConstraints* = TRUE / FALSE.
[b] Corresponding to SubmissionProperties:*allowPartialSubmission* = TRUE / FALSE.

Table 4.1.: Effect of Form:*submissionProperties* on completion and validation requirements for form submission is modelled via distinct sets of allowed transition into *final* state.

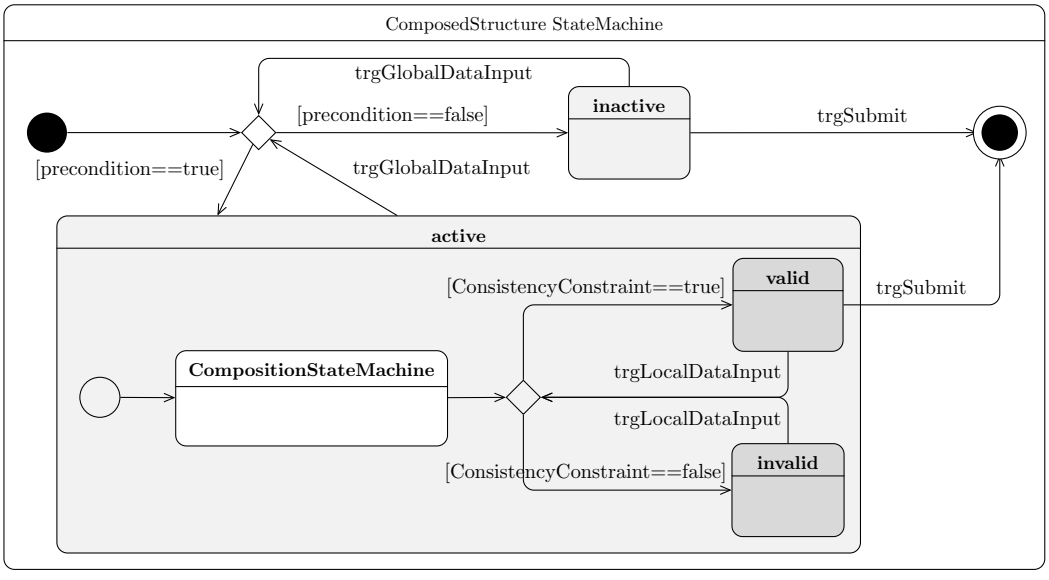

Figure 4.14.: *ComposedStructure state machine.*

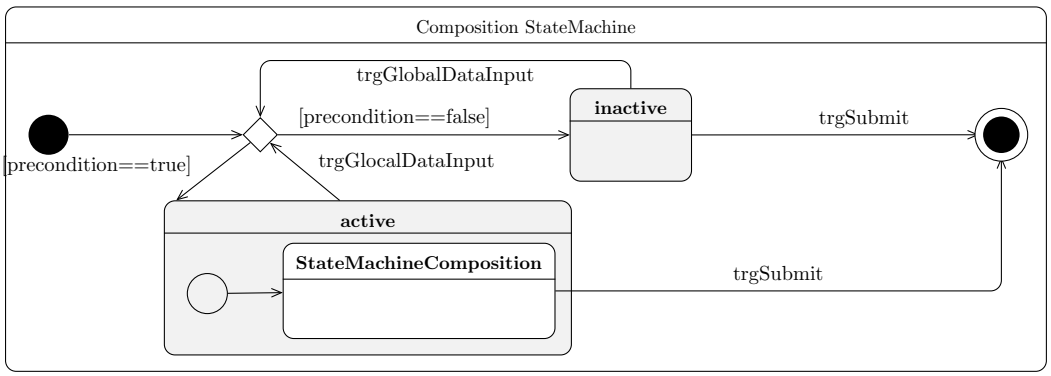

Figure 4.15.: *Composition state machine.*

properties of its components and the type of composition chosen. This section explains how the choice of *compositionType*, Fig. 4.4, influences completion order, relevance, completeness and validation of *StructureComposition*s.

Multiple *CompositionComponent*s CC can be combined to a StructureComposition of `sequential` $CC_1 ; CC_2 ; \ldots ; CC_n$, `parallel` $CC_1 \parallel CC_2 \parallel \ldots \parallel CC_n$, or `choice` $CC_1 \square CC_2 \square \ldots \square CC_n$ type. Every such StructureComposition may participate as *CompositionComponent* in another composition. If specified, the *relevance* of any *CompositionComponent* may be subject to a *precondition* g: $g(CC_0, \ldots, CC_n) \,\&\, CC$, possibly with functional dependencies on other *CompositionComponent*s $CC_0, \ldots, CC_n$. The *precondition* has the form of a BooleanExpression as specified in Fig. 4.8.

4.1.4.1. Sequential Composition

The order of elements on a form often reflects dependencies among them. Mainly three types of such dependencies can be distinguished: *a*) purely semantic dependencies, such as in example Fig. 4.10, *b*) dependencies related to a form's completion logic, such as Fig. 4.12, or *c*) functional dependencies, such as the pre-population of a form component based on prior data input. If an element provides information required by another element, it will need to be placed 'before' that element, since otherwise missing information might interrupt the form completion flow. *Sequential* composition, Fig. 4.16a, explicitly models the existence of such logical inter-dependencies among *CompositionComponent*s, as well as their completion order.

Consider the example in Fig. 4.17: The response to question *Q1* (CC_1) determines the relevance of question *Q2* ($g(CC_1) \,\&\, CC_2$). Likewise, a particular answer choice selected from the enumerated response type of *Q2* results in an additional question prompt *if 'other', please specify* ($g(CC_2) \,\&\, CC_3$).

Correct completion of this composition requires the *CompositionComponent*s to be completed in a well defined order so that all *precondition*s can be evaluated. In order to guarantee their evaluability, relevance *preconditions* specified against one of the *CompositionComponent*s must also apply to all subsequent components in the composition. In example Fig. 4.17, the relevance of CC_3 is subject to *precondition*s on both CC_1 and CC_2. The assumption of *cascading relevance* in sequential compositions facilitates

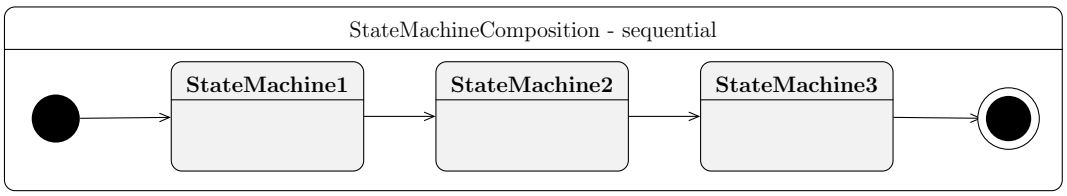

(a) SEQUENTIAL composition of *StateMachine*s.

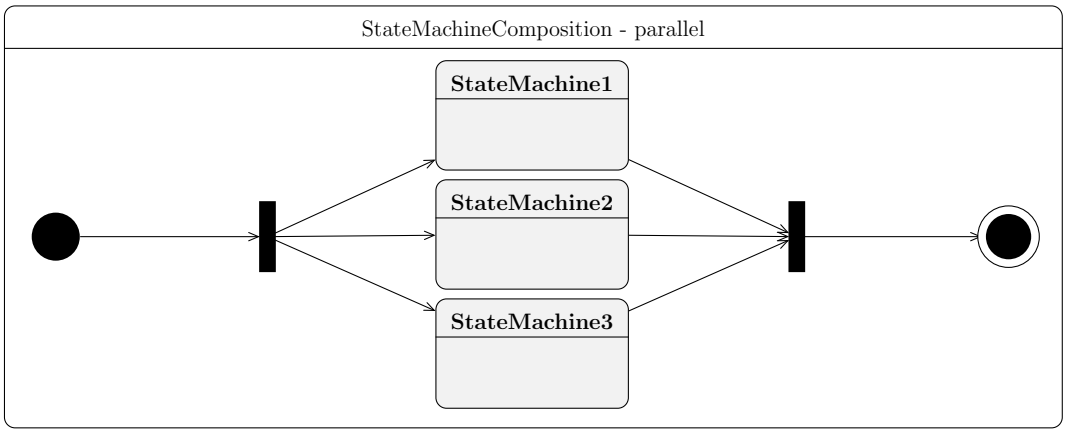

(b) PARALLEL composition of *StateMachine*s.

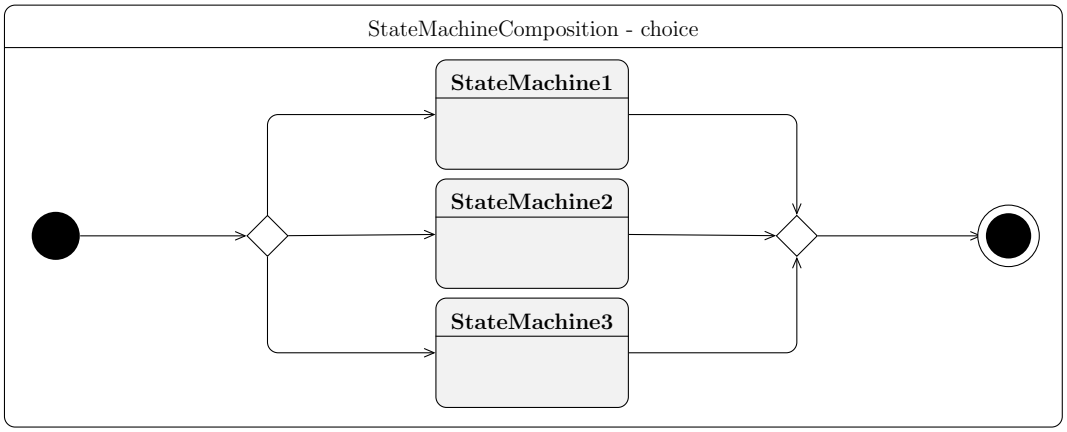

(c) CHOICE composition of *StateMachine*s.

Figure 4.16.: `Sequential` (a), `parallel` (b) and `choice` (c) composition of *StateMachine*s.

the specification of relevance constraints in those cases:

$$CC_1\,;\, g(\,CC_1\,)\,\&\,CC_2\,;\, g(\,CC_2\,)\,\&\,CC_3\ , \tag{4.1}$$

instead of

$$CC_1\,;\, g(\,CC_1\,)\,\&\,CC_2\,;\, g(\,CC_1\,,\,CC_2\,)\,\&\,CC_3\ . \tag{4.2}$$

Validation behaviour of a sequential composition is defined by the termination behaviour of the *StateMachine*s associated to the included CompositionComponents, *Simple-Structure state machine*s in the case of example Fig. 4.17. The *StateMachineComposition*

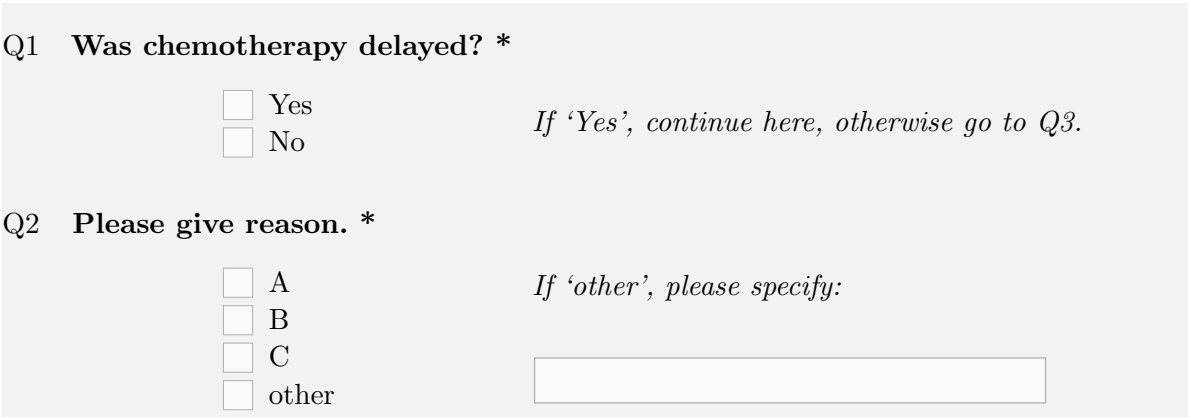

Figure 4.17.: Form components *Q1* (CC_1), *Q2* (CC_2) and 'if other' (CC_3) in `sequential` composition.

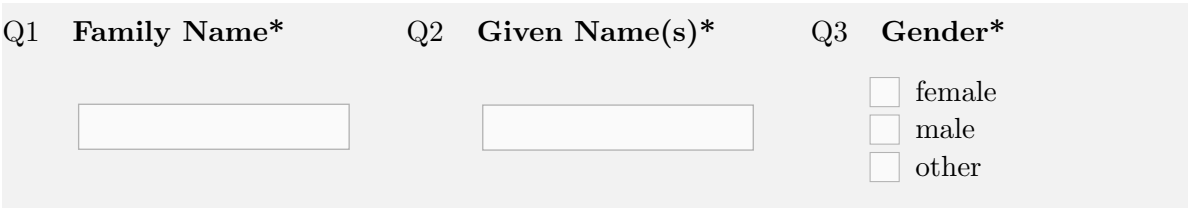

Figure 4.18.: Form components *Q1* (CC_1), *Q2* (CC_2) and *Q3* (CC_3) in `parallel` composition.

corresponding to `sequential` composition terminates when the state machines of all its *active* *CompositionComponent*s terminate according to the rules defined in Section 4.1.3.

4.1.4.2. Parallel Composition

Form components without logical dependencies, such as in example Fig. 4.18, can be completed independently from each other. Their completion and validation behaviour is modelled as `parallel` composition, Fig. 4.16b. The order of *CompositionComponent*s in a `parallel` composition corresponds to the recommended completion order and may be implemented in form design. However, successful form completion does not require the user to adhere to that order. Therefore, relevance constraints across siblings in a parallel composition are not permitted. As for `sequential` composition, the *StateMachineComposition* corresponding to `parallel` composition terminates when the statemachines of all its *active* *CompositionComponent*s terminate according to the rules defined in Section 4.1.3.

4.1.4.3. Choice Composition

A third form logic pattern, 'indeterminate exclusive choice', is represented in the example Fig. 4.19. It is 'indeterminate' since *active* components of the composition are not

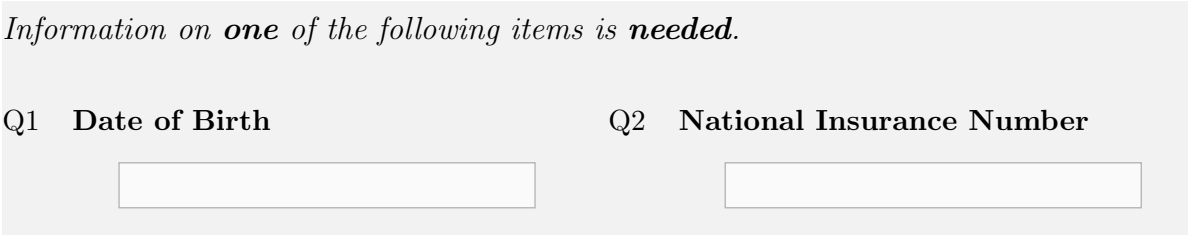

Figure 4.19.: Form components *Q1* (CC_1) and *Q2* (CC_2) in `choice` composition.

	Sequence ;	**Parallel** ‖	**Choice** □
Validation of StructureComposition [a]	all	all	single
Strict completion order of siblings	✔	–	–
Relevance *precondition* expressions across siblings	✔	–	–
ConsistencyConstraints across siblings [b]	✔	✔	–
LocalPrepopulationAssignments across siblings [c]	✔	–	–

[a] Number of 'relevant' *CompositionComponent*s required to terminate (according to validation scenarios in Table 4.1) for StructureComposition to terminate.
[b] ConsistencyConstraint validation performed after all CompositionComponents have been completed: no requirements on ordering.
[c] LocalPrepopulationAssignment may inform user interaction: StructureInComposition elements that act as Variable dependencies must preceed the *assignmentTarget*.

Table 4.2.: Restrictions on validation and completion order, and other functional dependencies among StructureComposition siblings by their `CompositionType`.

determined by predefined form logic, instead the user may choose which of various *CompositionComponent*s to complete.

If guaranteed completion of exactly one of the composition components is important ('exclusive choice'), this pattern cannot be expressed in neither sequential, nor parallel composition: Relevance *precondition*s and *minRequiredResponse* attributes would need to be set in a way to ensure all composition elements to be 'required', while only one single composition element may be *active* at any time. 'Cascading relevance' in sequential composition makes the definition of such constraints impossible. On the other hand, *precondition*s among siblings in parallel compositions are not permitted. The Forms-Metamodel therefore provides a `choice CompositionType`, Fig. 4.16c, that models such behaviour explicitly.

Similar to `parallel` compositions, `choice` composition siblings are considered independent from each other and constraints across siblings are not allowed. A choice composition is considered *valid*, when exactly one *CompositionComponent* is *valid*. The *StateMachineComposition* corresponding to `choice` composition terminates when the statemachine of *exactly one* of all its *active* *CompositionComponent*s terminates.

Table 4.2 summarises validation behaviour and completion order of those compositions, as well as resulting requirements on cross-dependencies among composition siblings.

4.1.5. Model Implementation and Validation

The Forms-Metamodel, Section 4.1.2, was implemented in the Eclipse Modeling Framework (EMF) [155]. Constraints that could not directly be accommodated in the relationships of the metamodel were expressed as model constraints in the Object Constraint Language (OCL) [156] and implemented using the *OCLinEcore* language provided by the Eclipse Platform. Table A.1 comments on these constraints.

The resulting metamodel was then tested by creating form specifications as instances of the Forms-Metamodel, using the *dynamic XML Metadata Interchange (XMI) instance* capability of the Eclipse Platform. The metamodel was modified iteratively until the design requirements, Section 4.1.1, were found to be satisfied.

Further, the Forms-Metamodel was validated against existing standards for form design. Comparisons to two representative metamodels are presented here: ISO/IEC 19763, specifies a metamodel framework for interoperability as introduced in Section 3.1.3.2. Part 13 of this standard, ISO/IEC 19763-13:2013, proposes a metamodel for the registration of forms, focusing on the documentation of form specifications to facilitate interoperability of form-captured data. Since generation of software artifacts from form specifications is not explicitly included in the scope of this standard, the ability of the Forms-Metamodel to support generation of data capture artifacts is demonstrated by comparison to the form definition language of the OpenClinica Framework, as introduced in Section 3.3.

Model transformations were defined to verify correspondences and identify differences between the Forms-Metamodel and the metamodels provided by these standards. The Atlas Transformation Language (ATL) [157] was used for specifying metamodel mappings and for executing model transformations in the Eclipse Platform.

Section 4.1.5.1 shows an example instance model which llustrates the use of the Forms-Metamodel. Transformation steps, common to most transformations between Forms-Metamodel and other form-related metamodels are detailed in Section 4.1.5.2. Section 4.1.5.3 and Section 4.1.5.4 present results of the comparison between the Forms-Metamodel and the OpenClinica forms metamodel and ISO/IEC 19763-13:2013, respectively.

4.1.5.1. Example Forms-Metamodel Instance

Figure 4.20 illustrates the usage of the Forms-Metamodel for the creation of data capture specifications on the example of form fragment Fig. 4.17. Both structural and behavioural composition are demonstrated.

This form fragment represents an instance of Group for reporting delays in chemotherapy treatment. Its validation behaviour is determined by the choice of sequential composition for its three components (ordered), instances of StructureInComposition *G1-Q1*, *G1-Q2*, *G1-Q3*. All fields are non-repeating and mandatory (min/maxReqResponses=1), however, the relevance of *G1-Q2* depends on the answer to *G1-Q1*, and the relevance of *G1-Q3* on the answer to *G1-Q2*. This is expressed by a *precondition* comparing an instance of Constant to an instance of Variable which references the preceeding instance of StructureInComposition. The first and second field are labelled by context-specific *number*s, expressed as instances of TextElement.

The actual question and answer domain for each question element in G1:Group are

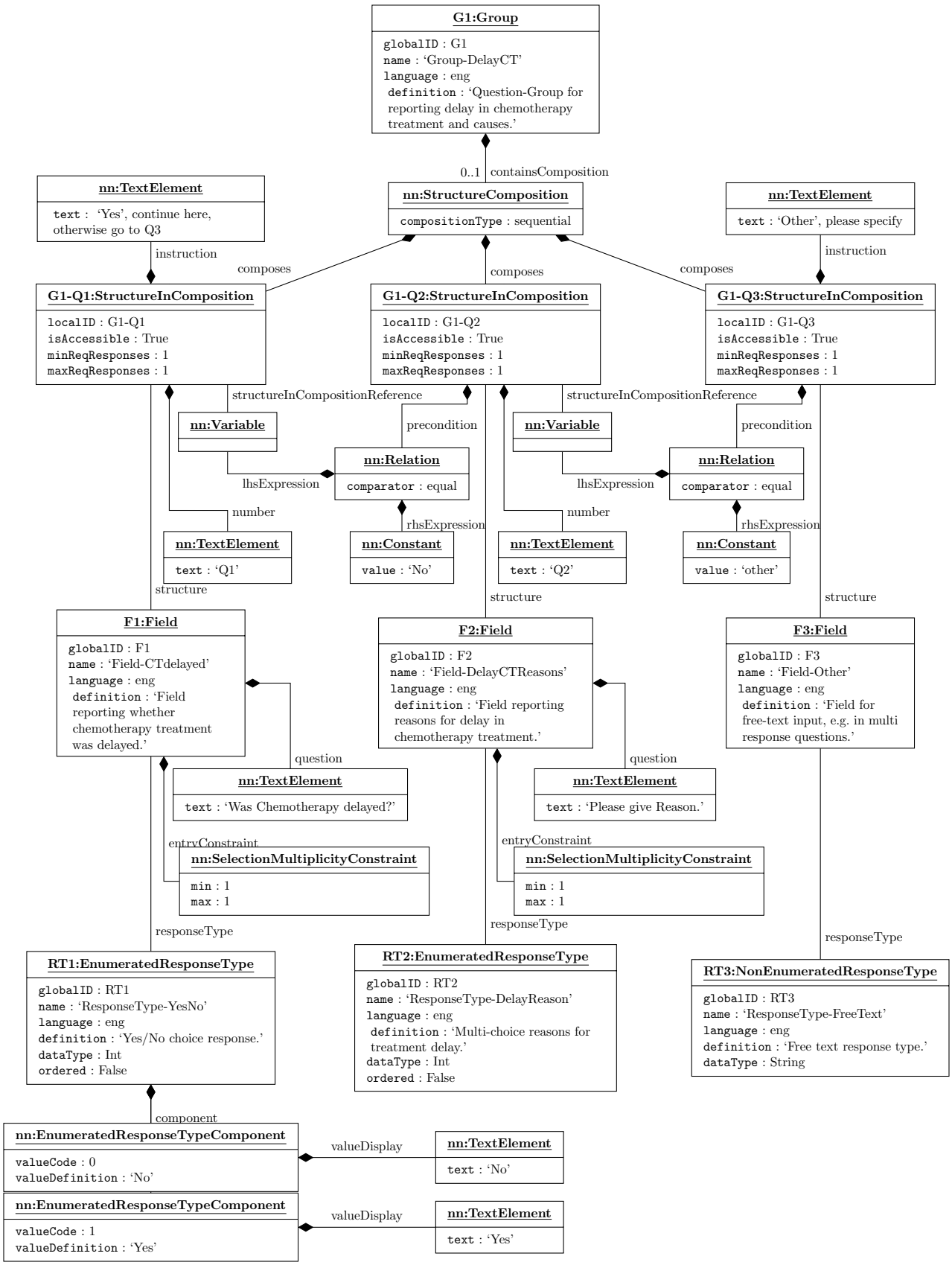

Figure 4.20.: Example Forms-Metamodel instance, based on Fig. 4.17. Instances named 'nn' represent unnamed elements. The EnumeratedResponseTypeComponents of RT2:Enumerated-ResponseType are not represented for space reasons.

provided by globally identifed instances of Field, referenced by the StructureInComposition instances. These define the intended meaning of the question, the question text shown to the user, and the *responseType*. The field question corresponds to an instance of TextElement, as specified for F1:Field and F2:Field.

A globally identifed *responseType* is referenced by each Field instance. F1:Field and F2:Field, both link to instances of EnumeratedResponseType, whereas F3:Field links to an instance of NonEnumeratedResponseType. Instances of *SimpleResponseType* specify their intended meaning in the same way as other globally defined structure elements. Instances of EnumeratedResponseType further define *valueCode* and *definition* for their EnumeratedResponseTypeComponent instancess as well as the value choices that are to be displayed on the form.

In this example, input to the instances of EnumeratedResponseType associated to F1:Field and F2:Field are both restricted by *entryConstraint*s permitting exactly one selection from the provided value domain. The answer options of RT2:Enumerated-ResponseType are not represented in Fig. 4.20 for space reasons.

While F1:Field and F2:Field are specifically designed for reporting in the context of treatment delays of chemotherapy, the meaning of F3:Field is not defined as precisely. Contextual information about its usage, allowing correct interpretation of data collected against this field, is provided through its inclusion into G1:Group and its logical dependence on the answers to F1:Field and F2:Field.

4.1.5.2. Common Transformation Steps

The Forms-Metamodel is designed for the creation of form specifications (instances of Form metaclass) from existing form fragments (instances of Group and Field metaclasses), each of which describes a default way of reporting observations. As such, it defines how reporting fragments can be combined and re-used in the context of new form specifications. Furthermore, it permits their extension with context-specific constraints, annotations and presentation information via the StructureInComposition metaclass. In contrast, most other form-related metamodels, especially those close to a particular implementation technology, view form components only in the immediate usage context on a specific form. Re-use of components with 'local modifications' might be possible, but is not the concern of these metamodels. Due to the modular nature of the Forms-Metamodel, the transformation of a form specification into an instance of such metamodels or into an actual form implementation, requires multiple steps. Since these steps are common to most transformations, they can be treated separately by introducing an intermediate metamodel derived from the Forms-Metamodel.

This section defines this intermediate metamodel, called 'Forms-Metamodel-Template' in the following, and outlines the main transformation steps involved in the conversion from Forms-Metamodel (FM) to Forms-Metamodel-Template (FMT): *a*) combination of *Constraint*s, *Annotation*s and PrepopulationAssignments specified against both FM:StructureInComposition and FM:*Structure* elements, and *b*) creation of *localID* attributes that allow form components derived from FM:*Structure* elements to be uniquely identifiable within the scope of a FMT form specification.

The most notable difference between FM and FMT concerns the relation between StructureInComposition and *Structure* elements: The Forms-Metamodel-Template only

allows form component properties to be specified in a single place. FMT:Field and FMT:Group are no longer considered form fragments in their own right, instead they become *specialisations* of an abstract FMT:*StructureInComposition* metaclass, Fig. 4.21a. As such, they are uniquely identified within a FMT:FormTemplate by their *localID*. Every FM:StructureInComposition *structure* reference in the Forms-Metamodel results in the creation of a FMT:Field or FMT:Group in the Forms-Metamodel-Template, compare Fig. 4.21b to Fig. 4.4b.

The transformation '*Forms-Metamodel* → *Forms-Metamodel-Template*' also derives the *localID* of any FMT:*StructureInComposition* from the *localID* of the included FM:-*Structure* and its position within the FM:Form hierarchy: A field *F4* in group *G1*, which itself is in the direct scope of form *Fo1*, would be identified as Fo1:G1-1:F4-1. Multiple inclusions of the same FM:*Structure* within a given direct scope are disambiguated by their occurrence index: *F1* is present twice in the direct scope of *Fo1*, Fig. 4.21b, resulting in *localID*s Fo1:F1-1 and Fo1:F1-2.

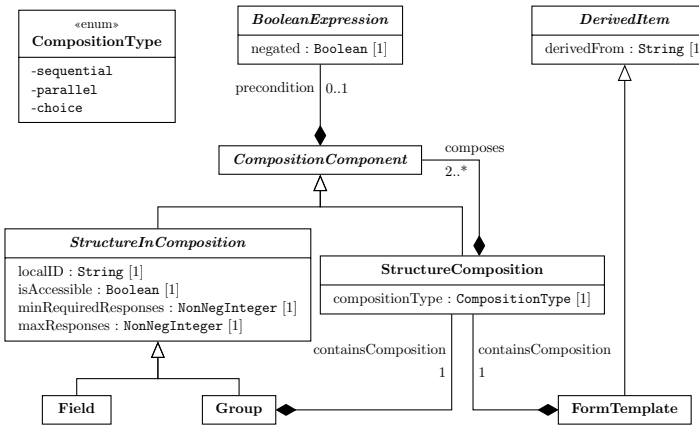

(a) Forms-Metamodel-Template *StructureComposition*.

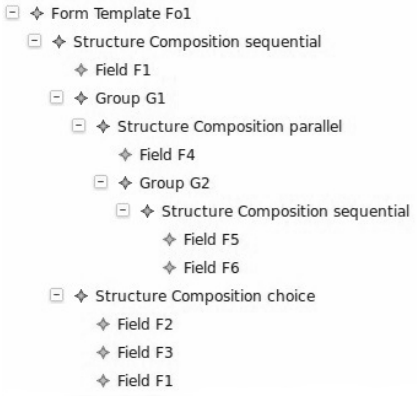

(b) Forms-Metamodel-Template StructureComposition instance.

Figure 4.21.: (a) StructureComposition metamodel and (b) model instance.

FMT:FormTemplate instances are considered the product of a transformation process, *derivedFrom* a Forms-Metamodel instance. FMT:FormTemplate attributes and relations are identical to those of FM:Form; FMT:Group and FMT:Field combine attributes and properties of FM:Group and FM:Field and their respective FM:StructureInComposition. However, FMT:*Annotation*, FMT:*Constraint* and FMT:*PrepopulationAssignment* are only specified once, either against FMT:*StructureInCompositon* elements if they apply to both FMT:Field and FMT:Group, or against FMT:Field, FMT:Group or FMT:Form directly.

The transformation combines constraints from FM:*Structure* and FM:StructureIn-Composition via logical AND, so that the resulting form specification requires all specified constraints, general and context-specific ones, to be fulfilled. For constraints that involve specification of limits, such as ValueRangeConstraint, FileSizeConstraint and SelectionMultiplicityConstraint, this implies that only values between the highest *min* and the lowest *max* value are permissible.

In addition to these differences, all references to FM:*Structure* elements in the Forms-Metamodel are replaced by *localID* references in the Forms-Metamodel-Template. To facilitate further transformation steps, other referenced FM:*FormElement*s, such as *Sim-*

pleResponseType and UnitOfMeasure, are included by the FMT:FormTemplate metaclass via UML:*composition* relationship.

All mapping relations between Forms-Metamodel and Forms-Metamodel-Template are summarised in Table A.4 in the Appendix.

The form specification resulting from this transformation process no longer allows the original form *Structure* component to be distinguished from its context-specific specialisation, StructureInComposition. As a consequence, the back transformation '*Forms-Metamodel-Template* → *Forms-Metamodel*' is not unique, since decisions about the placement of contextual information, at the 're-usable' FM:*Structure* or at its context-specific modification, have to be made. This information may be recovered partially by comparing a FMT:*StructureInComposition* to the original FM:*Structure* from which it has been derived.

Figure 4.22 shows the result of the transformation of Forms-Metamodel instance Fig. 4.20 into an instance of the Forms-Metamodel-Template. Note that FMT:Field instances now combine the attributes and properties of FM:*Field* and FM:StructureInComposition instances. Former references to instances of FM:*FieldSimpleResponseType* are converted into *containment* relationships.

4.1.5.3. OpenClinica

This section compares the Forms-Metamodel with the form definition language used by the OpenClinica Framework. This language is optimised for the specification of clinical data collection forms and is used as reference to evaluate the expressiveness of the Forms-Metamodel with regard to the generation of data collection instruments from form specifications.

OpenClinica Form-Metamodel The metamodel used by the OpenClinica Framework for form generation, Fig. 4.23, distinguishes between CRF, Section and Item as main form components. Every Item is required to be part of a Section (Item:*section_label*) and multiple Items may further be grouped into Groups (Item:*group_label*).

Sections provide for visual structuring of the form and can be nested (*parent_section*). Groups allow common behaviour to be assigned to multiple Items, such as 'repetition' or 'hiding'. Items combine textual elements for user guidance with *data_type* and *response_type*. Additionally, they support simple (*width_decimal*, *required*) and more sophisticated (*validation*) validation constraints, predefined (*default_value*) or computed (*response_values_or_calculations*) default values and relevance constraints (*item_display_status* in combination with *simple_conditional_display*).

Form components in the OpenClinica forms metamodel are identified by their *crf_name*, *section_label*, *group_label* and *item_name*. The *globalID* attribute of Form and *localID* attributes of other *StructureInComposition* components in the Forms-Metamodel provide corresponding identifiers.

Mapping between Form Metamodel and OpenClinica Metamodel Mapping relations between Forms-Metamodel and OpenClinica forms metamodel (OC) are summarised in Table A.5. The main properties of the mapping and differences between both metamodels are introduced in the following.

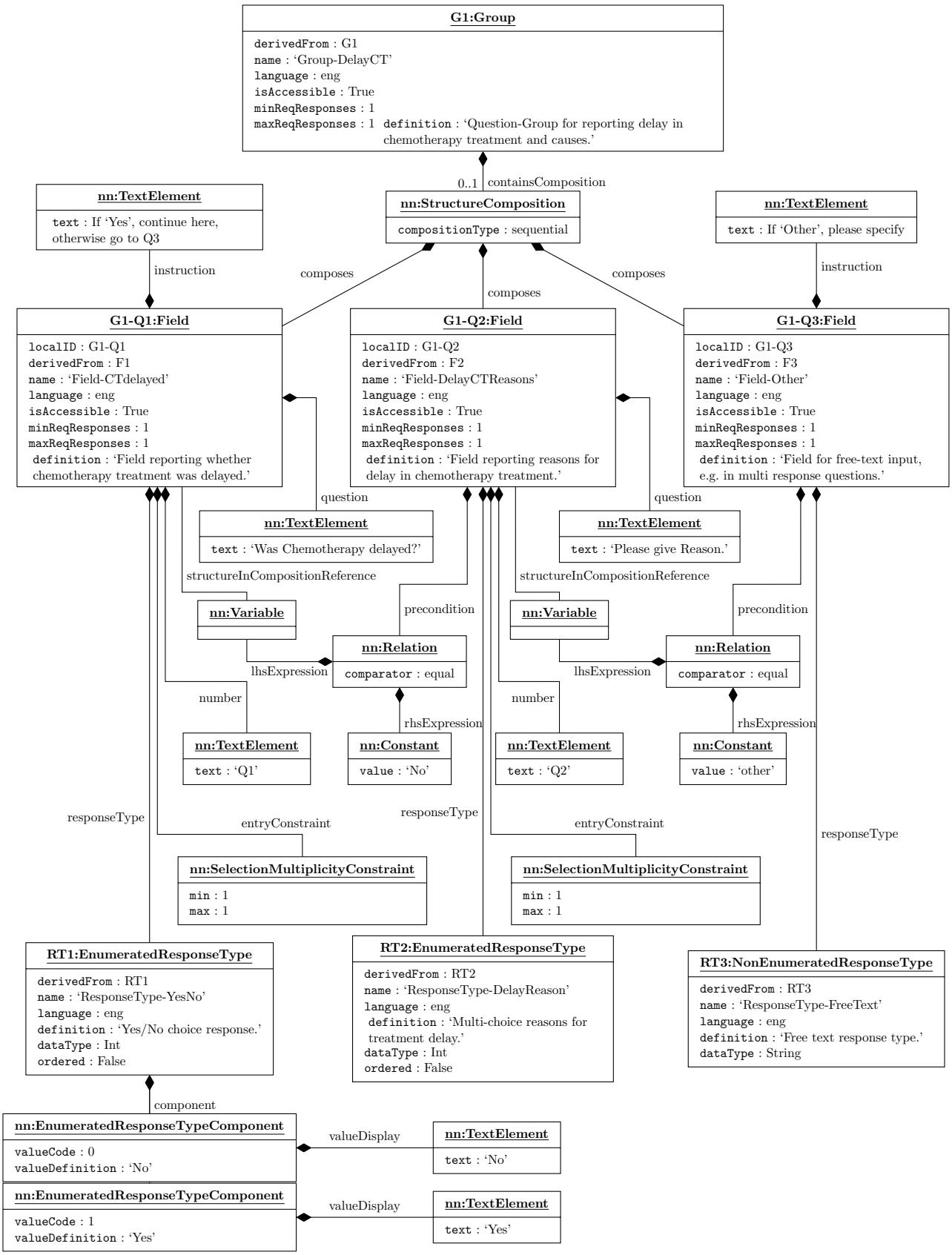

Figure 4.22.: Forms-Metamodel-Template instance, resulting from the transformation '*Forms-Metamodel → Forms-Metamodel-Template*' of Fig. 4.20. Instances named 'nn' represent unnamed elements. The EnumeratedResponseTypeComponents of RT2:EnumeratedResponseType are not represented for space reasons.

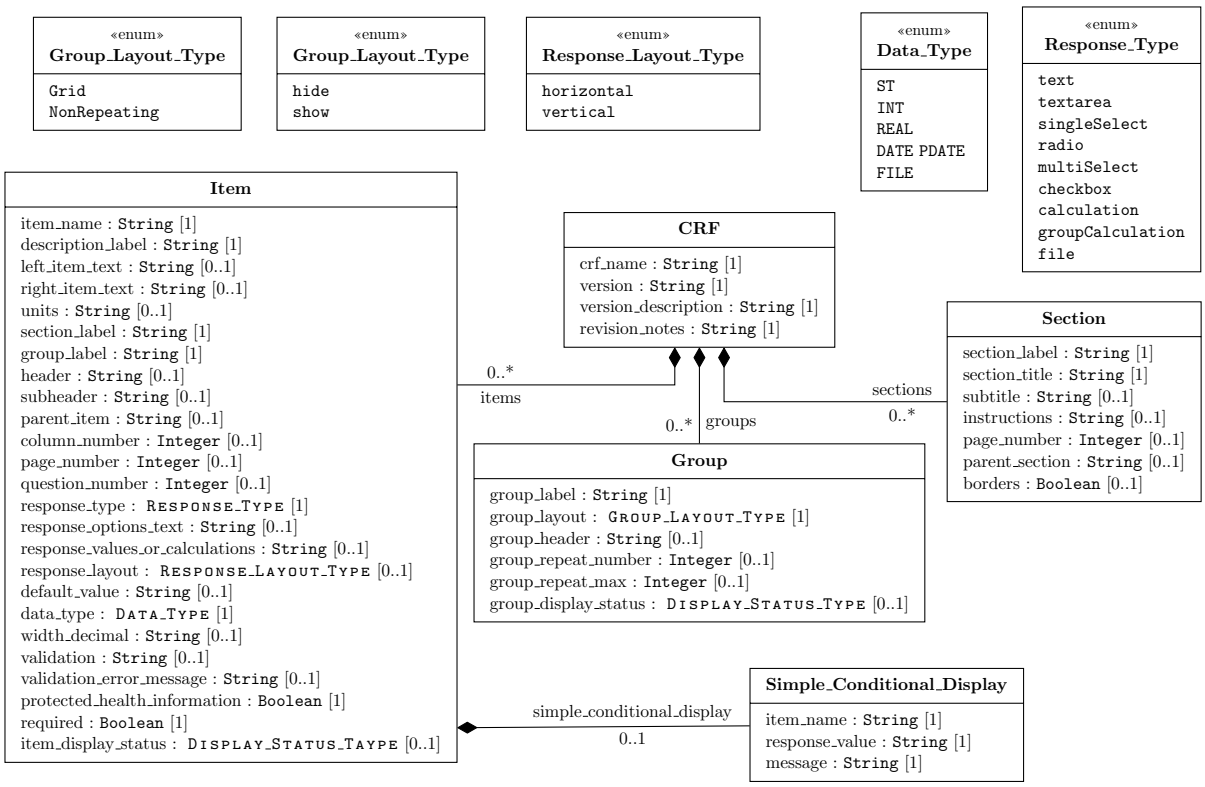

Figure 4.23.: OpenClinica's Form generation model

The OC:Item concept of the OpenClinica forms metamodel directly corresponds to FM:Field. Its textual components can be identified with FM:*InteractionElement* (only FM:TextElement). The Forms-Metamodel distinguishes FM:Groups for form structuring from those purely expressing shared behaviour (OC:Group) via specification of FM:-LogicalHierarchy at the FM:Form level. FM:Groups marked-up through this mechanism correspond to OC:Sections, others to OC:Groups.

Neither OC:Sections, nor OC:Items may be 'repeating'. Translating FM:StructureIn-Composition:*minRequiredResponses* and FM:StructureInComposition:*maxResponses* therefore requires the creation of dedicated OC:Groups with appropriate *group_repeat_number* and *group_repeat_max* attributes. The OC:Group:*group_layout* attribute has to be set according to the permitted number of responses and FM:SimplePresentation attributes *repeatingSimpleStructureAs* and *repeatingComposedStructureAs*.

While the Forms-Metamodel allows conditional relevance of all FM:Composition-Components, the OpenClinica forms metamodel foresees this only for OC:Groups (*group_-display_status*) and OC:Items (*item_display_status*). The notion of FM:Groups acting as conditional form sections therefore has to be approximated by the creation of a conditional OC:Groups within a (permanent) OC:Section.

OC:Items need to be placed in a section (OC:Item:*section_label*) which in turn may be nested into a section hierarchy (OC:Section:*section_label*). Correct attribution of these elements to their respective 'parent' OC:Section requires identification of the closest preceding 'section' FM:Group within the FM:*ComposedStructure* hierarchy. These FM:Groups can be identified with the help of FM:LogicalHierarchy markup.

Both, *data_type* and *response_type* are required for the definition of OC:Items. However, the Forms-Metamodel strictly separates the data type that is expected to be entered against a FM:Field (FM:*SimpleResponseType*) from its presentation (FM:InputFieldPresentation). Latter may be specified only on the FM:Form level. For FM:Field with FM:EnumeratedResponseType, FM:SelectionMultiplicityConstraint specifies the number of expected answer choices. The combination FM:EnumeratedResponseType, FM:SelectionMultiplicityConstraint:*min* = 1, FM:SelectionMultiplicityConstraint:*max* = 3 and FM:InputFieldPresentation:*selectorType* = `Checkbox`, for example, would translate into OC:Item attributes *response_type*=`checkbox` (allowing selection of multiple items) and *required*=TRUE, as well as *response_options_text* and *response_values_or_calculations*, corresponding to the FM:SimpleResponseType of the FM:Field. The constraint that no more than three selections from the enumerated value domain are accepted has no direct correspondence in the OpenClinica forms metamodel.

The OpenClinica forms metamodel provides a dedicated `calculation` *response_type* that can be used in combination with *response_values_or_calculations* to define pre-population values. The notion of `calculation` as 'unchangeable computed value' corresponds to FM:LocalPrepopulationAssignment with *valueLocked*='true', however, only simplest FM:*assignmentExpression*s can be expressed in the OpenClinica forms metamodel. OC:Item:*default_value* allows for pre-population of `single-select` *response_types*.

FM:ValueRangeConstraints and FM:PatternConstraints have their direct correspondence in OC:Item:*validation*. A *width_decimal* constraint may indicate the maximum length and number of decimal places in input fields and can be expressed as regular expression in FM:PatternConstraint.

OC:Simple_Conditional_Display specifies simple conditions, via a reference to *item_name* and specification of *response_value*, under which the respective OC:Item (*item_display_status*='hide') will be visible. This mechanism allows *preconditions* on the relevance state of FM:Fields to be expressed. However, the *item_name* reference is limited to OC:Items with predefined *response_options_text* and `single-select` *response_type*. More sophisticated conditions and the conditional display of OC:Groups can only be expressed in a dedicated 'rule' language and must be specified within the OpenClinica Framework.

In general, the expression language used in the OpenClinica forms metamodel for form generation is limited to relations between one referenced OC:Item and a constant value. Relations between multiple OC:Items, such as in FM:*Expression*s, are not possible, nor is the combination of multiple relations into OC:*BooleanExpression*s. As a consequence, Forms-Metamodel *consistencyConstraint*s across multiple form elements cannot be implemented.

The OpenClinica forms metamodel contains various features that do not have direct correspondence in the Forms-Metamodel but can be expressed as part of FM:StylesheetPresentation: OC:Items are attributed specific presentational information such as *column_number*, *page_number* and *response_layout*. Latter indicates whether response options are to be displayed horizontally or vertically. Specification of a *parent_item* results in indented presentation of the current OC:Item.

The *protected_health_information* attribute represents a concept specific to the domain of medical data capture and as such is not included in the Forms-Metamodel.

4.1.5.4. ISO 19763-13

In this section the Forms-Metamodel is validated against the latest 'Committee Draft' [95] of the form metamodel developed within ISO/IEC 19763, Section 3.1.3.2. Improvements for both metamodels are suggested.

ISO Form-Metamodel ISO/IEC 19763-13[1] defines Form_Design as 'container' for various types of *Form_Design_Element*s, namely Section_Element, Question_Element and *Presentation_Element*, Fig. 4.24.

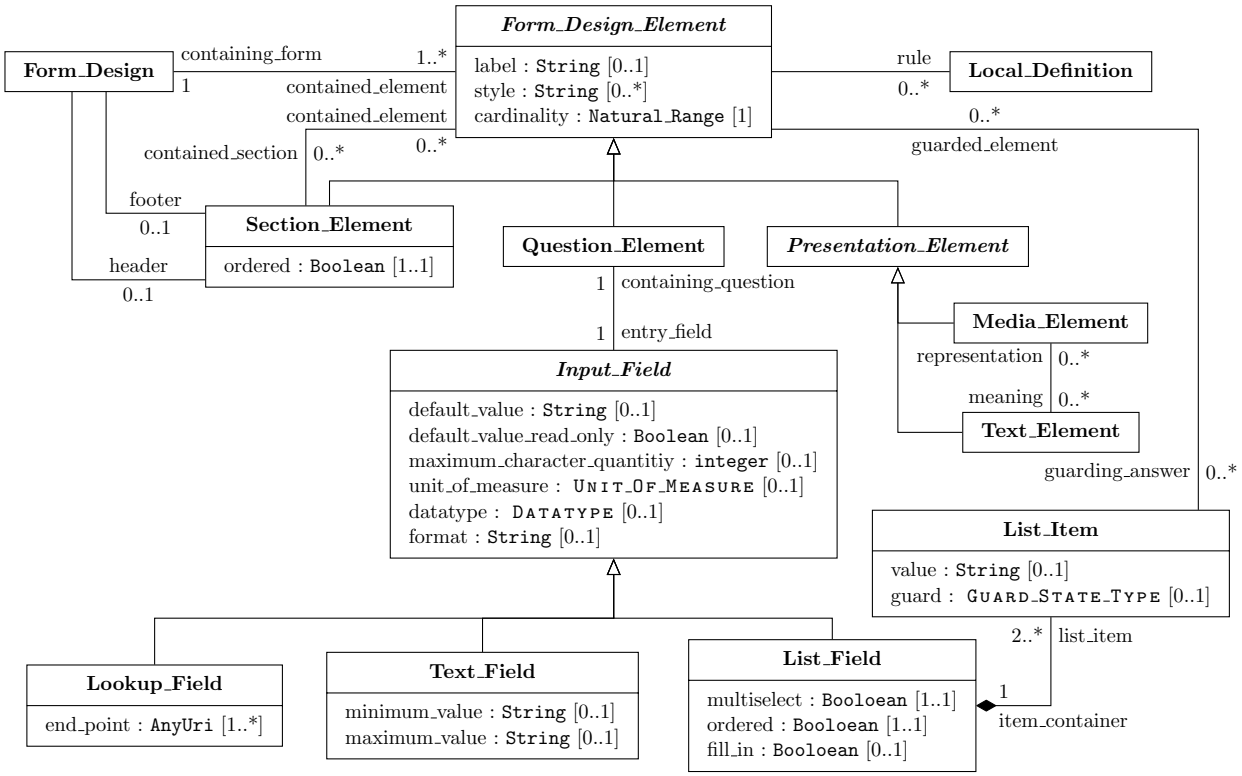

Figure 4.24.: Form components in ISO/IEC 19763-13, adapted from [95].

Both Form_Design and Section_Element may aggregate other *Form_Design_Element*s as *contained_element*s. Semantic significance of the order of contained_elements within a Section_Element must be indicated by setting the *ordered* attribute. Every *Form_Design_Element* occurs with a certain number of repetitions (*cardinality*) in its *containing_form* or Section_Element.

Section_Elements may contain *Presentation_Element*s: Media_Element or Text_Element. Text_Elements may also be directly associated to both, Section_Element and Question_Element, Fig. 4.25. ISO/IEC 19763-13:2013 distinguishes three types of TextElements: Prompt, representing the textual information that defines the semantics of the associated component, Number, as visual indicator of form completion order and identifier for

[1]Names and cardinalities of metaclass attributes and associations in ISO/IEC 19763-13 are undergoing harmonisation. For the definition of model mappings, it was therefore necessary to resolve naming and cardinality inconsistencies in the current 'Committee Draft' [95].

form elements, and AdditionalText for complementary information such as 'instructions'. Associations to any of those elements are optional for both Section_Element and Question_Element, allowing for example the definition of a Section_Element without *section_title* if it is used for grouping purpose only.

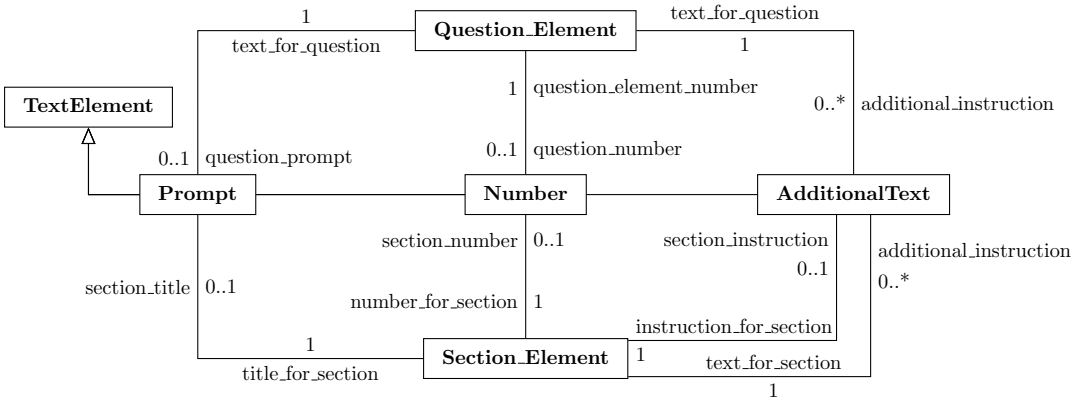

Figure 4.25.: Associations between Question_Element, Section_Element and Text_Element types in ISO/IEC 19763-13, adapted from [95].

Question_Elements are characterised by their associated *entry_Field* for data input. *Input_Field*s share common characteristics, such as constraints on *datatype*, the maximum number of characters used in the field and the *format* of the response. A *unit_Of_Measure* may be associated to any *Input_Field*, as well as a *default_value* which can be protected from user modification (*default_value_read_only*).

Text_Field represents a specific type of *Input_Field* that allows input of any characters that comply to the *format* attribute. It further provides additional attributes for specifying the permissible *minimum_value* and *maximum_value* for numeric *datatype*s.

List_Field corresponds to an *Input_Field* with predefined answer choices: List_Items. Depending on the setting of *multiselect*, only one or multiple of these items can be selected. If the order of answer choices is important, this can be indicated by setting the *ordered* attributes. Further properties of List_Field and List_Item (*fill_in*, *multiselect*, *guard*, *guarded_element*) are discussed in the following paragraphs. Similarly to questions and sections, usage information of List_Items is modelled via associations to the respective TextElement types, Fig. 4.26.

Lookup_Field is intended to represent an *Input_Field* with dynamic answer choices, such as an up-to-date list of patient names retrieved from a database.

Mapping between Forms-Metamodel and ISO/IEC 19763-13:2013 Direct correspondences between Forms-Metamodel-Template and ISO/IEC 19763-13:2013 metaclasses, their attributes and relations, are compared side-by-side in Table A.6.

The remainder of this section focuses on *differences* between ISO/IEC 19763-13:2013 (ISO) and Forms-Metamodel (FM). Possible modifications to the Forms-Metamodel resulting from this discussion are summarised in Table A.7.

Inheritance Structure ISO/IEC 19763-13:2013 defines two main form metaclasses: ISO:Form_Design and ISO:*Form_Design_Element*. Instances of these metaclasses may be

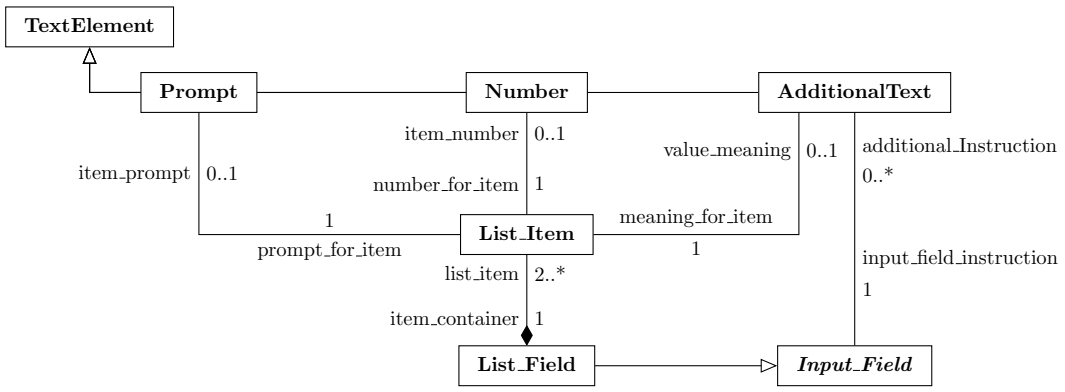

Figure 4.26.: Associations between *Input_Field*, List_Item and Text_Element types in ISO/IEC 19763-13, adapted from [95].

registered, maintained and related to each other via mappings among 'model elements' as defined by ISO/IEC 19763-10. ISO:*Form_Design_Element* represents the main visible elements of forms: ISO:Section_Element, ISO:Question_Element and ISO:*Presentation_Element*. ISO:*Input_Field*s only exist in combination with a specific ISO:Question_Element.

FM:*Structure*, defining the main types of data-entry elements on a form, broadly corresponds to ISO:*Form_Design_Element*, whereas FM:Form, a specialisation of FM:*Structure*, corresponds to ISO:Form_Design. Although ISO:Form_Design may have multiple *contained_element*s, it is not equivalent to ISO:Section_Element in its role as 'form element container', since it lacks various ISO:Section_Element properties: *rule*s, 'form title' and *ordered* attribute. Unambiguous definition of a ISO:Form_Design therefore requires a single 'main' ISO:Section_Element to be created. This is also required for the transformation between FM:Form and ISO:Form_Design, so that FM:*ComposedStructure* properties can be translated.

Both metamodels can be harmonised by separating the roles of FM:Form and FM:Group. Instead of sharing the bulk of their properties as specialisations of FM:*ComposedStructure*, FM:Form could exclusively serve for the definition of form-wide properties, Fig. 4.11, whereas FM:Group retains its current capabilities. Such a change would simplify the inheritance hierarchy of the Forms-Metamodel and avoid ambiguities related to the allowed uses of different specialisations of FM:*ComposedStructure*, compare Fig. 4.27 to Fig. 4.1.

In contrast to ISO:*Presentation_Element*, FM:*InteractionElement*s only exist in combination with a FM:*Structure* and are not modelled as specialisation of FM:*FormElement*. However, the definition of FM:*InteractionElement*s as independent form components would facilitate their re-use across form specifications. This might be helpful in cases where the same textual or media elements are to be used across forms, for example in order to allow predefined copyright statements or institutional information to be included in multiple form specifications. To achieve this, FM:*InteractionElement* could be made a specialisation of FM:*FormElement*, Fig. 4.27. Direct derivation from FM:*Structure* would result in inheritance of multiple undesired properties. This is the case for ISO:*Presentation_Element* which is derived from ISO:*Form_Design_Element* and thus inherits properties such as *cardinality*, *rule* or *contained_section*.

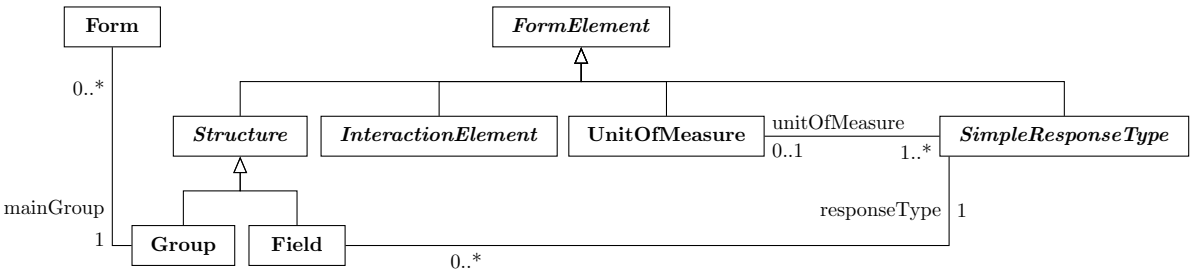

Figure 4.27.: Proposed modifications to Forms-Metamodel inheritance hierarchy (Fig. 4.1): FM:Form associates single *mainGroup*, replacing FM:*ComposedStructure*. Rules to prevent inclusion of FM:Forms into FM:StructureComposition are no longer necessary. FM:*InteractionElement* is defined as specialisation of FM:*FormElement*.

FM:InteractionElement vs. ISO:Presentation_Element ISO/IEC 19763-13:2013 permits the use of ISO:Media_Element only in combination with an ISO:Text_Element that specifies its *meaning*, whereas the Forms-Metamodel allows FM:TextElement and FM:-MediaElement to be used interchangeably. Thus, the Forms-Metamodel permits media content to play a primary role in 'user interaction', independent of any further textual information: a video clip might be included in a digital form to explain the topic and content of a given section.

The 'role' of a FM:MediaElement may be specified via its *explanationText*, an optional text note that serves for documentation and is not intended to be visible to the form user. However, in situations where a dependency between multiple FM:*InteractionElement*s has to be expressed, a dedicated association, such as ISO:Text_Element:*representation*, is advantageous. Consider the example of a 'multi-step' FM:Group:*instruction*, consisting of several FM:TextElements, each of which is illustrated by a FM:MediaElement.

In order to allow both, FM:MediaElements as primary information content, as well as explicit dependency relations between FM:*InteractionElement*s, a recursive relation *complements* could be added to FM:*InteractionElement*, Table A.7. This relation would indicate that one FM:*InteractionElement* element is intended to complement the information content provided by the other, without assuming any precedence between textual and media content. A similar relation might also be added to ISO:*Presentation_Element*.

FM:BooleanExpression vs. ISO:Local_Definition ISO:Local_Definition allows the definition of logical expressions: References to ISO:*Form_Design_Element*s can be used as ISO:Variables and three types of properties may be queried ('value' and 'relevance') or set ('default') at run-time. ISO:Local_Definition:predicate defines the condition for a *rule* to apply, corresponding to a *precondition* FM:*BooleanExpression* in the Forms-Metamodel. ISO:Local_Definition:*consequence* defines either a condition that must hold, or an assignment to be applied when the ISO:Local_Definition:*predicate* is fulfilled. Former involves 'value' and 'relevance' properties and can be translated into FM:*Constraint* and relevance *precondition*, latter makes use of the 'default' property and can be translated into FM:-LocalPrepopulationAssignment. In contrast to FM:LocalPrepopulationAssignment, specification of default values via ISO:Local_Definition does not allow the *default_value_read_only* attribute of the corresponding ISO:*Input_Field* to be set. Otherwise, both approaches fulfill the same functions and are similarly expressive.

ISO/IEC 19763-13:2013 allows for the grouping of multiple *consequence*s to a single *predicate* expression. This facilitates form design in situations where a single 'event' triggers multiple changes or additional constraints.

No restrictions on the scope of ISO:*Variable*s, or the kind of ISO:*Form_Design_Element*s they may be referring to, are suggested by ISO/IEC 19763-13:2013. The same mechanisms may therefore apply to all kinds of ISO:*Form_Design_Element*s, allowing for example an ISO:*Presentation_Element* to be displayed ('relevant') conditional on some *predicate*, or to change its 'value' text. Such conditional relevance of FM:InteractionElements, independent from the relevance state of their defining form element, is deemed unnecessary in the Forms-Metamodel.

FM:StructureComposition, Ordering and Validation Logic The Forms-Metamodel defines the composition of form components and its resulting implications on form completion order and validation behaviour using the FM:StructureComposition metaclass with its different CompositionTypes, see Section 4.1.2.5, 4.1.3 and 4.1.4. ISO:*Form_Design_Element*:*ordered* in ISO/IEC 19763-13:2013 indicates the significance of element order in a *contained_element* sequence. In its effect on form component order, this attribute is equivalent to `sequential` (*ordered* = TRUE) and `parallel` (*ordered* = FALSE) composition in the Forms-Metamodel.

In contrast to 'cascading relevance' in `sequential` compositions, Fig. 4.17, 'ordering' in ISO/IEC 19763-13:2013 does not imply strict functional dependencies among its (ordered) *contained_element*s. Relevance constraints expressed as ISO:Local_Definition must therefore always specify the full constraint with all its dependencies. Mapping between an *ordered* = TRUE ISO:Section_Element and a Forms-Metamodel `sequential` composition requires the constraint expressions to be expanded or reduced, similar to the transition between Eq. (4.1) and Eq. (4.2) in Section 4.1.4.

ISO/IEC 19763-13:2013 provides a mechanism identical to `sequential` composition trough List_Item:*guard*. This attribute allows multiple ISO:*Form_Design_Element*s to be rendered *inactive*, based on the ISO:List_Item that has been chosen from the ISO:List_Field of a particular ISO:Question_Element.

For a single *guard* and *guarded_element*, the behaviour corresponds to a simple `sequential` FM:StructureComposition with two FM:*CompositionComponent*s, the initial question and a further form element with relevance *precondition*, (1a) in Table 4.3. Repeated use of this mechanism allows for the creation of nested 'guarded' ISO:*Form_Design_Element*s that show 'cascading relevance' behaviour in the same way as `sequential` compositions, compare (1b) in Table 4.3 to Eq. (4.1) in Section 4.1.4.

ISO/IEC 19763-13:2013 does not allow the significance of 'order' among multiple *guarded_element*s to be specified. The mapping into FM:StructureComposition in (2), Table 4.3, is therefore ambiguous.

A *multiselect* ISO:List_Field may result in simultaneous activation of multiple 'guarded_element' sequences, (3) in Table 4.3. Again, the importance of order among these sequences of form elements cannot be specified. At design-time it is not known which of the available ISO:List_Item will be selected and which of the *guarded_element* ISO:*Form_Design_Element* sequences will be *active*. The ISO:*Form_Design_Element* sequences therefore need to be independent, which corresponds to `parallel` FM:StructureComposition.

	List_Field:-*multiselect*	List_Item with *guard*	List_Item:-*guarded_element*	StructureComposition
(1a)	FALSE	I_1	E_1	$\{Q_0\,;\ g(I_1)\,\&E_1\}$
(1b)	nested *guarded_element*s	E_1 is Question_Element with List_Field and List_-Item I_1' guarding E_2		$\{Q_0\,;\ g(I_1)\,\&E_1\,;\ g(I_1')\,\&E_2\}$
(2)	FALSE	I_1	$(E_1, E_2, \ldots, E_n)$	$\{Q_0\,;\ g(I_1)\,\&\{E_1, E_2, \ldots, E_n\}\}$
(3)	TRUE	I_1 I_2 I_3	$(E_1, E_2, \ldots, E_n)$ $(E_1', E_2', \ldots, E_n')$ $(E_1'', E_2'', \ldots, E_n'')$	$Q_0\,;\left\{\begin{array}{ll} g(I_1)\&\{E_1, E_2, \ldots, E_n\} & \| \\ g(I_2)\&\{E_1', E_2', \ldots, E_n'\} & \| \\ g(I_3)\&\{E_1'', E_2'', \ldots, E_n''\} & \end{array}\right\}$

Table 4.3.: Mapping between ISO:List_Item:*guarded_element* and FM:StructureComposition. ISO:Question_Element Q_0 with *entry_field* ISO:List_Field and multiple ISO:List_Items $I_1, \ldots, I_n$ are assumed.
For multiple *guarded_element*s (case (2)), the mapping into FM:StructureComposition is ambiguous: $\{E_1, \ldots, E_n\}$ indicates a FM:StructureComposition of undefined *compositionType*.

'Order' in ISO/IEC 19763-13:2013 is defined as ISO:Section_Element property and therefore always applies to a whole 'group' of ISO:*Form_Design_Element*s. To ensure that Section_Element:*contained_element*s can be completed in arbitrary order, conditions such as those valid for `parallel` composition siblings, Table 4.2, need to hold. Relevance of *contained_element* siblings therefore must not be constrained on the basis of data entered against other siblings. Consider an additional question *Q4 Are you married - Yes/No* added to the `parallel` composition example Fig. 4.18, together with an optional dependent question *Q5 Birth Name*. In the Forms-Metamodel, this case can be represented as composition of `parallel` and `sequential` FM:StructureCompositions:

$$Q1 \parallel Q2 \parallel Q3 \parallel \{Q4;\ g(Q4)\,\&Q5\}\ . \tag{4.3}$$

Modelling this example through the use of ISO:Local_Definition requires the definition of a 'main' (*ordered* = FALSE) ISO:Section_Element, as well as an additional (*ordered* = TRUE) ISO:Section_Element. Alternatively, *Q5* could be represented as List_Item:-*guarded_element*. However, ISO/IEC 19763-13:2013 provides this alternative only if the 'guarding' ISO:Question_Element has a ISO:List_Field.

The Forms-Metamodel notion of `choice` composition has no correspondence in ISO/IEC 19763-13:2013. Situations of choice, similar to example Fig. 4.19, may be translated into ISO/IEC 19763-13:2013 by defining suitable ISO:Local_Definitions against the 'relevance' property of the participating ISO:*Form_Design_Element*s:

> Local_Definition:*predicate*:
> Section_Element("Section1").*Form_Design_Element*("Q1").value='empty'
> Local_Definition:*consequence*:
> Section_Element("Section1").*Form_Design_Element*("Q2").relevance=TRUE

and

Local_Definition:*predicate*:
Section_Element("Section1").*Form_Design_Element*("Q2").value='empty'
Local_Definition:*consequence*:
Section_Element("Section1").*Form_Design_Element*("Q1").relevance=TRUE

However, without a notion of 'empty' in ISO/IEC 19763-13:2013, above constraints need to be implemented as ISO:BinaryOperation. This obscures the intent of modelling 'indeterminate exclusive choice' from multiple alternative response options. Correct reverse transformation of such constructs into `choice` compositions cannot be guaranteed.

FM:SimpleResponseType vs. ISO:Input_Field In contrast to FM:*SimpleResponseType*, ISO:*Input_Field* exclusively exists in combination with ISO:Question_Element. As such, it not only defines basic properties of a reusable value domain, compare ISO11179:-Enumerated_Value_Domain, but also context-specific constraints, such as the allowed range of entry values or a *default_value*. This information is specified in the Forms-Metamodel by combining a FM:Field with FM:*SimpleResponseType* and FM:*EntryConstraint*s.

ISO/IEC 19763-13:2013, does not provide a dedicated ISO:*Input_Field* for binary objects, such as FM:BlobResponseType, that allows 'files' as question responses. Applications of that response type may range from simple 'file-upload' input fields, used to 'attach' a file, to interactive input fields that permit the user input of a drawing or recording of a spoken answer, and return this response as binary object of some *MIMEType*. A similar type of input field can also be included in ISO/IEC 19763-13:2013. Direct derivation from ISO:*Input_Field*, however, will result in unnecessary attributes, such as *maximum_character_quantity*.

ISO:Lookup_Field intends to use dynamic information from a (web)service *end_point* for the creation of a list of answer choices, similar to ISO:List_Field. This functionality is frequently used in digital forms, for example in order to provide an 'up-to-date' list of patient IDs from a database query. A corresponding response type is missing in the Forms-Metamodel, and its specification in ISO/IEC 19763-13:2013 provides little detail.

In addition to *guard* and *guarded_element*s, ISO:List_Field differs from FM:EnumeratedResponseType by its optional *fill-in* attribute. 'Fill-in' fields are extensions to predefined lists of answer choices that allow individualised responses, different from the predefined values, to be entered by the user, example Fig. 4.17. As suggested by Eq. (4.1), 'fill-in' values can be modelled as two distinct FM:Field*s*, the first with its associated FM:EnumeratedResponseType and the second represented by a FM:NonEnumeratedResponseType. Both FM:Field components form a `sequential` composition in which the second component only becomes *active* if the 'other' FM:NonEnumeratedResponseTypeComponent is selected. Likewise, in ISO/IEC 19763-13:2013, 'fill-in' values can be represented as additional 'guarding' ISO:List_Item that specifies an ISO:Question_Element with ISO:Text_Field as its *guarded_element*.

Both approaches correctly describe relevance condition and validation logic of 'fill-in' fields. However, they do not acknowledge their role as 'value domain extensions'.

ISO/IEC 19763-13:2013 therefore proposes explicit modelling of 'fill-in' fields through the ISO:List_Field:*fill_in* attribute. This approach, however, only models the 'label' of the alternative answer choice, such as 'other', not the properties of its response.

An extension to the Forms-Metamodel that allows explicit modelling of 'fill-in' fields is presented in Fig. 4.28. In addition to multiple FM:*EnumeratedResponseTypeComponent*s,

an optional FM:FillInComponent may be defined with every FM:EnumeratedResponseType. The FM:FillInComponent contributes a *valueCode* to the FM:EnumeratedResponseType which, just like the *valueCode* of FM:EnumeratedResponseTypeComponents, is specified at design-time and must conform to the same *dataType*. In contrast to FM:EnumeratedResponseTypeComponent, FM:FillInComponent may or may not need *valueDisplay*s to appear in the list of answer choices, since the 'fill-in' input field may be placed directly in this list. As specialisation of FM:NonEnumeratedResponseType, FM:FillInComponent additionally defines the *dataType* of the 'fill-in' response value and an optional *instruction*, such as 'if other, please specify'. ISO:List_Field:*fill_in* could be remodelled in a similar fashion.

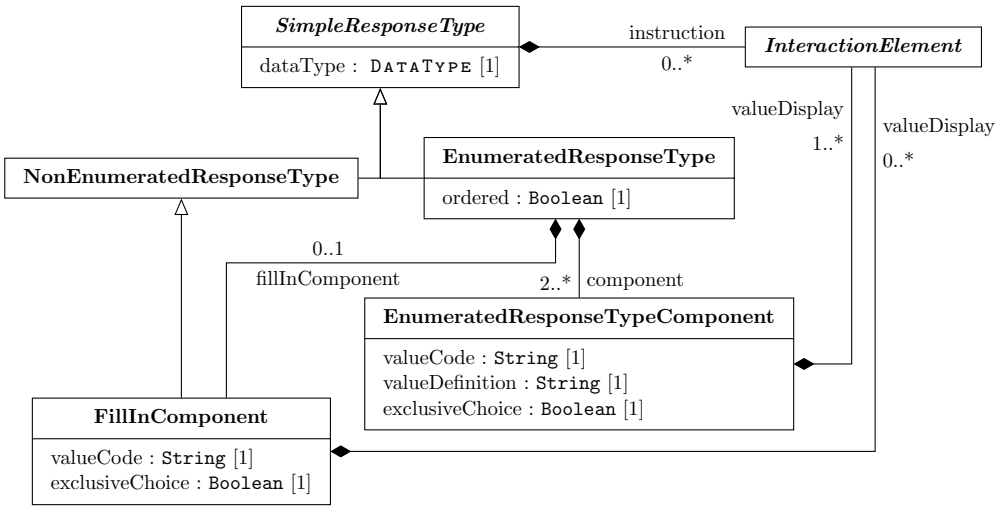

Figure 4.28.: Extension to Forms-Metamodel FM:*SimpleResponseType* to support 'fill-in' fields in predefined answer choices. An *exclusiveChoice* option has also been added to FM:*EnumeratedResponseTypeComponent* and *FillInComponent*

The number of required and the maximum number of permitted selections from an FM:EnumeratedResponseType may be specified via FM:SelectionMultiplicityConstraint. In the default case (*minRequiredResponses*=1, *maxResponses*=1), one answer choice (*valueCode*) must be selected from the EnumeratedResponseType. In other cases, at least *minRequiredResponses* data items and not more than *maxResponses* selections have to be made. ISO:List_Field only distinguishes *multiselect* = TRUE or FALSE response options.

None of the metamodels takes into account that selection of a particular answer choice may rule out selection of any of the others, regardless of the corresponding FM:SelectionMultiplicityConstraint. Such modification of the actual FM:SelectionMultiplicityConstraint from its original setting to 'exactly one' may be required for any of the following reasons: Logical inconsistency, such as in example Fig. 4.29a, or selection of a 'none of the available options applies' answer choice, Fig. 4.29b.

An *exclusiveChoice* attribute was added to FM:EnumeratedResponseTypeComponent in Fig. 4.28 to account for this behaviour.

In situations where no suitable answer choice is available, Fig. 4.29b, 'fill-in' fields may be used to permit entry of alternative responses. The 'fill-in' value may then be considered an exclusive choice option, such as in Fig. 4.30a, or an additional answer

1. **Your favourite team sports:**
Select at least two.

- ☐ Football
- ☐ Volleyball
- ☐ Hockey
- ☐ Rugby
- ☒ Prefer individual sports.

(a) Logical inconsistency.

1. **Your favourite team sports:**
Select at least two.

- ☐ Football
- ☐ Volleyball
- ☐ Hockey
- ☐ Rugby
- ☒ None of the above.

(b) 'None applies'.

Figure 4.29.: Different types of 'exclusive choice' options from predefined answer sets.

1. **Your favourite racket sports:**
Select at least two.

- ☐ Tennis
- ☐ Squash
- ☐ Hockey
- ☐ Cricket
- ☒ None of the above, other

Badminton

(a) Exclusive choice.

1. **Your favourite racket sports:**
Select at least two.

- ☐ Tennis
- ☒ Squash
- ☐ Hockey
- ☐ Cricket
- ☒ other

Badminton

(b) Non-exclusive choice.

Figure 4.30.: 'Exclusive choice' (a) and 'non-exclusive choice' (b) from predefined answer sets with 'fill-in' fields.

choice that applies together with predefined ones Fig. 4.30b. A 'fill-in' field that is used as non-exclusive choice option needs to fulfill the requirements defined by the corresponding FM:SelectionMultiplicityConstraint. Its multiplicity must be adjusted dynamically to guarantee the collection of *minRequiredResponses* selections as defined in the FM:-SelectionMultiplicityConstraint. In example Fig. 4.30b instructions indicate that at least *two* selections have to be made. If only 'other' is selected, two input fields for data input should be available. If 'other' and an additional FM:EnumeratedResponseTypeComponent, such as 'Squash', is selected, only one field. In general, the number of available input fields for a FillInComponent must equal SelectionMultiplicityConstraint:*minRequiredResponses* less the number of selected FM:EnumeratedResponseTypeComponents.

Presentation vs. Semantic Significance Forms-Metamodel and ISO/IEC 19763-13:2013 assign semantic significance to aspects of form design that are considered purely presentational by the respective other metamodel.

The *isAccessible* attribute in FM:*StructureInComposition* defines whether a form component is 'accessible' for the user, that is, whether the user is made aware of its existence and may know its values. Consider the example in Fig. 4.31 with questions from a 'mental status' questionnaire: Simple questions are asked and the participant's an-

swers compared to the correct responses in order to infer about the mental status of the participant. Evaluation of a completed form requires knowledge of the correct responses to each of its questions. These values may be 'stored' in FM:Fields via the FM:LocalPrepopulationAssignment mechanism. In this example, the information whether these 'correct response' FM:Fields were visible during form completion, is significant for the analysis of the resulting data.

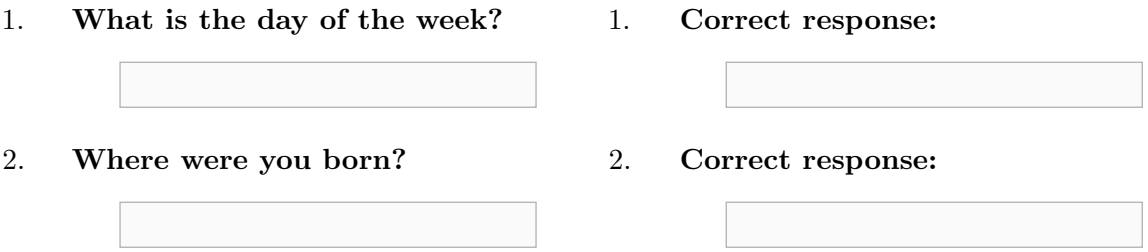

Figure 4.31.: Example questions from 'mental status' questionnaire. Each question field may be associated to a 'hidden' FM:Field (*isAccessible* = FALSE) that contains the correct response data.

Other situations where *isAccessible* may be used include automatic recording of additional information in digital forms, such as a user's 'IP-address', 'GEO-location' or the 'local time' when a form element was last modified. Such an attribute may also be added to ISO:*Form_Design_Element*.

ISO:Form_Design:*header* and ISO:Form_Design:*footer*, graphically accentuated parts of a form that appear on all its pages, have no correspondence in the Forms-Metamodel. Presentational 'mark-up' of included FM:*Structure* elements does not account for the role of 'header' and 'footer' as omnipresent context modifiers throughout a form specification. As such, the Forms-Metamodel should support this notion directly, not only through Form:*presentation*. Two optional references can be added to the FM:Form metaclass: Form:*header* and Form:*footer* to mark up any of the FM:StructureInComposition elements in the direct scope of FM:Form, Table A.7.

Reusability of Form Components The Forms-Metamodel aims to facilitate re-use of *Structure* elements in new contexts. The scope of variable references in functional dependencies, such as in *Constraint*s and LocalPrepopulationAssignments, is therefore limited in order to ensure portability of a form fragment into any larger data capture context. Similarly, the scope of variables in ISO:Local_Definition would need to be limited to the contained ISO:*Form_Design_Element*s and *rule*s be defined on the level of the 'parent' ISO:*Form_Design_Element* that contains all dependencies of the ISO:Local_Definition.

ISO/IEC 19763-13:2013 defines context-specific properties, such as *cardinality*, *question_number* or *section_number* and presentation information (*style*), on the level of the individual ISO:*Form_Design_Element*. If a specific ISO:*Form_Design_Element* is to be reused in a different ISO:Form_Design, these properties will likely require adaption. In the Forms-Metamodel, such allowed context-specific adaptions are modelled explicitly so that generic properties of the respective FM:*Structure* can be distinguised clearly from characteristics acquired in the specific usage context (FM:StructureInComposition). Transformation from

the Forms-Metamodel (FM:StructureInComposition) into the Forms-Metamodel-Template (FMT:*StructureInComposition*) corresponds to the derivation process into context-specific form elements, similar to ISO:*Form_Design_Element*s.

This approach works well for functional dependencies. FM:*InstructionElement*s, however, may have an additional semantic context dependency that cannot be modelled in this way. In particular the content of FM:StructureInComposition:*number* associations will change depending on the position of a FM:StructureInComposition within a form specification. It might therefore be preferable not to specify any *number* associations. If needed, a suitable numbering scheme could be inferred from FM:StructureComposition:*compositionType*, and the FM:LogicalHierarchy of a FM:Form. A StructureInComposition:*isNumbered* attribute might be needed to indicate whether a FM:StructureInComposition is to be numbered or not.

Annotation ISO/IEC 19763-13:2013 proposes two distinct types of model mappings, Metamodel Framework for Interoperability (MFI) mapping (ISO/IEC 19763-10:2013) and ISO:MDR_Mapping. Former defines relations between sets of MFI:Model_Elements, such as ISO:*Form_Design_Element*s. Latter defines sets of mappings with `MDR_ASSOCIATION_TYPE` between ISO11179:Data_Element (*data_element_identifier*) and ISO:Question_Element (*question_element_identifier*) pairs, as well as between ISO11179:Concept (*concept_identifier*) and ISO:Section_Element (*section_element_identifier*) pairs.

FM:*Annotation* provides similar mapping functionality. The Forms-Metamodel distinguishes annotations of *general validity* between FM:*Structure* elements (FM:StructureAnnotation) and annotations that only convey *context-specific* information between FM:StructureInComposition elements (FM:LocalAnnotation).

FM:StructureAnnotation allows the same relation types to be defined between FM:*Structure* elements that ISO/IEC 19763-10:2013 provides for mappings between ISO:*Form_Design_Element*s, Table A.2.

FM:LocalAnnotation adds an additional relation type that indicates 'semantic dependence' between annotation subject and annotation object. This may be used in cases similar to example Fig. 4.10 or in 'question piping', where the meaning of the annotation subject is defined by its usage context, specifically, another preceding form component.

FM:ExternalAnnotation is intended as more generic version of ISO:MDR_Mapping. It defines relations between any Forms-Metamodel component and some external concept, such as ISO11179:Data_Element or ISO11179:Concept from a Metadata Registry (MDR), or a concept from an external ontology. However, like ISO:Lookup_Field, the lookup mechanism for this model reference is not modelled in detail.

4.1.6. Summary

Based on a review of existing technologies and standards for form-based data capture, a metamodel for 'forms' was developed, supporting structural and behavioural composition of Data Capture Instruments (DCIs) from form components.

The Forms-Metamodel was shown to subsume all important features related to the generation of DCIs that are present in the form definition language of the OpenClinica Framework. Furthermore, the Forms-Metamodel allows a more fine-grained specification of constraints and intended form behaviour, compared to this domain-specific solution.

Comparison to ISO/IEC 19763, an upcoming meta-standard for form registration, confirmed the ability of the Forms-Metamodel to document the intended properties and behaviour of DCIs in an domain- and technology-independent way. While both metamodels were found to be mostly compatible in their documentation features, at the time of writing ISO/IEC 19763-13:2013 leaves important aspects of form logic and behaviour undefined. In particular, an expression language for the specification of constraints and a model for form behaviour were missing.

Both metamodels also differ in their approaches towards element reuse and compositionality: The Forms-Metamodel explicitly models the composition of form elements by reuse and context-specific modification of globally defined elements, according to specific rules that are defined as part of the Forms-Metamodel. The scope of ISO/IEC 19763-13:2013, on the other hand, is limited to the definition of single forms and their components. ISO/IEC 19763-13:2013 assumes the relations of form components to other existing form fragments to be documented by external annotations.

Detailed mapping rules across the components of the different metamodels were developed based on EMF implementations. They are documented in Appendix A.1, together with proposed improvements to both metamodels.

4.2. Metamodel for Markov Model-based Simulations

The development of a metamodel for Markov model-based health-economic assessments is motivated by the lack of open standards for the exchange of simulation specifications and the difficulty in documenting all assumptions relevant for the interpretation of simulation results. Section 4.2.1 proposes metamodels suitable for the specification and documentation of Markov models and their input parameters, as well as their use in Markov model-based simulation studies. An algorithm for the computation of simulation outputs is presented in Section 4.2.2. Section 4.2.3 validates the expressiveness of the proposed metamodels against existing studies in the field of Hadron Therapy and relevant reporting guidelines.

4.2.1. Metamodels

Metamodels for Markov models and Markov model simulations are presented in this section. Figure 4.32 shows the inheritance hierarchy of MarkovModel and *MarkovModelComponent*s, Fig. 4.32a, and their relations, Fig. 4.32b. The MarkovModel metaclass is derived from metaclasses that allow for the 'global' identification and definition of MarkovModel instances. As for *FormElement* in Section 4.1, inheritance from *NamedItem* and *IdentifiedItem* may be replaced by metaclasses of a suitable model registration metamodel. *MarkovModelComponent*s are attached to every MarkovModel and uniquely identifiable within the scope of this MarkovModel by their *localID*. *MarkovModelComponent*s represent the elements of Markov models, as introduced in the previous Section 3.3.2.2. Every State is characterised by one of three different StateTypes, as well as its associated *PayOff*s which represent Cost and Utility measures.

Transitions connect one *sourceState* to one *targetState* and assign a TransitionProbability to this connection. *PayOff*s may also be associated to Transitions. The components shown

in Fig. 4.32b define the structural aspects of the Markov model which are typically transferable between contexts. The values assigned as utility and cost measures, as well as the values of transition probabilities, however, tend to vary across population groups, treatment strategies and jurisdictions. *PayOff* and TransitionProbability are therefore classified as *CohortSpecificValue* that allows multiple 'cohort-specific' values to be associated to any of its instances. CohortValueSet represents this association between a Cohort and a *Value*. A Cohort, for the purpose of MarkovModel, represents the population group for which certain *Value*s apply. Its members share epidemiological and medical characteristics and undergo sufficiently similar medical interventions in comparable localities, so that the same transition probability, utility and cost values are applicable to all of them.

*Value*s are considered globally identifiable items, just like MarkovModels. They may represent constant *Estimate*s, Fig. 4.33, for some model parameter, such as the cost associated to a particular treatment, or the probability for developing a certain late side effect. However, some modelling contexts, for example related to mortality risks, demand time-dependency of model parameters to be taken into account. The properties of *Estimate* are covered in more detail in Section 4.2.2, Fig. 4.36.

TimeDependentValue allows for ValidityIntervals to be defined that associate an Estimate to the time interval (*validFrom*, *validUntil*) during which it is valid. Multiple Estimates can thus be combined. Any definition of time-dependency requires a reference point in time from which on the dependency of a parameter may be measured. TimeDependentValue assumes this reference point to be the beginning of the simulation, cycle 0. The metamodel foresees a sub-type of TimeDependentValue, AgeDependentValue where the reference point is the birth of a person and time-dependency is expressed in terms of a person's age. If required, TimeDependentValue could be generalised by allowing a specific reference point to be selected from predefined options. However, the metamodel presented in Fig. 4.33 proved sufficiently expressive for the Cost-Effectiveness Analyses (CEAs) that have been considered, compare Section 4.2.3.

MarkovModelSimulation (MMS), Fig. 4.34 provides the framework for simulating multiple existing MarkovModels and for comparing the results of different Cohorts. For clarity, metaclasses that form part of the MarkovModel metamodel are prefixed 'MM:' in the following. Figure 4.34a shows the inheritance of *MarkovModelSimulationComponent*s and Fig. 4.34b their relations.

Like MM:MarkovModel, instances of MarkovModelSimulation may be registered in a model registry. MarkovModelSimulation contains two types of components, MarkovModelReference and SimulationCohort.

MarkovModelReferences are used for pooling existing MM:MarkovModel instances and for defining their role and parameters within a MarkovModelSimulation.

The MarkovModelReference metaclass specifies the *numberOfCycles* that a referenced Markov model has to be run, the StateStartPopulation of its states and the cohort to be used in the simulation. The *targetStateRef* of StateStartPopulation identifies the MM:State of the referenced Markov model that is to be populated. Its *startPopulation* may be defined in terms of a specific *value* (PopulationValue) or in terms of the result of a previous simulation (PopulationValueFromSimulation). In latter case, one or more *sourceStateRef*s map the population of one or more Markov model states into a single state of the current Markov model.

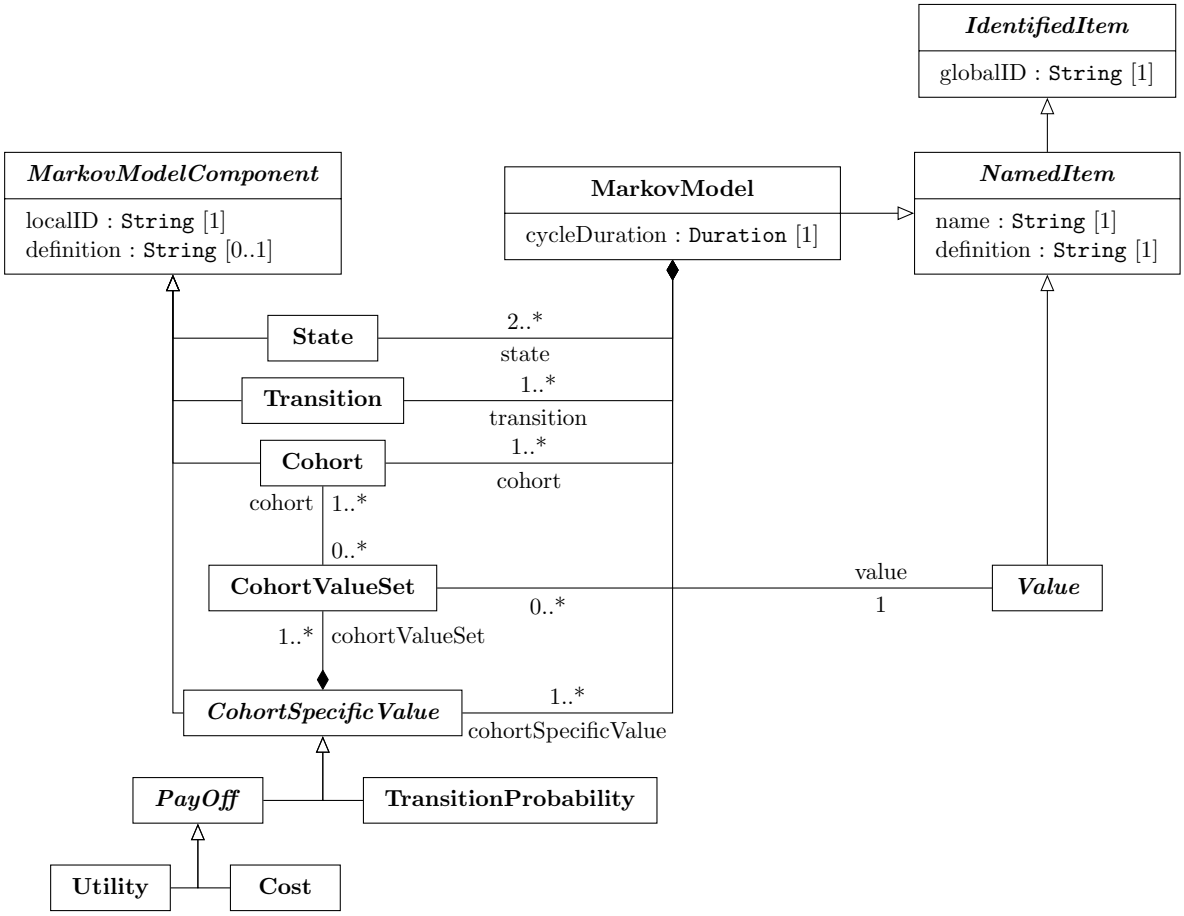

(a) MarkovModel and *MarkovModelComponent* inheritance.

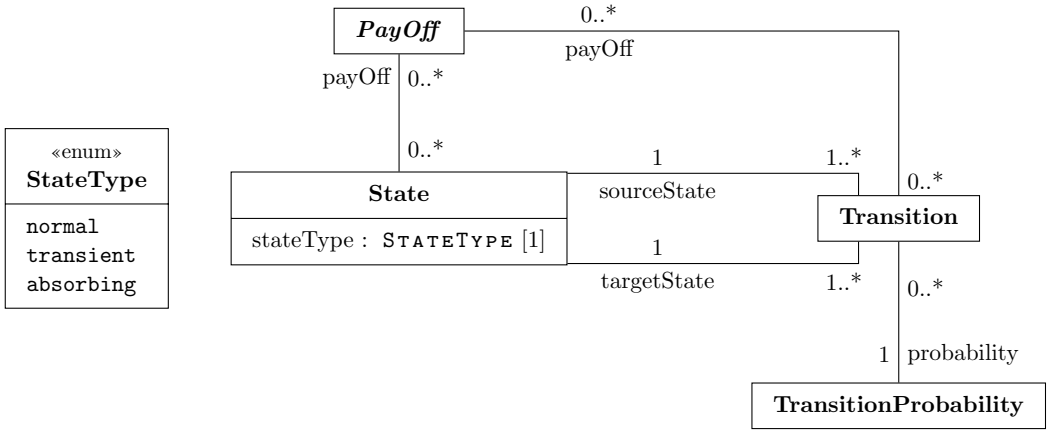

(b) Relations among *MarkovModelComponent*s.

Figure 4.32.: Markov model metaclasses MarkovModel and *MarkovModelComponent* (a), and relations among its specialisations (b).

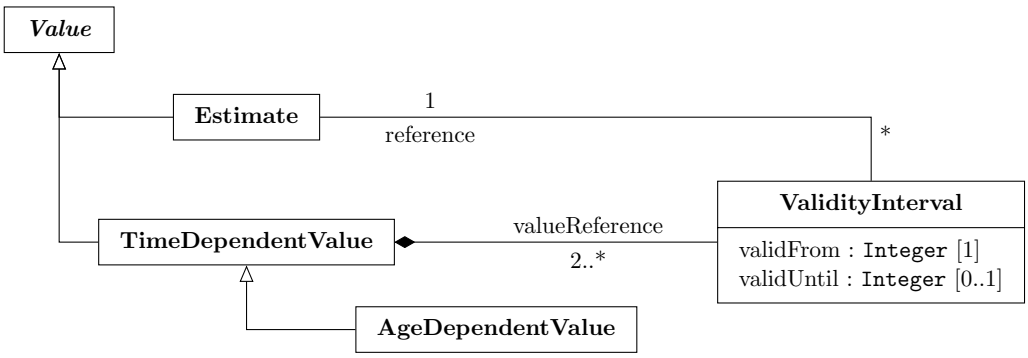

Figure 4.33.: Markov model simulation metaclass *Value*.

Multiple included MM:MarkovModel instances will use different names or identifiers for their MM:Cohort instances and not all defined cohorts may be relevant for a particular Markov model simulation. In order to select the subset of MM:Cohort instances relevant for the simulation, MarkovModelSimulation specifies its own SimulationCohorts and allows instances of MM:Cohort to be mapped to one of those.

Necessity and usage of attributes *halfCycleCorrection* and *evaluationType*, linked to MarkovModelSimulation, and *initialAge*, linked to SimulationCohort will be shown in the following section.

4.2.2. Computational Model and Outputs

This sections presents an algorithm for the computation of simulation outputs based on the parameters defined by MarkovModel and MarkovModelSimulation metaclasses.

The flow-chart in Fig. 4.35 summarises the computation process and the inputs and outputs involved. It divides the process into three major steps: The right-most column specifies the computation steps for the evaluation of a single Markov model. Multiple such evaluations may be chained to obtain combined outcome measures, centre column. A Markov model simulation computes these combined outcome measures for multiple SimulationCohorts in order to allow for inter-comparisons. The individual process steps and their relations to the Markov model and Markov model simulation metaclasses are defined in the following.

4.2.2.1. Markov Model

Assume an instance of MarkovModel MM with s states $S_1, \ldots, S_s$ (instances of State) and $s \times s = s^2$ possible transitions $T_{11}, \ldots, T_{ij}, \ldots, T_{ss}$ (instances of Transition) between *sourceState* S_i and *targetState* S_j. Every transition T_{ij} may occur with its associated transition probability p_{ij} (instance of TransitionProbability). This defines the structure of MM and its cohort-specific transition probabilities.

Multiple measures for cost $c_{i,1}, \ldots, c_{i,k}$ (instances of Cost) and utility $u_{i,1}, \ldots, u_{i,k}$ (instances of Utility) can be associated to every state S_i. Only cost values may be associated to transitions $T_{i,j}$: $c_{ij,1}, \ldots, c_{ij,k}$, since utilities characterise health states, not medical events.

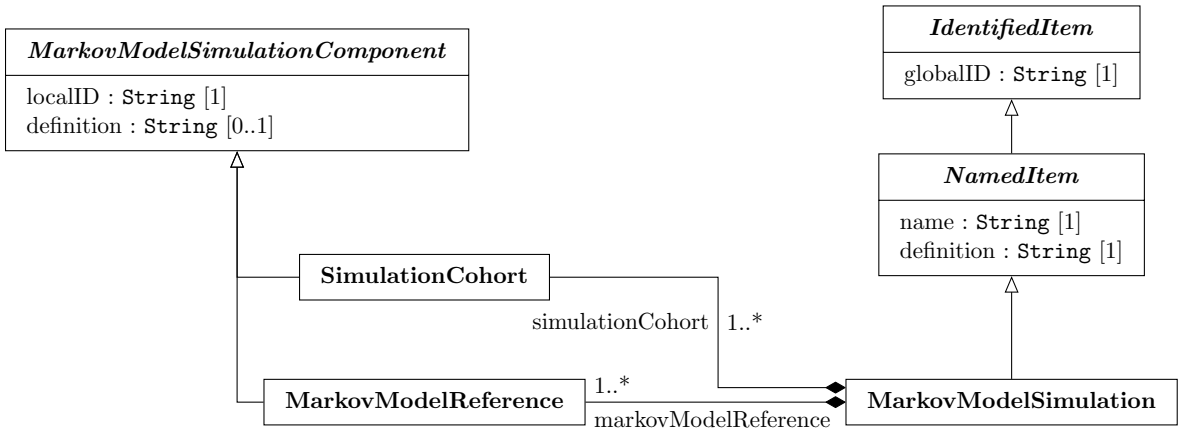

(a) MarkovModelSimulation and *MarkovModelSimulationComponent* inheritance.

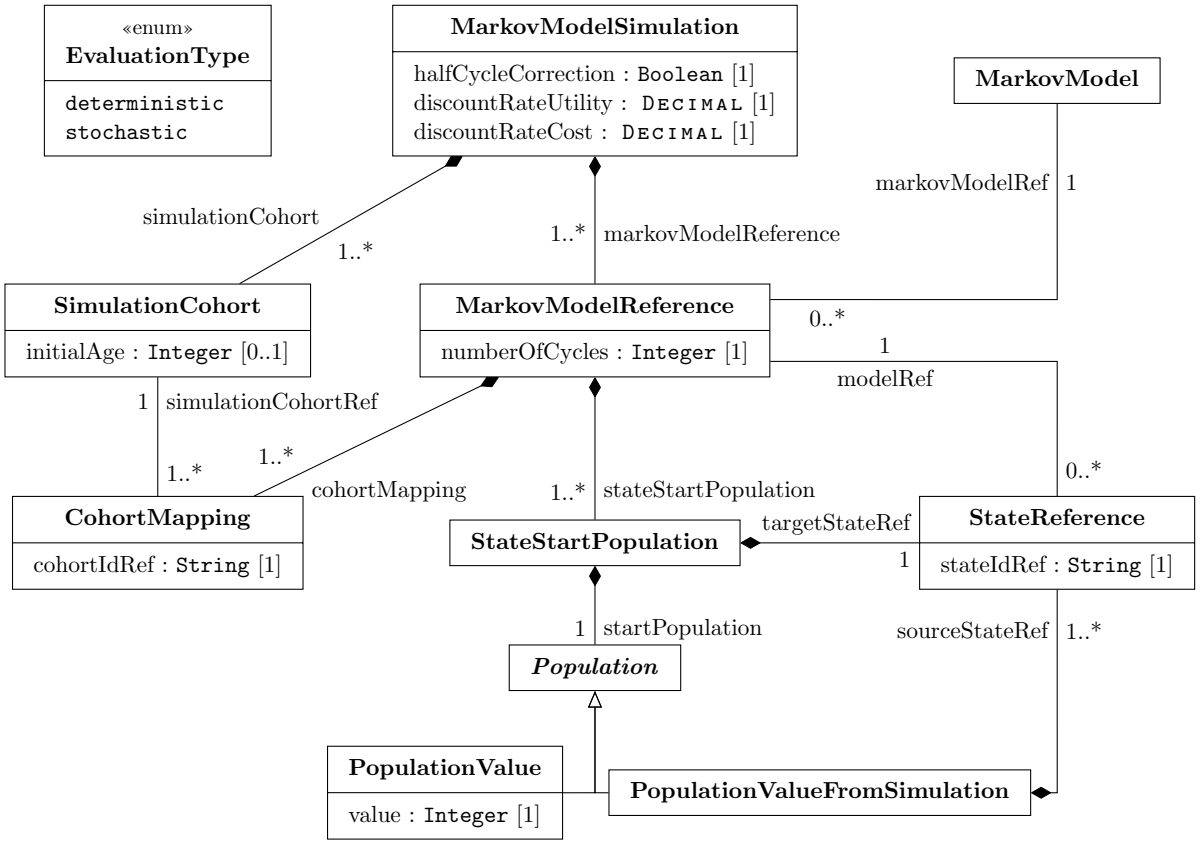

(b) MarkovModelSimulation.

Figure 4.34.: Markov model simulation metaclasses MarkovModelSimulation and *MarkovModelSimulationComponent* (a), and relations among its specialisations (b).

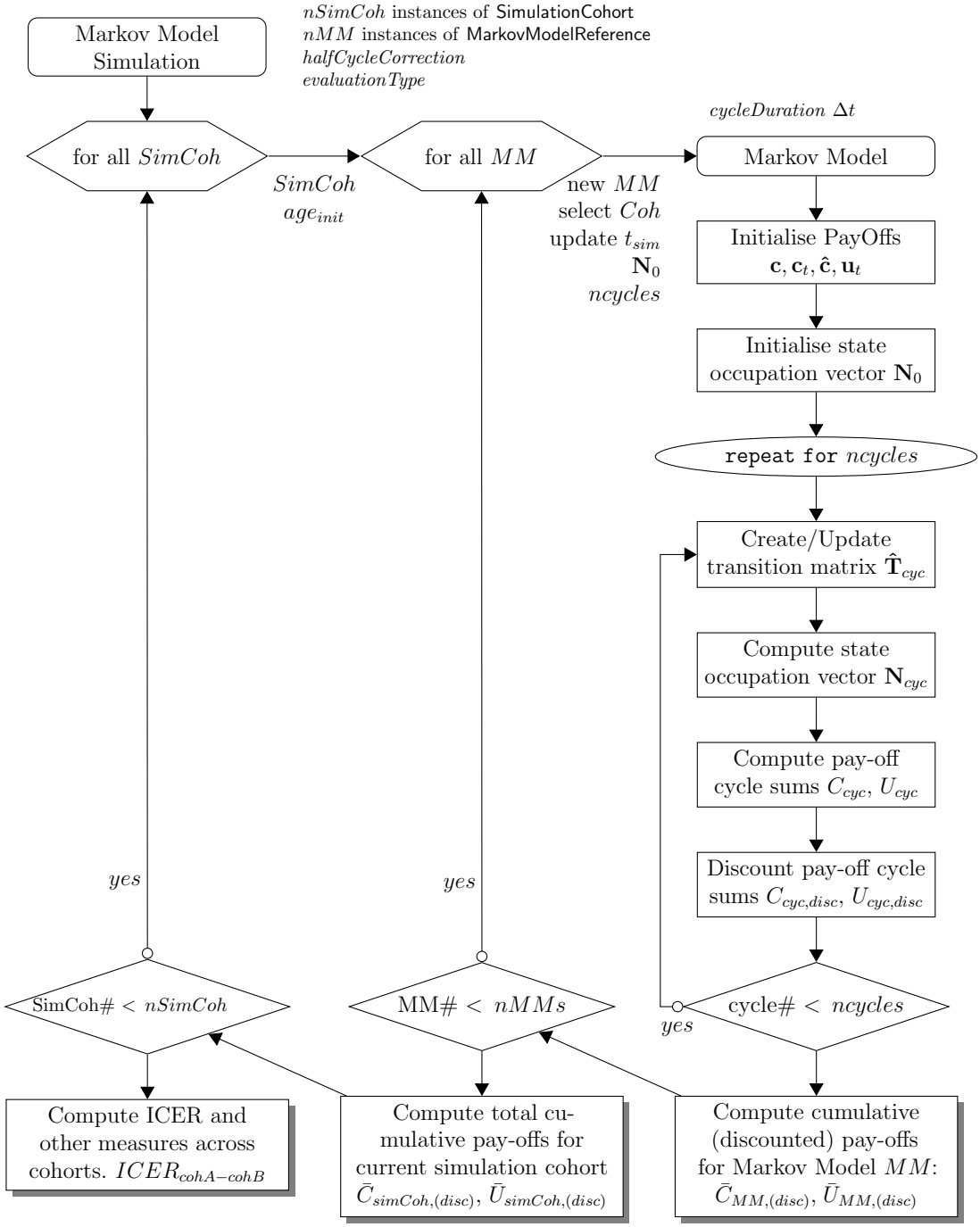

Figure 4.35.: Algorithm for the computation of Markov model simulations based on information expressed by MarkovModelSimulation and MarkovModel metamodels.

The Markov model allows transition probabilities, as well as cost and utilities to be defined as time-dependent values. However, explicit time-dependency is more likely to be used for transition probabilities. The algorithm therefore assumes utility and cost values to be constant. If time-dependency for these values is important, they need to be reinitialised in every Markov cycle, in the same way as transition probabilities.

The evaluation of the Markov model in Fig. 4.35 begins with the initialisation of (constant) pay-off values associated to states and transitions. Values may only be initialised with respect to a MM:Cohort. The following computational steps therefore assume a specific cohort *Coh* to be selected.

Since computation follows discrete time steps of *cycleDuration* Δt, one-off cost values of dimension [*money*] and of dimension [*money*]/[*time*] require separate treatment. Utility values are typically quantified in terms of Quality-Adjusted Life Years (QALYs)/[*time*]. These can be identified based on the UnitOfMeasure associated with any *Estimate*, Fig. 4.36.

The following naming convention is used throughout the remainder of this section: $\mathbf{c}_t = (\bar{c}_1, \ldots, \bar{c}_i, \ldots, \bar{c}_s)$, with $\bar{c}_i = \sum_k c_{i,k}$ and $c_{i,k}$ of dimension [*money*]/[*time*], indicates the cycle-length dependent cost contributions associated to all states; $\mathbf{c}$, indicates the constant cost contributions with dimension [*money*]. Similarly for utilities, $\mathbf{u}_t = (\bar{u}_1, \ldots, \bar{u}_i, \ldots, \bar{u}_s)$, with $\bar{u}_i = \sum_k u_{i,k}$ indicates the cycle-length dependent utility contributions associated to all states. Costs associated to transitions must not depend on the cycle length. They may be expressed as a 'transition-cost matrix' $\hat{\mathbf{c}}$ with entries $\bar{c}_{ij} = \sum_k c_{ij,k}$.

State occupation, the number of individuals or proportion of the cohort, in each state of the model, $N_1, \ldots, N_i, \ldots, N_s$ evolves over time, with every Δt increment. The 'state occupation vector' $\mathbf{N}_{cyc} = (N_{1,cyc}, \ldots, N_{i,cyc}, \ldots, N_{s,cyc})$ represents the state occupation for any given cycle *cyc*.

Assuming the general case of a Semi-Markov model, probability parameters may be time-dependent and the following computation steps must be repeated for every cycle, until a termination condition is fulfilled. Typically, evaluation stops when the maximum number of cycles, *ncycles*, specified by MMS:MarkovModelReference:*numberOfCycles*, has been reached.

An initial transition matrix, $\hat{\mathbf{T}}_{cyc=1}$ with entries $p_{ij,cyc=1}$ has to be created, and needs to be updated in every subsequent cycle to account for time-dependency of probability values. Selection of the correct probability value requires knowledge of the reference point relative to which the ValidityIntervals of the time-dependent probability values are defined: the simulated time t_{sim} that passed since the start of the simulation, or the current average age of the cohort *age*. Former is given by the product of current cycle number *cyc* and the cycle length Δt, latter by the sum of t_{sim} and the cohort's initial age age_{init} at the beginning of the evaluation.

The Markov model requires the StateType of every State to be defined. This provides an alternative definition of the transition probabilities p_{ii}, the probability for staying in S_i, which facilitates model specification, particularly for time-dependent probabilities. For the total population to be conserved throughout the simulation, values in a probability vector must sum to 1. This allows the following rules to be applied for

the computation of p_{ii} in dependence of the *stateType* of S_i:

$$\begin{array}{lrcl} \texttt{normal}: & p_{ii} & = & 1 - \sum_j p_{ij} \\ \texttt{transient}: & p_{ii} & = & 0 \\ \texttt{absorbing}: & p_{ii} & = & 1\,. \end{array} \tag{4.4}$$

In the first cycle, the initial state occupation vector $\mathbf{N}_0$ is updated to $\mathbf{N}_1$ by multiplication with transition probability matrix $\hat{\mathbf{T}}_1$, or generally for subsequent cycles[2]:

$$\mathbf{N}_{cyc} = \mathbf{N}_{cyc-1} \cdot \hat{\mathbf{T}}_{cyc}\,. \tag{4.5}$$

The increment in utility U_{cyc} and cost C_{cyc} accrued in any simulation step is referred to as the 'cycle sum'. For pay-offs related to states, it can be computed from the updated state population vector $\mathbf{N}_{cyc}$, Eq. 4.6a and 4.6b. Cost measures associated to transitions have to be evaluated based on the population proportion that underwent the transition T_{ij} in a given cycle, Eq. 4.6c. They are then assigned to the respective target state S_j of the transition, Eq. 4.6d:

$$U_{cyc} = \mathbf{N}_{cyc} \cdot \mathbf{u}_t \Delta t \tag{4.6a}$$

$$C_{cyc,\text{states}} = \mathbf{N}_{cyc} \cdot (\mathbf{c}_t \Delta t + \mathbf{c}) \tag{4.6b}$$

$$C_{cyc,\text{transitions}} = \sum_j \sum_i p_{ij,cyc} N_{i,cyc-1} \bar{c}_{ij} \tag{4.6c}$$

$$C_{cyc} = C_{cyc,\text{states}} + C_{cyc,\text{transitions}}\,. \tag{4.6d}$$

In order to reflect the depreciation of pay-offs over time, utilities U_{cyc} and costs C_{cyc} collected in every cycle may be discounted at individual (yearly) discount rates $r_{utility}$ and r_{cost}, yielding the 'discounted cycle sum':

$$U_{cyc,disc} = \frac{U_{cyc}}{(1 + r_{utility})^{t_{sim}}} \tag{4.7a}$$

$$C_{cyc,disc} = \frac{C_{cyc}}{(1 + r_{cost})^{t_{sim}}}\,, \tag{4.7b}$$

where t_{sim} corresponds to the simulated time-span (in years) that has passed when reaching cycle *cyc* of the current Markov model MM.

This process is repeated until the termination condition is fulfilled and the final state population vector $N_{ncycles}$ has been reached. Pay-off sums U_{cyc} and C_{cyc} are retained for every cycle so that the 'cumulative' utility $\bar{U}_{MM}$ and cost $\bar{C}_{MM}$ can be computed for the

[2]This representation assumes 'right stochastic matrices' with row vectors as probabilities; p_{ij} thus represents the probability of moving from state i into state j and $\sum_j p_{ij} = 1$.

simulated Markov model MM:

$$\bar{U}_{MM} = \sum_{cyc}^{ncycles} U_{cyc} \tag{4.8a}$$

$$\bar{C}_{MM} = \sum_{cyc}^{ncycles} C_{cyc}\,, \tag{4.8b}$$

and likewise for the discounted cumulative pay-offs $\bar{U}_{MM,disc}$ and $\bar{C}_{MM,disc}$.

4.2.2.2. Chained Markov Models

The start population $\mathbf{N}_0$ for a given Markov model MM may need to be determined on the basis of a a prior decision process, including initial costs and utilities. The Markov model simulation metamodel defines a generic way to express these initial conditions: Multiple Markov models $MM_1, \ldots, MM_{nMM}$ may be included in a single MarkovModelSimulation by means of MarkovModelReference. The simulation steps described in the previous section are repeated for all Markov models $MM_1, \ldots, MM_m$. MarkovModelReference specifies the cohorts relevant for the evaluation of each of these Markov models through CohortMapping: This provides a way to 'bind' the cohorts defined in distinct Markov models to a simulation cohort defined in Markov model simulation. For example, the current simulation cohort $simCoh$ 'CRT' may be mapped to cohort Coh 'CR' for the current Markov model MM_i and to cohort 'ConventionalRadiotherapy' in the following Markov model MM_{i+1}. MarkovModelReference also defines the *numberOfCycles* over which the respective Markov model is to be simulated.

Parameters are exchanged between consecutively evaluated Markov models. The final state occupation vector $\mathbf{N}_{ncycles,MM_{i-1}}$ resulting from evaluation of MM_{i-1} is mapped into states of MM_i and forms its initial state occupation vector $\mathbf{N}_{0,MM_i}$. For example, the population of states 'treatment-related death' and 'death - other causes' in MM_{i-1} may both be mapped into state 'dead' in MM_i.

Also, the overall simulation time t_{sim} at the end of evaluation of MM_{i-1} needs to be transferred to MM_i, in order for the cohort age to be computed (for AgeDependentValues) and for discount rates to be applied correctly in subsequent Markov models.

After simulation of all nMM Markov models, the total (discounted) cumulative pay-off for a given simulation cohort $\bar{U}_{simCohort}$ and $\bar{C}_{simCohort}$ can be computed from the individual (discounted) cumulative pay-offs resulting from each of the nMM Markov model evaluations:

$$\bar{U}_{simCohort,(disc)} = \sum_{MM}^{nMM} \bar{U}_{MM,(disc)} \tag{4.9a}$$

$$\bar{C}_{simCohort,(disc)} = \sum_{MM}^{nMM} \bar{C}_{MM,(disc)}\,. \tag{4.9b}$$

4.2.2.3. Markov Model Simulation

Above computations are repeated for all *nSimCoh* SimulationCohort instances specified by the Markov model simulation. This results in cumulative cost and utility estimates, Eq. 4.9 for all simulation cohorts, from which further estimates for health economic decision making can be derived.

The *initialAge* specified by each simulation cohort is used to compute the cohort *age* in each Markov model based on the total accumulated simulation time t_{sim}.

MarkovModelSimulation further specifies attributes *evaluationType*, *halfCycleCorrection*, *discountRateCost* and *discountRateUtility*. The latter two have already been introduced in the previous section.

State occupation in discrete-time Markov processes is evaluated either at the beginning or at the end of each cycle. Depending on the cycle duration and overall simulation time of the model, this may lead to over- or under-estimation of state membership at any cycle and thus to over- or under-estimation of the outcome measures. So-called 'half-cycle correction' is a computational mechanism that (approximately) corrects for this effect.

Depending on the `EVALUATIONTYPE` of the Markov model simulation, costs, utilities and transition probabilities are based on fixed value estimates or may be drawn from a parameter distribution that accounts for the variability of the underlying measure.

Figure 4.36 shows the metamodel proposed for the specification of *Estimate*s.

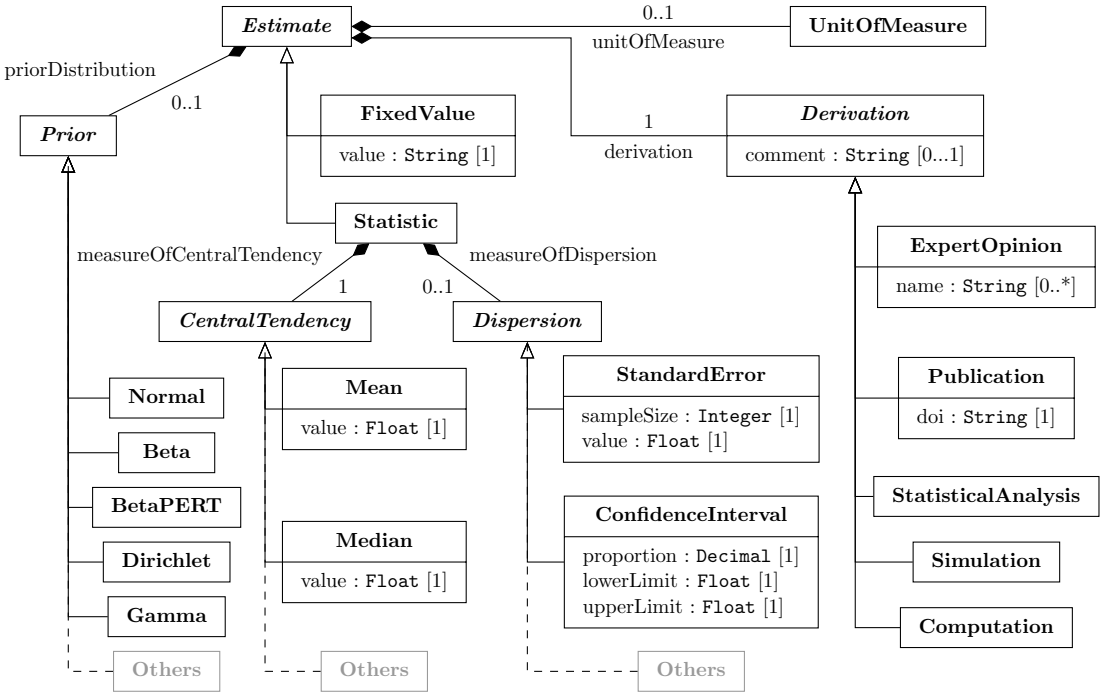

Figure 4.36.: Metamodel for Estimates used in Markov models.

Deterministic estimation uses a fixed estimate, such as the *value* attribute of FixedValue, or the *measureOfCentralTendency* of a Statistic.

Probabilistic computation uses parameter values, randomly drawn from suitable probability distributions. This probability distribution corresponds to the 'conjugate prior' distribution of the likelihood distribution of the random variable whose measurement is

reported as *Estimate*. Since prior distributions and their parameters are directly linked to the data from which an *Estimate* has been derived, Prior is modelled as a property of *Estimate* in Fig. 4.36. Guidance on the choice of suitable prior distributions for different types of data and the derivation of distribution parameters is given in [158].

4.2.2.4. Simulation-based Health-Economic Assessment

The outputs of Markov model simulations may be interpreted in the context of a health-economic assessment. The metamodel shown in Fig. 4.37 illustrates aspects of this context for the following discussion.

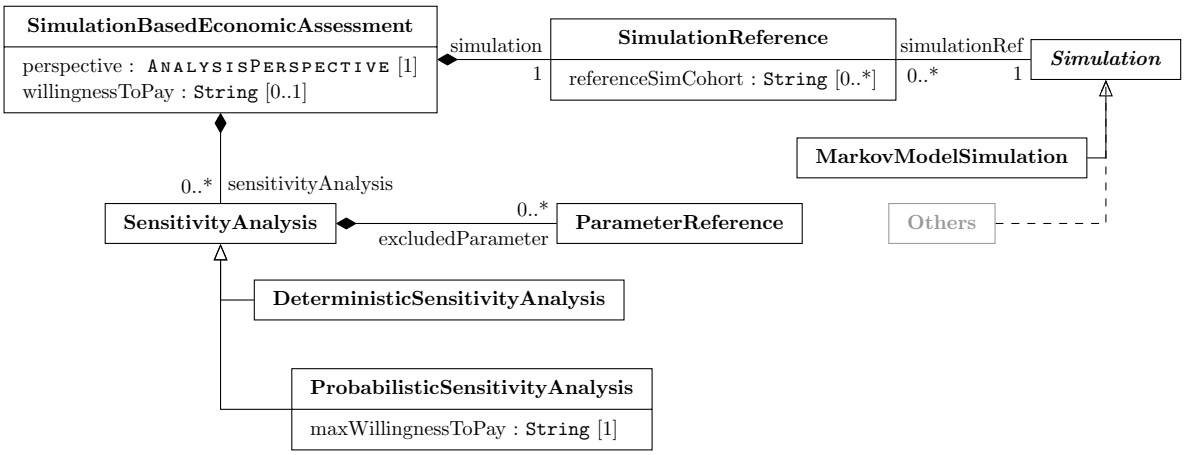

Figure 4.37.: Metamodel of usage context of Markov model simulation for simulation-based health-economic assessments.

.

Cost-Benefit Analysis (CBA) investigates differences between treatment options, typically between a new therapy T_1 versus an established alternative T_0. The outputs $\bar{U}_{simCohort}$, and $\bar{U}_{simCohort}$, Eq. 4.9, of multiple simulation cohorts in a Markov model simulation provide the data necessary for the evaluation of relative costs $\Delta C = C_1 - C_0$ and benefits $\Delta U = U_1 - U_0$ between those treatment options. Multiple *referenceSimCohort*s for a given *Simulation* may be specified as 'established alternatives' against which the remaining simulation cohorts are to be compared.

Results of costs and benefits are often illustrated in so-called 'cost-effectiveness' plane diagrams [159], where the abscissa indicates the difference in cost and the ordinate the difference in effectiveness between test and reference strategy. Incremetal Cost-Effectiveness Ratio (ICER), the ratio of relative costs and relative benefits $\Delta C/\Delta U$ is reported as a measure of cost effectiveness for therapy options that are potentially acceptable. This is the case when the new treatment is either less costly and less efficient or more costly and more efficient than the alternative, corresponding to the first and third quadrant in the 'cost-effectiveness' plane. In these cases, a decision about acceptance of the test-technology can only be made based on an assumption about the Willingness-To-Pay (WTP) for the improvement in outcome. WTP is typically measured in dimensions $[outcome]/[money]$and defines an upper threshold on the ICER between two treatments. If the ICER of the test-treatment lies below this threshold, the treatment would be

considered cost-effective. In principle, such a decision could be based on a single ICER estimate as obtained from the data of a single evaluation of Markov model simulation.

However, the model structure and its parameters are subject to uncertainties that may influence the outcome of the decision analysis [160]. The context metamodel in Fig. 4.37 only considers 'parameter uncertainty'. Two types of sensitivity analysis are typically performed to represent the impact of parameter uncertainty [161]:

In Deterministic Sensitivity Analysis (DSA) a single, or multiple, input parameters are varied over a justifiable range and the influence of this variation on the outcome measures, is quantified. In Probabilistic Sensitivity Analysis (PSA), the uncertainty in model parameters is represented by probability distributions, and all parameters are varied simultaneously. Due to the use of prior distributions, this is also considered 'a bayesian approach to sensitivity analysis' [158]. Model outputs are replicated in multiple repetitions, each using a distinct set of probabilistically determined input parameters and yielding different cost and utility outputs.

The effect of this variability on decision making depends on the WTP. Several techniques were developed to interpret the effect of uncertainty on decision making. Commonly reported is the so-called Cost-Effectiveness Acceptability Curve (CEAC) [162, 163]:

For every individual outcome of a PSA, the most cost-effective therapy option is determined in function of the WTP, for example by employing the 'net benefit approach' [164]. It allows costs and effects to be converted into the same unit, for a given WTP, so that the treatment with the maximum net benefit can be selected. Repeating this evaluation over a range of WTP values indicates the treatment option that is 'most-likely' to be cost-effective, under the assumption of a certain WTP.

A further commonly reported measure is the Expected Value of Perfect Information (EVPI) [165]. It measures the 'expected value of future research', based on the average opportunity loss that would be caused if the decision derived from PSA was mistaken. This analysis may be performed on all parameters at once or on single parameters or parameter groups individually in order to identify research priorities.

4.2.3. Validation

No open standard for the specification and documentation of Markov models was available for comparison and evaluation of the metamodels presented in Section 4.2.1. Markov model and Markov model simulation metamodels were therefore assessed by their ability to specify the parameters used in Markov model-based health-economic evaluations, and by how well they support the documentation of health-economic studies as recommended by reporting guidelines.

4.2.3.1. Specification of Health-Economic Modelling Studies

The metamodels proposed in Section 4.2.1 were tested on health economic analyses in Hadron Therapy (HT): The study characteristics of [84] (base-case analysis) were fully implemented as instances of Markov model simulation and Markov models. Further Markov model-based studies [80–83] were tested for compatibility with the metamodels.

Studies [80, 81, 83] compare different treatment modalities for a single tumour type, and [82, 84] additionally differentiate multiple tumour types or disease stages. Due to

differences in transition probabilities, costs and utility, each combination 'treatment type - medical condition' is represented by a dedicated instance of MM:Cohort.

In all studies initial costs, determined by treatment modality and medical condition, are applied to each of these cohorts. Initial costs can be expressed in the MarkovModel by introducing an initial state that represents the patient cohort in cycle $cyc = 0$, directly after treatment, and assigning cohort-dependent treatment costs to *each* of its outgoing transitions. To ensure that patients leave the state, this state must be 'transient', and cannot be repopulated, that is, have no incoming transitions. The model used in [83] sends patients through a 'post-treatment' state. It is not clear whether this choice is medically motivated, or necessary due to a limitation of the simulation software in attributing cost measures to transitions. Assigning 'initial costs' to each cohort might be more convenient than the assignment to transitions. The MarkovModel metaclass could be easily extended to support this pattern.

The simulation in [84] is divided into two phases, where the first phase corresponds to one single evaluation of transition probabilities (one Markov cycle) that determines additional initial costs and the state distribution for the second simulation phase. Since both phases use different cycle durations (6 months and 1 year), two instances of MarkovModel need to be created, each corresponding to one of the simulation phases. Both Markov models can then be combined in one Markov model simulation, as described in Section 4.2.1.

All studies use cost and either 'life years' or QALYs as outcome measures. Computation of 'life years' does not require additional input to the Markov model. However, for its computation the simulation code must recognise the states that do not count towards the cumulative life-time. For the reviewed models, recognition of 'absorbing states' as 'death states' is sufficient. Wider application of the MarkovModel metamodel may require introduction of an additional State attribute that indicates whether time spent in the particular state should be excluded from accounting.

Pay-off values are specified either with their *prior* distribution, if probabilistic sensitivity analysis is to be carried out, or with a range around which the value is to be varied in deterministic (one- or multi way) sensitivity analysis. Former is supported by *Estimate* as in Fig. 4.36, support for latter may be added by specifying the VariabilityRange linked to *Estimate* with attributes *lowerLimit* and *upperLimit*.

An interesting question is whether the overall run-time of the simulation should be considered a property of Markov model or of the Markov model simulation. The reviewed studies do not have to make this distinction as they create a dedicated model structure for their specific analysis. If however, existing model structures are to be reused, this question arises. The proposed metamodels attribute the overall run-time of a given MarkovModel to the MarkovModelSimulation in which it is embedded (MMS:MarkovModelReference:-*numberOfCycles*). This allows the run-time of a Markov model, potentially designed to simulate the full lifetime of a cohort, to be restricted and to be replaced by a second (third, fourth, etc.) model that better represents the conditions of the aged patient cohort. Such execution of multiple Markov models in succession must be supported by their *Values*, in particular, TimeDependentValues need to cover the relevant simulation time periods and ages of the patient cohort. Time periods during which an event may *not* occur, need to be explicitly specified with *zero* transition probability. For example 'cardiac events' in [81] are assumed to occur *starting from* 10 years after treatment and

then throughout lifetime, or in [80] 'all episodes of hypothyroidism[3]' were assumed to occur *within* the first four years after the primary diagnosis.

Time-dependent costs are used by [80] to represent the loss of earnings over lifetime, between age of 20 to 65. The Markov model supports time-dependency of all values, however, the algorithm, Section 4.2.2, assumes utility and cost values to be time-independent. To account for time-dependency, the algorithm may be generalised by moving initialisation of utility and cost vector into the *cycle repetition* loop.

An example for multiple transitions ('normal death', 'death from cancer', 'death from adverse events') leading into the same state ('death') is given in [82]. This is a convenient way of modelling situations where transition probabilities are available as 'excess-rates', such as a disease-specific mortality in 'excess' of the age-dependent mortality of the healthy population, or when different costs are associated to these transitions. While the MarkovModel only allows one TransitionProbability per Transition, it does not exclude multiple transitions to be declared between the same source and target states. The computational algorithm, however, assumes *not more than one* such transition to be defined. Computations of transition costs and of total transition probability could be adapted to support computation of more than one transition between the same source and target state, or instead, one absorbing target state could be defined for every transition.

Costs are typically composed of 'unit costs', specifying the price of a single unit, and 'resource use' specifying the number of units required per intervention or time. Additionally, certain costs may only be considered applicable to a portion of the population in a certain state. For example, in [84], patients who suffer from 'acute pneumonitis $\leq$ grade 3' may, with a certain probability, be admitted to hospital for a certain 'number of days' and a certain 'cost per day'. From these numbers the total average cost of being in the state can readily be computed.

MarkovModel considers 'unit costs', 'resource use' and 'applicable proportion' part of the *Derivation* information of an *Estimate* and only includes the resulting average cost explicitly as *Value*. Each of the individual items can be described as distinct *Estimate* themselves and the average cost be considered as 'derived from' a Computation of these values. However, this modelling approach raises the question how uncertainty of the combined value should be determined. The value of each individual component is uncertain, with parameter range or suitable prior distribution specified. To compute variability of the average value, the simulation engine would need to recognise the specified cost *Value* as a computation of individual values and then either determine an 'average' range or prior for this new statistic, or evaluate the Computation, with uncertain *Estimate*s, each time the cost value is drawn.

Additionally, use of 'historic' cost values, or values in different currencies, requires their current value to be projected and transferred into the reference currency of the study. Standard methods and information sources exist for such transformations and their application to cost *Value*s can be modelled. The derivation of a suitable metamodel for these transformations, however, is not part of this thesis.

All studies report incremental cost and utility, as well as ICER between test treatments and established alternative. Deterministic sensitivity analysis is performed in [80–82], probabilistic sensitivity analysis in [83, 84]. Only [84] reports CEACs and EVPI in

[3] A common endocrine disorder in which the thyroid gland does not produce enough thyroid hormones.

dependence on the WTP.

4.2.3.2. Reporting Requirements

Substantial literature exists on the reporting and design of economic evaluations in health care. Recently, these guidelines have been reviewed [122] and summarised in a checklist of 24 items to be included when reporting economic evaluations of health interventions [94]. While these guidelines were elaborated with publication-based reporting in mind, they do summarise the information that is considered essential for identification, interpretation and reproducibility of health-economic analyses.

The degree to which instances of the proposed metamodels provide the recommended information is analysed below, following the classification of [122].

Title & abstract, Introduction Recommendations related to 'Title & Abstract' and 'Introduction' aim at ensuring identifiability of health-economic evaluations among other articles, and availability of a succinct but comprehensive summary, as well as background information. Instances of MarkovModel and *MarkovModelSimulation* registered by a model registry are readily identifiable, and detectable with the help of annotation and classification schemes.

Methods - General 'Target population and subgroups' investigated, the 'setting and location' in which the analysis is undertaken and the 'comparators', that is the interventions or strategies under comparison, any combination of these characteristics is represented by an instance of MM:Cohort. Details about their properties may be documented by MM:*MarkovModelComponent*:*definition*, or dedicated reporting slots for each of these characteristics may be added to MM:Cohort. 'Time horizon' and 'discount rate' are documented as part of MarkovModelSimulation. The 'perspective' chosen for the analysis determines the costs considered. As such, it may be documented within the scope of a MarkovModel.

Methods - Outcomes & Costs The 'choice of outcomes' is limited by MarkovModel to cost, life time and utility. Methods used for identifying suitable studies for the computation of model parameters ('synthesis-based estimates' of outcomes and costs, as well as 'preference-based outcomes') and the methods of their computation are not documented as part of MarkovModel. However, since the *Derivation* of every input parameter is documented, this information can be obtained by analysing the *Value*s used.

Methods - Model Based Economic Evaluations The 'choice of model' is limited to Markov model as one subtype of possible modelling structures, and its 'model assumptions', such as states and transitions, are documented by MarkovModel.

Methods - Analytical Methods 'Analytic methods' used in the derivation of model input parameters are not directly documented by MarkovModel, but through the *Derivation* of *Estimate*s. 'Study parameters' themselves, such as values, ranges and prior probability distributions, are specified as instances of *Estimate*. Methods for the 'characterisation of model uncertainty' are considered separate from the model itself. They are represented by a distinct metamodel that defines the interpretation

of a Markov model simulation in the context of health-economic assessments, see Fig. 4.37. The combination of this metamodel with MarkovModelSimulation allows the type of sensitivity analysis performed, as well as its results, to be documented. Subgroup analysis for the 'characterisation of heterogeneity' may be part of this model, however, Fig. 4.37 does not aim to be comprehensive in this regard.

Discussion 'Study findings' may either be documented as linked results, that is instances of *Estimate* with suitable *Derivation*, or may be replicated by interpreting the standardised study specification with a simulation tool. 'Limitations' of the study need to be documented on all levels, that is at the derivation of input parameters, as well as at the Markov model and Markov model simulation level. Interpretation of the 'generalisability' of the results and the level to which they 'agree with current knowledge' is considered part of a secondary analysis process. A metamodel for this process may be devised, however, it is not part of this thesis. Its results can be documented in a similar way as the results of other secondary analysis processes.

Further recommendations, specific to *model-based* health economic assessments [89], additionally demand for explicit justification of modelling and simulation choices, such as the choice of cycle lengths, use of 'half-cycle correction', extensive validation of the decision model itself and reliability of the simulation code. Former aspects are explicitly documented by the metamodels. Existence of an open exchange standard for Markov model simulations may encourage the development of a trusted code-base for simulation tools that guarantee correct model evaluation.

4.2.3.3. Suggestions for Improvements

While all of the tested studies can be described in terms of the metamodels presented in Section 4.2.1, the following modifications may be envisaged: MarkovModel might be extended by an *initialCost* attribute of type `String` at MM:Cohort metaclass, and an *excludedFromAccounting* attribute of type `Boolean` (default FALSE) at MM:State, indicating whether time spent in that state should be excluded from the overall utility, such as live years. Both MM:Cohort and MMS:SimulationCohort may be extended by attributes *populationGroupDescription*, *settingDescription*, *treatmentDescription* in order to explicitly separate reporting slots for each of these characteristics. Likewise an attribute *limitations* of type `String` may be added to both metamodels to allow for reporting of possible limitations of model design and input parameters.

4.2.4. Summary

In response to challenges in documenting the assumptions and results of health-economic assessment studies, metamodels for Markov model-based simulation studies were developed: the Markov model metamodel allows specification of stochastic models of disease progression, and the Markov model simulation metamodel defines the role of Markov models within a simulation study.

These metamodels were tested on Markov model-based simulation studies in HT, and were found to be sufficiently detailed to describe the input parameters of a computational algorithm for Markov model-based health-economic assessments. Furthermore, complete

model instances provide documentation of study assumptions and parameters, and thus fulfill most of the requirements stipulated by reporting guidelines.

Additional metamodels are needed, for example to define properties and provenance of input parameters, or to declare simulation parameters that are common to a class of simulations and important for the interpretation of simulation results, but beyond the scope of the Markov model simulation metamodel. These metamodels, such as *Estimate* in Fig. 4.36 or SimulationBasedEconomicAssessment in Fig. 4.37, could only be touched upon in this section and are likely to require further refinement.

4.3. Application to Hadron Therapy

This section illustrates the use of the metamodels for data capturing forms, Section 4.1, and Markov model-based analyses, Section 4.2, in the architecture proposed in Section 3.2. A research case relevant to Hadron Therapy is postulated in Section 4.3.1 and the benefits of the proposed architecture are demonstrated on its example.

First, the usage of the Forms-Metamodel for supporting the creation of data capture artifacts, documentation and query of captured data is illustrated in Section 4.3.2. Section 4.3.3 then discusses, how form-related metadata can be used to discover similar data sources, to investigate data interoperability, and to improve the homogeneity of reporting. The use of analysis models, such as the Markov model, is described in Section 4.3.4.

4.3.1. Research Case

Due to the current lack of evidence, Section 1.2, the question of cost-effectiveness of Hadron Therapy (HT) compared to, or in combination with, alternative therapies is likely to remain an important question for the field in the near future, particularly for tumour sites where no major differences in clinical effectiveness had been shown. Answering these questions on the basis of single large-numbered trials is unrealistic; instead, evidence will need to be combined from a variety of sources. Decision analytic models, such as Markov models, may be used for their synthesis.

This research scenario requires the *collection of new* and the *synthesis of existing evidence*, particularly regarding *a*) survival, *b*) the subjective well-being of patients over the prolonged life-time, and *c*) costs related to the occurrence of clinically important adverse events during and after therapy. For projecting outcomes beyond the duration of clinical studies, Markov models similar to the ones used in [80–84] are likely to be employed. Health-states may represent the occurrence of (certain combinations of) adverse events, possibly combined with the characteristic of 'tumour control' or the lack thereof. Details in model structure, such as the relevant (combinations of) adverse events and the allowed transitions between them, depend on tumour type, location and, possibly, treatment strategy. The following discussion assumes Markov models of the general form shown in Fig. 4.38. Such models can be expressed as instances of MarkovModel and combined for evaluation in MarkovModelSimulation.

Model input parameters include *a*) transition probabilities, quantifying the likelihood for relevant adverse events, tumour recurrences, or death, *b*) measures of quality-of-life

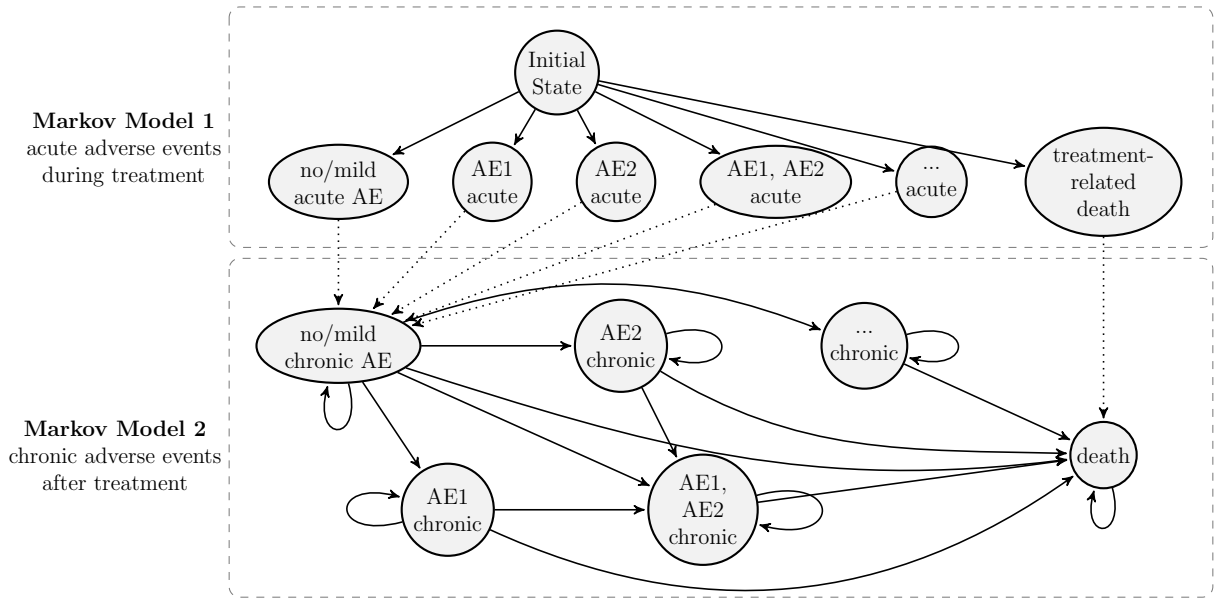

Figure 4.38.: General Markov model for investigation of treatment-related adverse events after radiation therapy as in [166], generalisation of [84].

for the distinct health states, and *c*) costing data, accounting for the costs of alternative therapeutic options, costs for the management of adverse events, and - dependent on the analysis perspective - opportunity costs to society. As mentioned in Section 4.2.2, input parameters of the Markov model, *Estimate*s, may be derived from other data through prior processing.

Case study Selected aspects of this scenario are used to demonstrate the benefits of the proposed architecture in the context of HT.

The application of the Forms-Metamodel for supporting multi-site data capture is illustrated on the example of adverse event reporting, Section 4.3.2. This includes the creation of form specifications, and the generation of a data capture system based on these specifications. Section 4.3.3 shows that form-captured data can be queried in terms of form and study metamodels. The metadata provided by form specifications and information about the data collection context, is - in many cases - sufficient to identify interoperable data sets that can undergo a joint analysis. The discussion of interoperability has to be constrained to *general* cases, not taking into account details of the specific analysis. These interoperability scenarios rely on the reuse of data capture fragments, and the certainty that the logical constraints specified among the components of these fragments are truthfully implemented through model-driven generation processes. More detailed analysis requires further metamodels that cover all analysis processes, Fig. 3.4. The ability of the metamodel-based approach to encourage reuse of reporting fragments within a domain is discussed in this context. Results of an analysis process that acts on form-collected data are documented as instances of Statistic, as defined in Fig.4.36. These values can then be used in further studies. Section 4.3.4 discusses the derivation of secondary analysis services for simulation studies based on the Markov

model that has been developed.

4.3.2. Usage of Forms-Metamodel for Data Capture

This section outlines the role of the Forms-Metamodel in the software architecture, Section 3.2. Its potential to support clinical research data collection in multi-site studies is illustrated on the foregoing case study.

Data Collection Example Figure 4.39 shows a selection of questions that may be used to collect data for the evaluation of adverse events in clinical studies. Recording of adverse events is part of the quality assurance in clinical practice and supports decision making by contributing to the evidence base of type, incidence and severity of adverse effects linked to specific therapies.

1. **Symptom or Location:** *Enter valid CTCAE 4.0 term.*

2. **Severity:**
Select CTCAE 4.0 score.
- ☐ 1 - mild
- ☐ 2 - moderate
- ☐ 3 - severe
- ☐ 4 - life threatening
- ☐ 5 - death

3. **Serious?**
Indicate whether observed adverse event is serious.
- ☐ Yes
- ☐ No

4. **Linked to treatment:**
Indicate likelihood of the observed adverse event being linked to protocol treatment.

unrelated	unlikely	probable	possible	definite
☐	☐	☐	☐	☐

Figure 4.39.: Collection of question fields for the evaluation of adverse events in clinical studies.

F1 in Fig. 4.39 asks for the name of an observed adverse event in terms of the Common Terminology Criteria for Adverse Events (CTCAE), a standardised classification of side effects that is used in assessing cancer therapy treatments. CTCAE also defines a scale (1-5) for scoring the severity of adverse events, together with standard definitions for its meaning (mild - death), *F2*. The severity scale provides more refined meanings for individual adverse event terms and states whether their occurrence indicates medical intervention. Adverse events that require medical intervention (typically grade > 3) are frequently classified as 'serious adverse event'. *F3* explicitly asks whether the evaluated adverse event is considered 'serious'. A positive response may trigger a dedicated section on the form to become active, in order for an incidence report to be completed. *F4* asks for the likelihood that the observed adverse event has been caused by the treatment that the patient has undergone as part of the clinical study protocol.

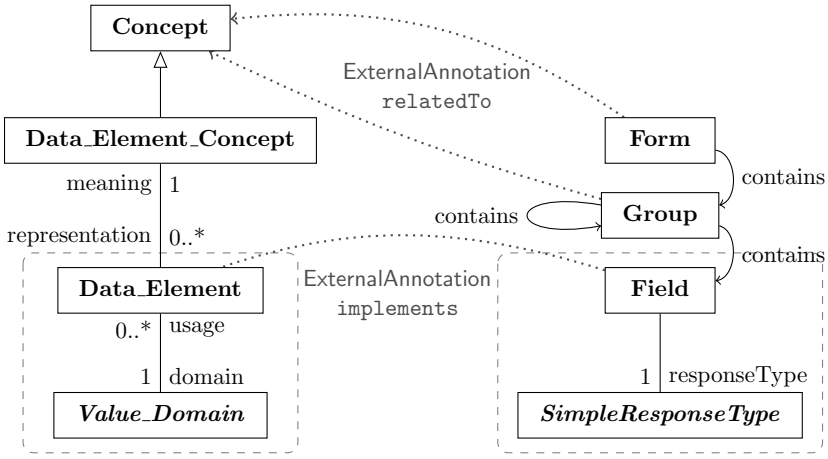

Figure 4.40.: Derivation of Fields from CDEs and annotation of form components.

4.3.2.1. Creation of Form Specifications from Form Fragments

Form fragments correspond to instances of Form, Group and Field metaclasses. This section shows how these fragments may be created and (re-)used.

Derivation of Field Specifications from Common Data Elements Existing MDRs may already provide Common Data Element (CDE) definitions for describing the data items that are to be recorded against individual form questions. The questions in example Fig. 4.39 can be identified with CDEs from the cancer Data Standards Repository (caDSR) and their data element concepts and value domains, Table 4.4.

FM:Field instances may be derived from such CDEs. Table A.3 specifies mapping rules for the transformation of elements from an ISO/IEC 11179 MDR into FM:Field, FM:*SimpleResponseType* and FM:UnitOfMeasure.

This derivation relation between Field instances and CDEs may be documented by FM:ExternalAnnotation with predicate `implements` as in Fig. 4.40. Through the ISO/IEC 11179 metamodel this annotation also establishes a link between the respective Field instance and the ISO11179:Data_Element_Concept associated to the CDE.

Registration of Form Fragments Created form fragments, Field, *SimpleResponseType* and UnitOfMeasure instances, may be stored in a repository, using their *globalID* as unique identifier. Additional registration and administration attributes can be inherited from existing standards, such as ISO/IEC 11179: *Registered_Item* (ISO/IEC 11179-3:2012, 8.1.2.1) and *Administered_Item* (ISO/IEC 11179-3:2012, 8.1.2.2).

The Forms-Metamodel allows fields to be grouped into larger data capture fragments. Fields *F1* to *F4* from example Fig. 4.39 may form a FM:Group instance *G1* for the reporting of adverse event information in clinical studies. Again, FM:ExternalAnnotation may be used to indicate the relation of *G1* to a concept system: Group *G1* could be asserted to be `relatedTo` the concepts 'adverse event' and 'reporting' in a concept system, such as the NCI Enterprise Vocabulary Service (EVS), Fig. 4.40.

Field	Data Element		Data Element Concept		Value Domain	
	ID	Name	ID	Name	ID	Name
Q1	3125302	CTCAE v4.0 Low Level Term Name	2943909	Adverse Event CTCAE term	3125301	CTCAE v4.0 Low Level Term Name
Q2	2944515	Adverse Event Severity Grade	2747735	Adverse Event Severity	2943992	Adverse Event Severity Grade
Q3	2199908	Serious Adverse Event Indicator	2013053	Serious Adverse Event Occurrence	2181608	Yes No Character Indicator
Q4	1285	CTC Adverse Event Attribution Scale	2188792	CTC Adverse Event Attribution	2015190	Attribution Scale

Table 4.4.: CDEs corresponding to questions in Fig. 4.39, with data element concept and value domain from caDSR.

Creation of Form-Specifications Form fragments can be combined as illustrated in Fig. 4.4b. Two distinct forms may be created from the adverse event recording group *G1* in Fig. 4.39: A form specifically for the reporting of adverse events during treatment or shortly after (annotation concept: 'routine adverse event reporting') and a form for long-term follow-up (annotation concept: 'long term follow up'). While both forms would use the same reporting group *G1* without modifications, their usage context differs and represents two distinct specialisations of an 'adverse event reporting' group.

4.3.2.2. Generation of Data Capture System

Once a form specification has been created, it can be transformed into different target models, as illustrated in Figure 4.41.

The transformation into PSMs may involve intermediate steps, such as the Forms-Metamodel-Template discussed in Section 4.1.5.2. Two types of target PSMs are of importance here: *a*) other *form metamodels*, such as the Case Report Form (CRF) definition language of the OpenClinica forms metamodel in Section 4.1.5.3, or ISO/IEC 19763-10:2013 in Section 4.1.5.4, and *b*) *datamodel metamodels*, such as *XML schema*, or *SQL*. After transformation into the respective PSM, the PSM can be serialised into software artifacts, corresponding to forms as data capture instruments or data schemas for storing form-collected data. This illustrates a significant advantage of the model-driven approach: Provided, a transformation between source and target model has been established, front- and back-end services for data capture and storage of the collected data can be created automatically from a form specification, thus lowering technical expertise and costs required for their initial creation and maintenance.

The quality of implementation, that is the degree to which the properties of a form specification are translated into properties of the data capture system, is determined by the quality of the transformations and the capabilities of the target technologies. Verification of the degree to which a software artifact represents a truthful implementation of its specification is an important aspect of quality assurance for information systems. The Model-Driven Engineering (MDE) approach allows this characteristic to be established,

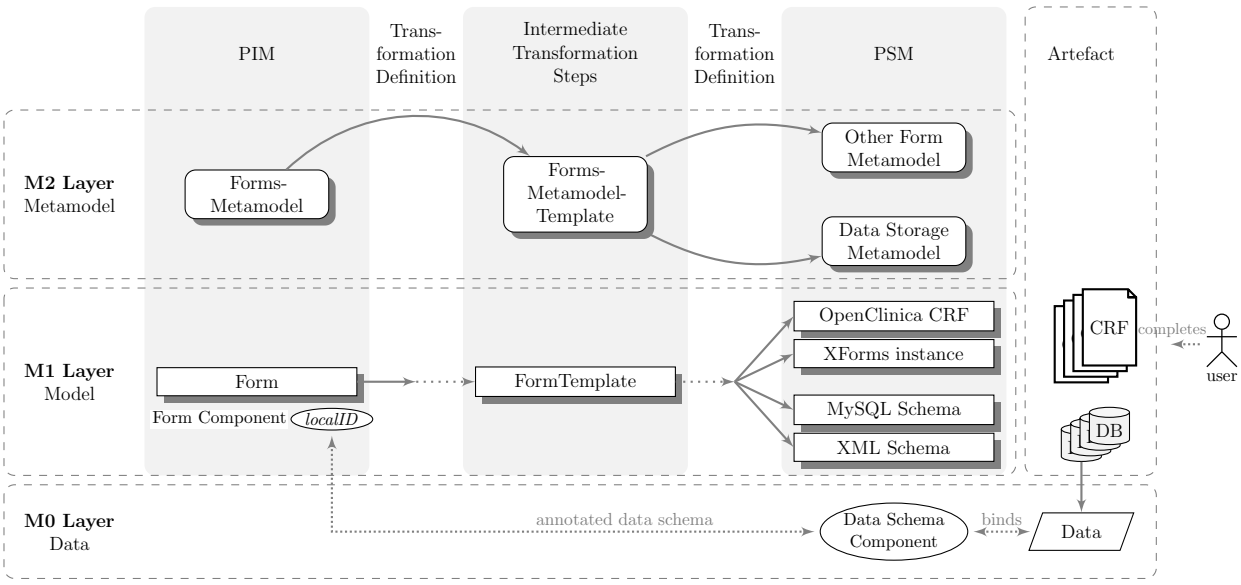

Figure 4.41.: Usage of Forms-Metamodel for data interoperability in clinical studies.
A form specification may be transformed into Platform Specific Model (PSM) instances, such as specification of data capture instruments or of data modeling standards, which can then be serialised into software artifacts.

not only for a single implementation, but for all artifacts created by the same set of transformation rules between two metamodels, PIM and PSM.

Generation of Reporting Artifacts As shown on the example of the OpenClinica forms metamodel in Section 4.1.5.3, the Forms-Metamodel is sufficiently detailed for form specifications to be transformed into implementable form representations that can be serialised into data capture instruments. Limited expressiveness of the target PSM will result in differences between the original design intent and the implementation and need to be documented as such. For example, the OpenClinica forms metamodel only provides limited support for conditional relevancy of form components.

Figure 4.42 shows an excerpt of the adverse event reporting group *G1* from Fig. 4.39, with additional 'start date' field, in an *XForms* implementation. The group is used within a larger form and multiple submissions are permitted (FM:StructureInComposition:-$maxResponses > 1$).

Generation of Data Model The Forms-Metamodel also specifies sufficient information for a data model to be created that can store the data collected against a given form specification.

Figure 4.43 models the relations between data submitted against the different types of form components. Data is collected against a DataCaptureInstrument, an implementation of a form specification, FM:Form. The implementation is characterised by the model mapping and generator service used for its creation, *generatorRef*. FormData represents the data collected by one data submission of a specific DataCaptureInstrument instance, such as the *Xforms* implementation shown in Figure 4.42. The *globalID* attribute establishes

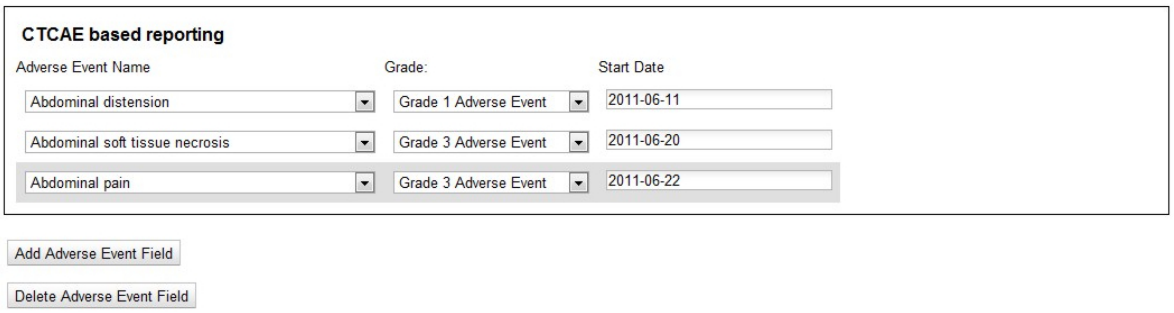

Figure 4.42.: *XForms* implementation of adverse event reporting group, Fig. 4.39.

the relation between FormData and the FM:Form from which the DataCaptureInstrument was derived. The Forms-Metamodel permits multiple FM:Group or FM:Field instances to be 'contained' in a FM:Form or FM:Group through the composition mechanism of FM:*ComposedStructure*. As part of such a composition (FM:StructureInComposition) FM:Group and FM:Field elements may occur multiple times (FM:StructureInComposition:-*maxResponses* > 1). In a data model, these repetitions need to be disambiguated (*fieldRepeatKey*, *groupRepeatKey*) in order to maintain the context of collection of every single data item.

Submission of the adverse event reporting group Fig. 4.42 will result in three GroupData structures with distinct *groupRepeatKey*s, each of which *contains* three FieldData structures. This allows distinction of data items that were collected against the same form structure (*localID*) but in different repetitions of their enclosing superstructure. Data values collected in 'groups' can thus be identified.

FM:Field instances with FM:EnumeratedResponseType may collect more than one value, depending on their associated FM:SelectionMultiplicityConstraint. The model in Fig. 4.43 therefore specifies two specialisations of *FieldData*: FieldDataValue corresponding to a single data *value*, and MultiValuedFieldData that may contain multiple FieldDataValue, disambiguated by *selectionRepeatKey*.

Data Annotation Generation of both data schema and reporting artifacts from a given form specification not only facilitates and speeds-up iterative form design, it also allows for automatic annotation of form-collected data. The *localID* of FM:StructureInComposition elements can be carried through to the data schema, as indicated in Figure 4.43, so that any data item associated to the schema will be linked to the form fragment against which it was collected. The semantics of the respective data item is then described by this form component and its usage within the form specification.

In example Fig. 4.42, the data entered against the first field *F1* in the third repetition of the adverse event reporting group *G1* can be identified as representing one of multiple *Adverse Event* terms. ExternalAnnotation provides information about the meaning of permitted entry values and identifies the entry value as standardised CTCAE term, Section 4.3.2.1. LocalAnnotation within its enclosing group *G1* may specify that values recorded within *G1* provide complementary information to the adverse event reported in *F1*. Likewise, *EntryConstraint*s and ConsistencyConstraints, or other aspects of form logic that may affect this particular data item, are documented by the form specification.

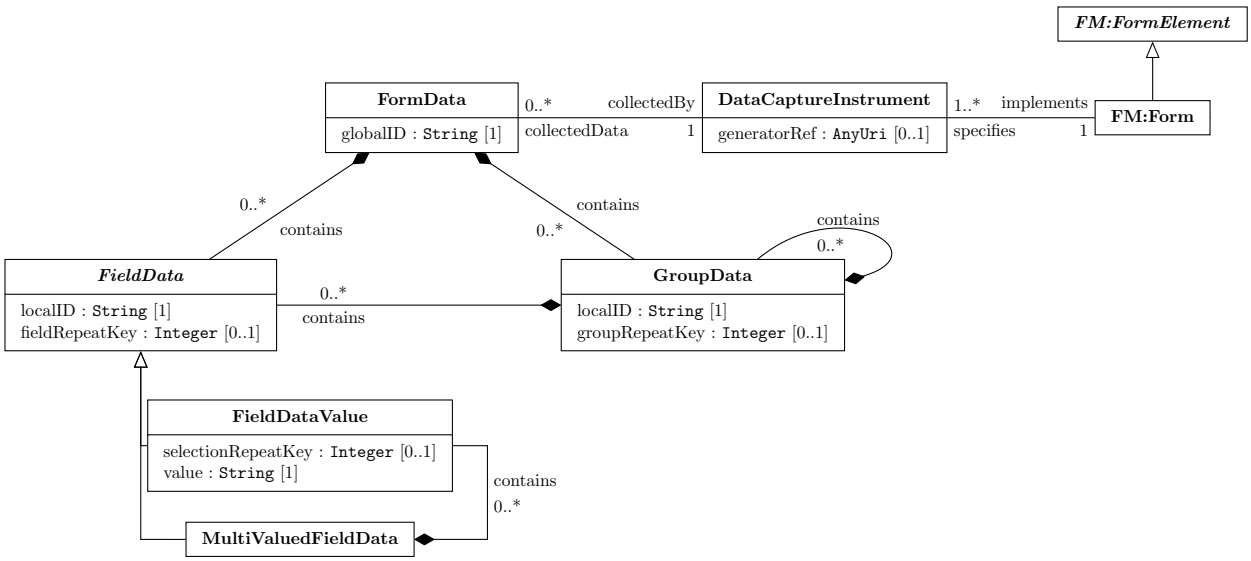

Figure 4.43.: Relation between form specification FM:Form, its implementation as DataCaptureInstrument and submitted data. Every submitted data item can be related to the form element (*localID*) against which it was collected.

ExternalAnnotation at higher-level structures may specify the usage context of the reporting fragments *G1* and *F1*, such as the use for 'adverse event reporting' in 'long-term follow up'.

4.3.3. Metadata-based Data Selection for Analysis

First, a context model for the use of data capture instruments in clinical studies is developed, Section 4.3.3.1. Section 4.3.3.2 then shows how the Forms-Metamodel, in combination with information about its usage context, can facilitate the identification of suitable existing data sources for meta-analysis. Section 4.3.3.3 explains how it may support pre-coordination of data collection in future studies so that collected data can be guaranteed to interoperate.

4.3.3.1. Clinical Study as Context for Data Capture

The specific context in and for which data capture forms are used, affects the interpretation and usage possibilities of the collected data. Naturally, information models for usage context are specific to a particular application domain, whereas the Forms-Metamodel provides a generic definition language for data capture forms, independent from any specific application domain.

Figure 4.44 presents a domain-specific metamodel that describes the usage of forms in the context of clinical studies. The model structure is based on the Clinical Data Standards Consortium's Operational Data Model (CDISC-ODM) study model [127]. However, its scope is strictly limited to aspects that affect the interpretation of form-collected data: A Study is identified by its *studyID*. As study-related metadata may change over time, it is grouped into versioned MetadataSets. Study-metadata of interest in this context is the StudyProtocol and the form specifications associated to StudyEvents.

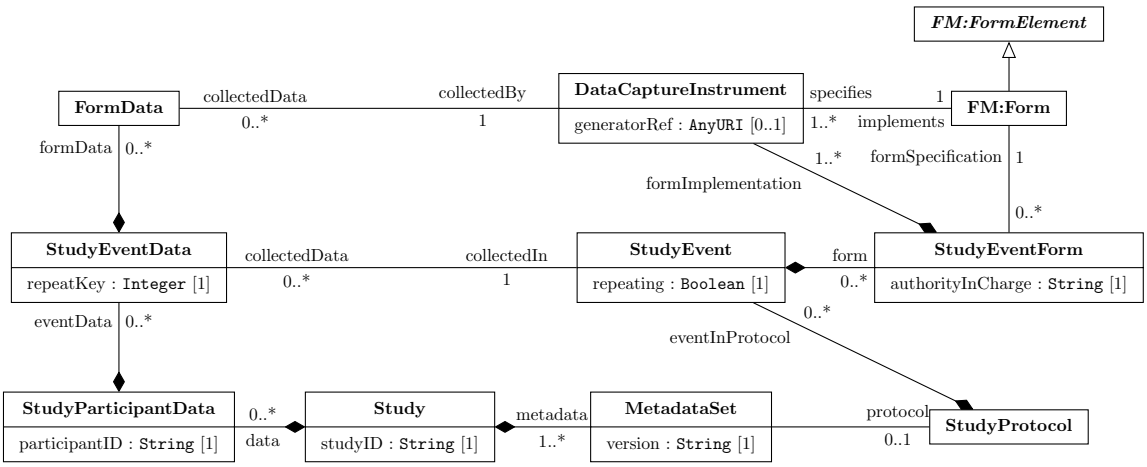

Figure 4.44.: Simple application model for the use of the Forms-Metamodel in the context of clinical studies.

The study protocol defines aspects of study design and conduct, such as the patient population that may participate in the study, the type of treatment, and treatment randomisation. It also defines StudyEvents, 'data collection events' such as a patient visit. By definition, data is collected as part of a StudyEvent, for example data on the occurrence of adverse events after therapy as part of a 'regular follow up' event.

In contrast to CDISC-ODM the metamodel in Figure 4.44 distinguishes between a form specification and its implementation. StudyEventForm represents the form that a single individual is required to complete as part of the StudyEvent. It refers to one single form definition FM:Form and associated DataCaptureInstruments, implementations generated from this definition. Multiple DataCaptureInstruments may be associated to the same form definition because different implementation technologies might be used in parallel (paper, digital).

During the lifetime of the study, its participants undergo the study events defined in the protocol and data is collected according to their associated study event forms. This results in a collection of completed data capture instruments for every study participant and study event. The structure of FormData maps to the components of the form specification (FM:Form) according to metamodel Fig. 4.43. StudyParticipantData comprises the data collected against all StudyEvents that a particular study participant underwent over the course of the study.

The information provided by an instance of this application model precisely specifies the context and circumstances of collection of any data item as part of a clinical study. In particular, it documents changes in the study protocol that affect data capture instruments and allows this information to be associated to every collected data item automatically.

As suggested by the application model, 'data', the data items collected against every form component, and 'metadata', the study protocol, study event definitions and associated form specification as well as the actual data capture instruments, can be maintained separately.

Query over Study Data The metamodels introduced here and in Section 4.3.2.2 provide the basic components for a query language over form-collected data in the context of clinical studies. Study:*studyID*, MetadataSet:*version*, StudyEvent:*studyEventID*, StudyEventForm:*studyEventFormID* and DataCaptureInstrument:*dciID* provide the keys to identify a particular form specification and the FormData submitted against it. Within FormData, the data collected against form components may be navigated by their *localID* and the corresponding 'repetition key' in case of repeating StructureInComposition elements. StudyParticipantData:*participantID* allows the data pertaining to a particular study subject to be identified.

All data collected against a single form fragment of *localID* within a given study *studyID* could thus be queried and be returned for every *participantID*, including all possible repetitions, such as repeating study events, or sections that repeat on a form.

4.3.3.2. Selection of Data Sources and Interoperability

As discussed in Section 2.1, contextual information is required to infer the meaning of existing data. In the proposed architecture, this contextual information is defined in terms of distinct metamodels, such as the context model for data collection in clinical studies shown in Fig. 4.44, and the Forms-Metamodel. Metadata relating to this context may be queried, individually for each metamodel, to infer about the meaning of data.

Assuming data collection has taken place with DCIs developed according to Section 4.3.2.1 and 4.3.2.2, the next step in the research scenario is the identification of suitable data sources: Individual Patient Data (IPD) meta-analyses should follow a 'protocol' that defines outcomes and patient characteristics to be analysed, similar to 'real' clinical studies.

Identification of Clinical Studies In this example, comparability of the clinical context is resolved manually by inspecting study descriptions, selecting suitable studies and identifying the study events of interest. Clinical studies, potential data sources, are frequently registered in public databases such as ClinicalTrials.gov with details about condition, eligibility criteria, interventions and randomisation. Based on this information, suitable studies for the 'recruitment' of a virtual patient cohort can be identified. With a sufficiently detailed study metamodel and formal definition of eligibility criteria [167], this process may be automated.

Having ensured that medically comparable studies are selected, interoperability of study data depends upon the observations reported in those studies and the requirements of the given analysis process.

Identification of Relevant reporting Fragments The following assumes that multiple comparable studies have been identified and that definitions of the CRFs used in these studies are available, conform to the Forms-Metamodel or a comparably expressive meta-standard. As Fig. 4.44 indicates, StudyEventForms represent aspects of study *metadata*. They are clearly distinguishable from *data* collected in the respective study and may therefore be made publicly available in the same way as other aspects of the study protocol. For simplicity, it is further assumed that study protocols and form designs remained unchanged over the course of these studies.

If the form specifications were used according to the methodology proposed in Section 4.3.2, they can be expected to provide an accurate record of the kind of data collected throughout the run-time of the study. They thus allow those studies to be identified that collected data to the same requirements.

Adverse event data is of particular relevance for the research scenario outlined before. Relevant reporting fragments can be identified by reviewing the form specifications associated with each of the studies, or querying for ExternalAnnotation of *annotationType* `relatedTo` with *annotationObject* concept 'adverse event' or related, such as defined for the example fragment in Fig. 4.39, Section 4.3.2.

Suppose, each of the identified studies defines a follow-up form that contains a section about adverse event reporting. In terms of the Forms-Metamodel this corresponds to an instance of metaclass Form, containing a StructureInComposition identified by its *localID* and defined by a globally identified instance of metaclass Group – compare metamodel characteristics in Fig. 4.21a.

Interoperability The following considerations require prior identification of 'comparable' clinical contexts based on a study specification that conforms to a metamodel, as shown in Fig. 4.44. Interoperability between data sets can then be discussed in terms of the properties of form specifications since these define logical constraints on and among single observations.

A decision about the interoperability of data collected in these studies can be reached in the following cases:

Identical Forms Two of the identified studies use the same form specification with *globalID Fo1*. In terms of the Forms-Metamodel, those two form specifications are identical and expected to collect the same data items to identical requirements.

'Equivalent' Forms Semantic 'equivalence' of two forms may be asserted by StructureAnnotation with `ANNOTATIONPREDICATE sameAs` through the Forms-Metamodel, or through a mechanism provided by the model registry, such as Model_Mapping in ISO/IEC 19763-10:2013. In the case of HT, multiple languages are likely to be used in follow-up forms, reflecting the geographic distribution of centres. An assertion of semantic equivalence between multiple form specifications in different languages asserts that each of these forms collects data to the same requirements, regardless of its language.

Identical Form Fragments (Groups) Assume two distinct follow-up form specifications, *Fo1* and *Fo2*, whose adverse event collection groups are *derivedFrom* the same group structure, identified through its *globalID GAE1*. Both form specifications collect data to the requirements of *GAE1*, refined by context-specific specialisations of *GAE1* in *Fo1* and *Fo2*, respectively. Such differences are limited to adjustments towards stricter validation constraints, pre-population of values, as well as the accepted and required number of completed repetitions of the *GAE1* reporting group. Since contained fields and their logical relations are identical, the data collected against any of these contextualised fragments can be expected to suffice the same requirements that are imposed by the *GAE1* reporting template.

Other cases If different reporting fragments are used, closer inspection is required. Assume a further form specification *Fo3* with a distinct adverse event reporting group, *derivedFrom globalID GAE2*, to be encountered. Both reporting groups, *GAE1* versus *GAE2*, may be compared with regard to their contained StructureInComposition elements. However, even if identical substructures are used in both groups, their completion logic may be sufficiently different to hinder general interoperability. For example, if a particular question is *required* to be completed in one reporting group, whereas its completion is *optional* in the other reporting group, a computing algorithm that *expects* the corresponding data item to exist, will fail. Therefore, general interoperability cannot be *assumed* between any pair of distinct reporting fragments, even if its constituents are identical.

In latter case, however, the Forms-Metamodel provides the query language for a detailed assessment of both reporting fragments, in order to conclude on interoperability on a case by case basis, depending on the requirements of the joint analysis purpose. Two form fragment may collect different but *commensurate* data for a given analysis. In this case, their interoperability with regard to this particular analysis may be *asserted*.

The Forms-Metamodel developed here provides the basis for future research on more fine-grained interoperability conditions.

Form Specification versus Implementation Above considerations are based on form specifications and on the assumption that these specifications are truthfully implemented into DCIs. Under this condition, any logical constraints on and among form components translate into properties of the collected data.

However, implementations of the same form specification may differ in the context of distinct studies. FormData, in Fig. 4.44 is therefore assumed to be collected not against a form specification, but against a DataCaptureInstrument that has been created by a *generator* according to a form specification.

The Forms-Metamodel attempts to minimise discrepancies between intended form design and final implementation by specification of its *preferredAccessMode*. This access mode may limit the functionality of the DCI and may affect the quality of collected data in terms of correctness and completeness. For example, *F1* in the adverse event reporting fragment from Fig. 4.39 would be represented as a free-text field in a paper-based implementation, whereas the use of valid CTCAE terms could be guaranteed in a digital form. Therefore, a different form specification might be preferable for paper-based CRFs.

4.3.3.3. Pre-coordination of Data Collection across Studies

For future joint analyses to succeed, commensurate data needs to be collected. The Forms-Metamodel supports this in three ways: *a*) It allows components of forms to be shared and reused, independently from any implementation. This is more flexible than coordination of data capture through reuse of *entire* paper-based CRFs, since it requires less coordination and agreement between reporting sites, in terms of the observations reported, as well as the reporting technology. At the same time, the contextual information provided by fragments allows interoperability of data collected in different contexts to

be assessed. *b*) Due to this characteristic, interoperability between different data sources can be surveilled automatically. If incompatibilities are identified, modification of the form specifications may be suggested, such as inclusion of further variables or exchange of reporting fragments by established and commonly used domain templates. Changes in data capture during an on-going study may result in inconsistent documentation if the collected data and its schema do not reflect the evolution of data capture instruments. The model-driven approach allows changes in form specification to be propagated to both, data capturing artifacts and back-end services, without additional implementation cost. *c*) Based on the language constructs provided by the Forms-Metamodel, content and properties of form specifications may be constrained. Sets of constraints can be developed that define the characteristics of forms permitted within a given domain. The validity of forms with respect to those criteria can then be tested and the use of interoperable reporting fragments be enforced.

Two main types of constraints can be identified: *content* constraints, requiring the inclusion of certain types of questions in every form or data collection process, and *form-property* constraints, that may for example enforce annotation of form components with concepts from a specific ontology. Constraints on form properties can be expressed through a suitable constraint language and knowledge of the Forms-Metamodel. Since the Forms-Metamodel is developed in Unified Modeling Language (UML), OCL may be used for this purpose. Content constraints, on the other hand, will refer to other registered user-models in the architecture or to classification schemes in which those models are included. In the context of the research scenario outlined before, a constraint may be formulated that requires form specifications used in follow-up events to include a particular type of adverse event reporting fragment. The definition of such constraints requires knowledge of the metamodels describing clinical studies and forms.

4.3.4. Analysis

Two distinct types of analysis services were introduced in Section 3.2. Those acting on *primary* data obtained through data collection instruments are discussed in Section 4.3.4.1, those acting on *derived* data, in Section 4.3.4.2.

Any analysis process produces outcome values, termed *Estimate* in Fig. 3.4. These may represent the input for further analyses, such as for meta-analyses or modelling studies that synthesise the evidence obtained from multiple clinical studies. The results obtained from those analyses may likewise be documented as instances of *Estimate*. Their provenance is described by the analysis process that lead to their creation, identified by a *derivation* association. Assumptions about the parameters of secondary analyses processes are thus well-documented.

4.3.4.1. Analysis of Primary Data

No detailed metamodel for analysis processes acting on primary data has been developed as part of this thesis. However, for the following argumentation, this type of *analysis* is sufficiently described as a 'processing instruction' based on an 'internal data representation'. The processing instruction might be expressed in terms of (statistical) computing

languages, such as R [168], Stata [169] or others, and the internal data representation might correspond to a 'dataframe', or 'table' in those languages.

The data-set required by an analysis process may be provided through a query expression over available data sources, in combination with suitable pre-processing that transforms the data returned by the query into the internal data representation required by the analysis. Such a query may be expressed in terms of concepts of the study metamodel and the Forms-Metamodel, as seen in Section 4.3.3.1. The combination of query and pre-processing of form-collected data to conform to the requirements of an analysis process is referred to as *mapping* in the following. Analysis services may be connected to form-collected data through such mappings.

Detailed investigation of the properties of such mappings will allow more fine-grained decisions about data interoperability than those discussed in Section 4.3.3.2.

In the context of the research scenario from Section 4.3.1, transition probabilities between adverse event-based health states for Markov models, such as Fig. 4.38, will need to be determined, for example by means of IPD meta analysis. This requires information on the 'current health-state' of each individual patient at multiple time points. Such data is obtained from repeating study events, 'follow-up' visits, in which the same DCIs are administered at every repetition. The 'current health-state' of an individual at each of these events can be established from observation of a particular adverse event, or a combination of adverse events. Statistical analysis processes, such as [170, 171], may then be used to derive transition probabilities between health states. The results of this analysis are documented as instances of *Estimate* in Fig. 4.36.

4.3.4.2. Analysis of Derived Data

The Estimate derived in the context of this case study represents a transition rate between two adverse event-based health states for a well defined patient population. It may be used in the definition of a Markov model to describe the transition probability between two health states, for example between 'no/mild chronic AE' and 'AE1' in the second model in Fig. 4.38. These health states can be represented as instances of MM:State, connected by an instance of MM:Transition, Fig. 4.32. The transition probability associated to this transition is specific to the particular patient cohort from which it was derived. Its use in the Markov model is therefore linked to an instance of MM:Cohort, and expressed as MM:*CohortSpecificValue*. Further parameters of this Markov model are described in the same way, with instances of *CohortSpecificValue* that associate instances of *Value* with instances of MM:Cohort. The same applies to the parameters of the first Markov model in Fig. 4.38.

Both instances of Markov model may be combined into a Markov model simulation, Fig. 4.34: The two Markov models are represented by instances of MMS:-MarkovModelreference with *markovModelRef* referencing the respective Markov model instance in the architecture. Relations between both Markov models, indicated as dotted lines in Fig. 4.38, are specified through MMS:StateStartPopulation.

An analysis service may be derived from this fully defined Markov model simulation that collects the input parameters *Estimate* and computes the outputs $\bar{U}_{simCohort}$, and $\bar{C}_{simCohort}$ for every instance of SimulationCohort according to the algorithm presented in Section 4.2.2. These results can be interpreted in the context of SimulationBase-

dEconomicAssessment and additional simulations be performed for sensitivity analysis, Fig. 4.37. Final outcomes such as ICERs between multiple alternative treatments are thus documented through the successive invocation of analysis services that perform operations on selected clinical information. The parameters relevant to any of those operations are accessible as models whose semantics is defined by their metamodels.

4.3.5. Summary

A methodology of usage of the Forms-Metamodel to support data capture and analysis across distributed study centres was illustrated on the example of HT:

Form components, in terms of the Forms-Metamodel, can be derived from existing CDEs and be combined into larger form fragments and form specifications from which data capture systems, including reporting artifacts and data models, can then be generated. By annotating the data model, links between a computable specification of the DCIs and the collected data are obtained as part of the generation process, thus providing free and accurate documentation of the collected data.

Since study metadata, including the DCIs used for data collection, are not subject to data privacy restrictions, they may be made publicly available. This information can be used to discover data sets and to assess their interoperability with regard to a given analysis purpose. Studies using identical DCIs or form fragments can thus be identified, and conversion-mappings between data captured against differing DCIs can be asserted, without the need to request access to confidential data. Furthermore, the ability to reuse and share form components in an implementation-independent way, and to automatically compare the properties of DCIs across studies may be used to encourage pre-coordination of data collection towards specific analysis goals.

In the field of particle therapy, such pre-coordination will be important to ensure interoperability of collected data for comparative analyses of treatment effectiveness and quality-of-life outcomes. Based on IPD meta-analyses, parameter *Estimate*s for different outcomes can be otbained for subgroups of the patient population. They can then be combined into Markov model simulation studies in order to estimate the relative cost-effectiveness of HT compared to alternative treatment options, for different tumour sites, populations and health systems. Using the Markov model and Markov model simulation metamodels, modelling assumptions of such studies can be specified and their results be documented.

4.4. Conclusion

A metadata-driven software architecture for clinical data capture and analysis was proposed in the previous Chapter 3, and two of its main components were developed in this chapter. The architecture's ability to support the evidence derivation process in Evidence-Based Medicine was demonstrated on an example from Hadron Therapy.

A metamodel for the specification of data capture forms was developed to support the collection of high-quality data in multi-centre data collection scenarios. Its two distinctive features are indispensable for its usage in the proposed architecture as they allow for model-driven generation of DCIs from form specifications: Due to its

expressiveness, the Forms-Metamodel supports processes of user interface generation and data documentation. This ensures consistency between the properties of DCIs, the collected data and their documentation. It reduces the cost of form design, as well as of the creation and maintenance of data capture services. Furthermore, the ability to compose new forms from existing model fragments allows form components to be shared and reused, regardless of any particular implementation technology. This may increase reporting homogeneity, leading to improved data interoperability.

Information derived from analysis processes also requires adequate documentation to ensure its correct use and interpretation. In response to the need for better documentation of simulation studies for health-economic assessments, metamodels for Markov model-based simulations were developed.

In order to benefit from the advantages of the proposed architecture, further research beyond the metamodels developed in this thesis is required, most importantly towards further metamodels and their interrelations: *a*) Metamodel of clinical studies: This metamodel provides the clinical context of data capture, including information about patient cohorts and study protocol. A detailed standard should also provide means to specify temporal relations between study events, and thus between their associated form specifications. An extension to the Forms-Metamodel might be considered to allow constraints *between* distinct forms to be defined, in addition to constraints between form components. *b*) Metamodel of statistical analyses over form-collected data: Such a metamodel should allow statistical analyses to be defined in terms of concepts of form and clinical study metamodels, so that the queries required for data collection can be generated automatically. Understanding the relation of logical constraints among analysis input parameters to constraints among form components, may allow data interoperability to be discussed with regard to the requirements of a particular data analysis purpose. *c*) Further analysis metamodels, and more detailed 'auxiliary' metamodels to define properties and provenance of input parameters, such as *Estimate* in Fig. 4.36 or SimulationBasedEconomicAssessment in Fig. 4.37.

Pre-coordination of data collection based on fixed form fragments may lead to the capture of redundant information. This is inefficient and may potentially result in inconsistent data sets. A calculus that computes an *optimised* form specifications from multiple form fragments and their composition type would therefore be valuable.

Finally, tooling needs to be developed that can interpret user-models and create corresponding software artifacts, such as data capture or analysis services. The general applicability of the proposed metamodels may encourage such developments.

5. Design of Ion Beam for Radiobiology

This chapter presents the results of first feasibility studies towards an ion beam facility based on the Low Energy Ion Ring (LEIR) at the European Organisation for Nuclear Research (CERN).

The main beam requirements for a bio-medical research facility in the context of Hadron Therapy (HT), and constraints imposed by the existing infrastructure, are established in Section 5.1. Section 5.2 briefly reviews the accelerator physics concepts required for the remainder of this chapter. Feasibility of slow extraction from the existing LEIR lattice is investigated in Section 5.3, based on analytical considerations and verified by particle tracking studies. Section 5.4 presents beamline designs for transporting the extracted beam towards the adjacent experimental area, as well as for 'horizontal' and 'vertical' delivery of ion beams. The results of these studies are concluded in Section 5.5.

5.1. Ion Beam Facility at LEIR

Among the arguments for establishing an ion beam facility dedicated to bio-medical research at CERN are the existence of significant parts of the required accelerator infrastructure, their guaranteed maintenance, and space availability for the installation of new research infrastructure.

In the following, capability and limitations of the existing accelerator infrastructure are compared to the requirements for radiobiological research with focus on HT: Section 5.1.1 first establishes the beam requirements that will be used for the following feasibility studies. Based on these requirements, the constraints imposed by the existing infrastructure and locality are then discussed in Section 5.1.2 and 5.1.3, respectively.

5.1.1. Requirements for Ion Beam Facility

As part of this research, a review of applications and existing facilities was conducted, and requirements for bio-medical ion beam facilities were collected in collaboration with members of the Particle Therapy Cancer Research institute (PTCRi) [172]. These findings were presented to the bio-medical community [173] and further refined during a follow-up meeting at CERN [98–100].

From the range of relevant applications, radio-biological research poses the strictest requirements on beam characteristics and facility infrastructure and therefore guides the choice of parameters for this study. Practical interest in radio-biological studies is mainly motivated by two fields: *Radiation protection*, studying the effect of ionising radiation on cells and cellular systems over a wide range of doses and dose rates, and *medicine*,

	Clinical	Radiobiology
Ions	mainly p, $^{12}_{6}$C	p to $^{20}_{10}$Ne
Energies	60 MeV/n to 400 MeV/n	10 MeV/n to at least 75 MeV/n
Dose rates	2 Gy min^{-1} to 5 Gy min^{-1}	
Field size	5 mm to 10 mm FWHM to 5 cm × 5 cm	
Field uniformity	better ±5 % across irradiation field	

Table 5.1.: Beam requirements for Hadron Therapy research.

interested in the beneficial uses of ionising radiation for therapeutic purposes, as well as its adverse side effects.

Requirements for latter, in particular for research related to HT[1] are reviewed here and summarised in Table 5.1. Besides suitable beam characteristics, the availability of support infrastructure and access programmes is key to the success of a bio-medical facility at CERN, as laid out in [99, 100].

Ion Species Particles from proton p to neon $^{20}_{10}$Ne are considered for radiobiological experiments at this facility:

Protons p and carbon ions $^{12}_{6}$C are essential as reference for current HT treatment practice. Although not currently used in clinical practice, helium $^{4}_{2}$He, $^{3}_{2}$He, lithium $^{6}_{3}$Li, boron $^{10}_{5}$B and oxygen $^{16}_{8}$O might provide ballistic and biological advantages in some clinical situations. Due to reduced lateral scattering compared to protons and reduced fragmentation compared to carbon ions, advantages are expected for example for the treatment of deep seated cancers or cancers close to critical structures. Nitrogen $^{14}_{7}$N and neon $^{20}_{10}$Ne are less likely to be used in a clinical setting, but of interest from a radiobiological point of view, in particular neon as reference to already existing radiobiological data.

Deuterium D, may lead to neutron contamination of the beam and is therefore likely to be restricted to radiobiological uses. While beams of lithium $^{6}_{3}$Li and boron $^{10}_{5}$B would potentially be of clinical interest, both, are known to be difficult to produce and handle.

Energy Measurements of Radiobiological Effectiveness (RBE) in function of Linear Energy Transfer (LET) and nucleon charge at various points on the Bragg curve are among the primary research objectives for the proposed facility [100]. This requires *in-vitro* cell survival experiments, with measurements taken on the plateau region of the Bragg curve, as well as on its rising slope and on the Bragg peak. The *minimum* useful beam energy is mainly determined by the experimental setup: For radio-biological experiments close to the Bragg peak, this energy needs to be sufficiently high for the

[1]Requirements for space radiation protection additionally include the need for higher beam energies, beyond the reach of LEIR, and a wider range of ions typically up to iron [174]. There clearly are synergies between radio-biological research for space radio-protection and therapeutic application of particle beams on topics such as carcinogenic potential, non cancer risk and acute effects of particle radiation and the effect of radio sensitisers or radio protectors [175].

particles to reach and penetrate the sample. With typical values[2] for the thickness of vacuum window, beam instrumentation and flask for cell culture, a minimum thickness of approximately 1 mm water equivalent length needs to be penetrated. In order to allow data taking on the Bragg peak, with minimum amount of absorber material, beam energies starting from about 10 MeV for protons and about 15 MeV/n to 20 MeV/n for carbon ions would be desirable[3]. The *maximum* beam energy should be sufficiently high to allow data taking on the plateau of the Bragg Curve. Maximum energies of at least 75 MeV/n would be required for carbon ions. Higher energies would be preferable; they will be required to allow measurements sufficiently far away from the rising shoulder of the Bragg peak with heavier nuclei.

To simulate treatment situations with human phantoms, the range of available beam energies needs to cover typical treatment depths in tissue: 3.5 cm to 27.5 cm are desirable for treating patients [176, 177], corresponding to energy ranges of 60 MeV/n to 250 MeV/n for protons and 120 MeV/n to 400 MeV/n for carbon ions.

Dose Rates For radio-biological experiments, the total dose required depends on the type of experiment; the irradiation time should be kept below approximately 10 minutes for practical reasons and to avoid the onset of cellular repair mechanisms during irradiation, resulting in desired dose rates of 2 Gy min^{-1} to 5 Gy min^{-1} for most mammalian cell experiments. For clinical applications, dose rates about 2 Gy min^{-1} for a volume up to one litre are typical values [22], corresponding to approximately 10^{10} s^{-1} protons or 10^{8} s^{-1} carbon ions delivered to the patient [178]. Dose variations across the sample area should be minimised, and for experiments with direct clinical relevance, total absorbed dose should be known with an accuracy of at least ±5 % at the level of one standard deviation [179].

Field Size and Uniformity *Broad beams* are considered more versatile than *micro-beams*. Adjustable beams between *pencil beam*, with a spot-size of about 5 mm to 10 mm Full-Width Half-Maximum (FWHM), to broad beam with fields up to 5 cm × 5 cm are considered sufficient for clinically oriented phantom studies, *in-vivo* small-animal studies, as well as for *in-vitro* cell studies. Raster or spot-scanning would be desirable for testing ballistic properties in phantoms and for in-vivo studies.

5.1.2. LEIR

The Low Energy Ion Ring (LEIR) was first proposed in 1993 [180] for accumulation of heavy ions to achieve the required luminosity for Pb-Pb collisions in the Large Hadron Collider (LHC). It was created from a previous synchrotron, the Low Energy Anti-proton Ring (LEAR), designed to decelerate and store anti-protons[4]. Commissioned in 2005 [183], LEIR now forms part of the LHC injection chain between Linear Accelerator 3 (LINAC3) and Proton Syncrotron (PS), as illustrated in Fig. 5.1.

[2]Bi-material vacuum window Kevlar & Mylar ∼ 300 µm water equivalent; ionisation and wire chambers ∼ 100 µm to 200 µm water equivalent; Polymethylmethacrylate (PMMA) flask ∼ 0.6 mm to 2.4 mm water equivalent.

[3]Based on *Stopping and Range of Ions in Matter* (SRIM) `http://www.srim.org/`, version 2008.04.

[4]See [181, 182] for an historic overview of LEAR's achievements.

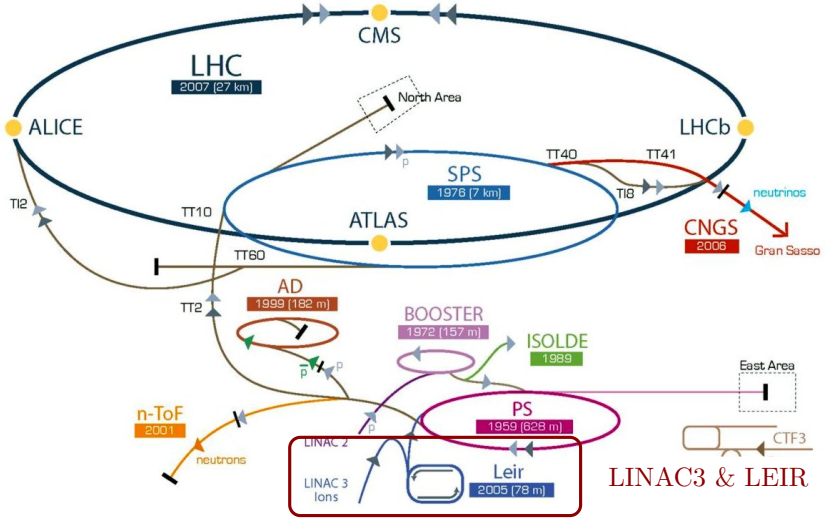

Figure 5.1.: LINAC3 and LEIR in LHC injection chain.

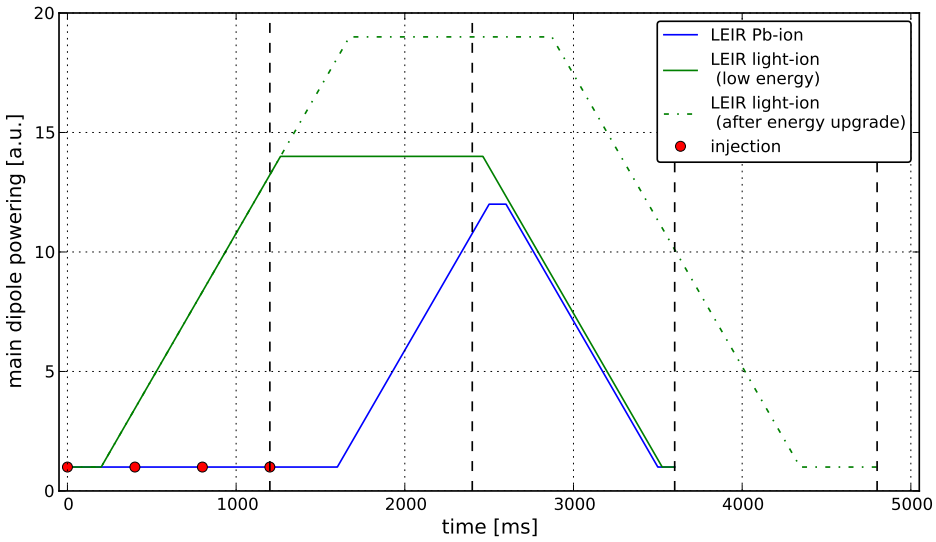

Figure 5.2.: Magnet cycle of LEIR for heavy ion operation [184] (blue) and tentative cycle for proposed light ion operation (green).

Its role is to transform several long, low-intensity pulses from LINAC3 (25 µA to 50 µA), 200 µs, 50 % efficiency: $3 \cdot 10^8$ to $6 \cdot 10^8$ Pb^{54+} per LINAC3 pulse) into short, high-intensity pulses ($9 \cdot 10^8$ Pb^{54+}) that are extracted towards the PS. The revolution time at extraction energy is 700 ns. A 3.6 s cycle for lead ion operation in LEIR [184] is sketched in Fig. 5.2 (blue). Further machine parameters for Pb^{54+} operation are listed in [184, Section 35.13].

A possible operational cycle for slow extraction of light ions from LEIR is also shown in Fig. 5.2. It assumes injection of a single LINAC3 pulse, followed by an acceleration ramp up to $B\rho = 4.8$ T m. Extraction of the accelerated beam is then achieved by debunching of the beam and ramping of the extraction elements. Figure 5.2 indicates an extraction spill of 1.2 s which can be extended as requested by the experiment. After extraction, the main

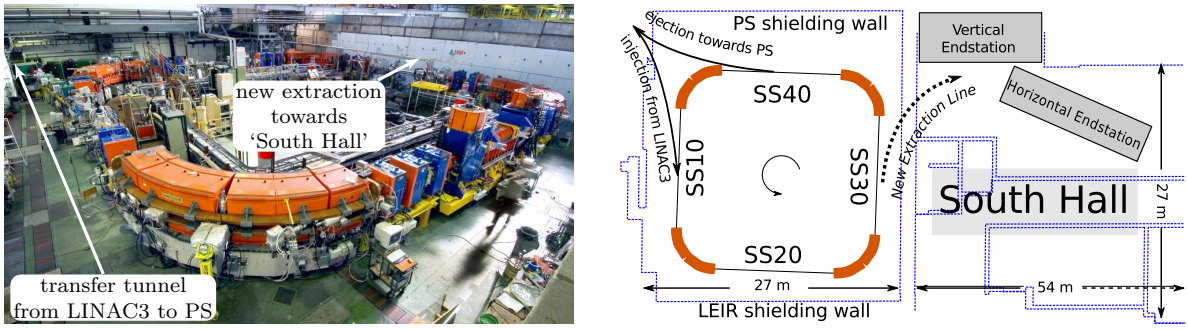

(a) Photograph of current LEIR, from [183].

(b) LEIR and South Hall.

Figure 5.3.: Current LEIR lattice and new ejection from Straight Section 30 (SS30) towards 'South Hall'. Approximate distances and possible positions for new beam transport lines and experimental endstations are indicated in (b). Orange color indicates dipole bending magnets in both figures, blue color indicates quadrupole magnets in (a).

dipoles are ramped down. The whole cycle duration needs to be a multiple of the so-called 'basic period' which presently lasts 1.2 s. Increasing the extraction energy to 430 MeV/n (6.64 T m) requires upgrade of the main dipole power supplies, see Section 5.1.3.4.

Figure 5.3a shows a photograph of the LEIR lattice. Its properties will be explained in detail in section 5.3.1.1, further information on LEIR and its use for LHC operation can be found in [184].

5.1.3. Local Constraints

Fulfilling the requirements outlined in Table 5.1 is subject to a number of constraints given by the existing infrastructure: the LEIR lattice, the injection and pre-acceleration chain and the location itself. In particular, continued use as part of the LHC infrastructure implies that modifications of LEIR must not impact on its performance for heavy ion injection.

5.1.3.1. Location and Space Availability

LEIR is located on the CERN Meyrin site, bordering to the PS ring structure. While most of the surrounding area is occupied by office spaces and machine halls, the 'south hall' area adjacent to LEIR is currently used as storage space. Clearing that area could free approximately 1500 m^2 for the installation of experimental beamlines, laboratories and offices. Figure 5.3b shows the location of LEIR, the adjacent south hall with approximate distances and indicates possible positions for beamlines and future experimental endstations.

5.1.3.2. Ion Species

The capability of the ion source and pre-acceleration stages of LEIR determines the ion species that can be made available for biomedical applications. While the current Electron Cyclotron Resonance (ECR) ion source could, in prinicple, generate most of the ion species identified in Section 5.1.1, components in the heavy ion front-end are not

suited for light ion transport. The Radio Frequency Quadrupole (RFQ) is designed for charge-over-mass ratios $Q/A \approx 1/8$, far below the values expected for light ions.

Various options for upgrades of the LEIR injector are presently being investigated [185]. One of them foresees the use of a commercial ECR ion source, acceleration in a new dedicated light-ion RFQ and injection into the present LINAC3 line with a switch-yard. Such an upgrade would allow ion species to be switched within short time intervals and thus also within consecutive LHC fillings, so that light-ion beams could potentially be provided in parallel to LHC ion operation.

5.1.3.3. Extraction Method

The main methods of beam extraction from synchrotrons are *fast extraction*, based on fast kickers deflecting the beam, and *slow extraction*, based on resonant amplitude growth of the circulating beam. Extraction towards the new experimental area for bio-medical studies needs to take place from Straight Section 30 (SS30), as indicated in Fig. 5.3.

Due to space constraints in the LEIR lattice, implementation of a fast extraction scheme is not easily possible: Extraction kickers cannot be installed in the preceding Straight Section 20 (SS20), and usage of existing kicker magnets would require delicate closed orbit manipulations. Therefore, the implementation of a slow extraction scheme is being studied. Such a scheme had already been used for anti-proton extraction from LEAR, the ancestor of LEIR, and is employed by all synchrotron-based ion beam therapy centres. The working principle of a slow extraction is explained in Section 5.2.3, and first results of this feasibility study are presented in Section 5.3.

5.1.3.4. Extraction Energies

Magnetic field strength $|\mathbf{B}|$ and the bending radius ρ of lattice dipoles determine the maximum magnetic rigidity $B\rho$ of the circulating beam. While the bending limit of LEIR's magnets would allow for a maximum $B\rho = 6.67\,\mathrm{T\,m}$, its currently installed power supplies limit beam rigidity to $B\rho = 4.8\,\mathrm{T\,m}$. For $Q/A = 1/2$, this corresponds to maximimum extraction energies of approximately 430 MeV/n and 240 MeV/n, respectively.

Minimum extraction energy in the proposed slow extraction scheme is governed by the available machine aperture and tune stability. Latter mainly depends on the stability of quadrupole power supplies. First estimates on these limits can be inferred from LEAR experience, where a slow extraction scheme had been employed before [186]. Its lowest extraction momentum of $100\,\mathrm{MeV}/c_0$ (corresponding to 5.5 MeV kinetic energy) for anti-proton extraction was critically limited by the stability of power supplies[5]. Maximum extraction energy from LEAR was constrained by the maximum achievable sextupole strength for resonance excitation and chromaticity correction. An upper momentum limit of $1.7\,\mathrm{GeV}/c_0$ (corresponding to 1 GeV kinetic energy) was reached, and further increasing the maximum extraction energy to 1.27 GeV had been planned[6].

[5] However, two distinct sets of power supplies were employed in LEAR, optimised for low and high currents, respectively. The current LEIR setup only uses a single set of power supplies which is not optimised for low currents. Minimum extraction energies with the current configuration are therefore likely to be higher than the estimates inferred from LEAR operation.

[6] The former LEAR lattice contained twice as many sextupoles as the current LEIR lattice, thus allowing sufficient resonance excitation and chromaticity correction up to high energies.

These minimum and maximum values in extraction energy translate into possible magnetic rigidities between $(B\rho)_{\min} = 0.34\,\mathrm{T\,m}$ and $(B\rho)_{\max} = 6.67\,\mathrm{T\,m}$. For ${}^{12}_{6}\mathrm{C}^{6+}$ this corresponds to an energy range of about 1.5 MeV/n to 430 MeV/n.

5.2. Accelerator Physics Concepts

This section provides the accelerator physics concepts that are needed for the remainder of this chapter. More details can be found in standard accelerator literature, such as [187–190].

First, linear particle motion in accelerators, Section 5.2.1, and resonances, Section 5.2.2, are introduced. Section 5.2.3 then prepares the ground for the slow extraction feasibility study, section 5.3, by explaining how resonant processes can be used for controlled beam extraction. This material is covered in depth in the Proton-Ion Medical Machine Study (PIMMS) design study for a hadron therapy facility [176, 177].

5.2.1. Linear Particle Motion

Accelerators use electromagnetic fields $\mathbf{E}$ and $\mathbf{B}$ to manipulate beams of charged particles. The motion of particles with charge q and velocity $\mathbf{v}$ in these fields is determined by the Lorentz force:

$$\mathbf{F}_{\mathrm{L}} = q\,(\mathbf{E} + \mathbf{v} \times \mathbf{B})\,. \tag{5.1}$$

An accelerator lattice consists of a sequence of elements used for beam manipulation, diagnostics, etc., aligned along the *reference orbit* or *equilibrium orbit*. The reference orbit with curvature $\rho = \rho_0$ is defined by the trajectory of a particle with design momentum $p = p_0$ that experiences a centrifugal force due to its circular acceleration:

$$|\mathbf{F}_{\mathrm{cf}}| = \frac{p^2}{m \cdot \rho}\,. \tag{5.2}$$

To keep a particle on the reference orbit, the Lorentz force, Eq. (5.1), must counteract the centrifugal force, Eq. (5.2). This equilibrium condition defines the magnetic rigidity $B\rho$ of the beam:

$$B\rho = \frac{p}{q}\,, \tag{5.3}$$

with $B = B_0$ the main dipole field strength. A curvilinear right-handed coordinate system ($\hat{\mathbf{x}}$, $\hat{\mathbf{z}}$, $\hat{\mathbf{s}}$) is defined with $s\hat{\mathbf{s}}$ being the distance along the reference orbit measured from some fixed reference point in the lattice, and $x\hat{\mathbf{x}}$ and $z\hat{\mathbf{z}}$ the horizontal and vertical component of the displacement from the reference orbit, Fig. 5.4[7].

[7] The configuration depicted in Fig. 5.4, with $\hat{\mathbf{x}}$ pointing towards the centre of the accelerator lattice for positively charged particles moving anti-clockwise, corresponds to the coordinate system employed by the Methodical Accelerator Design (MAD-X) [191], the tracking programme used for simulations in Section 5.3 and 5.4.

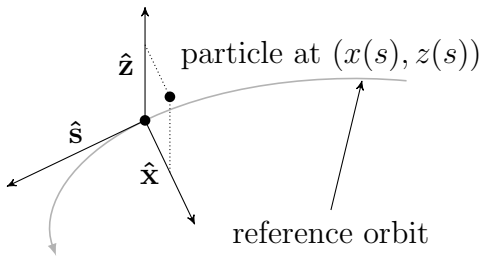

Figure 5.4.: Curvilinear coordinate system along $\hat{\mathbf{s}}$.

5.2.1.1. Magnetic Fields

A transverse two-dimensional magnetic field can be expressed as

$$\mathbf{B} = B_x(x, z)\hat{\mathbf{x}} + B_z(x, z)\hat{\mathbf{z}}\,. \tag{5.4}$$

Close to the axes, the magnetic field can be approximated by its Taylor expansion. The vertical component of the magnetic field in the horizontal plane, B_z, is given by:

$$B_z(x, z = 0) = \sum_{n=0}^{\infty} \frac{1}{n!} \frac{\partial^n B_z}{\partial x^n} x^n = B_0 + \left(\frac{\partial B_z}{\partial x}\right)_{x=0} x + \frac{1}{2!}\left(\frac{\partial^2 B_z}{\partial x^2}\right)_{x=0} x^2 + \dots\,, \tag{5.5}$$

where the constant term B_0 corresponds to a *dipole* field component, the linear term to a *quadrupole* field and the quadratic term to a *sextupole* field. Magnets are characterised by their coefficients in the Taylor expansion $B_n = \frac{\partial^n B_z}{\partial x^n}$. In order to allow characterisation of magnetic elements independently of the beam momentum, their coefficients are usually normalised by the magnetic rigidity $B_0\rho$. The normalised coefficient k_n for a $2(n+1)$-pole can thus be written as:

$$k_n = \frac{1}{|B_0\rho|} \frac{\partial^n B_z}{\partial x^n}\,. \tag{5.6}$$

5.2.1.2. Hill's Equation and Twiss Functions

Most particles in an accelerator will have coordinates and momenta that slightly differ from the properties of the ideal particle defining the reference orbit. Particles with deviating spatial properties undergo *betatron oscillations* about the reference orbit, an oscillatory motion in the transverse plane ($\hat{\mathbf{x}}$, $\hat{\mathbf{z}}$). Due to *dispersion*, particles with momenta different from the design momentum p_0 follow different equilibrium orbits, so-called *off-momentum closed orbits*. Consequently, off-axis and off-momentum particles will perform betatron oscillations around their off-momentum closed orbit.

In a linear lattice, containing only bending (dipole) and focusing (non-skew quadrupole) elements, the two transverse planes are decoupled and betatron motion can be described

by *Hill's equations*:

$$\frac{d^2x}{ds^2} + \left(\frac{1}{\rho^2} - k(s)\right) x = 0 \tag{5.7a}$$

$$\frac{d^2z}{ds^2} + k(s)\, z = 0\,, \tag{5.7b}$$

where ρ and $k(s) = k_1$, the focusing strength along the lattice, are evaluated for the closed orbit of a particle with momentum p[8]. Both equations can be written in the general form

$$\frac{d^2y}{ds^2} + K(s)\, y = 0\,, \tag{5.8}$$

where y represents either horizontal or vertical displacement and $K(s)$ is the generalised potential. A synchrotron lattice with circumference C typically consists of N identical sections of length L each. $K(s)$ therefore fulfils the periodicity relation $K(s) = K(s+C) = K(s+L)$. Hill's equation has periodic solutions that can be expressed in terms of trigonometric functions:

$$y_\beta(s) = \sqrt{\beta(s)\,\epsilon}\,\cos(\mu(s) + \mu_o)\,, \tag{5.9}$$

where the *phase advance* $\mu(s)$ is defined by

$$\mu(\Delta s) = \int_{s_0}^{s_0+\Delta s} \frac{ds}{\beta(s)} \tag{5.10}$$

and the *betatron amplitude function* $\beta(s)$ can be identified with the amplitude function of the oscillation. The phase advance for a full turn around a circular accelerator $\mu(\Delta s = C)$ divided by 2π equals the number of betatron oscillations that particles undergo when traveling around the ring. This quantity is called the *tune* Q. Tune Q, phase advance $\mu(s)$ and $\beta(s)$ are properties of the lattice, whereas the *emittance* ϵ is a property of a single particle or a statistical characteristic of an ensemble of particles. The derivative of $y(s)$ with respect to s, $y' = \frac{dy}{ds}$, denotes the divergence of the particle. Two further parameters can be derived from β which, together with β itself, form the *Twiss* or *Courant Snyder* parameters:

$$\alpha = -\frac{1}{2}\frac{d\beta}{ds}\,, \tag{5.11}$$

$$\gamma = \frac{1+\alpha^2}{\beta}\,. \tag{5.12}$$

A particle with initial condition $(y_0,\, y_0')$ follows an ellipse in *phase space* $(\hat{\mathbf{y}},\, \hat{\mathbf{y}}')$, Fig. 5.5a, described by the Courant-Snyder invariant:

$$C(y, y') = \gamma(s)\, y^2(s) + 2\,\alpha(s)\, y(s)\, y'(s) + \beta(s)\, y'^2(s) = \epsilon\,. \tag{5.13}$$

[8]This takes off-momentum particles with $p \neq p_0$ into account implicitly; an explicit treatment of the inhomogeneous Hill's equation (5.16) follows in section 5.2.1.3.

The phase space area enclosed by this motion is equal to $\pi\epsilon$, its shape and orientation are given by the Twiss parameters and thus depend on the position s in the lattice. For many applications, a representation of phase-space that is invariant to the position s is preferable. This is achieved by *normalised coordinates*:

$$Y = \frac{y}{\sqrt{\beta}}\,, \tag{5.14a}$$

$$Y' = y'\sqrt{\beta} + y\frac{\alpha}{\sqrt{\beta}}\,, \tag{5.14b}$$

which transform the Courant Snyder invariant, Eq. (5.13) and Fig. 5.5a, into a circle, as illustrated in Fig. 5.5b.

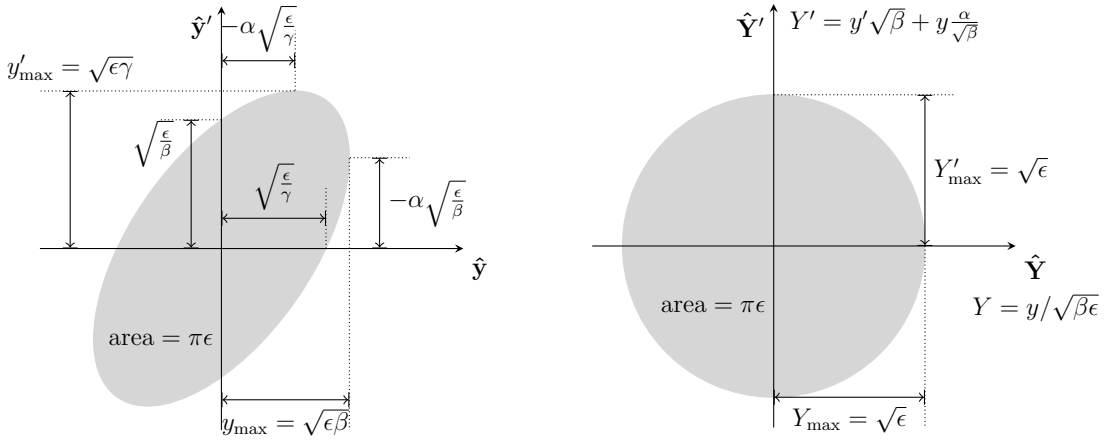

(a) Real phase-space, $\epsilon = \gamma\, y^2 + 2\alpha\, y\, y' + \beta\, x'^2$.

(b) Normalised phase-space, $\epsilon = Y^2 + Y'^2$.

Figure 5.5.: Phase-space trajectory of single particle undergoing betatron oscillation around its equilibrium orbit in real (a) and normalised (b) phase-space.

The emittance of a beam shrinks with increasing energy due to *adiabatic damping*. The *normalised emittance* ϵ^* defines a quantity that is invariant to changes in beam energy:

$$\epsilon^* = \beta_{\text{rel}}\,\gamma_{\text{rel}}\,\epsilon\,, \tag{5.15}$$

with the relativistic parameters β_{rel} and γ_{rel}.

For a Gaussian beam with standard deviation σ, the phase space area described by the root mean squared (r.m.s.) emittance $\epsilon_{\text{rms}} = \pi\frac{\sigma^2}{\beta}$ contains 39% of the beam. For aperture considerations, measures of multiples of r.m.s. emittances are used that contain a larger fraction of the beam. Typically values between $2\,\sigma$ to $2.5\,\sigma$ are chosen for these *geometric* emittances.

5.2.1.3. Dispersion and Chromaticity

Dispersion describes the momentum dependency of a particle's closed orbit from the bending power of dipole magnets, equation (5.3). For a particle with momentum deviation

$\delta p = p - p_0$ from the design momentum p_0, Hill's equation (5.8) takes the form:

$$\frac{d^2y}{ds^2} + K(s)\, y = \frac{1}{\rho}\frac{\delta p}{p_0}\,. \tag{5.16}$$

The solution of this equation is a linear combination of the solution of the homogeneous Hill's equation (5.8) y_β, Eq. (5.9), and of the solution of the inhomogeneous equation (5.16):

$$y(s) = y_\beta(s) + d(s)\frac{\delta p}{p_0}\,, \tag{5.17}$$

where the *dispersion* $d(s)$ is the solution of the inhomogeneous equation and $d(s)\,\frac{\delta p}{p_0}$ describes the *off-momentum closed orbit*. In analogy to normalised coordinates, *normalised dispersion* D and D' can be defined by replacing y, y' in Eq. (5.14) by d and d', respectively.

Also the effects of higher order magnets, such as the focusing or defocusing strength of quadrupole magnets, are momentum dependent. A particle with momentum higher than the reference momentum $\frac{p-p_0}{p_0} = \frac{\delta p}{p_0} > 0$ has a higher magnetic rigidity and thus experiences less focusing than an on-momentum particle. Such momentum-dependencies on focusing strength are referred to as *chromatic aberrations*. Their effect can be described by deviations Δk in the quadrupole gradient strengths which give rise to tune deviations ΔQ in the tune of (off-momentum) particles relative to the lattice (on-momentum) tune:

$$\Delta Q = \frac{1}{4\pi}\oint \beta(s)\,\Delta k(s)\,ds \approx Q'_{\mathrm{nat}}\,\frac{\delta p}{p_0}\,, \tag{5.18}$$

where the *natural chromaticity* Q'_{nat} of a lattice expresses the chromatic effects caused by its quadrupoles:

$$Q'_{\mathrm{nat}} = -\frac{1}{4\pi}\oint \beta(s)\,k(s)\,ds \tag{5.19}$$

with the normalised quadrupole gradient $k(s)$. More generally, the *chromaticity* Q' of a lattice is defined as the derivative of betatron tune versus the fractional change in momentum and can have further contributions from sextupoles:

$$Q' = Q'_{\mathrm{nat}} + Q'_{\mathrm{6pole}}\,, \tag{5.20}$$

where the sextupole contribution is given by

$$Q'_{\mathrm{6pole}} = -\frac{1}{4\pi}\oint k_2(s)\,\beta(s)\,d(s)\,ds\,, \tag{5.21}$$

with the normalised sextupole gradient $k_2(s)$ and the dispersion function $d(s)$. Lattices typically are composed of discrete magnetic elements with lengths l_i. In thin-lens approximation, assuming only small changes in Twiss parameters over the lengths of these elements, the integrals in Eqs. (5.18) and (5.19) can be replaced by sums over all elements i in the lattice with constant k_i over the length of each element.

5.2.1.4. Particle Transport

The solution of a second order linear differential equation, such as Hill's equation Eq. (5.8), is uniquely specified by the value of the function $y(s)$ and its derivative $y'(s)$ at a position $s = s_i$. The relation between phase space coordinates $(y(s_1),\, y'(s_1))$ and $(y(s_2),\, y'(s_2))$ at two distinct positions in the lattice s_1, s_2 can be represented as

$$\begin{pmatrix} y_2 \\ y_2' \end{pmatrix} = \hat{\mathbf{M}}_{21} \cdot \begin{pmatrix} y_1 \\ y_1' \end{pmatrix} \,, \tag{5.22}$$

with the *transfer matrix* $\hat{\mathbf{M}}_{21}$ and phase advance $\Delta\mu = \mu(s_2) - \mu(s_1)$ between the two points in the lattice:

$$\hat{\mathbf{M}}_{21} = \begin{bmatrix} \sqrt{\frac{\beta_2}{\beta_1}}\left(\cos(\Delta\mu) + \alpha_1 \sin(\Delta\mu)\right) & \sqrt{\beta_1\beta_2}\sin(\Delta\mu) \\ \frac{\alpha_1-\alpha_2}{\sqrt{\beta_1\beta_2}}\cos(\Delta\mu) - \frac{1+\alpha_1\alpha_2}{\sqrt{\beta_1\beta_2}} & \sqrt{\frac{\beta_1}{\beta_2}}\left(\cos(\Delta\mu) - \alpha_2\sin(\Delta\mu)\right) \end{bmatrix} . \tag{5.23}$$

In normalised coordinates, transfer matrix $\hat{\mathbf{M}}_{21}$ reduces to a simple rotation in phase space:

$$\hat{\mathbf{M}}_{21-\mathrm{norm}} = \begin{bmatrix} \cos(\Delta\mu) & \sin(\Delta\mu) \\ -\sin(\Delta\mu) & \cos(\Delta\mu) \end{bmatrix} . \tag{5.24}$$

Equation (5.22) can be extended to include dispersive effects:

$$\begin{pmatrix} y_2 \\ y_2' \\ \left(\frac{\delta p}{p_0}\right)_2 \end{pmatrix} = \begin{bmatrix} \hat{\mathbf{M}}_{21} & \begin{matrix} \delta_{21} \\ \delta_{21}' \end{matrix} \\ \begin{matrix} 0 & 0 \end{matrix} & 1 \end{bmatrix} \cdot \begin{pmatrix} y_1 \\ y_1' \\ \left(\frac{\delta p}{p_0}\right)_1 \end{pmatrix} \,, \tag{5.25}$$

where δ_{21}, δ_{21}' describe the coupling between transverse and longitudinal motion and are obtained from

$$\begin{pmatrix} \delta_{21} \\ \delta_{21}' \end{pmatrix} = \begin{pmatrix} d(s_2) \\ d'(s_2) \end{pmatrix} - \hat{\mathbf{M}}_{21} \cdot \begin{pmatrix} d(s_1) \\ d'(s_1) \end{pmatrix} . \tag{5.26}$$

5.2.2. Resonances

Linear motion as discussed before only considers dipole and quadrupole magnetic field components that are used to bend particle trajectories and to achieve stable oscillations around a design orbit. However, additional higher field components are present in a real lattice, due to magnet imperfections or by design. These deviations from perfect guiding fields can result in the excitation of resonant transverse particle motion. If perturbations are sampled periodically, their effect can build up and destabilise transverse motion. Zones of instability are described by the resonance relation

$$l\, Q_x + m\, Q_z = p \,, \tag{5.27}$$

where l, m and p are integer values. For example, in an uncoupled resonance of order $l = n + 1$, the particle returns every l-th turn to the same position $x(s)$ and angle $x'(s)$. A $2(n+1)$-pole magnet can excite this resonance, leading to an increase in the amplitude

of the particle's motion. The case of a sextupole magnet ($n = 2$, $l = 3$) exciting a third order resonance is discussed in more detail in the following Section 5.2.2.1.

5.2.2.1. Third-order Resonance

In an unperturbed lattice, particles of third-integer tune $Q = p \pm \frac{1}{3}$, where p is integer, will return to their initial position in phase space every three turns. The resonance-driving effect of a sextupole magnet can be described as perturbation to this motion. Controlled growth of the amplitude of particle motion can be exploited to extract particles from a synchrotron. This application will be shown in more detail in Section 5.2.3, its principles are introduced here.

The magnetic field components of a sextupole magnet can be derived from its scalar potential. With Eq. (5.5), they can be expressed in terms of the second derivative of the field B_z in the horizontal plane. For a *normal* sextupole, this yields:

$$\begin{pmatrix} B_x \\ B_z \end{pmatrix} = \begin{pmatrix} \partial^2 B_z \\ \partial x^2 \end{pmatrix} \cdot \begin{pmatrix} x \cdot z \\ \frac{1}{2} \cdot (x^2 - z^2) \end{pmatrix} \ . \tag{5.28}$$

A particle passing through the sextupole will thus experience a vertical force, due to B_x, and a horizontal force, due to B_z. In thin-lens approximation, the effect on a particle's trajectory can be described by kicks:

$$\Delta x' = -\frac{B_z \, l_s}{B\rho} = -\frac{1}{2} \, k_2 \, l_s \, (x^2 - z^2) \tag{5.29a}$$

$$\Delta z' = \frac{B_x \, l_s}{B\rho} = k_2 \, l_s \, x \, z \ , \tag{5.29b}$$

where l_s is the length of the magnet and k_2 the normalised sextupole gradient as defined in Eq. (5.6). In normalised coordinates, Eq. (5.14):

$$\Delta X = 0 \quad \text{and} \quad \Delta X' = -\frac{1}{2} \, \beta_x^{3/2} \, k_2 \, l_s \, (X^2 - \frac{\beta_z}{\beta_x} \, Z^2) \tag{5.30a}$$

$$\Delta Z = 0 \quad \text{and} \quad \Delta Z' = 2 \, \beta_x^{3/2} \, k_2 \, l_s \, \frac{\beta_z}{\beta_x} \, X \, Z \ . \tag{5.30b}$$

Unless $Z = 0$, sextupole magnets couple motion in the horizontal and vertical plane. For the application of third order resonance extraction, Section 5.2.3, $Z \ll X$ so that the influence of vertical motion can be neglected to first order. Using the definition of the *normalised sextupole strength*

$$S = \frac{1}{2} \, \beta_x^{3/2} \, \frac{B_z l_s}{B\rho} = \frac{1}{2} \, \beta_x^{3/2} \, l_s \, k_2 \ , \tag{5.31}$$

and only considering horizontal motion ($Z = 0$), Eq. (5.29) can be replaced by

$$\Delta X = \Delta Z = \Delta Z' = 0 \quad \text{and} \quad \Delta X' = S X^2 \ . \tag{5.32}$$

The effect of sextupole kicks on particle motion at third-integer tune can now be

computed by transporting a particle of tune Q over three turns through the lattice using Eq. (5.24), and applying sextupole kicks Eq. (5.32)[9]. The resulting changes in position ΔX_3 and divergence $\Delta X_3'$ over these three revolutions are known as *spiral step* and *spiral kick*, respectively:

$$\Delta X_3 = \tilde{\epsilon}\, X' + \frac{3}{2} S X X' \,, \tag{5.33a}$$

$$\Delta X_3' = -\tilde{\epsilon}\, X + \frac{3}{4} S (X^2 - X'^2) \,. \tag{5.33b}$$

In general X and X' may include dispersive effects so that

$$X = X_\beta + D \frac{\delta p}{p_0} \,, \tag{5.34a}$$

$$X' = X_\beta' + D' \frac{\delta p}{p_0} \,, \tag{5.34b}$$

where X_β, X_β' describe particle motion relative to the off-momentum equilibrium orbit given by $\mathbf{D}\frac{\delta p}{p_0}$.

Identification of Eq. (5.33a) with $\frac{\partial \mathbf{H}}{\partial X_\beta'}$ and Eq. (5.33b) with $-\frac{\partial \mathbf{H}}{\partial X_\beta}$, and integration yields the *Kobayashi Hamiltonian* [192]:

$$\mathbf{H} = \frac{1}{2}\, \tilde{\epsilon}\, (X_\beta^2 + X_\beta'^2) + \frac{S}{4} (3 X_\beta X_\beta'^2 - X_\beta^3) \,, \tag{5.35}$$

with

$$\tilde{\epsilon} = \epsilon - 3S \left(D \frac{\delta p}{p_0} \right) \,. \tag{5.36}$$

The first term of the Hamiltonian describes unperturbed particle motion in the linear machine ($S = 0$), which corresponds to circles in normalised phase space. The size of these circles depends on $\tilde{\epsilon}$ which consists of the *modified tune distance* $\epsilon = 6\,\pi\,\delta Q$ of a particle from resonance and a dispersion-dependent term.

The second term of the Hamiltonian describes the perturbation due to a sextupole magnet that distorts the phase space trajectories into triangular form. With increasing excitation strength S this effect becomes stronger until, at a certain level of excitation, the closed trajectories open up; the particles on these open trajectories are unstable. The trajectories separating phase space areas of stable and unstable motion are called *separatrices* and connect the three unstable *fixed-points* of the system. Stable (P_0) and unstable fixed-points (P_1, P_2, P_3), Eq. (5.41), fulfill the condition $\frac{\partial \mathbf{H}}{\partial X} = 0$ and $\frac{\partial \mathbf{H}}{\partial X'} = 0$ and are illustrated in Fig. 5.6.

Equating the general Hamiltonian $\mathbf{H}(X, X')$ with the Hamiltonian at the position of one of the unstable fixed-points $\mathbf{H}(X_{\mathrm{FP}}, X'_{\mathrm{FP}})$ yields an equation for the separatrices:

$$\left(-X + \sqrt{3}\, X' + \frac{4\tilde{\epsilon}}{3S} \right) \cdot \left(X + \sqrt{3}\, X' - \frac{4\tilde{\epsilon}}{3S} \right) \cdot \left(\frac{SX}{4} + \frac{\tilde{\epsilon}}{6} \right) = 0 \,. \tag{5.37}$$

[9] A detailed derivation can be found in [176].

A general equation for the separatrices, also taking into account dispersive effects, can be formulated:

$$h = \frac{4\pi}{S}\widetilde{\delta Q} = \left(X - D\frac{\delta p}{p_0}\right)\cos\alpha + \frac{1}{2}\left(X' - D'\frac{\delta p}{p_0}\right)\sin\alpha \ , \tag{5.38}$$

with angle α between the horizontal half-axis of the stable triangle and the normal vector to one of the three separatrices, as indicated in Fig. 5.6. The tune distance from resonance $\widetilde{\delta Q} = \delta Q + Q'\frac{\delta p}{p_0}$ of a particle takes into account the tune distance $\delta Q = Q_0 - Q_{\text{res}}$ due to lattice tune, and the momentum-dependent tune shift $Q'\frac{\delta p}{p_0}$ of a particle with momentum offset $\frac{\delta p}{p_0}$ due to chromaticity. Figure 5.7 illustrates this relation.

The area of the largest *stable triangle*, the *acceptance*, can be derived from Eq. (5.38):

$$A_\Delta = \frac{4}{\sqrt{3}}\frac{\tilde{\epsilon}^2}{S^2} = \frac{48\pi\sqrt{3}}{S^2}(\widetilde{\delta Q})^2\pi \ . \tag{5.39}$$

This area of stability in phase space is determined by the ratio of tune distance and excitation strength $|\tilde{\epsilon}/S|$: The motion of a particle is stable if its single particle emittance $\epsilon_{\text{particle}}\,\pi = A^2_{\text{particle}}\,\pi$, defined by the particle's normalised amplitude $A = \sqrt{X^2 + X'^2}$, is smaller than the acceptance defined in Eq. (5.39):

$$A^2_{\text{particle}}\pi \leq \frac{48\pi\sqrt{3}}{S^2}(\widetilde{\delta Q})^2\pi \ . \tag{5.40}$$

The acceptance (5.39) of a particle close to resonance tune ($\widetilde{\delta Q} \approx 0$) approaches zero and thus the particle becomes unstable.

The orientation of this stable triangle in phase space is determined by the sign of S and the observation point in the lattice. The angle α in equation (5.38) can be described by an initial angle α_0 at the position of the resonance driving sextupole and the phase advance $\Delta\mu$ between resonance driving sextupole and the observation point: $\alpha = \alpha_0 - \Delta\mu$, where α_0 takes values $\{60°, 180°, 300°\}$ and $\{0°, 120°, 240°\}$ for $S > 0$ and $S < 0$, respectively. Approaching the resonance tune 'from above' ($\widetilde{\delta Q} > 0$) or 'from below' ($\widetilde{\delta Q} < 0$) determines the separatrix from which particles are extracted. Figure 5.8 illustrates the possible configurations for all combinations ($\widetilde{\delta Q}$, S) at the position of the resonance-driving sextupole ($\Delta\mu = 0$).

The stable triangle at any position along the lattice can be obtained by transporting the fixed-points found at the resonance driving sextupole Eq. (5.41) according to Eq. (5.22), which corresponds to a clockwise rotation of the phase space map in normalised phase space. Area and shape of the stable triangle remain unaffected by the transport.

Tune and amplitude dependence of stability condition Eq. (5.40) are frequently depicted in a so-called *Steinbach Diagram*. Figure 5.7 illustrates this for positive chromaticity: If a particle's amplitude A_p is sufficiently large and its tune distance from resonance $\widetilde{\delta Q}$ sufficiently small, its motion will approximate the separatrices between the unstable fixed-points, depicted in Fig. 5.6. Any further increase in amplitude, or decrease in tune distance, will result in unstable particle motion. For a given position in the lattice, particles then follow the open trajectories indicated in Fig. 5.8.

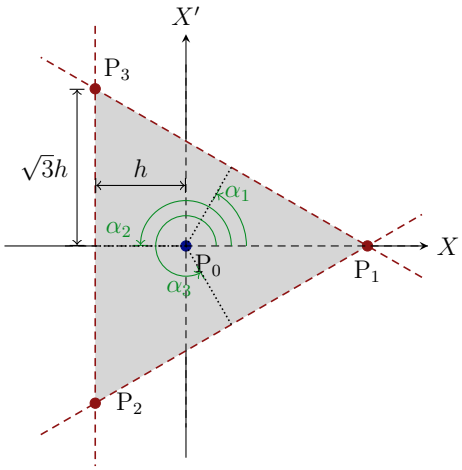

$$P_0 = (0,\, 0) \tag{5.41a}$$

$$P_1 = \left(\frac{4}{3}\frac{\tilde{\epsilon}}{S},\, 0\right) \tag{5.41b}$$

$$P_{2,3} = \left(-\frac{2}{3}\frac{\tilde{\epsilon}}{S},\, \pm\frac{2}{\sqrt{3}}\frac{\tilde{\epsilon}}{S}\right) \tag{5.41c}$$

Figure 5.6.: Separatrix at resonance driving sextupole with stable (P_0) and unstable fixed-points (P_1, P_2, P_3), Eq. (5.41), for zero dispersion $\mathbf{D} = 0$

Figure 5.7.: Steinbach diagram (stable configuration): Off-resonance lattice tune Q_0 with tune distance δQ from resonance. Beam is centred around design momentum p_0 with momentum spread $\pm\Delta p_\mathrm{b}$. The tune distance $\widetilde{\delta Q}$ of a particular particle in the beam is determined by the lattice tune Q_0 and a tune-shift $Q'\frac{\delta p}{p_0}$, caused by chromaticity and the particle's momentum off-set δp from p_0.

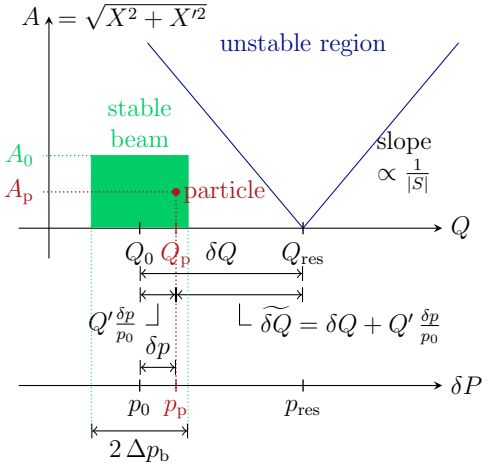

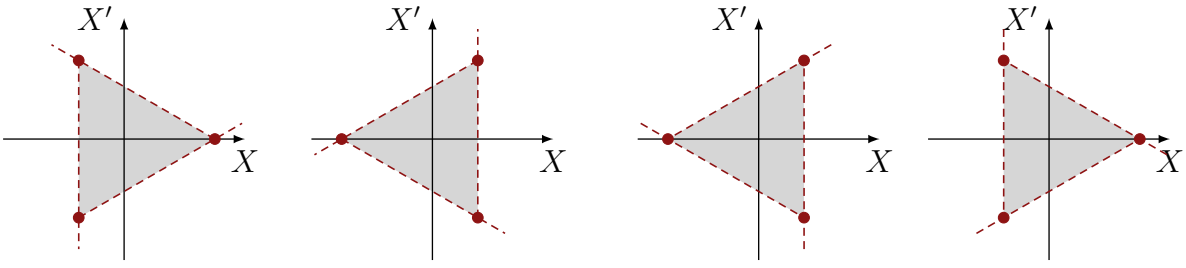

(a) $\widetilde{\delta Q} > 0,\ S > 0$ **(b)** $\widetilde{\delta Q} > 0,\ S < 0$ **(c)** $\widetilde{\delta Q} < 0,\ S > 0$ **(d)** $\widetilde{\delta Q} < 0,\ S < 0$

Figure 5.8.: Schematic illustration of the orientation of separatrices at the position of the resonance-driving sextupole for different configurations of $\widetilde{\delta Q}$ and $\operatorname{sgn} S$. Extended lines indicate the separatrices along which unstable particles diverge.

5.2.3. Third-order Resonant Extraction

The emittance growth and particular geometry of particle trajectories at a third-order resonance can be exploited to implement a *slow-extraction* scheme where a small portion of the circulating particles is being removed continuously - and over a large number of turns - from the circulating beam. Such a scheme can achieve low particle fluxes with extraction times typically of the order of several seconds to minutes.

5.2.3.1. Description of Extraction Process

During particle injection and acceleration, the machine needs to be tuned sufficiently far away from the resonance tune to allow for stable particle motion. Figure 5.9 illustrates this for extraction 'below resonance' with $Q_0 < Q_{\mathrm{res}}$. After reaching extraction energy the beam is debunched and parts of the stable beam are slowly driven into resonance. Different resonance-driving mechanisms are indicated in Fig. 5.9 and will be discussed in the following subsection.

The *stable* part of the beam corresponds to particles with amplitudes below the stability threshold given by Eq. (5.40). These particles continue circulating in the accelerator. Particles above this threshold are *unstable*. Their transverse (horizontal) oscillation amplitude increases according to Eq. (5.33a) so that the particles diverge along the separatrices Eq. (5.38). This amplitude growth can be exploited for extraction as it allows particles to jump across a thin septum by which they are kicked away from the circulating beam towards the extraction line. This process is described in more detail in Section 5.2.3.3. The remainder of this section discusses requirements for efficient extraction.

5.2.3.2. Resonance-driving Mechanisms

The flux of extracted particles is determined by the rate at which particles become unstable. Different methods for gradually bringing beam particles into resonance are illustrated in Fig. 5.9. This section outlines the most common of these methods; further information about simulation and comparison of these methods with regard to their suitability for medical ion beam facilities can be found in [193].

Radio-Frequency Knock-Out (RF-KO) (①, Fig. 5.9) is based on transverse excitation of the stable beam by applying band-limited noise signals. As the amplitude of the beam grows, beam particles exceed the stability limit due to their large amplitude, *amplitude selection* (Ⓐ, Fig. 5.9). The momentum spread of the extracted beam corresponds to the momentum spread of the stable 'waiting' beam. RF-KO is being used for extraction from medical accelerators, for example at the Heidelberger Ionenstrahl Therapiezentrum (HIT) [194] and the Centro Nazionale di Adroterapia Oncologica (CNAO) [178], and would provide a versatile option also for extraction of medical beams from LEIR. In combination with appropriate noise signal generators, existing machine elements could be used for this purpose.

Other methods are based on manipulating the tune of beam particles to approach resonance tune. Particles with the smallest tune distance from resonance $\widetilde{\delta Q}$ and largest amplitude A_{p} become unstable first, and soon particles with a variety of amplitudes and tune distances follow. The instantaneously extracted momentum spread of the

beam extracted by these methods depends on the resonance configuration, waiting beam amplitude and resonance-driving mechanism.

The simplest of these methods is *tune-driven* extraction through modification of the lattice tune by varying the strength of lattice quadrupoles, thus moving Q_0 closer to resonance tune Q_{res} (②, T in Fig. 5.9). This method has been used effectively at the Helmholzzentrum für Schwerionenforschung (GSI) to provide beams for patient treatment, despite its sensitivity to tune ripples and effects on the position stability of the circulating beam. As it does not require additional dedicated equipment to be installed in the lattice, this method would be well-suited for first experiments at LEIR. Two further methods are based on modifying the momentum p_{p} of beam particles in order to decrease their tune distance $\widetilde{\delta Q}$. The required change in particle momentum can be achieved in different ways: *Acceleration-driven extraction* (③, M in Fig. 5.9) slowly drives the whole waiting beam into resonance by modifying p_0, for example via a betatron core for inductive acceleration. As it requires the installation of dedicated equipment in the accelerator lattice, this method is less suited for LEIR. *Stochastic extraction* (④, M in Fig. 5.9) increases the beam's momentum-spread $\pm\Delta p$ via application of longitudinal Radio Frequency (RF)-noise. This method was implemented in LEAR previously [195], since it allows extraction with very low particle fluxes and long spill lengths.

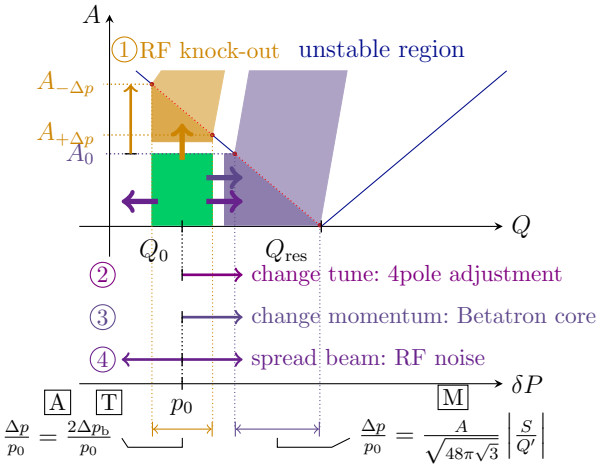

Figure 5.9.: Steinbach diagram illustrating different *driving mechanisms* for extraction: Parts of the stable beam can be driven into resonance by *amplitude increase* ①, *tune adjustment* ②, or *beam acceleration* ③ ④. The instantaneously extracted momentum spread depends on the selection mechanism: by amplitude A, tune T, or momentum M. Positive chromaticity $Q' > 0$ is assumed and resonance approached 'from below' resonance tune $\widetilde{\delta Q} < 0$.

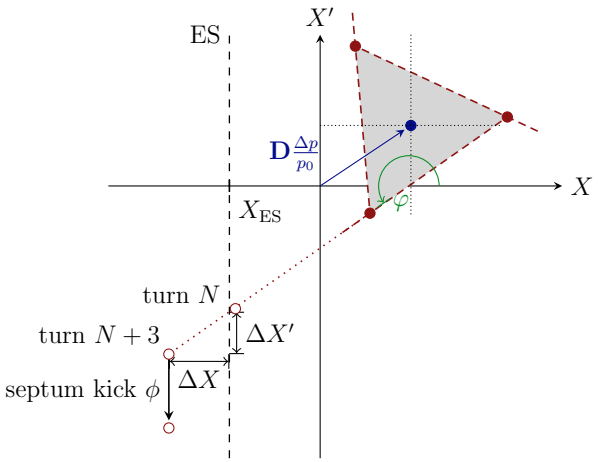

Figure 5.10.: Spiral step ΔX and spiral kick $\Delta X'$ across electrostatic ejection septum (ES).

5.2.3.3. Spiral Step and Kick across Electrostatic Septum

Once the motion of a particle has become unstable, its horizontal amplitude increases quadratically every three turns. After N turns the particle passes just outside the electrostatic ejection septum (ES) and spends the next two turns on other separatrices. On the third turn, $N+3$, the particle returns to the original separatrix, however, due to the increase in amplitude it is now located inside the ES, compare Fig. 5.10. The difference in amplitude between the N^{th} and the $N+3^{\text{rd}}$ turn consists of a radial and a divergence part, the spiral step and spiral kick, Eq. (5.33).

Taking into account orbit deviations, the spiral step at the position of the ES can be expressed as[10]:

$$\Delta X_{\text{ES}} = \left(\frac{3}{4} S \left((X_{\text{ES}} - X_{\text{OD}})^2 + (X'_{\text{ES}} - X'_{\text{OD}})^2 \right) - \frac{4}{3} \frac{\tilde{\epsilon}^2}{S} \right) \cdot \cos\varphi \,, \tag{5.42}$$

where X_{ES} is the transverse position of the electrostatic septum in normalised coordinates,

$$X_{\text{OD}} = D_{\text{ES}} \frac{\delta p}{p_0} + X_{\text{OC}} \,, \tag{5.43}$$

$$X'_{\text{OD}} = D'_{\text{ES}} \frac{\delta p}{p_0} + X'_{\text{OC}} \,, \tag{5.44}$$

represent deviations from the design orbit due to dispersive effects and orbit correction at the ES, and φ the angle between the separatrix and the horizontal axis, as illustrated in Fig. 5.10. The spiral kick can be obtained as the projection of ΔX_{ES} on the X' axis.

For an on-resonance particle and the ES positioned in a non-dispersive part of the beam-line, above expression simplifies to

$$\Delta X = \frac{3}{4} S \frac{1}{\cos\varphi} \left(X_{ES} - X_{\text{OD}} \right)^2 \,. \tag{5.45}$$

5.2.3.4. Virtual Sextupole

The Kobayashi Hamiltonian, Eq. (5.35), only takes into account the effect of one single sextupole on particle motion. The combined effect of multiple sextupoles on the resonance can be described by a driving term κ [197], for the third-order resonance:

$$\kappa \propto \sum_n S_n \exp(3i\mu_{x,n}) \,. \tag{5.46}$$

[10] Equation (5.42) is obtained by inserting one of the separatrices, Eq. (5.37), into Eq. (5.33) and transporting the result to the position of the ES. Dependence from phase-advance $\Delta\mu$ between resonance sextupole and ES can then be replaced by the angle φ between horizontal axis and separatrix. A detailed derivation can be found in [196].

The sum over all sextupoles in the lattice can then be replaced by a single *virtual sextupole* with the virtual sextupole strength S_{virt} and phase advance μ_{virt}:

$$S_{\text{virt}}^2 = \left[\sum_n S_n \cos(3\mu_{x,n})\right]^2 + \left[\sum_n S_n \sin(3\mu_{x,n})\right]^2 , \tag{5.47a}$$

$$\mu_{\text{virt}} = \frac{1}{3}\arctan\left(\frac{\sum_n S_n \sin(3\mu_{x,n})}{\sum_n S_n \cos(3\mu_{x,n})}\right) . \tag{5.47b}$$

5.2.3.5. Geometric Considerations

The slow extraction principle relies on a sequence of septa that successively impart deflections ϕ to the particles which - after phase advance $\Delta\mu$ to the next septum - translates into a physical displacement of the particle. At the first septum, typically a very thin ES, the kick needs to be directed away from the $\hat{x}$ axis, as illustrated in Fig. 5.10, in order to separate extracted and circulating sections of the separatrix. Further, the particle's X' coordinate should ideally have the same sign as its position coordinate in normalised phasespace, in order to drive the separated particles away from the axis of the machine and from the septum wires. Extraction therefore is best to be performed in the first ($X > 0$, $X' > 0$) or third ($X < 0$, $X' < 0$) normalised phasespace quadrant.

The separation resulting from a deflection ϕ after phase advance $\Delta\mu$ can be estimated by comparing the transport of two (on-momentum) particles to the position of the magnetic septum: Both particles start at the horizontal position of the ES and with the same X', but only one receives a kick ϕ. Equation (5.48) provides an estimate for the resulting gap that becomes available for the magnetic septum $\Delta\mu$ downstream:

$$\Delta x_{\text{MS}} = \phi\sqrt{\beta_{\text{ES}}\beta_{\text{MS}}}\sin(\Delta\mu) . \tag{5.48}$$

Orientations φ in which two of the three separatrices have the same distance to one of the septa result in particle losses. Since the three separatrices are separated by 120°, such losses will occur for angles $\varphi_{\max} > 60°$ (first quadrant extraction) and $\varphi_{\max} > 240°$ (third quadrant extraction) at the first septum, and for angles $\varphi_{\min} < \Delta\mu - 60°$ and $\varphi_{\min} < \Delta\mu - 240°$ at the second septum, depending on the phase advance $\Delta\mu$ between both septa. Ideally a phase advance of $\Delta\mu = 90°$ would be chosen between both ES and magnetic ejection septum (MS), so that the kick imparted on the particle by the first septum fully translates into a spatial separation at the second septum. In that case, the smallest possible angle at the ES would be limited to $\varphi_{\min} = 30°$ ($\varphi_{\min} = 210°$).

The orientation of the separatrices at the first septum depends on the sign of S, on $\widetilde{\delta Q}$, as well as on the phase advance $\Delta\mu$ between resonance driving (virtual) sextupole and septum. Assuming an intermediate separatrix angle between these limits, $\varphi = 45°$ ($\varphi = 225°$), geometrical considerations lead to the value pairs ($\Delta\mu$, α) given in Table 5.2 for extraction in the first or third quadrant and different resonance configurations ($\widetilde{\delta Q}$, S). The angle α can be determined by selecting α_0 of the extraction separatrix at the (virtual) resonance-driving sextupole, Fig. 5.6, and transporting it to the position of the ES: $\alpha = (\alpha_0 - \Delta\mu)$.

	$\widetilde{\delta Q} < 0$		$\widetilde{\delta Q} > 0$	
	1st quadrant	3rd quadrant	1st quadrant	3rd quadrant
$S < 0$	$\Delta\mu = 45°$ $\alpha = 135°$	$\Delta\mu = 105°$ $\alpha = 315°$	$\Delta\mu = 45°$ $\alpha = 315°$	$\Delta\mu = 105°$ $\alpha = 135°$
$S > 0$	$\Delta\mu = 105°$ $\alpha = 135°$	$\Delta\mu = 45°$ $\alpha = 315°$	$\Delta\mu = 105°$ $\alpha = 315°$	$\Delta\mu = 45°$ $\alpha = 135°$

Table 5.2.: Required phase-advance $\Delta\mu$, between (virtual) resonance sextupole and ES, and separatrix orientation α for different resonance settings ($\widetilde{\delta Q}$, S). The values assume $\varphi = 45°$ and $\varphi = 225°$ for first and third quadrant extraction, respectively. Values for $\Delta\mu$ are given modulo 120° to account for the freedom in choosing the initial separatrix α_0: $\alpha = \alpha_0 - \Delta\mu$, compare Fig. 5.6 and 5.8.

5.2.3.6. Hardt Condition

The trajectories of simultaneously extracted beam particles are typically not superposed because – due to the momentum spread of the beam – these particles are extracted at different tune distances $\widetilde{\delta Q}$. This is illustrated in Fig. 5.11a: *a*) the size of stable triangles differs due to tune shifts via the chromaticity, equation (5.39), and *b*) the positions of separatrices pertaining to particles with different momentum off-sets are shifted by the dispersion vector, equation (5.41).

The resulting 'misalignment' causes off-momentum particles to cross the ES at different X'. However, the ES has a finite length and is designed for transporting particles within a certain X' range. Particles exceeding the angular aperture will be lost either at the (inner) septum wires or the (outer) septum wall. If transported through the ES, initial misalignment increases the full divergence $\Delta X'$ of the extracted beam segment, which reduces the gap available for the MS, resulting in particle losses there.

Choice of suitable $\frac{Q'}{|S|}$ allows compensation of the dispersion shift ($\propto \mathbf{D} \cdot \delta p/p_0$) of off-momentum particles by increasing their stable phase space areas ($\propto \frac{Q'}{S} \cdot \frac{\delta p}{p_0}$) so that their extraction separatrices align, Fig. 5.11b. This can be achieved by removing the momentum dependence from separatrix equation Eq. (5.38). The resulting relation, known as *Hardt condition* [195], provides a condition for the magnitude of $\frac{Q'}{|S|}$ required to superpose the trajectories of off-momentum particles, in function of the normalised dispersion vector $\mathbf{D}$ and the orientation of the extraction separatrix at the ES:

$$D\cos(\alpha) + D'\sin(\alpha) = -4\pi Q' \frac{\operatorname{sgn}(\widetilde{\delta Q})}{|S|}\,. \tag{5.49}$$

The left hand side (LHS) of Eq. (5.49) is determined by the angle between the normal vector on the extraction separatrix, α, and the dispersion vector $\mathbf{D}$. Table 5.2 shows that a change in the sign of $\widetilde{\delta Q}$ reverses the sign of the LHS of Eq. (5.49) due to the change in α, whereas a change in the sign of S has no effect on the LHS. The term $\frac{\operatorname{sgn}(\widetilde{\delta Q})}{|S|}$ in the right hand side (RHS) of Eq. (5.49) compensates for this.

The example in figure 5.11a assumes $\widetilde{\delta Q} < 0$ ($\delta Q = 0$ and $\frac{\delta p}{p_0} < 0$) and a given

dispersion vector **D**. In this configuration, the stable triangle emittance of off-momentum particles needs to be increased in order to align with the extraction separatrices of on-momentum particles and to compensate for a dispersive shift in the opposite direction. This requires a high absolute value of the chromaticity and a positive sign ($Q' \gg 0$).

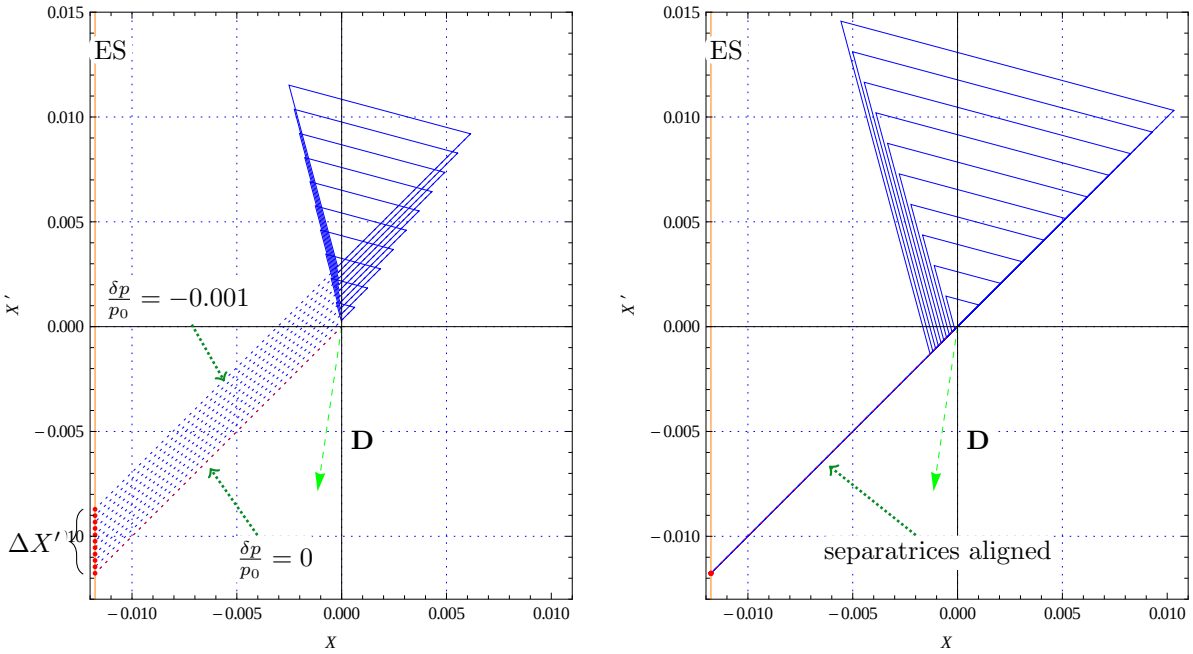

(a) Hardt condition not fulfilled. **(b)** Hardt condition fulfilled.

Figure 5.11.: Two extraction configurations with unfulfilled (a) and fulfilled (b) Hardt condition. Extraction separatrices in configuration (a) are 'misaligned', resulting in a larger divergence spread $\Delta X'$ of the extracted beam segment compared to configuration (b).

5.3. Slow Extraction Study (Transverse Aspects)

This section presents investigations into the feasibility of implementing a new slow extraction scheme in LEIR.

Equation (5.42), or in simplified form Eq. (5.45), defines a relation between the main parameters for the transverse aspects of the extraction process: normalised transverse horizontal position X_{ES} of the ES, normalised sextupole strength S, orientation of the extraction separatrix φ in normalised phase space and the resulting spiral step width ΔX. Derivation of a suitable extraction configuration for LEIR from this formula requires multiple steps which are presented in the following sections:

In order to relate above parameters to real coordinates, first, the position for the ES has to be determined, based on the constraints imposed by the LEIR lattice, Section 5.3.1. This choice defines relevant Twiss functions, so that an analytic estimate for suitable parameters (Δx, φ, S, Q') can be computed, Section 5.3.2. Particle tracking simulations based on this estimate are performed in Section 5.3.3 to verify and refine the analytic results and to derive parameters for the extracted beam segment. Section 5.3.4 discusses

the results and draws conclusions on the feasibility to implement a slow extraction scheme in LEIR.

5.3.1. LEIR-specific Constraints

This section describes two lattice configurations with horizontal tune $Q_H = 5/3$ and $Q_H = 7/3$, similar to the current LEIR and former LEAR configuration, respectively.

5.3.1.1. Lattice Parameters and selected Beams

LEIR, as currently in operation, has a 'square' lattice with 79 m circumference, composed of four straight sections (*SS10*, *SS20*, *SS30*, *SS40*) with a total length of 12.8 m each and four 90° bending sections (*ARC10*, *ARC20*, *ARC30*, *ARC40*), Fig. 5.12.

Several long, low-intensity ion pulses from Linear Accelerator (LINAC)3 are injected into Straight Section 10 (SS10) by means of a special stacking mechanism in transverse and longitudinal phase space [198]. For heavy-ion accumulation, injection is alternated with phase space cooling, achieved by an electron cooler [199] installed in the adjacent SS20. After accumulation and acceleration, fast kicker magnets installed in SS30 are used to extract a single short, high-intensity pulse from Straight Section 40 (SS40). A quasi two-fold periodicity was chosen for LEIR due to requirements of the injection mechanism and for effective electron cooling. Two RF cavities are installed in SS40.

Focusing is provided by quadrupole doublets in the injection section SS10 and the opposite section SS30, and by triplets in the cooling section SS20 and the extraction section SS40. Two families of sextupole magnets with four sextupoles each are installed in section SS10 and SS30 for chromaticity correction. In addition, two weaker sextupoles are present in SS40 and the bending magnets are equipped with entrance and exit Pole Face Windings (PFW) producing dipolar and sextupolar magnetic fields. Table 5.5 lists the properties of installed sextupole magnets. Multiple orbit correction magnets are present in LEIR, the ones used for orbit manipulations in SS30 (*DWHV21*, *DWHV32*, *DEHV22*, *DWHV22*, *DWHV31*, *DHV31*) are indicated in Fig. 5.12.

The nominal working point for optimised injection efficiency and Pb operation was found to be $Q_{\mathrm{H}} = 1.82$, $Q_{\mathrm{V}} = 2.72$. Details about the rationale underlying the design choices that led to the LEIR lattice are described in [184, Chapter 35].

Slow resonant extraction requires the lattice to be tuned close to a third-integer resonance. Two different tune configurations of the currently existing lattice are investigated in the first part of this study:

LEIR-like configuration, similar to the current configuration for LHC Pb-ion operation, but with horizontal tune $Q_{\mathrm{H}} = 5/3$. Figure 5.13a shows the lattice functions for this configuration with zero-dispersion in both SS20 and SS40.

LEAR-like configuration, similar to the former LEAR which implemented a slow extraction scheme based on horizontal tune $Q_{\mathrm{H}} = 7/3$. Figure 5.13b illustrates the four-fold periodicity and the lower values for horizontal betatron and dispersion functions that can be achieved in this configuration.

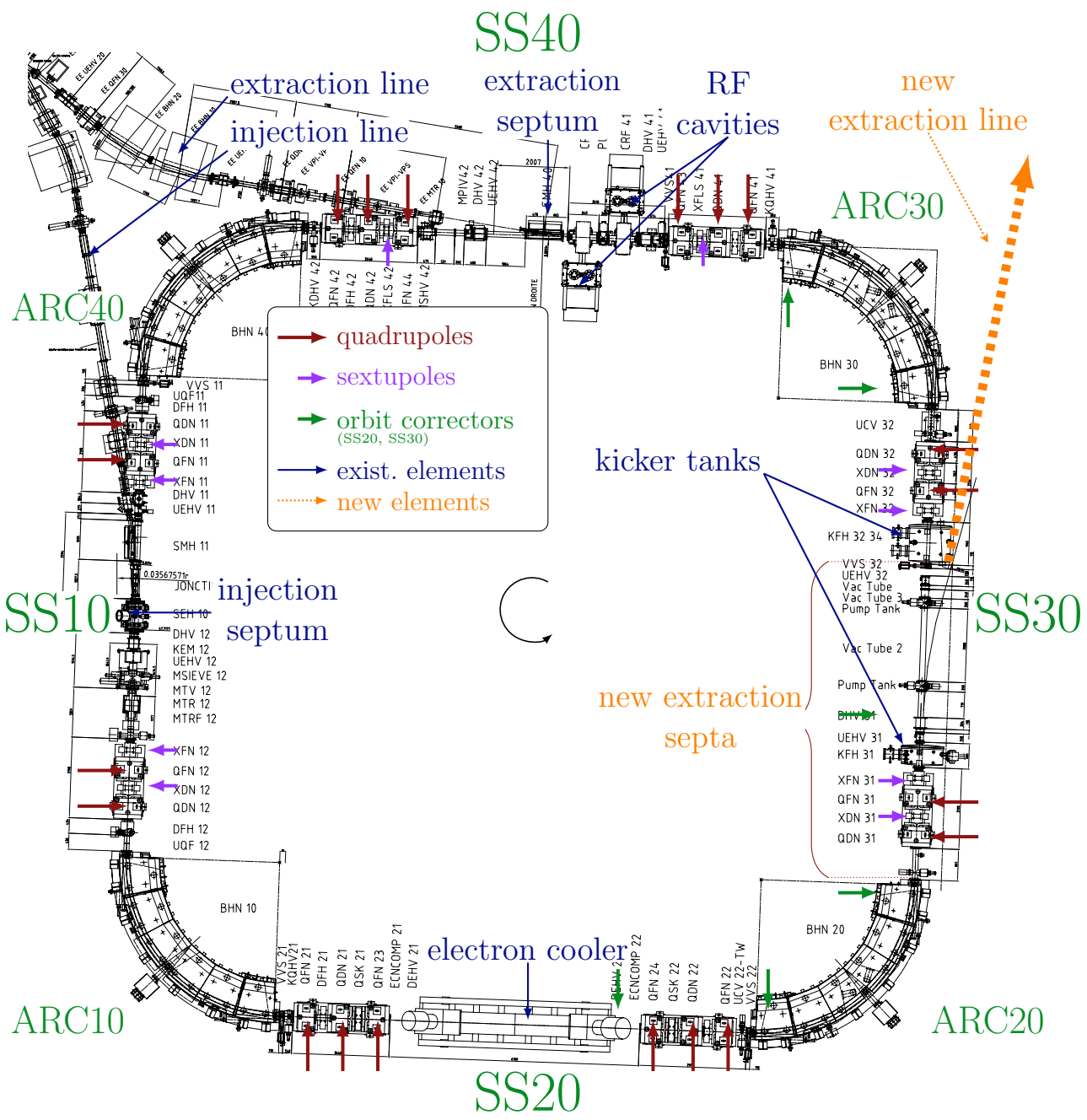

Figure 5.12.: The LEIR lattice. See Fig. 5.14 for a detailed view of the new extraction section SS30.

The optical functions of these configurations are summarised in Fig. 5.13 and Table 5.3, respectively. Due to the choice of the coordinate system, compare Fig. 5.4, dispersion functions assume negative values.

Beam properties at injection and potential extraction energies for LEIR are listed in Table 5.4. Values for beam emittances are based on the geometric emittances $\epsilon_{\mathrm{H,geom}} = 60\,\pi\,\mathrm{mm\,mrad}$, $\epsilon_{\mathrm{V,geom}} = 40\,\pi\,\mathrm{mm\,mrad}$ at injection energy ($^{208}_{53}\mathrm{Pb}$ at 4.2 MeV/n) after phase space stacking and before cooling according to [184, Section 35.13]. These numbers take into account the phase space covered to $2.5\,\sigma$ [198] and thus correspond to normalised

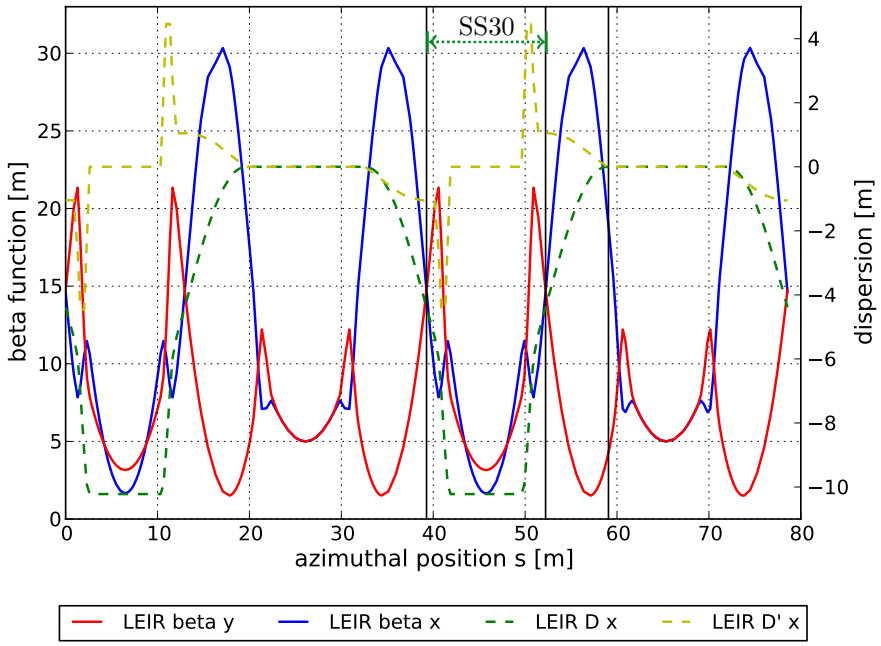

(a) Optical functions in LEIR-like lattice at third-integer resonance $Q = 5/3$.

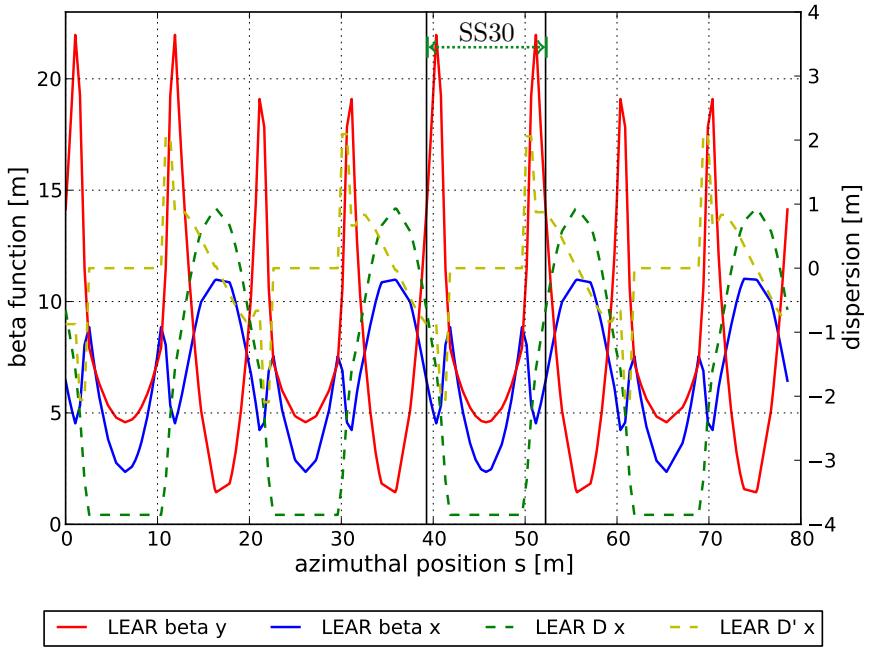

(b) Optical functions in LEAR-like lattice at third-integer resonance $Q = 7/3$.

Figure 5.13.: Lattice function of (a) LEIR-like and (b) LEAR-like lattices.

configuration	Q_{H}	Q_{V}	$Q'_{\mathrm{H,nat}}$	$Q'_{\mathrm{V,nat}}$	$\beta_{x,\mathrm{max}}$	$\beta_{y,\mathrm{max}}$	$d_{x,\mathrm{max}}$	$d'_{x,\mathrm{max}}$
LEAR	7/3	2.73	-2.71	-6.95	11.02	21.97	-3.85	-2.09
LEIR	5/3	2.72	-3.49	-4.54	30.34	21.34	-10.22	-4.46

Table 5.3.: Lattice Parameters for LEIR- and LEAR-like configurations.

		Injection	**Extraction**					
			P6	*P5*	*P4*	*P3*	*P2*	*P1*
E	[MeV/n]	4.2	10	20	30	40	240	430
$B\rho$ $(q/A = 1/2)$	[T m]	0.59	0.92	1.30	1.60	1.85	4.75	6.64
$\epsilon_{\mathrm{H,rms}}$	[π mm mrad]	9.61	6.22	4.38	3.57	3.08	1.20	0.86
$\epsilon_{\mathrm{H,geom\,(2.5\,\sigma)}}$	[π mm mrad]	60.04	38.85	27.40	22.31	19.27	7.49	5.36
$\epsilon_{\mathrm{V,rms}}$	[π mm mrad]	6.44	4.17	2.94	2.39	2.07	0.80	0.57
$\epsilon_{\mathrm{V,geom\,(2.5\,\sigma)}}$	[π mm mrad]	40.25	26.04	18.37	14.96	12.92	5.02	3.59
$(\Delta p/p_0)_{(1\,\sigma)}$	[10^{-3}]	$\pm$0.2						

Table 5.4.: Beam parameters at injection (4.2 MeV/n) and extraction energies: Configurations *P6-P3* correspond to minimum potential extraction energies 10 MeV/n to 40 MeV/n, configurations *P2* and *P1* to maximum extraction energy with the current power supplies (240 MeV/n) and after power supply upgrade (430 MeV/n, magnet limit).

r.m.s. emittances $\epsilon^*_{\mathrm{H,rms}} = 0.91\,\pi$ mm mrad and $\epsilon^*_{\mathrm{V,rms}} = 0.61\,\pi$ mm mrad, respectively[11]. In contrast to the current Pb-ion injection scheme, provision of bio-medical ion beams will not require longitudinal phase space stacking. The beam momentum at injection is therefore assumed to correspond to the momentum spread of the beam served by LINAC3, $\Delta p/p_0\,(1\,\sigma) = \pm 2 \cdot 10^{-4}$ [198].

Type	Number	Position	Max. integrated Strength [T m^{-1}]
XDN	4	*SS10*	5.23
XFN	4	*SS30*	5.23
XFLS	2	*SS40*	2.17
PFW	8	*ARCs*	5.4

Table 5.5.: Sextupole families in LEIR and limits on integrated strengths. Two sextupole families, focusing (XFN) and defocusing (XDN), are currently used for chromaticity adjustment. Members of XFLS and PFW can be powered independently and can be used for resonance excitation. All magnets XFN, XDN, XFLS have a length of 33.5 cm.

[11] These values are consistent with injection emittances obtained at medical synchrotrons, based on a 'Supernanogan' (Pantechnik SA) source for ion production [178, for carbon, p. 137] – a likely alternative (light-ion) source for a LEIR-based facility.

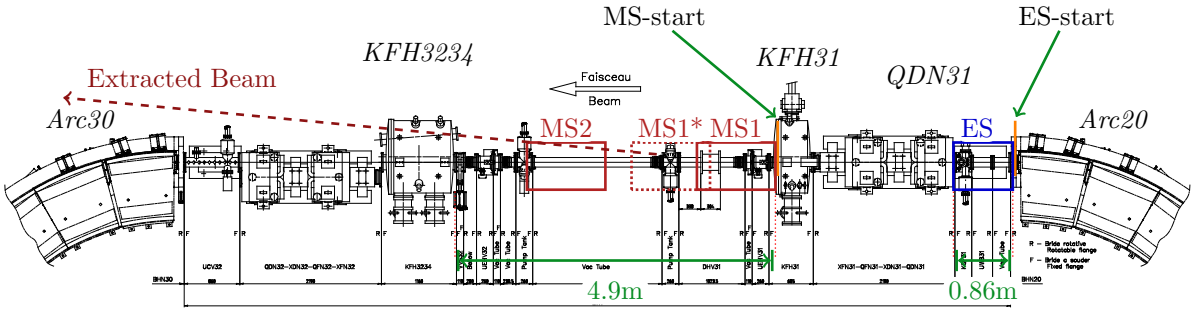

Figure 5.14.: New extraction section SS30 with proposed septa: electrostatic ejection septum (ES), possible locations for the first magnetic septum (MS1 or MS1*) and the second magnetic septum (MS2). Properties of electrostatic and magnetic septa are summarised in Table 5.7.

5.3.1.2. New Extraction Septa

Given the location of the new experimental area and space availabilities in LEIR, Section 5.1.3.1, the required new extraction septa need to be installed at the beginning of straight section SS30 as indicated in Fig. 5.12.

Extraction septa in the slow extraction scheme have the purpose to separate circulating and extracted parts of the beam. The first septum has to be very thin, therefore typically an *electrostatic ejection septum (ES)* with a thickness of about 0.1 mm is used. When sufficient separation between circulating and extracted particles is achieved, thicker septa can be placed. These *magnetic ejection septa (MS)* allow stronger deflection of the extracted beam so that the beam can exit the accelerator lattice through an extraction line.

Figure 5.14 provides a more detailed view of the space availabilities in SS30: 86 cm are available between the end of Bending Section 20 (ARC20) and the first quadrupole *QDN31*, and further 4.9 m between kicker tanks *KFH31* and *KFH3234*. Elements between these kicker tanks (pump tanks *PT31*, *PT32*, beam monitors *UEHV31/32* and orbit kicker magnet *DHV31*) can be moved, so that multiple magnetic septa may be installed.

Septum Positioning: Ideally, the positions of extraction septa in the lattice would be chosen under consideration of the resonance configuration [176], in order to achieve maximum beam separation at the second septum and to facilitate fulfilment of the Hardt condition. Their positioning in LEIR is constrained by space availability in *SS30*.

In order to maximise the total achievable deflection of the extracted beam, the ES needs to be placed as early as possible in SS30, between ARC20 and the first quadrupole *QDN31* as indicated in Fig. 5.14. Further septa can then be positioned in the remaining space between the two kicker tanks *KFH31* and *KFH3234*. Extraction from SS30 requires a minimum separation of 28 cm between extracted and circulating beam at the position of the kicker tank *KFH3234* due to the width of its kicker magnet. The tank itself is larger but can be adapted to accommodate a beam-pipe[12].

[12]In fact this has been the case for slow extraction from LEAR. However, as Fig. 5.14 shows, the position and angles of the existing beam pipe need to be modified.

	β_x [m]	D_x [m]	horizontal position [m]		position in SS30 [m]
			current	resulting	(to element centre)
SMH40	5.00	0	-0.036		
SEH10	3.28	-10.30	-0.050		
ES	7.84	-4.39		-0.045	0.430
further septa	< 5.57	-10.30		-0.050	
MS1					4.335
MS1*					5.335
MS2					6.735

Table 5.6.: Lattice functions for LEIR as in Pb-ion operation ($Q_{\mathrm{H}} = 1.82$) and horizontal positions of current aperture limiting elements *SMH40*, *SEH10*. Minimum possible horizontal positions for the new septa were obtained according to Eq. (5.50). Longitudinal positions correspond to those indicated in Fig. 5.14, and are measured from the beginning of SS30 to the centre of the respective element.

In a lattice exclusively designed for a slow extraction scheme, the transverse (horizontal) position of the ES would be chosen to make the ES the aperture limiting element in the lattice. However, in LEIR a certain minimum horizontal position is imposed by the requirement to maintain the acceptance of the machine for LHC operation.

This can be ensured by scaling the horizontal acceptance in the Pb-ion scheme to the positions of the new septa in the lattice: The horizontal aperture limitation scaled from a position s to a position s' in the lattice is given by

$$\mathrm{Max}\left\{ D(s') \cdot \mathrm{Min}\left(\frac{A(s)}{D(s)}\right) \;,\; \sqrt{\beta(s')} \cdot \mathrm{Min}\left(\frac{A(s)}{\sqrt{\beta(s)}}\right) \right\} , \tag{5.50}$$

where $A(s)$ corresponds to the aperture available at the primary position s in the lattice. The Min() terms in Eq. (5.50) select the locations s that limit the acceptance of the lattice due to maximum dispersion or betatron amplitude functions, respectively. For the LEIR lattice in Pb-ion operation, these positions correspond to the injection septum *SEH10* and the magnetic extraction septum *SMH40* in SS40. Table 5.6 summarises relevant beam functions for LEIR as in Pb-ion operation ($Q_{\mathrm{H}} = 1.82$) and the resulting minimum horizontal positions for the new septa: 45 mm for the new ES and 50 mm for any additional septa installed between *KFH31* and *KFH3234*.

The longitudinal positions of the septa (beginning of SS30 to centre of element) indicated in Fig. 5.14 are also listed in Table 5.6. It is further discussed in Section 5.3.4.3.

Septum strength: The maximum electric field E_{ES} of an electrostatic ejection septum determines the maximum kick ϕ_{ES} that can be imparted on beam particles:

$$\phi_{\mathrm{ES}} = \frac{e\, E_{\mathrm{ES}}\, l_{\mathrm{ES}}}{10^9 \cdot p\, \beta\, c} \,. \tag{5.51}$$

Septa	Unit	Electrostatic	Magnetic
Physical length	[m]	0.86	1.20
Effective length	[m]	0.66	1.00
Septum width	[mm]	0.1	10
Electric field strength	[$\mathrm{MV\,m^{-1}}$]	7	-
Magnetic field strength	[T]	-	0.5
Kick (240 MeV/n, $Q/A = 0.5$)	[mrad]	5.4	105.2
Kick (430 MeV/n, $Q/A = 0.5$)	[mrad]	3.2	75.4

Table 5.7.: Properties of possible extraction septa for LEIR.

For LEIR, this field is limited to approximately $E_{\mathrm{ES}} = 7\,\mathrm{MV\,m^{-1}}$ [200]. Assuming an effective length of $l_{\mathrm{ES}} = 66\,\mathrm{cm}$ (physical length of 86 cm as indicated in Fig. 5.14), this results in a maximum kick of $\phi = 5.4\,\mathrm{mrad}$ for particles with $E = 240\,\mathrm{MeV/n}$ and $\phi = 3.2\,\mathrm{mrad}$ for particles with $E = 430\,\mathrm{MeV/n}$.

Thin magnetic septa require a gap of at least 10 mm between circulating and extracted beam at their entrance and could withstand a magnetic field strength $B_{\mathrm{MS}} \approx 0.5\,\mathrm{T}$ [200]. With an effective septum length $l_{\mathrm{MS}} = 1\,\mathrm{m}$, such a septum could achieve a deflection $\phi = 75.4\,\mathrm{mrad}$ for 430 MeV/n particles ($Q/A = 1/2$):

$$\phi_{\mathrm{MS}} = \frac{e\,B_{\mathrm{MS}}\,l_{\mathrm{MS}}}{3.3356 \cdot p}\,. \tag{5.52}$$

The beam momentum p is given in units [GeV/c_0] in Eqs. (5.51) and (5.52), electric field strength E in [$\mathrm{V\,m^{-1}}$] and the magnetic field strength B in [T].

5.3.2. Resonance Configuration in LEIR

This section discusses constraints on and choices of the parameters in Eq. (5.42) (ΔX, φ, S), based on the theory introduced in Section 5.2.3. Its results guide the tracking studies performed in Section 5.3.3.

5.3.2.1. Spiral Step Size

The spiral step size ΔX determines the width of the extracted beam segment and has implications on extraction efficiency. Losses at the electrostatic and magnetic septum define a lower limit on the spiral step size, because the proportion of particles lost at both septa decreases with increasing spiral step size. Between ES and MS, extracted and circulating beams are separated by only few mm to cm and transported in the same beam pipe. The apertures of lattice elements between ES and MS, in combination with closed orbit displacements at their position, therefore limit the maximum spiral step size.

A typical beam width for medical beams is $\Delta x \approx 10\,\mathrm{mm}$ [176], also providing for good extraction efficiency. This will be the target spiral step size for this study, however, the achievable spiral step size will be governed by limitations on S and aperture constraints. In general, larger spiral step sizes require higher resonance excitation strengths S, Eq. (5.42),

which is limited by the available sextupoles in LEIR. These effects are discussed in detail in Section 5.3.3.

5.3.2.2. Quadrant and Angle of Extraction Separatrix

With the chosen coordinate system, Fig. 5.4, outward extraction corresponds to extraction in the second or third quadrant ($X < 0$). Geometric considerations, Section 5.2.3.5, suggest extraction into the third quadrant ($X' < 0$) as preferred choice.

The extraction angle is determined by the phase advance $\Delta\mu_{\mathrm{X_{res}-ES}}$ between (virtual) resonance-driving sextupole and ES. With the sextupoles installed in LEIR, the 'position' of the virtual sextupole can be freely chosen according to Eq. (5.47b).

However, the range of permissible angles φ is limited due to losses that would occur if particles on two separatrices are equally close to the ES or MS, depending on the relative phase advances between those septa. The phase advance between the centre of ES and the first possible position for the next septum after *KFH31*, indicated as *MS-start* in Fig. 5.14, is approximately $\Delta\mu_{\mathrm{ES-MS}} = 21°$ in the LEIR-like configuration and $\Delta\mu_{\mathrm{ES-MS}} = 31°$ in the LEAR-like configuration. Applying the considerations from Section 5.2.3.5 to third quadrant extraction with these phase advances yields a wide range of permissible values φ between 141° to 240° (LEIR) and 151° to 240° (LEAR), respectively.

The following estimation assumes an extraction angle of 45° in the third quadrant, $\varphi = 225°$, as indicated in Fig. 5.11.

5.3.2.3. Phase and Strength of Resonance-driving (virtual) Sextupole

The effect of multiple lattice sextupoles on resonance excitation S can be described by a single virtual sextupole with normalised sextupole strength S_{virt} and phase[13] μ_{virt}, Eq. (5.47). The phase advance $\Delta\mu$ required for achieving an angle $\varphi = 225°$ of the extraction separatrix at the ES depends on the configuration of the resonance, namely the sign of S, Fig. 5.8. Configurations with positive or negative S differ by a 60° rotation of the separatrices in phase-space. Since this can be compensated by modifying the phase advance $\Delta\mu_{\mathrm{X_{res}-ES}}$ between (virtual) resonance sextupole and ES, $S > 0$ can be assumed without restricting possible solutions.

To achieve a separatrix angle of $\varphi = 225°$ in this configuration (Fig. 5.8a or 5.8c), $\Delta\mu_{\mathrm{X_{res}-ES}} = 45° \pmod{120°}$ is required. The position of the (virtual) excitation sextupole in the lattice μ_{virt} can be calculated from the phase μ_{ES} of the ES and the phase-advance $\Delta\mu_{\mathrm{X_{res}-ES}}$:

$$\mu_{\mathrm{virt}} = \mu_{\mathrm{ES}} - \Delta\mu_{\mathrm{X_{res}-ES}} \,. \tag{5.53}$$

Based on these parameters ($\varphi = 225°$, $x_{ES} = -45\,\mathrm{mm}$, $\Delta x_{ES} = 10\,\mathrm{mm}$) a first estimate for the required sextupole excitation strengths S_{virt} can be obtained from Eq. (5.45).

[13] 'Phases' and 'positions' are used interchangeably in the following. 'Phase' hereby refers to the phase-advance between the beginning of SS10 and the respective (virtual) element.

Family		XFLS		PFW							
Element		41	42	11	12	21	22	31	32	41	42
μ_x mod(120°)	[°]	11	92	45	57	46	58	105	117	106	118
$\Delta\mu$	[°]	49	88	15	3	14	2	75	63	74	62
β_x	[m]	7.14	7.14	18.36	23.33	23.33	18.36	18.36	23.33	23.33	18.36
d_x	[m]	0.0	0.0	-3.80	-0.03	-0.03	-3.80	-3.80	-0.03	-0.03	-3.80

Table 5.8.: Horizontal betatron amplitude β_x and dispersion d_x functions at the positions of XFLS and PFW sextupole magnets. Phase positions of the individual sextupoles μ_x are given modulo 120° and correspond to phase-advances $\Delta\mu$ to the ES. (Based on LEIR-like configuration, $Q_{\text{Lattice}} = Q_{\text{res}} = 5/3$)

5.3.2.4. Fulfilling Hardt-Condition

Chromaticity adjustment can be used to superpose the extraction separatrices of off-momentum particles in order to minimise losses at ES and MS by fulfilling the Hardt condition, Eq. (5.49).

Dispersion vector $\mathbf{D}$ and sextupole strength S_{virt} in Eq. (5.49) are already defined by the lattice configuration and the foregoing considerations that lead to the parameter set (φ, x_{ES}, Δx_{ES}). The parameter α, describing the orientation of the extraction separatrix at the ES for which the Hardt condition should hold, is defined by the sign of S_{virt} and $\widetilde{\delta Q}$, as well as the extraction quadrant. Extraction into the third quadrant and positive S_{virt} have been selected. Table 5.2 lists the possible combinations found in LEIR and their corresponding parameters $\Delta\mu$ and α required for solving the Hardt condition.

With these assumptions, Eq. (5.49) can be evaluated and an estimate for optimal lattice chromaticity Q' be obtained.

All parameters used and obtained in this section are summarised in Table 5.9. Applying previous considerations to the parameters of LEIR and LEAR, Table 5.9a, yields analytic estimates for the required sextupole excitation strength S_{virt} and chromaticity Q', Table 5.9b, which serves as basis for the following tracking studies.

5.3.2.5. Sextupole Configuration

The sextupole families installed in LEIR, Table 5.5, allow creating arbitrary combinations of virtual sextupole strengths S_{virt} and phases μ_{virt} according to Eq. (5.47).

From Eq. (5.47a) follows that the resonance-driving term S cancels if members of the same sextupole families are separated by a multiple of 60°. Chromaticity correction sextupoles are typically arranged in this way, so are sextupole families XFN and XDN in LEIR. These can be used to correct the natural chromaticity of the lattice, for example to the chromaticity value given by the Hardt-condition.

Sextupoles for resonance-excitation would ideally be placed in dispersion-free regions of the lattice, in order not to affect lattice chromaticity, Eq. (5.21). *XFLS41* and *XFLS42* in *SS40* fulfil these requirements in the LEIR configuration. Pole Face Windings *XFW12*, *XFW21*, *XFW32* and *XFW41* are located in low-dispersion $D \approx 0$ areas, which also makes them suitable for resonance excitation, Table 5.8.

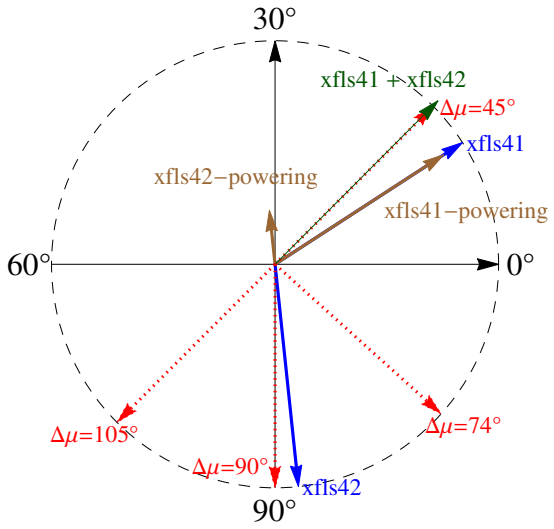

(a) XFLS sextupoles: Arrows in brown indicate the relative powering of *XFLS41* and *XFLS42* in order to achieve phase-advance $\Delta\mu = 45°$ (green) between virtual resonance-driving sextupole and ES.

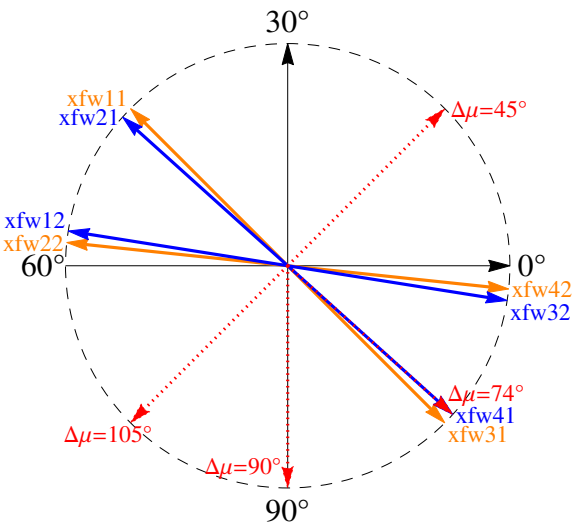

(b) PFW sextupoles: Sextupoles *XFW12*, *XFW21*, *XFW32*, *XFW41* (blue) are better suited than *XFW11*, *XFW22*, *XFW31*, *XFW43* (orange) for sextupole excitation due to low dispersion and high β-function, Table 5.8.

Figure 5.15.: Phases μ_x (mod 120°) of sextupoles (a) XFLS and (b) PFW. Virtual sextupole phases $\mu_{\mathrm{x,virt}} = (\mu_{\mathrm{x,ES}} - \Delta\mu)$ (mod 120°) for different phase advances $\Delta\mu$ from ES are indicated in red. (Based on LEIR-like configuration, $Q_{\mathrm{Lattice}} = Q_{\mathrm{res}} = 5/3$)

The excitation strength S_{virt} determines the slope of the stability limit ($\propto |1/S|$) in the Steinbach diagram, Fig. 5.7, and the size of the maximum spiral step, Eq. (5.42). Its maximum achievable value depends on multiple factors: *a*) The maximum integrated strength of any individual sextupole is limited by its characteristics, such as geometry, cooling, or power supplies, constraint. These limits are listed in Table 5.5. *b*) The achievable excitation strength S scales $\propto \beta_x^{3/2}$, Eq. (5.31). Sextupoles located at positions with large horizontal betatron amplitude therefore allow achieving higher excitation strengths S at same integrated strength $k_2 l$. Values for β_x are listed in Table 5.8. *c*) The excitation strength of a *virtual* sextupole S_{virt} , Eq. (5.47a), is limited by the maximum strengths S_i and positions $\mu_{\mathrm{x},i}$ of the contributing real sextupoles in the lattice. Figure 5.15 illustrates the positions μ_x (mod 120°) of LEIR sextupoles that may be used for resonance excitation: XFLS sextupoles in Fig. 5.15a and PFW in Fig. 5.15b. Various phase advances $\Delta\mu_{\mathrm{X_{res}-ES}}$ of the virtual sextupole from ES are indicated by red arrows as reference for the simulation studies in Section 5.3.3. In principle, a base of two independently powered sextupoles can achieve any position μ_{virt} in the lattice and thus any phase advance $\Delta\mu_{\mathrm{X_{res}-ES}}$. Figure 5.15a illustrates the relative powering of *XFLS41* and *XFLS42* to achieve a phase advance $\Delta\mu = 45°$.

Sextupole coefficients for a given resonance configuration can be found analytically. Estimates for S_{virt}, μ_{virt} and horizontal chromaticity Q'_{h} result from the foregoing considerations. Assuming an additional constraint on the vertical chromaticity Q'_{v}, sextupole

coefficients k_{2_i} of four independent families i can be computed:

$$\begin{pmatrix} S_{virt}\cos_{virt} \\ S_{virt}\sin_{virt} \\ 4\pi(Q'_H - Q'_{H,nat}) \\ -4\pi(Q'_V - Q'_{V,nat}) \end{pmatrix} = \begin{pmatrix} \sum\limits_f \gamma_f \cos_f & \sum\limits_d \gamma_d \cos_d & \gamma_{fls}\cos_{41} & \gamma_{fls}\cos_{42} \\ \sum\limits_f \gamma_f \sin_f & \sum\limits_d \gamma_d \sin_d & \gamma_{fls}\sin_{41} & \gamma_{fls}\sin_{42} \\ \sum\limits_f l_f\beta_f D_f & \sum\limits_d l_d\beta_d D_d & l_{fls}\beta_{41}D_{41} & l_{fls}\beta_{42}D_{42} \\ \sum\limits_f l_f\beta_f D_f & \sum\limits_d l_d\beta_d D_d & l_{fls}\beta_{41}D_{41} & l_{fls}\beta_{42}D_{42} \end{pmatrix} \cdot \begin{pmatrix} k_{2_f} \\ k_{2_d} \\ k_{2_{41}} \\ k_{2_{42}} \end{pmatrix}, \quad (5.54)$$

with the factor $\gamma_i = \frac{1}{2}\beta_i^{3/2} l_i$ for each magnet family i and $\cos_i$, $\sin_i$ as short-hand notation for $\cos(3\mu_i)$ and $\sin(3\mu_i)$, respectively. The sum $\sum\limits_i$ is to be taken over all members of the respective family i, with the values for the lattice functions μ, β and D, μ to be evaluated at the position s of each of its members.

Values for matching constraints in LEIR and LEAR configurations are listed in Table 5.9c.

5.3.3. Particle Tracking Study

This section describes particle tracking studies of the extraction process and presents their results. Tools and methods used for these studies are introduced in Section 5.3.3.1 and two extraction-driving mechanisms are simulated:

Momentum selection Ⓜ, corresponding to ③ or ④ in Fig. 5.9, provides a convenient way to explore different extraction configurations for multiple beam amplitudes simultaneously. The simulations in Section 5.3.3.2 therefore serve to illustrate difficulties and mitigation strategies in the extraction configuration and to identify suitable extraction geometries. Informed by their results, extraction by *tune selection* Ⓣ, corresponding to ② in Fig. 5.9, is simulated in Section 5.3.3.3 for extraction above and below resonance and different resonance excitation strengths. Extracted beam characteristics obtained from these simulations are compared in Section 5.3.3.4 and provide estimates of the transverse properties of the extracted beam segment that are used as start parameters in the transferline design, Section 5.4. Extraction by *amplitude selection* Ⓐ, ① in Fig. 5.9, generally yields smaller extracted beam emittances compared to extraction by *tune selection* Ⓣ, as discussed in Section 5.3.3.1. No dedicated simulations have therefore been performed for this extraction mechanism. Properties of all resonance-driving options are summarised in Table 5.10.

Trackings for this feasibility study were exclusively performed on the LEIR-like lattice configuration, in which zero-dispersion regions at the position of resonance excitation sextupoles, Table 5.8, allow decoupling of resonance excitation and chromaticity correction. This is not easily possible in the LEAR-like lattice configuration due to the lack of zero-dispersion regions, compare Fig. 5.13b.

5.3.3.1. Tools and Tracking Procedure

During the resonance-driving process, the motion of particles in normalised horizontal phase space changes from a circular shape, characteristic for stable motion, into a triangular shape, characteristic for motion close to third-integer resonance. If this process is performed sufficiently slowly, particle emittances are preserved. Under this assumption,

Lattice functions	Unit	LEIR-like lattice @ESin	LEIR-like lattice @MSin	LEAR-like lattice @ESin	LEAR-like lattice @MSin
D_x	[$m^{1/2}$]	-1.15	-4.11	-0.26	-1.64
D'_x	[$m^{1/2}$]	-7.86	-6.80	-2.50	-1.91
α_x		3.36	1.66	1.09	1.17
β_x	[m]	14.63	6.20	6.45	5.55
Septa					
horizontal position	[m]	-0.045	-0.050	-0.045	-0.050
maximum kick [a]	[mrad]	-3.2	-75.4	-3.2	-75.4
$\Delta\mu_{ES-MS}$ [b]	[°]	21		31	

[a] Based on estimations in Table 5.7, 430 MeV/n.
[b] $\Delta\mu$ from *ES* to *MS-start* in Fig. 5.14.

(a) Lattice functions at ES and MS.

	Unit	LEIR-like lattice	LEAR-like lattice
Separatrix			
min separatrix angle $\varphi_{\min}$	[°]	141	151
max separatrix angle $\varphi_{\max}$	[°]	240	240
nominal angle φ_0	[°]	225	225
Sextupole			
spiral step Δx [a]	[m]	-0.01	-0.01
phase advance $\Delta\mu_{\text{Xres-ES}}$	[°]	45	45
sextupole strength S [b]	[$m^{-1/2}$]	17.81	11.82
Hardt condition			
for $\widetilde{\delta Q} < 0$		$\alpha = \alpha_0 - \Delta\mu_{\text{Xres-ES}} = 315°$	
for $\widetilde{\delta Q} > 0$		$\alpha = \alpha_0 - \Delta\mu_{\text{Xres-ES}} = 135°$	
chromaticity Q'_x for HC		6.73	1.49

[a] Target spiral step width for on-momentum particles $\delta p/p_0 = 0$ at ES.
[b] Based on above parameters and Eq. (5.45).

(b) Analytic estimates for resonance configuration parameters.

Constraints	Unit	LEIR-like lattice horizontal	LEIR-like lattice vertical	LEAR-like lattice horizontal	LEAR-like lattice vertical
natural chromaticity Q'_{nat}		-3.49	-4.54	-3.17	-7.46
target chromaticity Q'_{HC}		6.73	0	1.49	0
sextupole strength S	[$m^{-1/2}$]	17.81		11.82	
$\Delta\mu_{\text{Xres-ES}}$	[°]	$45 + n \cdot 120$ $(S > 0)$			
sextupole length l	[m]	0.33535			

(c) Constraints for matching of sextupole magnets.

Table 5.9.: Resonance configuration parameters for LEIR and LEAR, based on analytic considerations in Section 5.3.2.

	M	T	A
constant	Q_L, $A_{\max}$	Q_L, $\delta p/p$	$A_{\max}$, $\delta p/p$
varying	δp	Q_L	$A_{\max}$
mechanism	acceleration	tune modification	transverse kicks
implementation	betatron core	exist. quadrupoles	noise signal generators & exist. dampers
simulation method	particles of all amplitudes extracted simultaneously, choose δp_i so that $\delta Q = 0$ to $\delta Q_{A_{\max}}$, Fig. 5.16	for given $A_{\max}$, choose lattice tune Q_L as in Fig. 5.17a, change Q_L until configuration Fig. 5.17b	for given $A_{\max}$, choose lattice tune as in Fig. 5.18a, increase particle amplitude $A_{\max}$ at $Q_L = \text{const}$
simulated	Section 5.3.3.2	Section 5.3.3.3	–

Table 5.10.: Comparison of resonance-driving options and their simulation. Simulation of momentum-driven M extraction conveniently allows testing extraction configurations for different beam amplitudes. Tune-driven extraction T is the easiest to implement, resulting in maximum extracted beam emittances. Extracted beam parameters based on this simulation, Section 5.3.3.4, are therefore used as estimates for the design of beam transfer lines in Section 5.4. Extraction by amplitude selection A is similar to either Fig. 5.17a (for high-amplitude particles) or 5.17b (for low-amplitude particles). Since resulting extracted beam segments are generally smaller than those obtained from T, no dedicated simulations have been performed for this extraction mechanism.

investigation of the transverse aspects of a slow extraction scheme does not require full simulation of the dynamic extraction process. Instead, tracking can be performed exclusively on the stability limit and the extraction be split into distinct tracking processes: for different stages of extraction, and for circulating and extracted beam segments [201].

Tracking Code and Lattice Model The MAD-X[14] [191] program was used for linear beam optics calculations and particle tracking studies. MAD-X is the successor of MAD-8, a tool for charged particle optics design in alternating-gradient accelerators and beamlines. It provides an interface to the Polymorphic Tracking Code (PTC) [202], libraries for particle tracking. MAD-X and PTC are used extensively for accelerator design related to high-energy physics projects at CERN.

Particle tracking studies were performed using *ptc_track*, a 'thick-lens' tracking code, based on the PTC libraries and integrated into MAD-X. Particles are specified by their individual starting coordinates in 6-D phase space (X, PX, Y, PY, T, PT) and are tracked individually, starting from the first element in a specified element sequence and for a given number of turns. For every observation point in the lattice and every simulated turn, each particle's coordinates in 6-D phase space are stored in a text file.

All simulations are based on a detailed optical model of LEIR[15] that is maintained at CERN. The lattice model includes dipole, quadrupole and sextupole elements as

[14]MAD - Methodical Accelerator Design: `http://mad.web.cern.ch/mad/`, release 5.00.00 and later.

[15]Element and sequence definitions in MAD-X convention are available from `http://project-leir-optics.web.cern.ch/project-LEIR-optics/2012/`.

introduced in Section 5.3.1.1, as well as orbit correctors and diagnostics. The dipole PFWs are modelled as thin sextupolar components without finite length, which seems a reasonable assumption given their field quality [203]. Orbit correctors are modelled as kicker elements that produce point-like kicks. The electron cooler was disabled for all simulations. Septa introduced for the simulation of the extraction process were modelled as point-like orbit correctors at the centre of their longitudinal position.

Data analysis scripts were implemented in Python[16], based on and extending *PyAccel* [204], an existing library for accelerator design.

Matching Tune and Orbit Correction: Nominal values for the vertical lattice $Q_V = 2.72$ were used in all studies. The horizontal tune was matched to $Q_H = 5/3 + \delta Q$ where the tune shift δQ depends on the particular tracking scenario and is reported with every tracking result in this section.

Six orbit correctors are available for manipulating the closed orbit in SS30: four at the entrance and exit of the two bending magnets delimiting SS30 (*DWHV21/22*, *DWHV31/32*) and further two in SS20 (*DEHV22*) and SS30 (*DHV31*). Their positions in the lattice are indicated in Fig. 5.12. The strengths of these elements were matched to obtain horizontal separations Δx from the unperturbed reference orbit at the positions of the electrostatic ejection septum (ES) and magnetic ejection septum (MS), and to close this 'orbit bump' in Bending Section 30 (ARC30). Constraints on the orbit excursion at ES and MS are reported with tracking results.

Matching Virtual Sextupole Excitation and Chromaticity: An analytic approach for computing sextupole coefficients for a given resonance configuration was introduced in Section 5.3.2.3. To provide a more flexible means of manipulating parameters S_{virt}, μ_{virt} in simulations, a numeric matching routine was implemented, using MAD-X's *macro* definition. Four constraints, S_{virt}, μ_{virt}, Q'_{h}, Q'_{v} can be specified, and the parameters $S_{\cos} = S_{\mathrm{virt}} \cos(3\mu_{\mathrm{virt}})$ and $S_{\sin} = S_{\mathrm{virt}} \sin(3\mu_{\mathrm{virt}})$ are calculated as the sum over the respective contributions of all sextupole families. Suitable solutions are searched by sweeping parameter ranges for the coefficients k_{2_i} of selected sextupoles and comparing the resulting sums $S_{\cos}$ and $S_{\sin}$ to the constrained parameters S_{virt} and μ_{virt} according to their definition[17]. Sextupole families *XFN* and *XDN* were used for chromaticity correction and matched using MAD-X internal chromaticity computation. The values for S_{virt}, μ_{virt} and Q'_{h} are reported with tracking results. Tune, orbit correction, sextupole excitation and chromaticity were changed iteratively until a stable configuration was found.

Extraction Schemes: Values for the horizontal lattice tune distance from resonance δQ, as well as horizontal chromaticity Q'_H are needed for simulation studies. Tracking on the stability limit additionally requires a value for the relative momentum off-set $\frac{\delta p}{p}$ of particles to be specified.

[16] Python Programming Language: `http://www.python.org/`

[17] In order to replicate the separatrix geometry for a given S found from analytic considerations, Fig. 5.8, the following relation had to be applied between sextupole powering coefficients in MAD-X $k_{2,\ MAD}$ and the normalised sextupole coefficient k_2 in Eq. (5.31): $k_{2,\ MAD} = -k_2$.

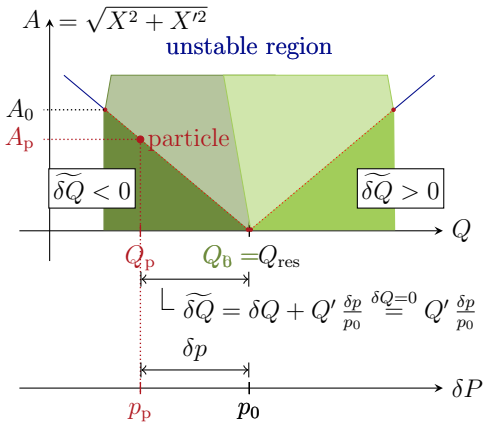

Figure 5.16.: Momentum selection [M]: Extraction below and above resonance at constant $(\widetilde{\delta Q}, \frac{\delta p}{p})$. Lattice tune on resonance $(\delta Q = 0)$, so that unstable particles are selected exclusively by their momentum off-set δp.

At a given resonance excitation strength S, the stability limit for a particle is described by its amplitude A_p and its tune distance from resonance $\widetilde{\delta Q}_\mathrm{p} = \delta Q + Q' \frac{\delta p}{p}$, as introduced in Fig. 5.7 and Eq. (5.40). The geometric horizontal emittance $\epsilon_\mathrm{H,geo}$ of the circulating beam provides an estimate for the largest particle amplitude at a given extraction energy:

$$\widetilde{\delta Q} = \delta Q + Q' \frac{\delta p}{p} = \sqrt{\frac{\epsilon_\mathrm{H,geo}}{48\,\pi\,\sqrt{3}} \cdot \left(\frac{S}{Q'}\right)^2}\,. \tag{5.55}$$

The relative momentum off-set $\frac{\delta p}{p}$ of a particle on the stability limit can thus be computed as a function of its emittance for a given lattice tune distance δQ and resonance configuration $(S,\, Q')$. Two types of simulations were performed to investigate the properties of extracted beams.

[M] Momentum Selection:
This configuration represents extraction methods that continuously increase the momentum off-set of beam particles at fixed lattice tune until all particles are extracted, such as ③ or ④ in Fig. 5.9. In these schemes, the extracted tune spread is given by the largest particle amplitude and the slope of the stability limit, according to Eq. (5.55). For every particle amplitude, extraction takes places at constant $(\widetilde{\delta Q}, \frac{\delta p}{p})$, so that the transverse properties of the extracted beam remain constant throughout the duration of the spill.

Figure 5.16 illustrates this extraction situation in a Steinbach diagram. A range of particle amplitudes $A = 0 \ldots A_0$ are extracted simultaneously at different tune distances below $(\widetilde{\delta Q} < 0)$ or above $(\widetilde{\delta Q} > 0)$ resonance. For convenience, the lattice is tuned on-resonance $\delta Q = 0$ so that sign and magnitude of $\widetilde{\delta Q}$ are determined exclusively by the relative momentum offset $\frac{\delta p}{p}$ of a particle and the chosen lattice chromaticity Q'.

With Eq. (5.55), these momentum off-sets are computed to represent particles of different amplitudes, and thus beam energies. Table 5.4 in Section 5.3.1 lists expected geometric horizontal emittances for a range of beam energies in LEIR. Based on these emittances, particles were selected: particles *P3-P6* for minimum extraction energies (40 MeV/n to 10 MeV/n), and *P1*, *P2* corresponding to maximum extraction energies at 240 MeV/n and 430 MeV/n, respectively.

T Tune Selection:
This configuration assumes that beam particles are 'driven' towards the stability limit by changing the lattice tune Q_0, configuration ② in Fig. 5.9: Particles with maximum amplitude A_0 are extracted at the beginning of the spill at large tune distance from resonance, Fig. 5.17a. Towards the end of the spill, particles of lower amplitude are extracted close to resonance tune, Fig. 5.17b. As a consequence, particles of a given amplitude but different $\frac{\delta p}{p}$ are extracted at different times during the spill. Figure 5.18 illustrates this for maximum amplitude particles. This results in changes of the transverse properties of the extracted beam which will be discussed in Section 5.3.3.4. During the major part of the spill, the full momentum spread of the beam, $2\,\Delta p_b$, is extracted, as indicated in Fig. 5.17.

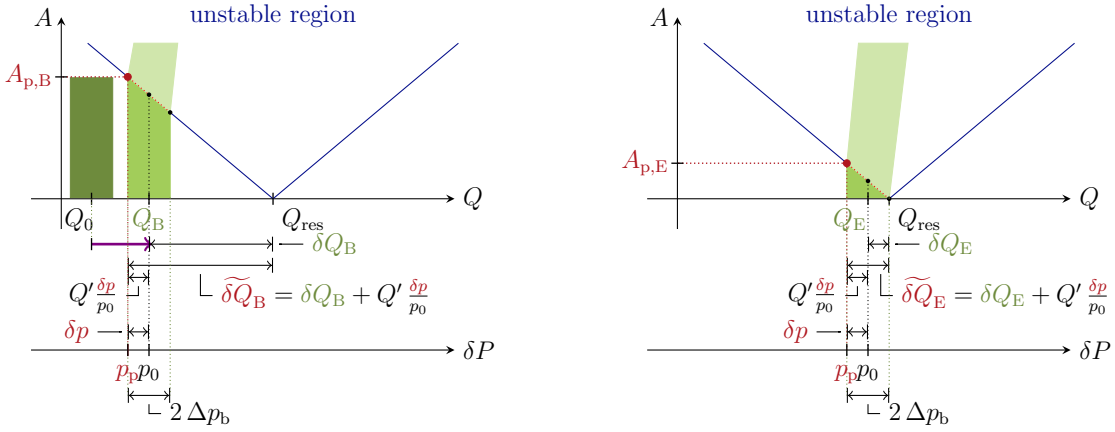

(a) Beginning of Spill **(b)** End of Spill.

Figure 5.17.: Tune selection in quadrupole-driven extraction T: Three particles are tracked for two tune configurations corresponding to 'beginning' (a) and 'end' (b) of spill. Beam momentum p_0 and momentum spread Δp_b remain constant during extraction. Only particles within a small range of emittances are extracted simultaneously at any moment throughout the duration of the spill.

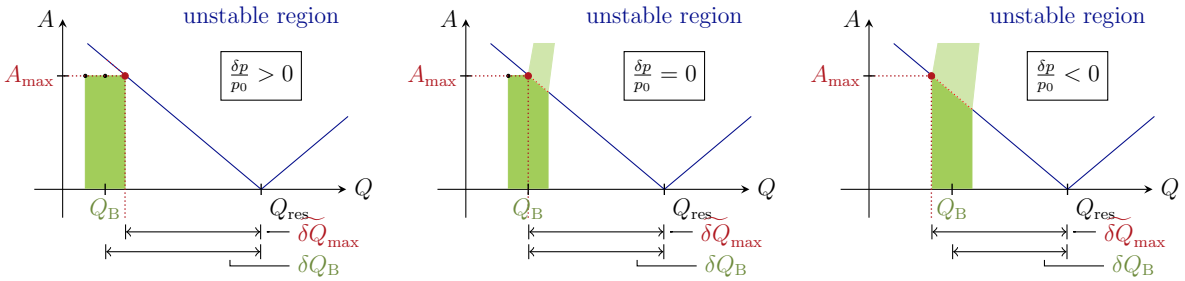

(a) $\frac{\delta p}{p_0} > 0$ **(b)** $\frac{\delta p}{p_0} = 0$ **(c)** $\frac{\delta p}{p_0} < 0$

Figure 5.18.: In tune-driven extraction, particles of a given amplitude but different $\frac{\delta p}{p}$ are extracted at different times of the extraction process. Figures a, b, c illustrate this for maximum particle amplitudes at the beginning of the spill and positive chromaticity.

Regardless of beam energy, a fixed beam momentum spread of $\Delta p/p_0 = \pm 2 \cdot 10^{-4}$ was assumed for these studies, corresponding to the beam momentum spread at injection. Two simulations were performed for every resonance configuration with three particles ($\delta p/p_0 = -2 \cdot 10^{-4}$, $\delta p/p_0 = 0$, $\delta p/p_0 = +2 \cdot 10^{-4}$) and two tune settings δQ. The tune settings were chosen to correspond to the 'beginning' and 'end' of extraction, as illustrated in Fig. 5.17. In the first configuration, the lattice tune distance from resonance δQ is determined from Eq. (5.55) so that a maximum emittance particle (*P6*) with $\delta p/p_0 = -2 \cdot 10^{-4}$ is on the stability limit[18]. Similarly, δQ at the end of extraction is computed to extract a particle with $\delta p/p_0 = +2 \cdot 10^{-4}$ very close to resonance tune.

Additional simulations were performed for selected configurations to investigate the variation in extracted beam parameters as the 'waiting beam' enters the resonance, Fig. 5.18.

A Amplitude Selection:
The start configuration for such simulations corresponds to Fig. 5.18a. However, instead of changing the lattice tune towards resonance, particle amplitudes are increased continously, ① in Fig. 5.9. Since the extracted beam properties in this configuration resemble those obtained from a single tracking of configuration T, resulting in smaller extracted beam emittances, no dedicated simulations were performed for this extraction mechanism.

Transverse Start Coordinates: With δQ and $\delta p/p$ given from previous considerations, suitable start coordinates (x, x', y, y', s, $\delta p/p$) can be found iteratively: First, transverse coordinates (x, x', y, y') are selected at a suitable position s, so that tracking (>3000 turns) results in stable particle motion. Then, the particle's amplitude is increased continuously by manipulating its coordinates in horizontal phase-space (x, x') until motion becomes unstable. Since typically $\epsilon_\mathrm{H} \gg \epsilon_\mathrm{V}$ in slow resonant extraction, particles were placed on the reference path in the vertical plane, thus neglecting coupling effects between the transverse planes.

Particle coordinates were considered sufficiently close to the stability limit when a small increase in sextupole strength S ($\Delta S \sim 2\%$) was sufficient to turn previously stable motion into unstable motion. This process can be carried out at any observation point in the lattice. For convenience, a dispersion-free region[19] was chosen.

At nominal S, resulting in stable particle motion on the stability limit, the phase space areas of the stable triangles were integrated and compared to the expected emittance according to Eq. (5.55) based on (S, Q', Q_0, $\delta p/p_0$). Then, particle motion was turned unstable by slightly increasing S as explained before.

The 'shoelace' formula was used for integration of the phase space area:

$$A = \frac{1}{2} \left| \sum_{i=1}^{n} x_i (y_{i+1} - y_{i-1}) \right| , \tag{5.56}$$

with polygon vertices (x_i, y_i) corresponding to the coordinates of the phase-space tra-

[18] Assuming extraction below resonance ($\widetilde{\delta Q} < 0$) and positive chromaticity $Q'_H > 0$, correspondingly, for extraction above resonance

[19] Marker *Ctrs40* in the LEIR lattice.

jectory of a single particle at the selected observation point in the lattice. The polygon has to close ($x_0 = x_n$ and $x_{n+1} = x_1$) and coordinates need to be ordered so that the edges of the polygon do not cross.

Coordinates of Unstable Particle on ES: Phase-space trajectories resulting from above tracking allow approximate estimation of the aperture requirements of circulating unstable particles, and of their spiral step across the septum. Since the amplitude of unstable motion grows quadratically with distance, it is not guaranteed that the estimates obtained from these particles describe the maximum amplitudes of spiral steps and orbit excursion that can occur for a given resonance configuration.

For better estimates, start coordinates very close to the septum have to be chosen. While the horizontal position x_{ES} of the septum is known, the divergence $x'(x = x_{\mathrm{ES}}) = x'_{\mathrm{ES}}$ at which particle cross the septum depends on resonance parameters and orbit corrections. It therefore has to be determined by tracking.

Phase space plots at the position of the ES, such as figure 5.19, show particles crossing the ES at some divergence x'_{ES}. The separatrices care be approximated as straight lines and the crossing points x'_{ES} computed for every particle. Particles starting from this position (x_{ES}, x'_{ES}) represent *a*) particles that just passed inside of the ES and continue circulating further three turns before crossing the septum with maximum spiral step, or *b*) particles that just crossed the septum wires, experience the kick of the ES, and are extracted. The following tracking processes are performed based on these coordinates.

Outermost Circulating Particles: The amplitude of particles passing inside the ES continues to grow over the following three turns, so that the trajectories of these particles require the maximum aperture for a given lattice configuration. Aperture limitations are detected by comparing the horizontal coordinates of the particles over these three turns with the apertures of LEIR elements.

After three turns, these particles cross the ES with maximum spiral step Δx and spiral kick $\Delta x'$. Both can then be computed as the difference between the particle's start position at the ES and its position after three turns.

Tracking Extracted Particles: The extracted beam segment consists of particles with a range of horizontal coordinates: Assuming perfect alignment of extraction separatrices for off-momentum particles, the segment is delimited by (innermost) particles that only just entered the ES, with starting coordinates very close to (x_{ES}, x'_{ES}), and (outermost) particles that underwent the maximum spiral step into the septum, with coordinates ($x_{\mathrm{ES}} + \Delta x$, $x'_{\mathrm{ES}} + \Delta x'$). While travelling along the ES, particles are deflected in the electric field of the septum by an angle ϕ. The simulation accounts for this by applying a single kick at the centre of the ES element ($x' \rightarrow x' + \phi$). Further particles without kick, start coordinates (x_{ES}, x'_{ES}), are tracked to represent the outermost particles of the circulating beam. All particles are tracked to the position of the MS, providing the results for figures such as Fig. 5.24.

Based on the horizontal positions of the tracked particles, the required orbit correction at the position of the MS and aperture requirements of the extracted beam are determined.

	S [$m^{-1/2}$]	φ [°]	α [°]	$\Delta\mu$ [°]	Q'	sgn $\delta\widetilde{Q}$	Sextupole	OC(ES) [mm]	OC(MS) [mm]
C1-M-BR-1	17.81	225	315	45	6.73	< 0	XFLS	0	0
C1-M-BR-2								20	25
C1-M-BR-3								25	30
C1-M-BR-4								28	30
C1-M-AR-1	17.81	225	135	45	6.73	> 0	XFLS	0	10
C1-M-AR-2								20	25
C2-M-BR-1	17.81	165	255	105	11.18	< 0	XFLS	10	30
C3-M-BR-1	17.81	195	285	75	10.26	< 0	XFLS	0	0
C4-M-BR-1	17.81	196	286	74	10.26	< 0	XFW41	14	28
C4-M-AR-1	17.81	196	106	74	10.26	> 0	XFW41	7	24

Table 5.11.: Selected resonance configurations for LEIR. All trackings were performed on resonance ($\delta Q = 0$) according to Fig.5.16 (momentum selection $\boxed{\mathrm{M}}$) for extraction below (BR) and above (AR) resonance.

The distance between outermost circulating and innermost extracted particle at the MS defines the maximum possible width of the septum.

5.3.3.2. Particle Tracking - Momentum Selection

Table 5.11 lists several resonance configurations that will be referred to by their number *C1* - *C4* throughout this section. First, procedure and challenges of the configuration process will be explained based on configuration *C1* which corresponds to the analytic estimate (LEIR) obtained from Section 5.3.2. Configurations *C2* - *C4* will then be discussed as possible solutions for LEIR.

Verification of Analytic Solution Figure 5.19 shows the phase-space coordinates of seven particles with different single-particle emittances at the position of the ES, tracked over multiple turns according to configuration *C1-M-BR-1*. Particles *P1-P6* correspond to beams with geometric emittances expected at different extraction energies from LEIR, Table 5.4. Particle *P0* represents a small-emittance particle, extracted very close to resonance tune.

The plots consist of three data sets, describing 'just stable' particle motion (marker: •••), unstable particle motion (marker: ⬟), and three turns in unstable motion, starting from the horizontal position of the ES (marker: ⬟). The last allows estimation of the maximum aperture requirements of the circulating beam over the last three turns before extraction and estimation of the maximum spiral step size.

Figure 5.19a clearly demonstrates the $\varphi = 225°$ extraction angle ($\varphi = 45°$ in the third quadrant) and the fulfilment of the Hardt-condition. Families *XFN*, *XDN* were used for chromaticity correction and the sextupoles *XLFS41* and *XFLS42* in dispersion-free *SS40* for resonance excitation. Sextupole phase and strength was adjusted following

the procedure outlined in 5.3.3.1, Table 5.9c lists the matching constraints used for this example.

To establish the aperture needs of unstable circulating particles, consider the trajectory of an unstable particle that just passes inside of the ES in its N^{th} turn, such as particles ⬟ in Fig. 5.19. It circulates two further turns, $N+1$ and $N+2$, as the outermost particle on the other two separatrices before crossing the ES with maximum step size in its $N+3^{\text{rd}}$ turn.

In real phase space, Fig. 5.19b, the regular shape of the separatrices is distorted due to the local optical functions. The trajectories of unstable particles in this configuration (*C1-M-BR-1*) extend far (>10 cm) into the aperture of the machine. Figure 5.19 also indicates that particles of different amplitudes undergo spiral steps of different sizes.

Spiral step sizes for configurations *C1* are compared in Fig. 5.20 in function of tune distance. Configuration *C1-M-BR-1* and *C1-M-AR-1* were adjusted to yield a 10 mm spiral step for particles extracted on-resonance $\widetilde{\delta Q} = 0$. However, extraction at very small tune distances is difficult to reproduce by tracking. Particles extracted at small $\left|\widetilde{\delta Q}\right|$ (*P0*) show spiral step sizes between 12 mm (extraction above resonance) and 13 mm (extraction below resonance). Spiral step sizes obtained from tracking are consistently higher than predicted analytically from Eq. (5.42). For the chosen extraction simulation method Ⓜ, particles extracted above and below resonance have different momentum offsets. Dispersion shift decreases the distance between particles extracted above resonance and the ES, resulting in lower spiral steps compared to particles extracted below resonance. These are further distanced from the ES, compare for example Fig. 5.19 (below resonance) to Fig. 5.25. The effect of orbit corrections on spiral step size is discussed in the following.

Aperture Limitations on Circulating Beam Circulating unstable particles in the last turns before extraction may exceed the available machine apertures. This is the case for the previous example, configuration *C1-M-BR-1*, Fig. 5.19a. For a given resonance configuration, aperture requirements depend on the length and orientation of the separatrices in phase space. The maximum separatrix length is determined by the size of the corresponding stable triangle ($\propto \widetilde{\delta Q}$) and its orientation and distance from the septum wires.

These effects can be mitigated by reducing the number of turns that unstable particles circulate before extraction, which requires reduction of the horizontal distance between ES and the unstable fixed-point of the extraction separatrix. Since the horizontal position of the ES is fixed due to constraints on the acceptance of the machine, Section 5.3.1, an orbit correction has to be introduced that makes the ES the aperture limiting element for slow extraction.

Local orbit corrections at the position of the ES and MS can be introduced with the available orbit correctors. Figure 5.21 shows three different possible configurations (*C1-M-BR-3*, *C1-M-AR-1*, *C2-M-BR-1*) in which the closed orbit is displaced towards the outside of the lattice. The orbit distortion only affects SS30 and adjacent bends ARC20 and ARC30, it can be closed throughout the remaining lattice. Generally, the shape of the orbit displacement depends on the ratio between the required orbit displacements at the ES and MS, since these two locations provide the main matching constraints.

The minimum amplitude of the orbit correction at the ES needs to be adjusted to

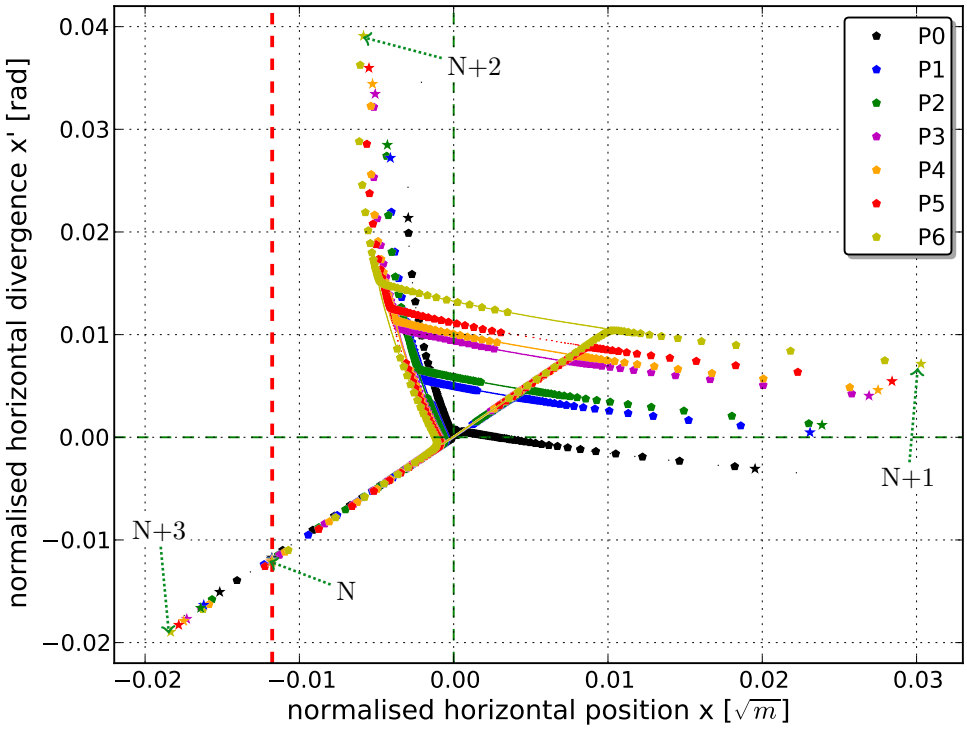

(a) Normalised coordinates.

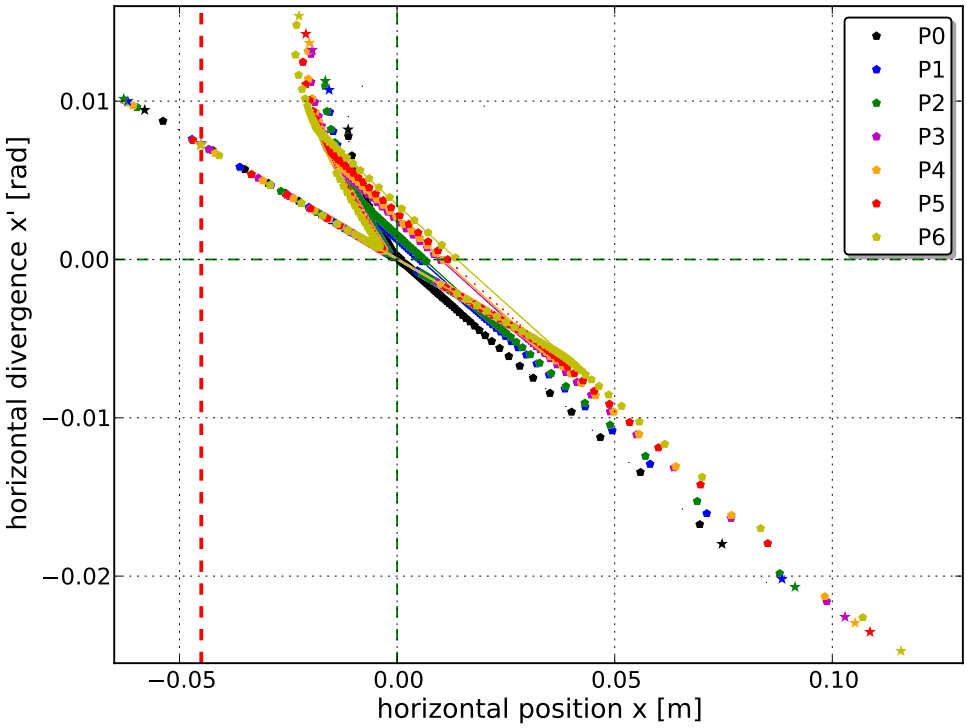

(b) Real coordinates

Figure 5.19.: Extraction geometry at ES, based on configuration *C1-M-BR-1* in (a) normalised and (b) real coordinates. Marker • • • indicates stable motion, ⬟ unstable motion. Last three turns in unstable motion, starting from the ES are represented by ⬟. *P1-P6* represent beams with geometric emittances corresponding to different extraction energies, Table 5.4. *P0* represents a small-emittance particle, extracted very close to resonance tune.

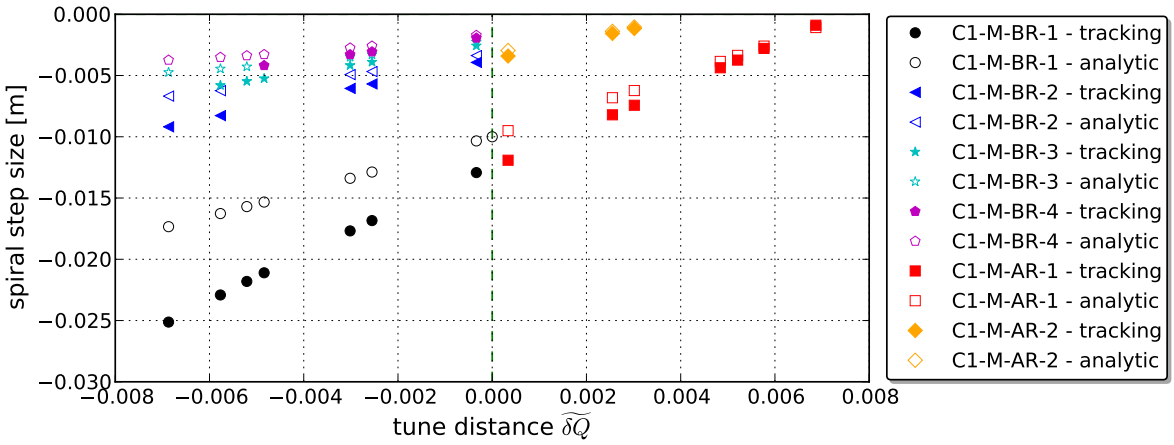

Figure 5.20.: Spiral step size in function of a particle's tune distance from resonance $\widetilde{\delta Q}$ for configurations *C1*. Filled markers represent simulation results, empty markers correspond to analytic estimates based on Eq. (5.42).

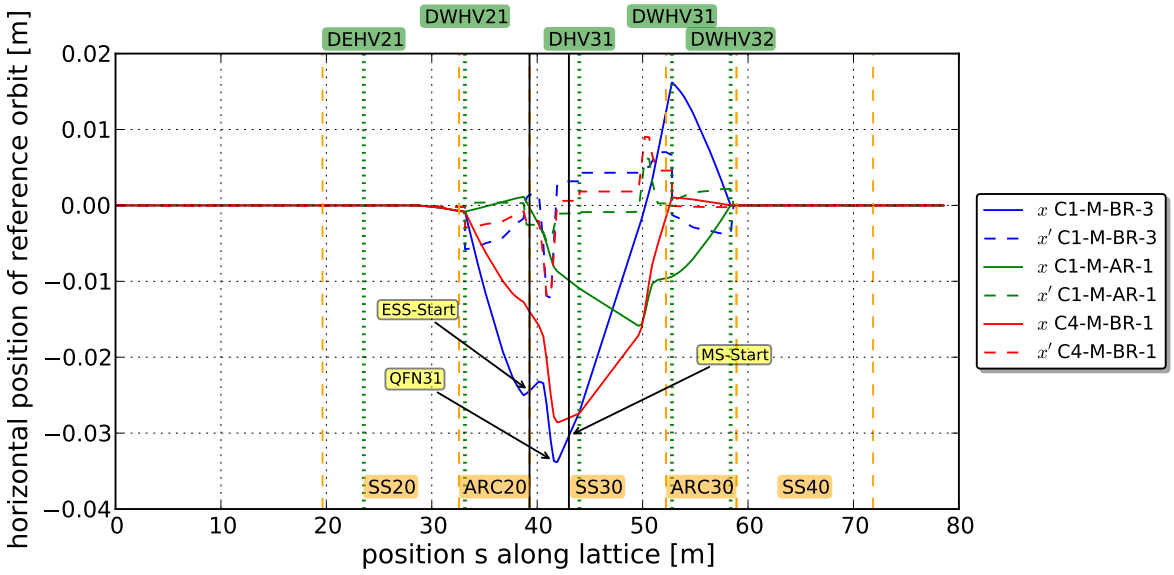

Figure 5.21.: Selected orbit corrections in LEIR: *C1-M-BR-3*, *C1-M-AR-1*, *C4-M-BR-1*. Dashed vertical lines indicate different sections of the LEIR lattice, dotted vertical lines the location of orbit correctors. The positions of ES and MS are indicated by black lines.

allow circulation of unstable particles over the last turns before extraction. It can be determined by iterative particle tracking with successively increased orbit displacement at the ES, until no lattice element is found to obstruct the motion of circulating unstable particles.

The maximum displacement may be limited by particle losses in the septum. Figure 5.22 illustrates this situation, comparing configuration *C1-M-BR-1* with configuration *C1-M-BR-3* where an additional orbit correction of 25 mm at the ES had been introduced. In this case, particle *P6* is extracted on the 'upper separatrix' before reaching the ES. Such particles may be lost in the septum because their divergence x' does not match the design

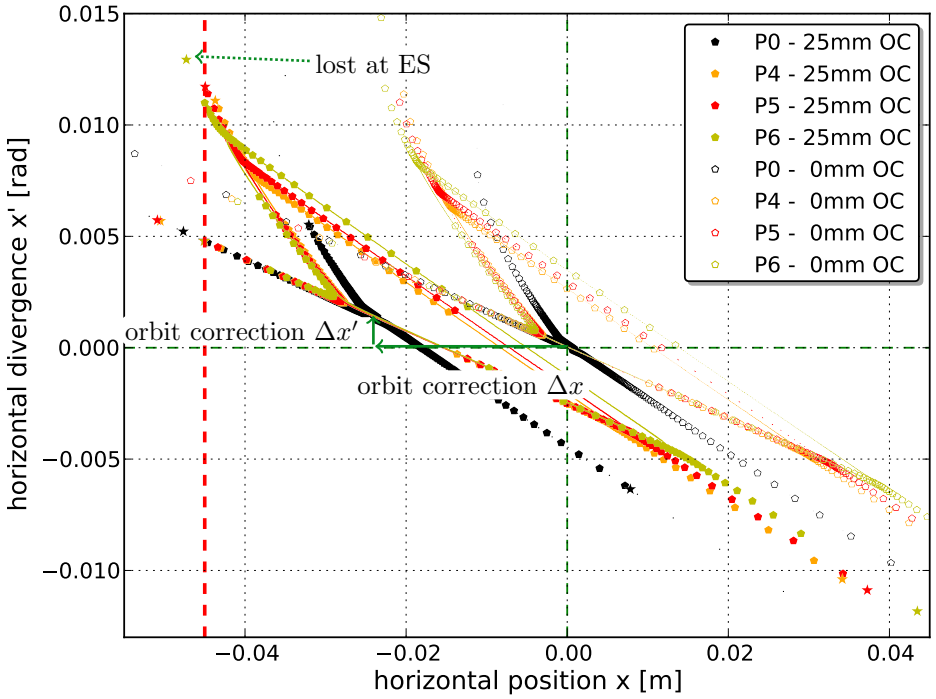

Figure 5.22.: Particle losses at ES due to amplitude of orbit correction. Extraction of selected particles (*P0*, *P4*, *P5*, *P6*) without orbit correction (*C1-M-BR-1*, empty markers) and with 25 mm orbit correction at ES (*C1-M-BR-3*).

divergence of the ES. Further increase of the orbit correction to 28 mm (*C1-M-BR-4*) results in *P5* and *P4* being lost in the same way.

As a result of reducing the number of circulation turns also the spiral step size decreases with increasing orbit displacement towards the ES, Fig. 5.20. In order to compensate for this effect, sextupole strength S or the extraction angle φ can be increased. Both requires readjustment of the Hardt condition and thus lattice chromaticity. Increasing φ in this extraction configuration (*C1-M-BR*), however, would also result in particles being extracted from the 'upper separatrix' already at smaller orbit corrections.

The horizontal position of the first MS imposes a further constraint on the required orbit correction: It must be configured to allow the circulating beam to pass inside the MS ($x = -0.05\,\mathrm{m}$) as close as possible, in order to make best use of the gap between circulating and extracted beam. Figure 5.23 shows circulating and extracted parts of the beam at the position of the MS for configuration *C1-M-BR-3*.

Aperture Limitations on Extracted Beam Spiral step size and orbit corrections at the ES and MS affect the properties of extracted beam particles. The maximum 'useful' width of the extracted beam segment is limited by aperture constraints over the first meters downstream of the ES, where circulating and 'extracted' beam are still transported in the same vacuum pipes: The extracted beam segment has to pass the first quadrupole doublet (*QFN31*, *QDN31*), sextupoles (*XFN31*, *XDN31*) and kicker magnet (*KFH31*), compare Fig. 5.14.

Figure 5.24 compares the horizontal positions of circulating (marker: •) and extracted

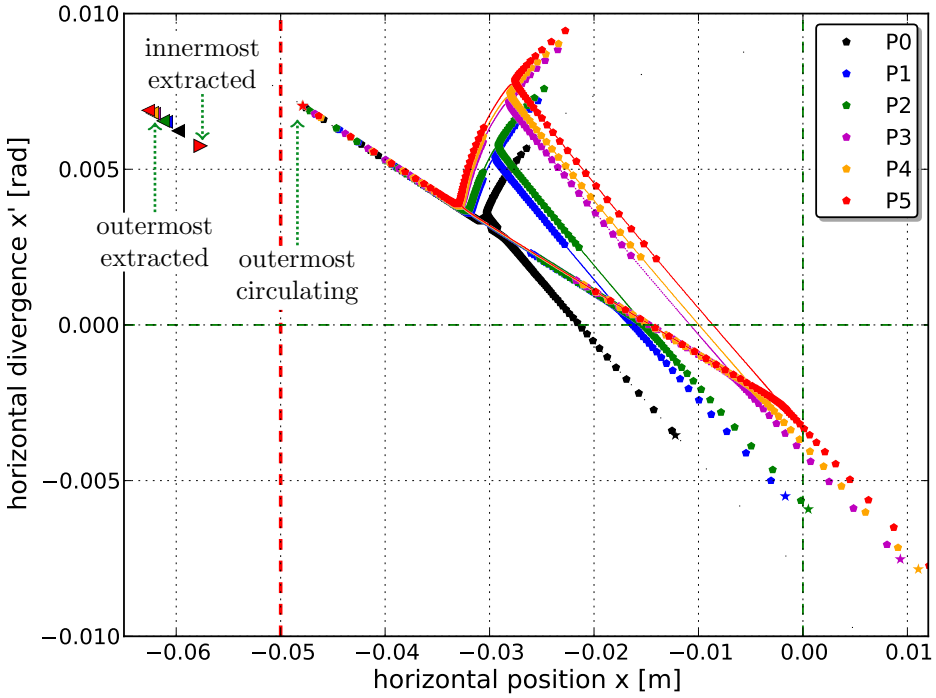

Figure 5.23.: Particles at MS with well adjusted orbit correction (*C1-M-BR-3*).

(marker innermost extracted: ▲, marker outermost extracted: ▼) particles to the available aperture (marker: ■) at lattice elements between ES and MS for configuration *C1-M-BR-1* and *C1-M-BR-3*. Maximum spiral step sizes resulting from configuration *C1-M-BR-1* are so large that parts of the extracted beam would be lost at elements *XDN31*, *QFN31*, *XFN31* and *KFH31*. Configuration *C1-M-BR-3* with 25 mm orbit correction at the ES results in smaller maximum spiral step sizes. It also adjusts the orbit correction at the MS in order to allow circulating particles to pass closely by the inner aperture of the MS, thus maximising the space available for placing a magnetic septum.

The orbit displacement at the position of the MS is required to be larger than at the position of the ES. With the orbit correctors currently installed, such orbit corrections result in orbit displacements similar to the ones shown in Fig. 5.21. In many cases, the orbit correction peaks at the position of *QFN31* where it exceeds the displacement required at the MS. Despite this, elements *QDN31*, *XDN31*, *QFN31*, *XFN31* do not impose strict limitations on the width of the extracted beam segment since apertures of quadrupoles and sextupoles could be increased to approximately ±84 mm and ±87 mm, respectively (marker: □).

Figure 5.24 further indicates that the maximum transportable spiral step size is limited by the aperture of the kicker magnet *KFH31* to approximately 15 mm, assuming a kick $\phi = 3.4$ mrad from the ES and depending on the shape of the orbit correction between ES and MS.

Possible Extraction Configurations Configurations *C1-M-BR-1* to *C1-M-BR-3* were found suitable only for the extraction of particles *P0-P1*. Further increase of the orbit correction at the ES (*C1-M-BR-4*) additionally permits extraction of particle *P2*, cor-

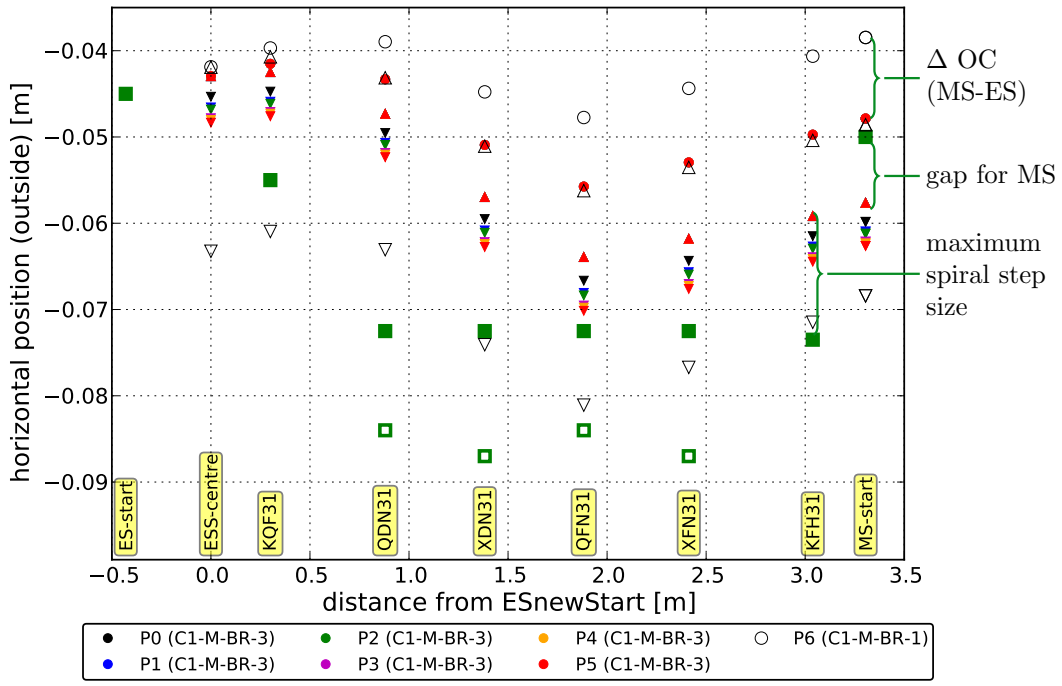

Figure 5.24.: Horizontal positions of circulating and extracted particles with element apertures between ES and MS, for configuration *C1-M-BR-1* and *C1-M-BR-3*, kick at ES $\phi = 3.2\,\text{mrad}$. Marker ● indicates circulating particles, ▲ innermost extracted particles and ▼ outermost extracted particles. Marker ■ represents the current apertures of lattice elements, □ the maximum available apertures after modification.

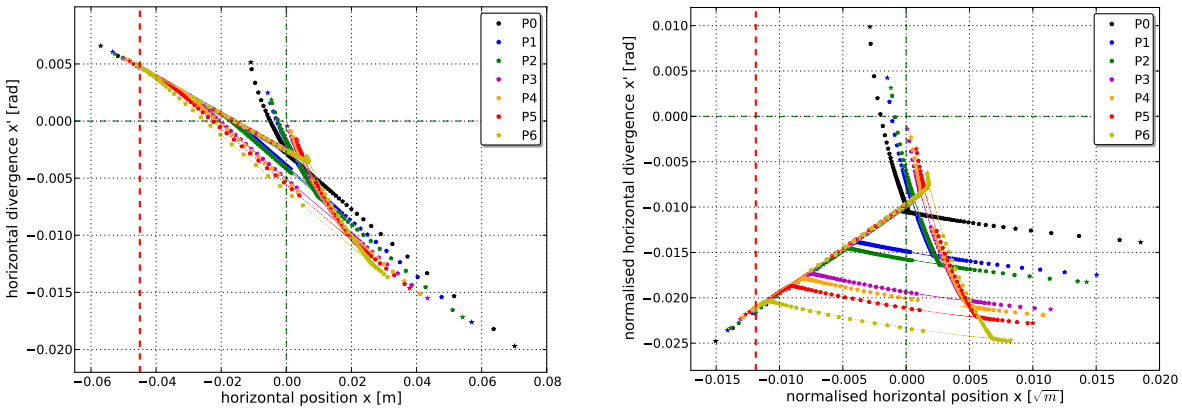

(a) At ES, real coordinates

(b) At ES, normalised coordinates.

Figure 5.25.: Configuration *C1-M-AR-1* at ES in real (a) and normalised (b) phase-space.

responding to emittances $<7.5\,\pi$ mm mrad[20]. According to Table 5.4, these extractable emittances would correspond to the geometric emittance of beams with energies above approximately 240 MeV/n. At lower energies, the high-amplitude component of the beam would be lost.

Figures 5.25a and 5.25b show the extraction geometry at the ES for extraction above resonance ($\widetilde{\delta Q} > 0$), *C1-M-AR*. Due to change of the sign of $\widetilde{\delta Q}$ the orientation of separatrices changed, compare Fig. 5.8c for extraction below resonance to Fig. 5.8a for extraction above reference, with additional 45° phase-advance due to transport to ES. Additionally, due to dispersion shift ($\delta p/p_0 > 0$, normalised dispersion vector pointing in third quadrant), separatrices are now shifted towards the ES. As consequence of these geometric changes, the amplitude growth of unstable particles extracted at large tune distance is interrupted already after a small number of turns, whereas small amplitude particles ($\widetilde{\delta Q} \approx 0$) circulate for many terms and are lost in element apertures.

Comparing extraction below (*C1-M-BR*) and above resonance (*C1-M-AR*), the following observations can be made: In both cases, the large effective distance to the ES ($X_{\mathrm{ES}}/\cos(225°)$ in normalised phase-space) results in the need for large orbit corrections to control particles extracted close to resonance *P0*. For momentum selection Ⓜ, the tune distance from resonance at which particles are extracted is determined by the momentum off-set of the particles. Dispersion shift ($D < 0$, $D' < 0$) therefore positions particles extracted at large tune distances (large $|\delta p|$) close to the ES in the case of extraction above resonance ($\delta p > 0$) and further away from the ES in the case of extraction below resonance ($\delta p < 0$). Maximum amplitude of orbit corrections is limited in both cases: Below resonance, particles will be lost at the ES due to extraction from a second separatrix, as seen in Fig. 5.22. Above resonance, the space between ES and reference orbit is occupied by stable circulating particles so that any outwards displacement of the reference orbit results in losses of high amplitude components of the beam, Fig. 5.25.

In order to overcome these aperture limitations, a more suitable separatrix orientation at the ES has to be chosen. The effective separatrix length can be reduced by decreasing the extraction angle to $|\varphi| < 45°$ in the second or third quadrant, as illustrated in Figs. 5.26a, 5.26b, 5.26c for $\varphi = 225°$, $\varphi = 195°$ and $\varphi = 165°$, respectively.

In real phase space, this rotation results in reorientation of the separatrices: Most notably, with increasing φ (extraction below resonance) the 'upper' unstable fixed-point (highlighted in Figs. 5.26d, 5.26e, 5.26f) moves away from the ES. This change in orientation allows orbit corrections of higher amplitude, without causing particles losses at the ES.

Due to the small phase-advance between ES and MS in LEIR, a wide range of separatrix angles (141° to 240°) is possible without risking losses at the MS. Therefore an angle $\varphi \ll 225°$ can be chosen, resulting in more favourable extraction configurations. *C2-M-BR-1*, using $\varphi = 165°$ in Fig. 5.27a, and *C4-M* in Fig. 5.27b, using $\varphi = 196°$, represent such configurations,

In order to fulfil the Hardt Condition in *C2-M-BR-1*, larger chromaticity is required, $Q' \approx 11$. An orbit displacement of 10 mm at the ES is sufficient to avoid losses of unstable

[20]Extraction of higher emittance particles results in losses at the inside of *KDHV21* and at the outside of *KDHV42*. Further losses (*C1-M-BR-1*, *C1-M-BR-2*) may occur at the outside of *KDHV41*, in the vicinity of *KDHV42* (downstream), in the vicinity of *KDHV21* (upstream), at *VPS22*, in Bending Section 10 (ARC10) and on the ES itself.

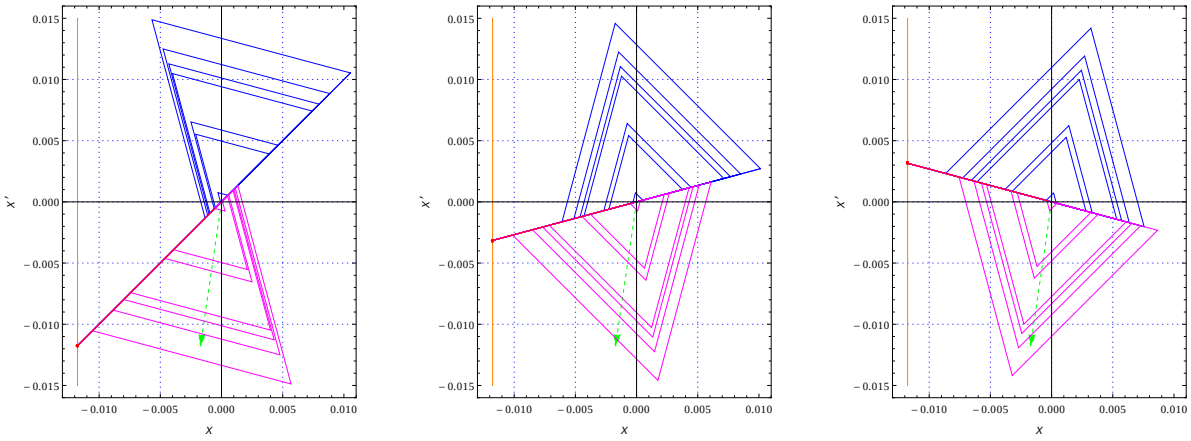

(a) $\Delta\mu = 45°$, $\varphi = 225°$ (Normalised phase-space).

(b) $\Delta\mu = 75°$, $\varphi = 195°$ (Normalised phase-space).

(c) $\Delta\mu = 105°$, $\varphi = 165°$ (Normalised phase-space).

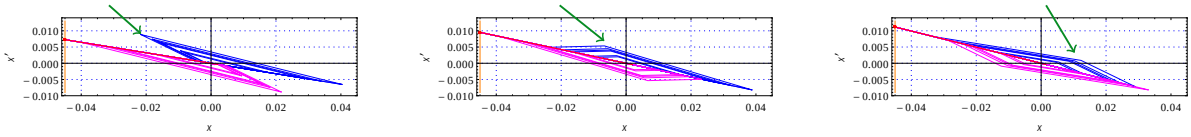

(d) $\Delta\mu = 45°$, $\varphi = 225°$ (Real phase-space).

(e) $\Delta\mu = 75°$, $\varphi = 195°$ (Real phase-space).

(f) $\Delta\mu = 105°$, $\varphi = 165°$ (Real phase-space).

Figure 5.26.: Separatrix orientations at ES for different extraction angles φ and extraction below (blue) and above (magenta) resonance in (a - c) normalised and (d - f) real coordinates. (Based on analytic solution with LEIR parameters and emittances *P0-P7*.)

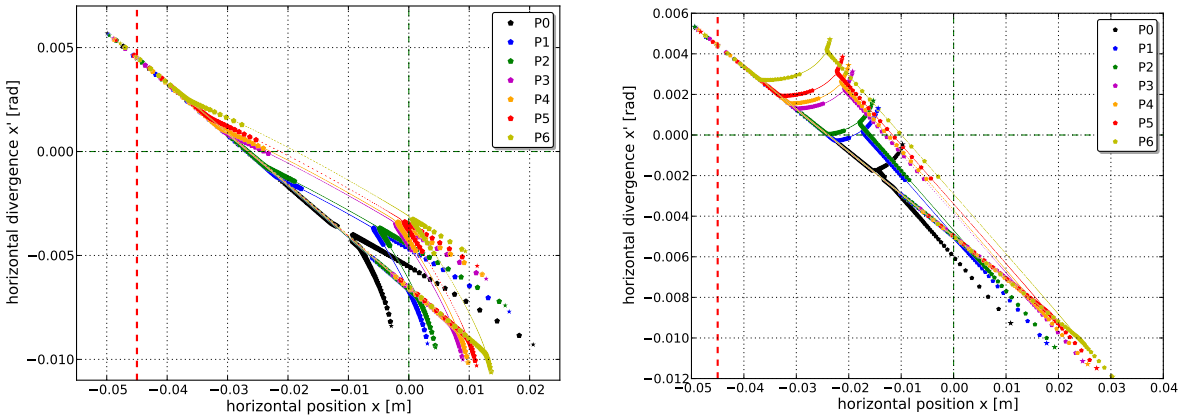

(a) *C2-M-BR-1* at ES, real coordinates.

(b) *C4-M-BR-1* at ES, real coordinates.

Figure 5.27.: Configurations *C2-M-BR-1* (a) and *C4-M-BR-1* (b) at ES.

Max. $B\rho$	$B\rho = 4.8\,\mathrm{T\,m}$					$B\rho = 6.6\,\mathrm{T\,m}$				
Sextupole	XFN	XDN	S41	S42	W41	XFN	XDN	S41	S42	W41
Limit [$\mathrm{T\,m^{-1}}$]	5.23	5.23	2.17	2.17	5.4	5.23	5.23	2.17	2.17	5.0
C1-M-BR-1	-3.93	3.08	-7.80	2.09	0.0	-5.49	4.30	-10.90	2.92	0.0
C1-M-BR-2	-3.81	2.93	-8.60	1.78	0.0	-5.32	4.09	-12.02	2.49	0.0
C1-M-BR-3	-3.78	2.89	-8.71	1.75	0.0	-5.28	4.04	-12.18	2.45	0.0
C1-M-BR-4	-3.77	2.88	-8.60	1.86	0.0	-5.27	4.02	-12.03	2.60	0.0
C1-M-AR-1	-3.90	3.05	-8.46	1.65	0.0	-5.45	4.26	-11.83	2.31	0.0
C1-M-AR-2	-3.82	2.94	-8.49	1.93	0.0	-5.34	4.11	-11.86	2.70	0.0
C2-M-BR-1	-5.10	3.89	8.97	0.18	0.0	-7.13	5.43	12.54	0.25	0.0
C3-M-BR-1	-5.00	3.76	-6.00	-9.62	0.0	-6.99	5.26	-8.39	-13.44	0.0
C4-M-BR-1	-4.71	3.56	0.0	0.0	-1.35	-6.58	4.98	0.0	0.0	-1.88
C4-M-AR-1	-4.71	3.56	0.0	0.0	-1.35	-6.58	4.98	0.0	0.0	-1.88

Table 5.12.: Powering levels of lattice sextupole families for configurations from Table 5.13 and maximum extraction energies of 240MeV/n($B\rho = 4.8\,\mathrm{T\,m}$) and 430MeV/n($B\rho = 6.6\,\mathrm{T\,m}$), respectively. Limits on integrated sextupole strengths from Table 5.5.

particles in element apertures before extraction; 30 mm displacement at the MS maximise space available for a magnetic septum.

Likewise *C4-M* for extraction below (*C4-M-BR-1*) and above resonance (*C4-M-AR-1*) allows circulation of unstable particles up to extraction with the orbit corrections given in Table 5.11.

Table 5.12 lists the integrated sextupole strengths needed for the configurations introduced before. Comparison with their limits shows that *XFLS41* cannot provide the sextupole strength required for *C1* and *C2*. In order to stay within powering limits, beam rigidity would need to be limited to $B\rho \approx 1.17\,\mathrm{T\,m}$ to $1.60\,\mathrm{T\,m}$, or sextupole strength be reduced by a factor ~ 3 at $B\rho = 4.8\,\mathrm{T\,m}$. However, the former corresponds to an upper limit on extraction energy of about 15 MeV/n to 30 MeV/n ($Q/A = 1/2$), and latter results in a reduction of spiral step size by a factor ~ 3. Alternatively, a stronger sextupole could be installed in place of the existing *XFLS41* or *XFLS42*, or the existing PFW could be used for resonance excitation.

Configuration *C4* represents a possible solution based on powering a single PFW (*XFW41*) in agreement with strength limitations. High β_x functions (factor ~ 3 higher compared to *XFLS41/42*), Table 5.8, together with an increased limit on the maximum achievable integrated strength, allow resonance excitation up to maximum extraction energies from LEIR.

However, increase in overall excitation strength in the lattice was observed to lead to strong amplitude detuning effects that distort resonance behaviour. For example, configuration *C3-M-BR-1* results in increased stable triangle emittance. In this configuration, the phase-advance of the virtual sextupole $\Delta\mu_{X_{res}-ES} = 75°$ is chosen similar to configuration *C4*, but is created by superposition of *XFLS41* and *XFLS42*. This angle requires strong powering of both *XFLS41* and *XFLS42*, Table 5.12, due to the relative

	S [$m^{-1/2}$]	φ [°]	α [°]	$\Delta\mu$ [°]	Q'	sgn $\widetilde{\delta Q}$	δQ [10^{-3}]	OC@ES [mm]	OC@MS [mm]
C4-AB-BR-0 [a]	17.81	196	286	74	10.26	< 0	-4.82	0	0
C4-AB-BR-1 [a]							-4.82	14	25
C4-AB-BR-2 [b]							-6.87	14	25
C4-AB-BR-3 [c]							-8.92	14	25
C4-AE-BR-0 [a]							-2.05	0	0
C4-AE-BR-1 [a]							-2.05	14	25
C4-AE-BR-2 [d]							-0.51	14	25
C4-AB-AR-0 [a]	17.81	196	106	74	10.26	> 0	4.82	0	0
C4-AB-AR-1 [a]							4.82	8	28
C4-AE-AR-0 [a]							2.05	0	0
C4-AE-AR-1 [a]							2.05	8	28
C5-AB-BR-1 [a]	40	196	106	74	10.0	< 0	-13.43	14	25
C5-AB-BR-2 [b]							-15.43	14	25
C5-AE-BR-1 [a]							-3.75	14	25
C5-AE-BR-2 [d]							-1.75	14	25

[a] Three particles corresponding to extraction on- and off-momentum $\delta p/p_0 = \pm 2 \cdot 10^{-4}$, Fig. 5.17.
[b] Single particle $\delta p/p_0 = 0$, Fig. 5.18b.
[c] Single particle $\delta p/p_0 = +2 \cdot 10^{-4}$, Fig. 5.18a.
[d] Single particle, lattice tune close to resonance, $\delta p/p_0 = 0$.

Table 5.13.: Tracking configurations for tune selection T. Trackings were performed at tune distances corresponding to the beginning (AB) and end (AE) of spill, according to Fig. 5.17. Configurations above (AR) and below (BR) resonance were studied, and orbit correctors (OC) at the ES and MS adjusted to avoid particle losses in the machine.

phase-advance of both sextupoles, compare Fig. 5.15.

Momentum selection M provides a convenient way to explore the extraction geometry of different configurations. The following section derives properties of the extracted beam for extraction by tune modification T. These studies are based on extraction configurations *C4*, using the PFWs.

5.3.3.3. Particle Tracking - Tune Selection

Simulations in this section are carried out according to the tune selection mechanism T that was introduced in Section 5.3.3.1, Fig. 5.17. Simulations were performed at tune settings corresponding to the beginning of the spill (*C*-AB-**) and towards the end of the spill (*C*-AE-**), as well as below and above resonance. Table 5.13 lists the simulation settings.

Figure 5.28 shows the extraction geometry of configuration *C4-BR* for extraction below resonance, and Fig. 5.29 configuration *C4-AR* for extraction above resonance. Since the Hardt-condition is fulfilled, particles extracted simultaneously - at the same lattice tune Q, but with different tune distances from resonance $\widetilde{\delta Q}$ due to the beam's momentum spread - are well aligned and enter the ES with similar divergence $x'(x = x_{\mathrm{ES}})$. As the lattice tune approaches resonance tune, the tune distance $\widetilde{\delta Q}$ at which particles of a

given momentum offset δp are extracted approaches zero, corresponding to the extraction of particles with diminishing amplitudes as sketched in Fig. 5.17. While the position of the stable fix-point remains constant for particles of a given momentum off-set, their corresponding stable phase shrinks with decreasing tune distance from resonance. As a consequence, the extraction separatrix and the crossing point x'_{ES} moves during the duration of the spill: towards positive x' for extraction below resonance, Fig. 5.28b, and towards negative x' for extraction above resonance, Fig. 5.29a.

At the very beginning of the extraction process when the stable waiting beam enters the resonance, particles of maximum amplitude *P6* are extracted at constant tune distance $\widetilde{\delta Q}$ but varying momentum off-set, compare Fig. 5.18 for extraction below resonance: $\delta p = +2 \cdot 10^{-4}$ (*C4-AB-BR-3*), $\delta p = 0.0$ (*C4-AB-BR-2*), $\delta p/p_0 = -2 \cdot 10^{-4}$ (*C4-AB-BR-1*). Similarly, towards the end of the spill, particles of lowest emittance are extracted at $\delta p \approx 0$ (*C4-AE-BR-2*). During this initial and final phase of extraction particle trajectories are further shifted and enter the ES with different x'_{ES} as shown in Fig. 5.28b.

A fixed orbit displacement therefore cannot provide optimal extraction conditions throughout the spill, potentially resulting in losses of particles in the ES and a reduction in the gap available for the MS, Figs. 5.28c and 5.29b. However, dynamic re-adjustment of orbit correctors might allow to compensate this effect.

Spiral step sizes resulting from *C4* are shown in Fig. 5.30. Application of the required closed orbit correction (marker: ●) reduces spiral step sizes compared to the unperturbed closed orbit (marker: ■), as already seen previously. With appropriate orbit correction, spiral steps sizes for extraction below resonance (*C4-BR*) vary between about 2 mm to 4 mm, for extraction above resonance (*C4-AR*) between 0 mm to 6 mm. Below resonance, the on-momentum particle achieves a larger spiral step width than the off-momentum particle ($\delta p/p_0 > 0$) that is closer to resonance tune, *C4-AE-BR1*. This is probably caused by a dispersion shift towards the ES which shortens separatrices and thus circulation time of unstable particles. This interpretation is consistent with the observation of higher maximum (*C4-AE-AR-1*) and lower minimum (*C4-AB-AR-1*) spiral step widths for extraction above resonance: In that case, particles close to resonance tune with negative momentum off-set are shifted away from the ES.

Figure 5.31 shows the horizontal trajectory of extracted particles at lattice elements between ES and MS. Particles correspond to minimum and maximum spiral step sizes for extraction below (*C4-A-BR*), Fig. 5.31a, and above (*C4-A-AR*) resonance, Fig. 5.31b. Comparing the positions of circulating particles at the beginning (*C4-AB*) and end (*C4-AE*) of the spill shows the horizontal shift that had been observed in phase-space plots at the MS: inward for extraction below resonance and outward for extraction above resonance. The figures compare the effects of two distinct ES kick amplitudes ϕ: gap widths between 9.8 mm ($\phi = 3.2°$) and 16.5 mm ($\phi = 5.4$ mrad) are achieved between (outermost) circulating and (innermost) extracted particles at the position of the MS. The effective gap available throughout the spill (assuming fixed orbit corrector settings) is reduced by the shift of the beam. A stronger kick $\phi = 5.4$ mrad would require apertures of *QFN31* and *XFN31* to be enlarged and would limit the maximum spiral step size to about 8 mm.

Using PFW *XFW41* for resonance excitation allows the spiral step size to be further increased by applying a higher resonance excitation strength S. Given the integrated

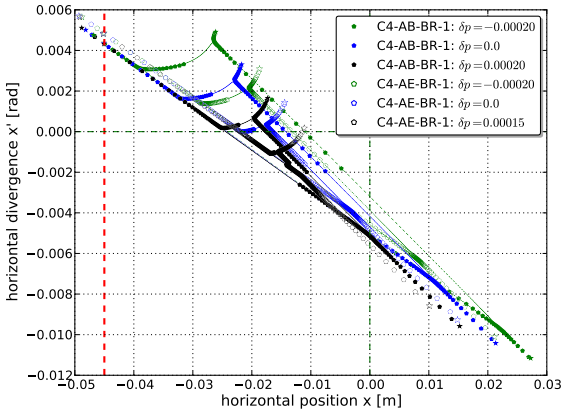

(a) At ES, real coordinates.

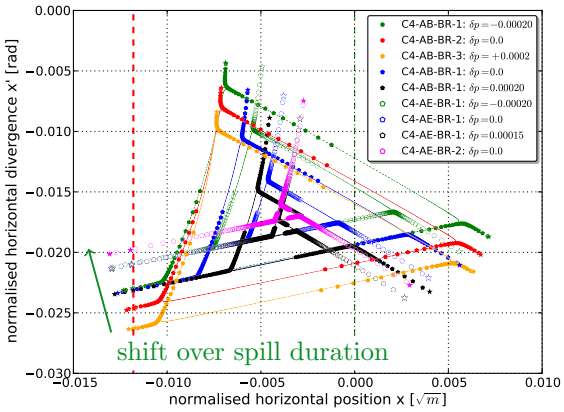

(b) At ES, normalised coordinates.

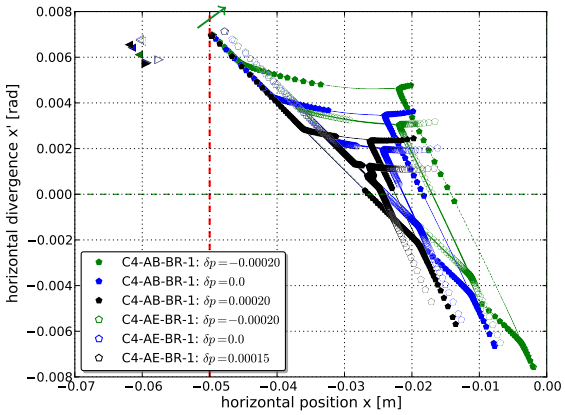

(c) At MS, real coordinates

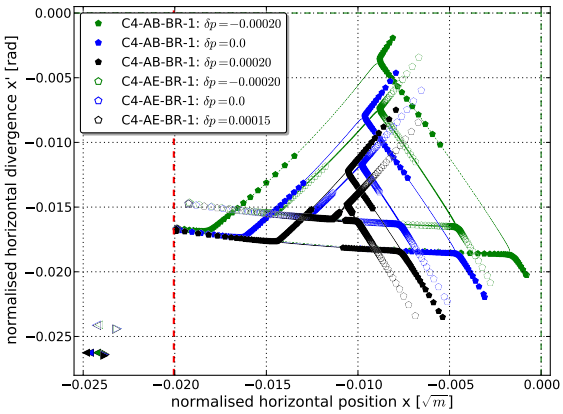

(d) At MS, normalised coordinates.

Figure 5.28.: Configuration *C4-BR* at ES (a, b) and MS (c, d). Filled markers represent extraction at the beginning of the spill (*C4-AB-BR-1*), empty markers the end of the spill (*C4-AE-BR-1*). (b) additionally includes *C4-AB-BR-2*, *C4-AB-BR-3*. *C4-AE-BR-1*.

strength limit of *XFW41* 5.4 T m^{-1} and $\beta_x \approx 23$ m follows $S_{\max} \approx 45\,\mathrm{m}^{-1/2}$ at maximum extraction energy $B\rho = 6.7$ T m. Simulation in configurations *C5-AB-BR* and *C5-AE-BR* yields integrated strength ~ 4 T m^{-1} for $S = 40\,\mathrm{m}^{-1/2}$. Fulfilment of the Hardt condition in this configuration requires a very high positive value of horizontal chromaticity $Q'_x \approx 24$. At maximum extraction energy, sextupole families *XFN* and *XDN* only allow chromaticity correction up to $Q'_x \approx 6.5$, so that the Hardt condition in configurations such as *C5* cannot be fulfilled.

Figure 5.32b clearly shows the resulting misalignment of simultaneously extracted particles. The extracted beam segment in this configuration has a finite 'height' $\Delta x'$ which is superposed on the change in x' over the duration of the spill.

This configuration yields spiral step sizes up to approximately 11 mm, Fig. 5.30. Trackings for extraction at constant tune distance from resonance, but varying particle momentum offsets, clearly show the momentum dependence of spiral step size for extraction below resonance and positive chromaticity: negative momentum offsets result in

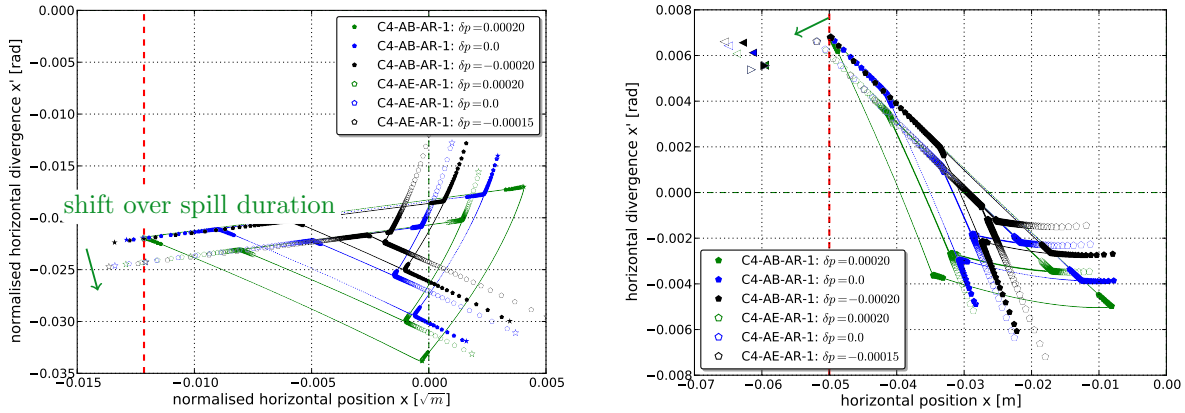

(a) At ES, normalised coordinates. **(b)** At MS, real coordinates

Figure 5.29.: Configuration *C4-AR* at ES (a) in normalised coordinates for comparison to Fig. 5.28b, and at MS (b) in real coordinates for comparison to Fig. 5.28c. Filled markers represent extraction at the beginning of the spill (*C4-AB-AR-1*), empty markers the end of the spill (*C4-AE-AR-1*).

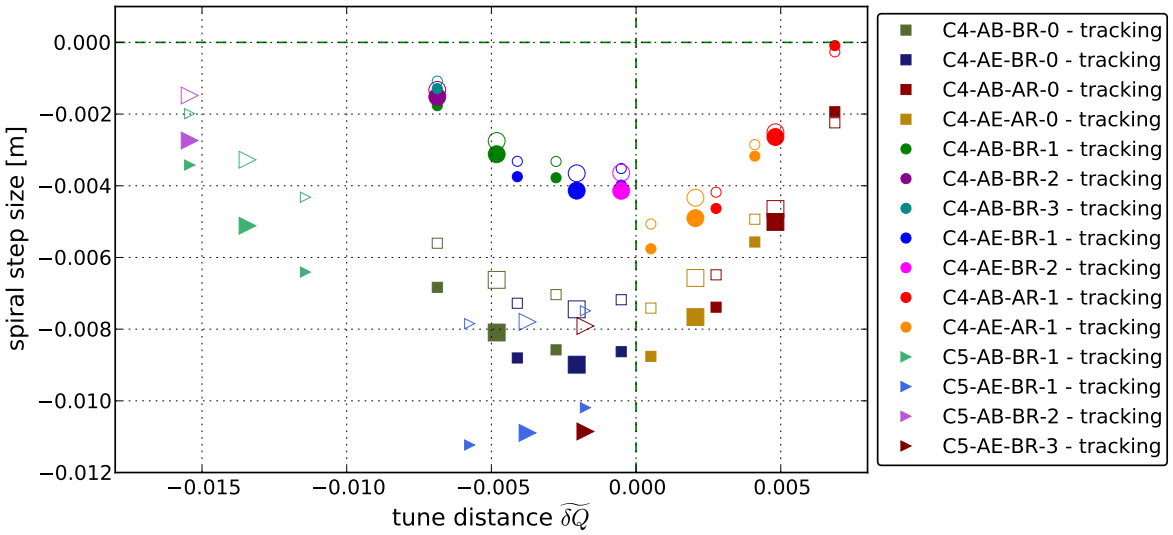

Figure 5.30.: Spiral step width versus tune distances for extraction configurations *C4* and *C5* in Table 5.13. Filled markers correspond to simulation results, empty markers to analytic estimations based on Eq. (5.42); enlarged markers represent on-momentum particles.

largest spiral step sizes, positive momentum offsets in smallest[21]. Close to resonance, this momentum-dependence seems to dominate the tune-dependence of spiral step width since particles with negative momentum offset achieve larger spiral step widths than particles with positive momentum offset that are extracted closer to resonance tune.

[21] Extraction at maximum $\widetilde{\delta Q}$: compare *C5-AB-BR-1* ($\delta p/p_0 < 0$) to *C5-AB-BR-2* ($\delta p/p_0 = 0$); Extraction at minimum $\widetilde{\delta Q}$: compare *C5-AE-BR-1* ($\delta p/p_0 > 0$) to *C5-AE-BR-2* ($\delta p/p_0 = 0$).

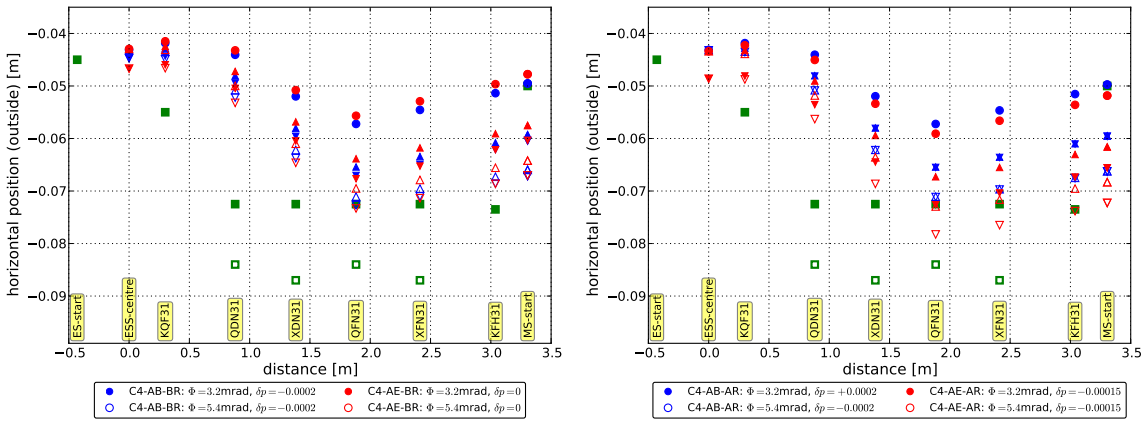

(a) Below resonance (*C4-A-BR*). **(b)** Above resonance (*C4-A-AR*).

Figure 5.31.: Horizontal positions of extracted particles between ES and MS for kicks $\phi = 3.2\,\text{mrad}$ (filled markers) and $\phi = 5.4\,\text{mrad}$ (empty markers). Particles were selected to cover the full range of spiral step widths occurring in trackings *C4*, compare Fig. 5.30. (a) corresponds to extraction below and (b) to extraction above resonance. Marker ● indicates circulating particles, ▲ innermost extracted particles and ▼ outermost extracted particles. Marker ■ represents the current apertures of lattice elements, □ the maximum available apertures after modification.

5.3.3.4. Characteristics of Extracted Beams

Figure 5.33 shows extracted beam segments in horizontal phase space at the entrance of the ES: Particles close to the septum wires at $x = -0.045\,\text{m}$, and particles that underwent the maximum spiral step Δx for the respective configuration. Maximum spiral step sizes in *C5*, Fig. 5.33b, are larger than those in *C4*, Fig. 5.33a, due to the higher sextupole excitation strength in this configuration.

Both plots represent extraction by tune selection T as discussed in the previous section. Therefore, two sets of particles are plotted in each figure, corresponding to extraction at the beginning of the spill (*C*-AB-BR*, large tune distance from resonance, lower x'), and at the end of the spill (*C*-AE-BR*, closer to resonance, upper x'). For configuration *C4*, Fig. 5.33a, particles are aligned at each extraction position because the Hardt condition is fulfilled. This clearly is not the case for *C5*, Fig. 5.33b.

The dependence of spiral step width from particle momentum offset $\delta p/p_0$ and tune distance from resonance $\widetilde{\delta Q}$ was discussed in the context of Fig. 5.30. This effect can also be observed in Fig. 5.33 on the particles extracted close to resonance tune (upper x'): Spiral step width Δx in the configuration close to resonance is dominated by the effect of dispersion shift away from the septum (larger Δx for $\delta p/p_0 \leq 0$), not by tune distance (larger Δx for smaller tune distance from resonance, corresponding to $\delta p/p_0 > 0$).

All tracking results were obtained from single particle tracking on the stability limit as described in Section 5.3.3.1. In reality, extraction is a dynamic process and particle or lattice properties are continuously changed to move particles towards the stability limit and replace those that have already been extracted. Differences in the characteristics of extracted beams resulting for different extraction mechanisms are briefly discussed in the following:

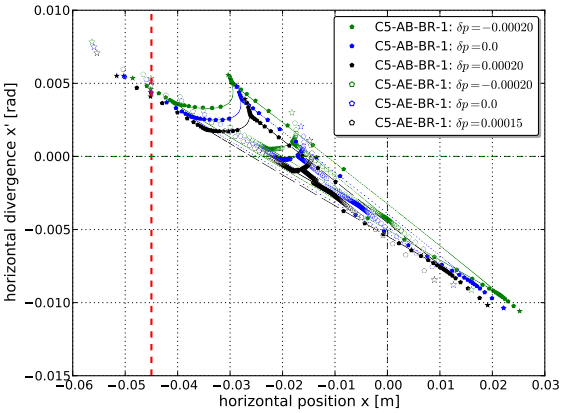

(a) At ES, real coordinates.

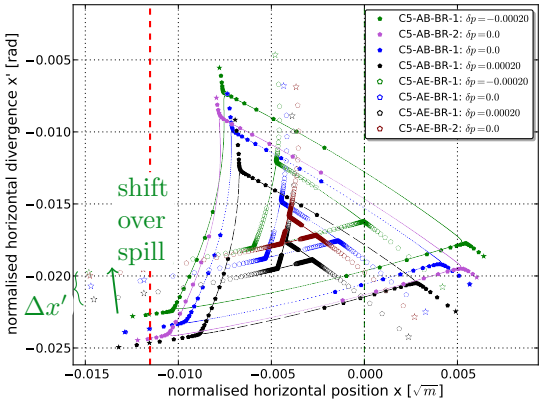

(b) At ES, normalised coordinates.

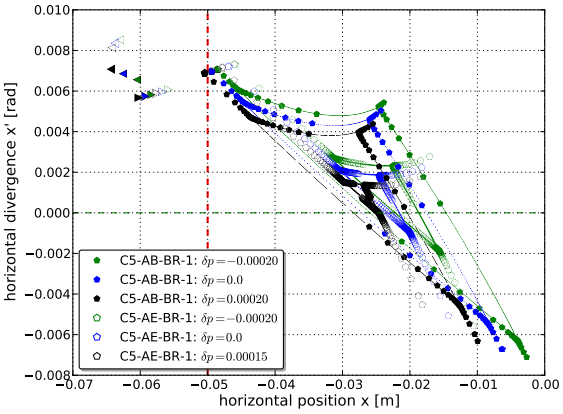

(c) At MS, real coordinates

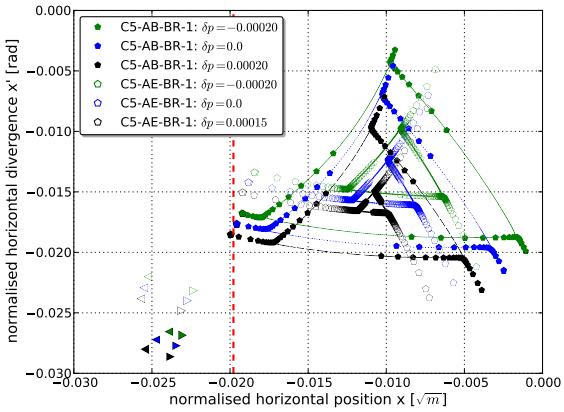

(d) At MS, normalised coordinates.

Figure 5.32.: Configuration *C5-BR* at ES (a, b) and MS (c, d). Filled markers represent extraction at the beginning of the spill (*C5-AB-BR-1*), empty markers the end of the spill (*C5-AE-BR-1*). (b) additionally includes *C5-AB-BR-2* and *C5-AE-BR-2*.

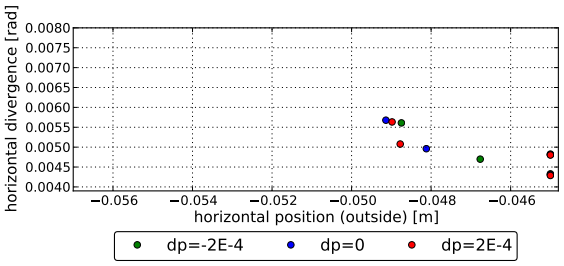

(a) Extracted beam segment *C4-*-BR-1*.

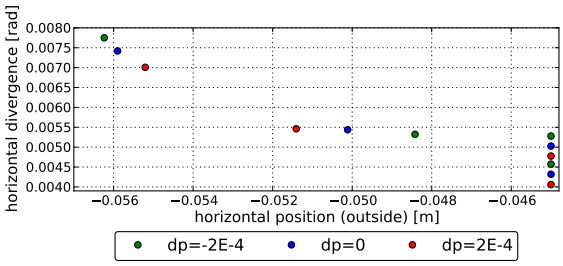

(b) Extracted beam segment *C5-*-BR-1*.

Figure 5.33.: Extracted beam segments at ES entry for Tune Selection T, tracking configurations *C4* (a) and *C5* (a).

Tune Selection T:
Integrated over the duration of the spill, the phase space area of the extracted beam segment is delimited by particles extracted at the two lattice tune extrema, corresponding to beginning and end of extraction, as shown in Fig. 5.33. The extracted beam segment forms a trapezoid whose height depends on two factors: *a*) Due to the change of lattice tune ΔQ over the duration of the spill, on-momentum particles are extracted at different tune distances $\widetilde{\delta Q} = \delta Q$. As the resonance tune is approached, the size of the stable phase space area decreases, which results in a divergence shift of the crossing point between extraction separatrix and ES. *b*) At any point during extraction (fixed lattice tune distance from resonance δQ), particles with different momentum offsets are extracted at different tune distances $\widetilde{\delta Q}$ due to chromaticity-caused tune shift.

This second component increases with beam momentum spread and can be corrected by fulfilling the Hardt condition, compare Fig. 5.33a to Fig. 5.33b. The first component cannot be corrected by the Hardt condition because the tune distance $\widetilde{\delta Q}$ at which a particle is extracted is not related to its momentum offset, Fig. 5.18. However, dynamic adjustment of orbit correctors during the extraction process could reduce or compensate this divergence shift.

Simulations here were performed for the extraction of particles with large horizontal emittance $\epsilon_\mathrm{H} \approx 40\,\pi\,\mathrm{mm\,mrad}$, corresponding to beam sizes for low energy extraction at around 10MeV/n, *P6* in Table 5.4. Since the displacement is directly caused by a change in stable phase space area, the effect of x' shift during extraction is expected to reduce towards higher extraction energies and smaller beam emittances.

Amplitude Selection A
In this configuration, the lattice tune for extraction would be chosen based on beam emittance and slope of the resonance, as illustrated in Fig. 5.18a. Since the lattice tune remains constant thoughout the extraction process, no shift in x' is expected during extraction. Constant relation between particle tune and particle momentum offset allows compensating dispersion related variations in extraction x' by fulfilling the Hardt condition.

Momentum selection M
Regarding its properties in horizontal phase space, this configuration is similar to amplitude selection. Relation between extraction tune and particle momentum offset is exclusively defined by the resonance configuration, so that particles extracted at different tune distances can be aligned by adjusting chromaticity or dispersion.

In all cases, the horizontal width of the extracted beam segment is defined by the maximum spiral step and is of the order of several millim. Since its divergence is much smaller, the extracted beam is often referred to as 'bar of charge' in horizontal phase space. Its width is independent of the beam momentum p_0, but varies due to the tune distance dependence of the spiral step, Eq. (5.42).

Even if the Hardt condition is fulfilled, and extracted off-momentum particles are well-aligned, the extracted beam has a certain divergence spread $\Delta x'$ of the order of $10^{-2}\,\mathrm{mrad}$ which is caused by coupling between the motion in vertical and horizontal plane and is therefore expected to increase with vertical emittance. This effect was not taken into account in the simulations discussed previously since coordinates in the vertical

plane were chosen on the reference orbit ($y = y' = 0$). The divergence spread caused by coupling at low energy extraction is estimated to 0.05 mrad in [176]. It decreases with increasing beam energy due to adiabatic damping in the vertical plane.

5.3.4. Summary & Discussion

This section investigated feasibility of slow extraction from SS30 in LEIR. Based on LEIR-specific constraints, Section 5.3.1, parameters for suitable extraction configurations were derived from analytic considerations, Section 5.3.2, and then verified and refined by particle tracking, Section 5.3.3. Tracking simulations in Section 5.3.3.2 and 5.3.3.3 indicate that suitable extraction configurations can be found on both sides of the resonance. Figure 5.30 suggests that for the same level of closed orbit correction, higher spiral steps are achieved for extraction below resonance, compare *C4-*-BR-0* and *C4-*-AR-0*. The following discussion is therefore based on this scenario.

For extraction below resonance, phaseadvance $\Delta\mu \approx 70°$ ($\varphi \approx 200°$) was identified to provide a suitable extraction geometry. This phaseadvance can be achieved by simultaneous powering of multiple LEIR sextupoles, such as *XFLS41* and *XFLS42*, or by using PFWs *XFW41* or *XFW21* which are placed at $\Delta\mu = 74°$ and $\Delta\mu = 14°$, respectively, Section 5.3.2.5. Given their integrated strength limits and high betatron amplitude functions, Table 5.8, excitation strengths up to $S = 45\,\mathrm{m}^{-1/2}$ (at maximum extraction energy) can be achieved with one of these PFWs, which is not possible with *XFLS41* or *XFLS42*. *XFW32* is less suited because orbit corrections in SS30 affect the reference orbit through this element. Additional powering of *XFW12* allows adjustment of the phase advance $\Delta\mu = 14°\pmod{60°}$, if needed.

In the following, effects of strong amplitude-dependent detuning, Section 5.3.4.1 and possible septum arrangements for low- and high-energy extraction scenarios, Section 5.3.4.2 and 5.3.4.3, are discussed. Section 5.3.4.4 concludes on the findings of this slow extraction study and suggests directions for further research.

5.3.4.1. Amplitude-dependent Detuning

Figure 5.34 shows the relation of extraction tune distance $\widetilde{\delta Q}$ to maximum stable particle amplitudes for selected configurations. Data points correspond to the square-root of the observed maximum stable emittances $A_{\mathrm{sim}} = \sqrt{\epsilon_{\mathrm{sim}}}$ from tracking simulations, lines represent the expected maximum stable amplitudes $A_{\mathrm{an}} = \sqrt{\epsilon_{\mathrm{an}}}$ based on Eq. (5.55) for two different excitation strengths, $S_{\mathrm{virt}} = 17.8\,\mathrm{m}^{-1/2}$ (dashed) and $S_{\mathrm{virt}} = 40\,\mathrm{m}^{-1/2}$ (dotted).

For small emittance particles and small S_{virt}, tracking results are in good agreement with theoretic values. Deviations from the expected emittance ϵ_{an} for *C1* (marker: ■) and *C4* (marker: ●) stay below ±10 %. However, larger deviations can be observed for configurations *C2* (marker: ▲), *C3* (marker: ▼) and *C5* (marker: ▶), particularly at high amplitudes.

Non-linear detuning depends on the strength and phase advances of all sextupoles, including those that are not contributing to resonance excitation. It may occur with a single strongly powered sextupole, such as in *C5*. Strong detuning effects were also observed when multiple sextupoles were powered to achieve a desired phase for the virtual

resonance driving sextupole, even if the resulting S_{virt} was relatively low. Configuration *C3* represents this case: deviations between observed and expected emittance values amount up to $\epsilon_{\mathrm{sim}}/\epsilon_{\mathrm{an}} \approx 1.6$ for maximum amplitude particles. Most extraction configurations discussed before were chosen to minimise such detuning effects while maximising effective resonance excitation strength S_{virt}. Extraction angles were therefore selected that rely on a single sextupole providing the main contribution to resonance excitation and only a small correction by a second. Further quantitative investigation of these detuning effects are needed for the development of better mitigation strategies.

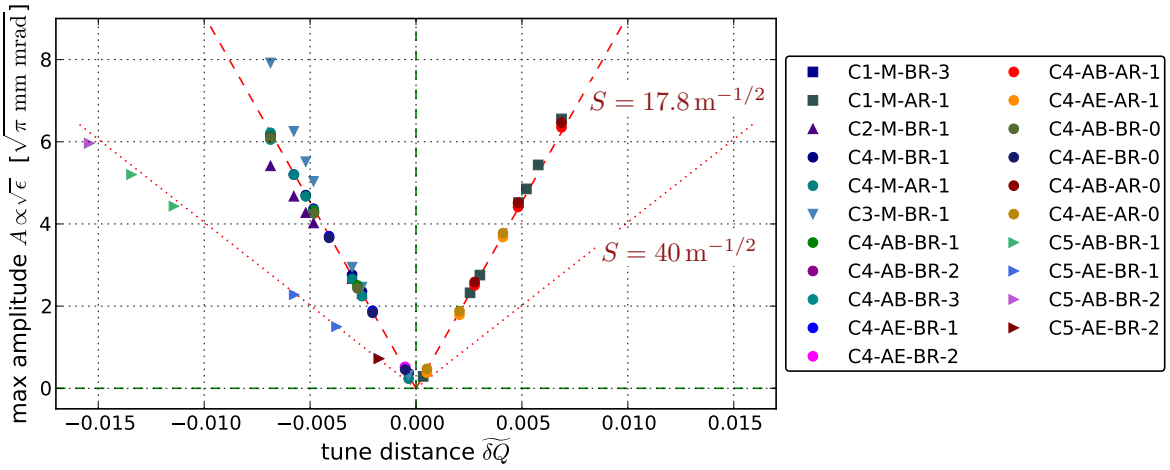

Figure 5.34.: Maximum stable particle amplitude $\propto \sqrt{\epsilon_{\mathrm{sim}}}$ from tracking for configurations *C1* (marker: ■), *C2* (marker: ▲), *C3* (marker: ▼), *C4* (marker: ●) and *C5* (marker: ▶) versus tune distance $\widetilde{\delta Q}$. Expected emittances according to Eq. (5.55) are indicated for $S_{\mathrm{virt}} = 17.8\,\mathrm{m}^{-1/2}$ (dashed line) and $S_{\mathrm{virt}} = 40\,\mathrm{m}^{-1/2}$ (dotted line).

5.3.4.2. Extraction Configurations

Based on considerations of extraction efficiency and machine limitations, several constraints on extraction parameters were identified in the previous sections. The most important requirements and constraints are summarised in Table 5.14. The following paragraphs discuss those requirements and conclude on the suitability of the investigated configurations for extraction from LEIR.

Extraction from current LEIR In a preliminary extraction scheme, based on the current magnets and power supplies installed in LEIR, extraction energy is limited to $E_{\mathrm{max}} = 240\,\mathrm{MeV/n}$ ($B\rho = 4.8\,\mathrm{T\,m}$), so that a maximum ES kick of up to $\phi = 5.4\,\mathrm{mrad}$ can be given. At this energy, XFN and XDN allow for chromaticity correction up to $Q'_{\mathrm{x}} \approx 11$ ($Q'_{\mathrm{y}} = 0$), so that the Hardt condition can be fulfilled for $\{\varphi = 196°,\ S \approx 19\,\mathrm{m}^{-1/2}\}$ as in *C4*. For higher resonance excitation strengths, such as those obtained in *C5* by using *XFW21* and/or *XFW41*, the Hardt condition cannot be fulfilled. Table 5.15a summarises extraction parameters for both configurations.

In order to minimise particle losses at the ES to <5 %, minimum spiral step sizes should exceed 2 mm. Except for high-amplitude particles in *C4*, this requirement is fulfilled in

	Unit	Current LEIR $B\rho$ up to 4.8 T m	High Energy $B\rho$ up to 6.7 T m
Min. spiral step $\Delta x_{\min}$ [a]	[mm]	2	2
Max. spiral step $\Delta x_{\max}$ [b]	[mm]	8	14
Max. Q'_{x} for Hardt-condition [c]		11	6.5
Max. S_{virt} [d]	[$\mathrm{m}^{-1/2}$]	62	45
Min. gap at entrance of MS [e]	[mm]	10	10
Min. separation at entrance of *KFH3234*	[mm]	28	28

[a] Required to keep losses at ES below 5 %, assuming thickness of septum wires ~ 0.1 mm, Table 5.7.
[b] Aperture limitation due to *KFH31*, depending on ES kick and orbit displacement at *KFH31*.
[c] Limited by integrated strengths of chromaticity correction sextupoles *XDN*/*XFN*, Table 5.5.
[d] Based on integrated strengths, Table 5.5, of single resonance excitation sextupole *XFW41* or *XFW21* ($\Delta\mu \approx 70°$).
[e] Separation between circulating and innermost extracted particles at entrance to MS, assuming 10mm septum width, Table 5.7.

Table 5.14.: Parameter requirements and constraints for low (current LEIR) and high energy (after upgrade) extraction from LEIR.

both configurations. To accommodate the beam in the extraction line, the apertures of *QFN31* and *XFN31* need to be enlarged by approximately 5 mm to 10 mm. The maximum spiral step size that can be transported past *KFH31* is limited by the ES kick and the amplitude of closed orbit displacement at the MS. Figure 5.31a (*C4*) indicates an upper spiral step limit of approximately 8 mm in these configurations. Low-emittance particles in *C5* slightly exceed this limit.

The gap available between the innermost transverse position of the MS at $x = -0.05$ m and the innermost particles of the extracted beam might be reduced due to dispersion shift of simultaneously extracted particles if the Hardt condition cannot be fulfilled. This effect can be observed in configuration *C5*, Fig. 5.32c, and is expected to be less pronounced at lower S.

In addition, extraction method T (Fig. 5.17) gives rise to variation of the divergence x'_{ES} of extracted particles throughout the spill, Section 5.3.3.4. Assuming fixed orbit displacement at ES and MS, this variation results in an additional reduction of the available gap width, for example to $\Delta x_{C5} \approx 12.4$ mm in *C5*, Fig. 5.32c. Figure 5.32b suggests that this variation in x'_{ES} between particles extracted towards the beginning and end of the spill (*C5-AB-BR-2*, *C5-AE-BR-2*) is contained within the divergence variation across on- and off-momentum particles at unfulfilled Hardt Condition. Gap widths between $\Delta x \approx 12$ mm to 14 mm and would provide sufficient space for the installation of a magnetic septum (width ≈ 10 mm) at the exit of *KFH31*, where the first magnetic ejection septum *MS1* is placed in Fig. 5.14.

Variation in the horizontal position of the extracted beam at the first MS could be mitigated by dynamically adapting the amplitude of orbit correction at this location: from the value chosen at the beginning of a spill (*C5-AB-BR*) to a slightly increased value (+3 mm) towards the end of the spill (*C5-AE-BR*). This way, an effective gap between $\Delta x \approx 14$ mm and $\Delta x \approx 16$ mm could be made available for the installation of a magnetic septum. Table 5.15b summarises these parameters.

C4		*C4-AB-BR-1*			*C4-AE-BR-1*				
$\frac{\Delta p}{p}$	$[10^{-4}]$	-2.0	0	$+2.0$	-2.0	0	$+1.5$	S	$17.8\,\mathrm{m}^{-1/2}$
ϵ_{geo}	[π mm mrad]	37.5	18.6	6.3	13.7	3.6	0.3	Q'_{x}	10.3
Δx	[mm]	1.8	3.1	3.8	3.7	4.1	4.0	$\Delta\mu_{\mathrm{x}}$	74°
$\widetilde{\delta Q}$	$[10^{-3}]$	-6.9	-4.8	-2.8	-4.1	-2.1	-0.5		
C5		*C5-AB-BR-1*			*C5-AE-BR-1*				
$\frac{\Delta p}{p}$	$[10^{-4}]$	-2.0	0	$+2.0$	-2.0	0	$+2.0$	S	$40.0\,\mathrm{m}^{-1/2}$
ϵ_{geo}	[π mm mrad]	35.5	27.1	19.6	5.2	2.3	0.5	Q'_{x}	10.0
Δx	[mm]	3.4	5.1	6.4	11.2	10.9	10.2	$\Delta\mu_{\mathrm{x}}$	74°
$\widetilde{\delta Q}$	$[10^{-3}]$	-15.4	-13.4	-11.4	-5.8	-3.8	-1.8		

(a) Extraction parameters for configuration *C4* and *C5*.

	dynamic orbit correction		fixed orbit correction	
	C4	*C5*	*C4*	*C5*
Min. gap (exit *KFH31*)				
$B\rho$ up to 4.8 T m [a]	16.3 mm	14.6 mm	14.2 mm	12.4 mm
$B\rho$ up to 6.7 T m [b]	9.6 mm	7.9 mm	7.5 mm	5.8 mm
Min. gap (exit *KFH31* + 1m) [c]				
$B\rho$ up to 4.8 T m [a]			19.6 mm	17.8 mm
$B\rho$ up to 6.7 T m [b]			10.7 mm	9.0 mm

[a] ES kick limited to 5.4 mrad.
[b] ES kick limited to 3.2 mrad.
[c] Interpolation, assuming additional 1 m drift with given kick.

(b) Gaps at MS for configurations *C4* and *C5*.

Table 5.15.: Extraction parameters (a) and available gap at MS (b) for configurations *C4* and *C5*.

Both misalignment effects are expected to decrease with increasing extraction energy: The effect of unfulfilled Hardt condition on the alignment of instantaneously extracted particles decreases due to a reduction in $\delta p/p \propto 1/B\rho$. Due to the reduced beam emittance, only a smaller range of tunes ΔQ is extracted, Eq. (5.55), resulting in reduced variability of x'_{ES} over the extraction process.

Reduction of excitation strength below $S \sim 20\,\mathrm{m}^{-1/2}$ would result in increased losses at the ES for low energy extraction (10-20MeV/n) due to reduced minimum spiral step size <2 mm. Lower S should, however, have no or even a positive effect on the extraction efficiency at the MS, since the Hardt condition could be fulfilled and thus a wider gap be made available. Detuning effects, such as those observed at large particle amplitude in *C5* (Fig. 5.34), would be suppressed. On the other hand, further increase of the excitation strength S, leading to a larger spiral step size, would improve extraction efficiency at the ES and reduce relative losses at the inside of the MS. Depending on orbit displacement at MS and maximum spiral step size, this may cause losses at *KFH31*.

Extraction after High-Energy Upgrade Replacement of the dipole power supplies in LEIR will allow higher extraction energies up to 430 MeV/n ($B\rho = 6.64\,\mathrm{T\,m}$). Due to increased beam rigidity, the maximum electric field of the ES then limits deflection to $\phi = 3.2\,\mathrm{mrad}$, thus reducing separation between circulating and extracted beam at the exit of *KFH31* to $\Delta x < 9.6\,\mathrm{mm}$, Table 5.15b. Installation of a magnetic septum at the position *MS-start* indicated in Fig. 5.14 will therefore result in particle losses,.

The maximum spiral step size in this configuration is constrained by *KFH31* to approximately 14 mm. Since horizontal chromaticity correction at maximum extraction energy is limited to $Q'_{\mathrm{x}} \approx 6.5$, high S for maximum spiral step sizes of this magnitude and simultaneous fulfilment of the Hardt-condition are incompatible.

Assuming $S = 40\,\mathrm{m}^{-1/2}$ as in *C5* and successful dynamic adaption of orbit corrections, Fig. 5.32c indicates that approximately 30% of the beam would be lost at the MS towards the end of the spill for extraction of low energy beams. Higher losses, up to approximately 50% towards the end of spill, are expected at larger beam momentum spread and if orbit corrections cannot be adapted dynamically. These values are based on $\epsilon_H \approx 40\,\pi\,\mathrm{mm\,mrad}$. At higher energies, a smaller range of tunes ΔQ is extracted, resulting in reduced variation in x'_{ES} during extraction and thus in smaller losses.

5.3.4.3. Placement of Downstream Septa

In order to increase the available gap width in the high energy extraction scenario, the first magnetic septum needs to be placed further downstream from the ES and from the position *MS-start* indicated in Fig. 5.14. An additional drift space of 1 m would result in a gap width $\Delta x = 10.7\,\mathrm{mm}$ for high energy extraction ($B\rho = 6.64\,\mathrm{T\,m}$, $\phi = 3.2\,\mathrm{mrad}$) and $\Delta x = 19.6\,\mathrm{mm}$ for low energy extraction ($B\rho = 4.8\,\mathrm{T\,m}$, $\phi = 5.4\,\mathrm{mrad}$), compare *C4* in Table 5.15b.

Both configurations, with a first magnetic septum placed immediately after *KFH31* (*MS1*) or 1 m downstream of *KFH31* (*MS1**), are illustrated in Fig. 5.14. Using a second magnetic septum (*MS2*), installed approximately 20 cm downstream of the exit of *MS1**, extracted beams up to $B\rho = 6.64\,\mathrm{T\,m}$ could be deflected to a horizontal position of $x = -42\,\mathrm{cm}$ ($l_{\mathrm{KFH31-MS}} = 1\,\mathrm{m}$) at the entrance of kicker tank *KFH3234* – sufficient to pass its kicker magnet.

For operation with *MS1** the orbit correction needs to be readjusted for the circulating beam to pass closely inside the MS at $x = -0.05\,\mathrm{m}$, leading to a slightly elevated orbit excursion at *KFH31*. The effect on the horizontal position, however, is small: <1 mm outwards shift compared to the foregoing extraction tracking studies.

In order to further improve extraction efficiency, in particular for configurations such as *C5* in which the Hardt condition cannot be fulfilled, the first magnetic septum may need to be installed even further downstream, possibly with an additional electrostatic septum inserted between *KFH31* and the first magnetic septum. Alternatively, a thinner (and weaker) magnetic septum may be placed first, followed by a second (stronger) magnetic septum. When increasing the phase advance between ES and the first MS, its influence on the minimum acceptable separatrix angle φ_{min} at the ES, as discussed in Section 5.2.3.5, needs to be taken into account.

All requirements and constraints discussed in this section are summarised in Table 5.14. Workable configurations *C4* and *C5* and their parameters are listed in Table 5.15. Start

parameters for the following beamline design study are based on septum configuration *MS1** and *MS2* in Fig. 5.14, installed at the positions indicated in Table 5.6. The central orbit of the extraction line is approximated as $x = -0.042\,\mathrm{m}$, $x' = -140\,\mathrm{mrad}$ at the entrance to *KFH3234* for beams of all energies.

5.3.4.4. Conclusion

Multiple mechanisms can be exploited to achieve slow resonant extraction of circulating beam particles, Section 5.2.3.2. In particular, *quadrupole-driven* extraction by tune selection [T] lends itself for implementation in LEIR since no additional equipment would be needed. Workable extraction configurations for this extraction mechanism were identified for low-energy extraction ($B\rho$ up to $4.8\,\mathrm{T\,m}$) from LEIR, Section 5.3.4.2. In this configuration, extraction can be achieved using one ES at the beginning of SS30, and one MS with gap width $\Delta x = 10\,\mathrm{mm}$, installed at the exit of *KFH31*.

Since less separation can be obtained between circulating and extracted beams at high-energy extraction ($B\rho$ up to $6.64\,\mathrm{T\,m}$), Table 5.15b, this configuration would result in major losses at the MS. For high-energy extraction, the MS would therefore need to be replaced by a thinner septum $\Delta x < 9\,\mathrm{mm}$ and be installed at least 1 m downstream of *KFH31*, compare *MS1* to *MS1** in Fig. 5.14. Additionally, a second magnetic septum *MS2* would need to be installed approximately 2.4 m downstream of *MS1**. Table 5.6 summarises the positions of these magnetic septa in SS30.

Alternatively, RF-KO, extraction by *amplitude selection* [A], could easily be implemented in LEIR, by using existing damper elements to impart transverse kicks on beam particles. As beginning *C*-AB-** and end *C*-AE-** configurations of the extraction process by *tune selection* [T], compare Fig. 5.17, resemble those of high- and low-amplitude extraction by means of *amplitude selection* [A], the foregoing findings are expected to also apply to this extraction mechanism.

High values for the horizontal chromaticity were chosen in the simulations for extraction by *tune selection* [T] in order to fulfill the Hardt condition as well as possible, given the powering constraints of sextupole families *XFN* and *XDN*. Since different criteria may apply to the choice of chromaticity for extraction by *amplitude selection* [A], dedicated studies for this extraction mechanism will be needed.

While the studies performed in this section indicate feasibility of slow extraction from LEIR and provide first estimates for the transverse phase space properties of the extracted beam segment, a detailed design proposal for a new slow extraction will require further investigations:

Particle tracking studies in Section 5.3.3 were based on a well-established lattice model of the current LEIR, see Section 5.3.3.1. Although not all error terms may be taken into account by this approximation, no major changes to the presented results are expected. A detailed error analysis, taking into account uncertainties in lattice, element alignment and beam properties, will be required to verify this assumption.

The presented study attempts avoiding the creation of stable islands and minimising amplitude detuning effects by careful selection and usage of one single, or few, resonance excitation sextupoles. Development of better mitigation strategies demands further quantitative investigation of detuning effects in LEIR.

Single particle tracking allows simulation of the positions of extremal beam particles throughout the lattice and at the extraction septa. Although the results obtained from these studies, in combination with aperture information and estimated septum properties, Table 5.7, indicate the viability of different extraction configurations and setups, information about loss levels can hardly be inferred. More detailed multi-particle simulation studies will therefore be needed to quantify expected particle losses and the resulting activation of extraction elements.

The two-septum configuration (*MS1/MS1**, *MS2*) proposed in Section 5.3.4.3 is based on tracking studies and analytic estimates of beam propagation to septum positions located downstream of *KFH31* with the aim to provide parameter estimates for the beamline design in the following Section 5.4. Further tracking studies are required to determine most suitable and versatile septum arrangements that simultaneously maximise extraction efficiency for all extraction energies and ensure sufficient horizontal separation at *KFH3234* for the installation of transfer line beam pipes and first quadrupole magnets.

Work on a detailed proposal for a new slow extraction scheme, including an optimised positioning setup of magnetic septa in SS30 and the orbit corrections required to minimise particle losses during the extraction process, is currently underway and will be available as CERN report [205].

5.4. Design of Beam Transfer lines

This section presents linear optic designs for two transfer lines: A horizontal beamline for energies up to the maximum extraction energy 430 MeV/n ($B\rho = 6.64\,\mathrm{T\,m}$), and a vertical beamline for energies up to 75 MeV/n ($B\rho = 2.55\,\mathrm{T\,m}$), based on the beam requirements established in Section 5.1.1.

After introducing design approach and constraints in Section 5.4.1, the components of the proposed beamlines and their characteristics are presented in Section 5.4.2. Section 5.4.3 evaluates the results and discusses possible improvements.

5.4.1. Design Criteria and Constraints

The use of the extracted beam for biomedical experiments demands variable beam sizes from a few mm FWHM pencil beams, to broad beams with at least 5 cm × 5 cm and high level of dose uniformity across the sample area, Table 5.1.

Different approaches for the formation of homogeneous broad beams are commonly used, based on active methods, such as higher order optical elements or 'beam wobbling', or passive methods using scatterers to increase the beam's emittance [206–208]. Modern ion therapy treatment centres rely on beam scanning systems which are able to perform the complex beam deliveries needed for patient treatment and medical physics experiments while at the same time providing the possibility to deliver homogeneous dose distribution across a large target area [209, 210].

A beam scanning system offers most flexibility and would therefore be the delivery mechanism of choice for radiobiological beamlines at LEIR. Since its implementation is time-intense and costly, this study investigates an upgradable solution to provide beams of sufficient quality for radio-biological experiments in a first implementation stage

already on a shorter timescale. The proposed design is based on a minimum number of first-order optical elements to guide the beam towards the endstations and to achieve a wide range of beam sizes in the target plane. Main constraints and design considerations are detailed in the following sections.

5.4.1.1. Space Constraints for Beam Transfer Lines

The schematic in Fig. 5.3b shows the storage area adjacent to LEIR which provides ample space for the installation of beam transport lines, connected experimental endstations and laboratories.

While no particular constraints are imposed on location and length of the horizontal transfer lines, vertical space availability is limited due to transport cranes installed across the site. The location indicated for the vertical end-station in Fig. 5.3b, maximises the possible height of the vertical transfer line and end-station: approximately 7.5 m from ground level, compared to only about 5.5 m at any other location. An installation height of 1.5 m above ground is assumed for LEIR, so that approximately 5.5 m are left for the beam optics required for a vertical beamline.

Alternatively, the vertical beamline may be placed underground, which is expected to provide advantages with regard to radiation protection. Since a given beamline design could be used for both scenarios and installation above ground poses stricter constraints due to space limitation, this scenario has been chosen for the following study.

5.4.1.2. Start Parameters for Beam Transfer Line

In order to use the Courant-Snyder formalism, Section 5.2.1.2, beam parameters ϵ, α and β have to be determined for the extracted beam. Parameters of the extracted beam in vertical phase space can be considered identical to those of the circulating beam. In horizontal phase-space, parameters need to be estimated from the characteristics of the extracted beam segment. Typically, a beam's emittance and optical functions are defined by closely fitting an ellipse, Eq. (5.13), to the particle distribution in phase space. However, this approach is less suited for representing the 'bar of charge' that is obtained from slow resonant extraction in horizontal phase space: Emittance ϵ, and thus the betatron amplitude function $\beta_x = \frac{\sigma_x^2}{4\epsilon}$ of the extracted beam, would depend strongly on the divergence spread $\Delta x'$ and spiral step-size Δx of the extracted beam. This would result in strong dependence of betatron amplitude function from extraction energy due to the effect of adiabatic damping on $\Delta x'$, and from tune distance at extraction due to varying spiral step size Δx.

Approximation by 'Unfilled Ellipse' The 'unfilled ellipse' approach [176, 211] is used to obtain a robust estimate of beam parameters in the horizontal phase-space: It considers the phase space area covered by the bar of charge as a small part of a larger, mainly 'unfilled' ellipse whose large half-axis is defined by the width Δx of the extracted beam segment, corresponding to the maximum spiral step. The emittance $\epsilon_{\text{unfilled}}$ of this 'unfilled ellipse' is chosen to be far greater than the actual emittance ϵ_{real} of the extracted beam segment. This makes the parameter estimates insensitive to variations in the extracted divergence and thus guarantees a more robust estimate of the β function.

Figure 5.35a illustrates this approach: Particles with different momenta $\delta p/p_0$ between $(\delta p/p_0)_{\min}$ and $(\delta p/p_0)_{\max}$ are extracted at the ES. The Hardt condition is assumed to be not perfectly fulfilled, so that particles with different $\delta p/p_0$ will not superpose but rather form several 'lines of charge' extracted at different x'. Their spiral step size Δx depends on the resonance configuration, according to Eq. (5.42). Figures 5.35a and 5.36 assume off-momentum particles to achieve larger spiral step sizes than on-momentum particles. The large axis of the 'unfilled ellipse' corresponds to the length of the maximum spiral step. The central orbit in the extraction line is defined as the centre position of the extracted 'line of charge' for on-momentum particles. This way, the momentum dependence of width Δx and divergence x' of extracted beam segments can be expressed by an initial dispersion vector $\mathbf{D}$ at the beginning of the transfer line. In zero-dispersion regions of the transfer line, extracted off-momentum particles will be horizontally centred relative to on-momentum particles; in regions with $D' = 0$, on- and off-momentum particles will have the same divergence, Fig. 5.35b.

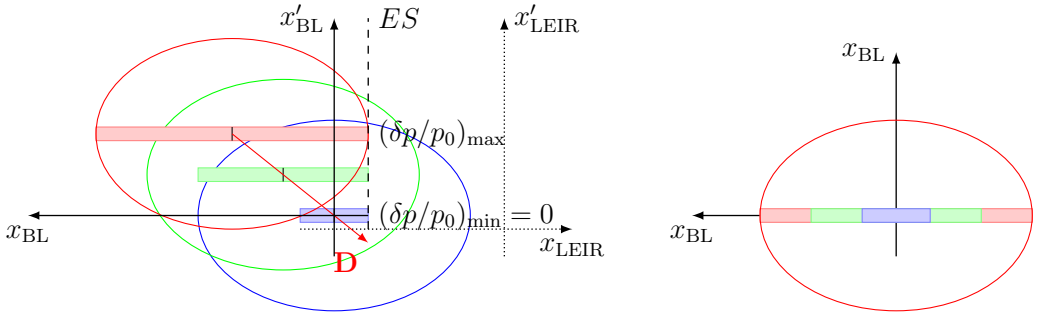

(a) Beam segments extracted at different tune distances due to particle momentum offset. Large half-axis of 'unfilled ellipse' defined by largest spiral step Δx, momentum-dependent displacements described by initial dispersion vector $\mathbf{D}$.

(b) Extracted beam after dispersion compensation in beamline: $D = D' = 0$. Position of on-momentum particles defines the centre of the beamline coordinate system $(x_{\mathrm{BL}}, x'_{\mathrm{BL}})$

Figure 5.35.: 'Unfilled ellipse approach' [211] for description of extracted beam segment: at the ES (a) and further downstream after dispersion correction (b).

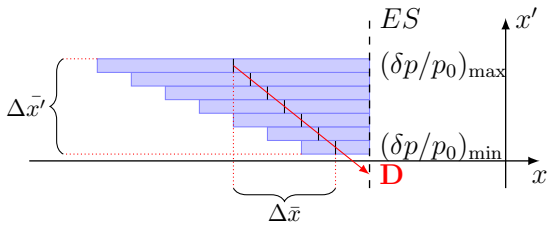

$$D_x = \frac{\Delta\bar{x}}{\Delta(\delta p/p_0)} \tag{5.57a}$$

$$D'_x = \frac{\Delta\bar{x}'}{\Delta(\delta p/p_0)} \tag{5.57b}$$

Figure 5.36.: Initial D and D' from extracted beam.

Computation Due to the single-particle tracking method used in Section 5.3, only few data points were available for each extraction configuration: Three sets of two particles, each corresponding to minimum, zero and maximum momentum offset, close to the ES and after a maximum spiral step into the ES, compare Fig. 5.33.

For applying the fitting approach described before, the extracted beam is assumed to consist of three momentum segments, each corresponding to one of the tracked particle pairs. Initial dispersion D and its derivative D' can then be estimated from the positions of on- and off-momentum segments in phase space, as indicated in Fig. 5.36. Computing the mean position of each momentum segment $(\bar{x}, \bar{y})$ from the coordinates of only two tracked particles, implies the assumption of constant particle density along each 'line of charge'.

The *real* emittance of the extracted beam segment after dispersion correction is approximated by a rectangle:

$$\epsilon_{\text{real}} = \Delta x_{\max} \cdot \Delta x' \,. \tag{5.58}$$

Its length $\Delta x_{\max}$ corresponds to the length of the momentum segment with the largest spiral step. Its height $\Delta x'$ is given by the divergence spread caused by coupling between horizontal and vertical plane. A value of 0.05 mrad [176] is used as estimate.

Horizontal betatron amplitude function β_{x} at the beginning of the beamline and emittance of the unfilled ellipse $\epsilon_{\text{unfilled}}$ need to fulfil the conditions

$$\Delta x_{\max} = 2\sqrt{\epsilon_{\text{unfilled}}\,\beta_{\text{x}}}\,, \tag{5.59a}$$

$$\epsilon_{\text{unfilled}} \gg \epsilon_{\text{real}}\,, \tag{5.59b}$$

but can otherwise be chosen freely. Following [176], $\epsilon_{\text{unfilled}} \approx 10 \cdot \epsilon_{\text{real}}$ is used here. In this approximation, the real width of the beam is no longer characterised by emittance and betatron amplitude function alone. Instead, the phase-advance μ from the extraction point must be known for calculating the real beam size as the projection of the bar of charge within the unfilled ellipse onto the $\hat{x}$-axis. Without the knowledge of phase-advance, a beam width estimate based on β and the emittance of the unfilled ellipse will overestimate the actual beam width at most locations.

Beam parameters, resulting from the extraction configurations discussed in Section 5.3.3.3, are listed in Table 5.16. They are of similar magnitudes as those obtained from synchrotrons for medical applications.

Table 5.17 summarises the start parameters for the beamline design study: They represent a combination of extremal values from the beam parameters derived from extraction tracking, Table 5.16: Values $\beta = 15\,\text{m}$, $\epsilon_{\text{unfilled}} = 2\,\pi\,\text{mm mrad}$ correspond to the maximum beam widths found from tracking. Most extraction configurations below resonance result in negative dispersion D and D'. Additionally, a large negative dispersion was found to complicate dispersion correction in the common part of the beamline, Section 5.4.2.1. Values $D = -4\,\text{m}$, $D' = -1$ were therefore chosen as conservative estimates. Since the small number of tracked particle coordinates did not allow a meaningful 'fit' to the particle distribution, no estimates for α could be obtained and a value $\alpha = 0$ was assumed. Start parameters in vertical phase space are approximated by the beam parameters of the circulating beam in LEIR at the position of the ES.

	D [m]	D'	$\Delta x_{\max}$ [mm]	ϵ_{real} [π mm mrad]	$\epsilon_{\text{unfilled}}$	β_{x} [m]
C4-AB-BR-1	-2.569	-0.100	3.8	0.0605	0.605	5.97
C4-AE-BR-1	-0.342	-0.066	4.1	0.0653	0.653	6.44
C4-AB-AR-1	5.804	0.050	4.6	0.0732	0.732	7.23
C4-AE-AR-1	3.772	0.031	5.8	0.0923	0.923	9.11
C5-AB-BR-1	-3.820	-1.285	6.4	0.1019	1.019	10.05
C5-AE-BR-1	1.336	-1.250	11.2	0.1783	1.783	17.59
PIMMS [176]	2.09	-0.017	10		1.65	15
MedAustron [196]	-2.24	0.023	10		5	5

Table 5.16.: Courant-Snyder parameters of extracted beam segments, estimated from extraction configurations Table 5.13 employing 'unfilled ellipse' approach.

	ϵ_{geo} [π mm mrad]	β [m]	$\Delta x_{\max}$ [mm]	D [m]	D'	α
Vertical Phasespace	3.6 - 26	15	–	0	0	-2.77
Horizontal Phasespace	2	15	11	-4	-1	0

Table 5.17.: Start parameters for beam transport line design, based on rounded values from configurations *C4-BR*, *C5-BR* at position of ES. Values for vertical phase space are taken from circulating beam in LEIR.

5.4.1.3. Reshaping Slow Extracted Beam

The actual horizontal size of the beam is small, as seen from the extracted beam segments Fig. 5.3.3.4, and depends on the phase advance μ between extraction septum ES and target plane. In medical machines, the particular shape of the extracted beam in horizontal phase space is exploited to achieve precise control of the horizontal beam size at the patient: PIMMS [176] proposes the use of a 'phase shifter' module, consisting of multiple quadrupoles, that provides control over the horizontal beam size via adjustment of horizontal phase advance, while keeping the optical functions β_x and α_x constant throughout the transfer line. Optical functions in the vertical plane are controlled independently from the horizontal plane by a 'stepper' module. The combined module consists of multiple quadrupoles and has a length of 13.6 m.

The limited space available between extraction point and the position where a vertical (upwards oriented) beamline can be installed does not allow μ_x to be controlled independently in this way. However, the dependence of horizontal beam size on phase advance is disadvantageous for the design process and setup flexibility – a (close to) normally distributed beam in both phase space planes is preferable.

Multiple small angle scattering results in an angular distribution that can be approx-

imated by a Gaussian with r.m.s. scattering angle [212, section 30.3]:

$$\theta_{\mathrm{rms}} = \frac{13.6\,\mathrm{MeV}}{\beta_{\mathrm{rel}}\, c\, p}\, Z \sqrt{\frac{x}{\widetilde{X_0}}} \left[1 + 0.038 \ln\left(\frac{x}{\widetilde{X_0}}\right)\right] , \tag{5.60}$$

where β_{rel}, c, p, Z are the relativistic β, velocity of light, momentum, and charge state of the particle in units of the electron charge e. The thickness of the scatterer is given in units of its radiation length $x/\widetilde{X_0}$. Equation (5.60) represents a good estimate for the r.m.s. scattering angle if the correction term $\propto \ln\left(x/\widetilde{X_0}\right)$ becomes small, that is $x \approx \widetilde{X_0}$.

The resulting increase in particle divergence leads to an increase $\Delta\epsilon$ in the emittance of a traversing beam [213]:

$$\Delta\epsilon_{k\,\sigma} = \frac{\beta}{2}(k\,\theta_{\mathrm{rms}})^2 , \tag{5.61}$$

where k indicates the number of standard deviations σ.

While such emittance 'blow-up' due to scattering is undesired in circular machines where it reduces the lifetime of the beam, a thin scatterer may be placed in a beam transfer line to transform the extracted bar of charge in horizontal phase space into an approximately Gaussian distribution [214]. This is applied for example at the NASA Space Radiation Laboratory (NSRL) beamline [206]: By using thin Cu-foils extracted particles are stripped to their highest charge state and at the same time the beam is prepared for down-stream manipulations with non-linear optical elements.

A similar approach is taken here to create a Gaussian beam distribution from the 'bar of charge' extracted from LEIR. Given its small initial value, the horizontal emittance after traversal of a thin scatter foil is assumed to be dominated by the emittance increment Eq. (5.61). The vertical emittance will be composed of the initial r.m.s. emittance and the emittance increment:

$$\epsilon'_{\mathrm{rms,\,x}} = \Delta\epsilon_{\mathrm{rms,\,x}} \tag{5.62a}$$

$$\epsilon'_{\mathrm{rms,\,y}} = \epsilon_{\mathrm{rms,\,y}} + \Delta\epsilon_{\mathrm{rms,\,y}} . \tag{5.62b}$$

By varying the magnitude of both β_x and β_y at the location of the scatter foil, the effect of the resulting r.m.s. scatter angle θ_{rms} on beam emittances can be adjusted to obtain similar beam emittances ϵ'_{rms} in horizontal and vertical plane:

$$(\epsilon'_{\mathrm{rms,\,x}} = \epsilon'_{\mathrm{rms,\,y}} = \epsilon'_{\mathrm{rms}})\ \&\ (5.62)\ \rightarrow\ \frac{\beta_x}{\beta_y} = \frac{\epsilon'_{\mathrm{rms}}}{\epsilon'_{\mathrm{rms}} - \epsilon_{\mathrm{rms,\,y}}} . \tag{5.63}$$

The following study assumes that $\epsilon'_{\mathrm{rms}} = 4.5\,\pi\,\mathrm{mm\,mrad}$ can be achieved in both planes, and for all energies, by selecting from a range of scatter foils and adjustment of β_x and β_y to suitable values. Figure 5.37 shows the required scatterer thickness for achieving this value for ϵ'_{rms} in dependence of beam energy and charge-over-mass ratio Q/A. A fixed value $\beta_y = 10\,\mathrm{m}$ is assumed for the vertical betatron function at the scatter foil; β_x is adjusted according to Eq. (5.63). Scatter foils up to approximately $4 \cdot 10^{-3}$ radiation lengths would thus be required for protons $Q/A = 1$ and foils up to approximately

$12.5 \cdot 10^{-3}$ for $Q/A = 1/2$ ions, such as carbon ${}^{12}_{6}C^{6+}$. For copper[22] as scatter material, this corresponds to thicknesses of up to 58 µm and 181 µm, respectively.

5.4.1.4. Uniform Dose Distribution across Sample

After traversal of the scatter foil, particles in both transverse planes can be assumed to be approximately normally distributed. This allows the expected level of dose uniformity across a given sample area to be estimated in function of the r.m.s. beam size in the target plane.

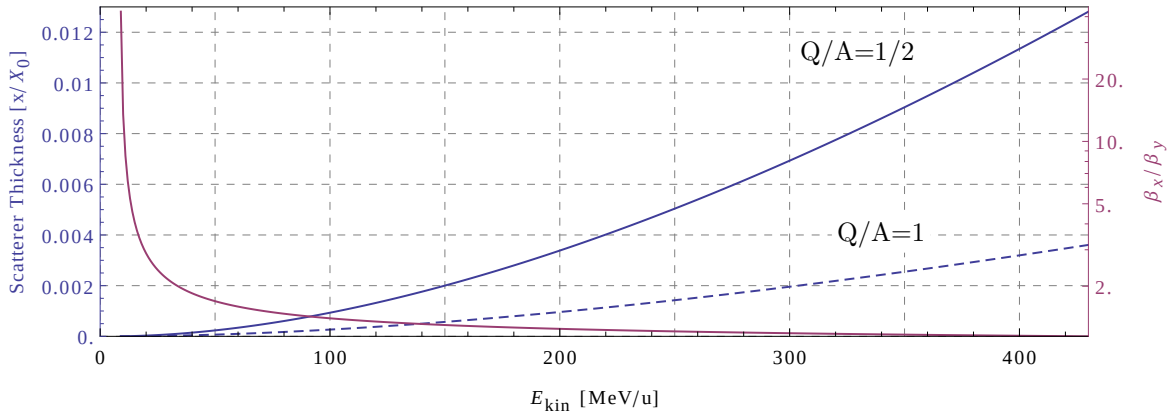

Figure 5.37.: Thickness of scatter material (in units of radiation length) required to achieve $\epsilon'_{\mathrm{rms}} = 4.5\,\pi\,\mathrm{mm\,mrad}$ for all relevant beam energies. The computation assumes $\beta_y = 10\,\mathrm{m}$ at the scatter foil and β_x to be scaled relative to β_y as indicated in the plot.

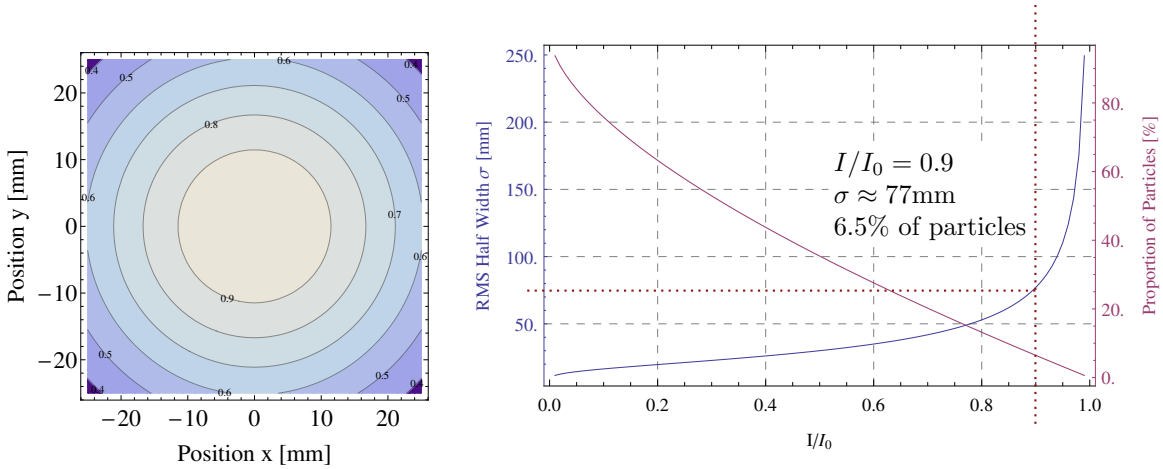

(a) I/I_0 for 2-D Gaussian beam.

(b) I/I_0 across 5 cm × 5 cm irradiation field.

Figure 5.38.: I/I_0 for 2-D Gaussian beam (a). Required r.m.s. half-width σ in function of desired beam homogeneity I/I_0 across 5 cm × 5 cm irradiation field (b). The right scale of (b) indicates the proportion of beam particles available for irradiation in the homogeneous field region.

[22] Copper Cu: $\widetilde{X_0} = X_0\,\rho = 1.435\,\mathrm{cm}$, $X_{0,\,\mathrm{Cu}} = 12.86\,\mathrm{g/cm^2}$, $\rho = 8.960\,\mathrm{g/cm^3}$ [212, table 6.1].

Like the particle density distribution $\rho(x, y)$, the intensity distribution in the target plane $I(x, y)$ corresponds to a two-dimensional normal distribution:

$$I(x,y) \propto \rho(x,y) = \frac{1}{\sqrt{2\pi}\sigma_x \sqrt{2\pi}\sigma_y} \, \mathrm{e}^{-(\frac{x^2}{2\sigma_x^2}+\frac{y^2}{2\sigma_y^2})} \,, \tag{5.64}$$

where the r.m.s. beam half-width $\sigma = \sqrt{\beta\,\epsilon_{\mathrm{rms}}}$ is defined by the beta function β in the target plane and the r.m.s. emittance ϵ_{rms} of the beam. If the distribution is further assumed to be symmetric in both planes ($\sigma_{\mathrm{x}} = \sigma_{\mathrm{y}} = \sigma$), the r.m.s. beam size σ required to limit intensity fluctuations $I(x, y)/I(x = 0, y = 0)$ across an irradiated (square) field of 5 cm × 5 cm ($x = y = \pm 2.5$ cm) can be computed from Eq. (5.64). Fig. 5.38a visualises intensity variations across such a field.

By increasing the r.m.s. beam size σ, a given target area can be irradiated more homogeneously. Requirements on σ for various uniformity limits I/I_0 are shown in Fig. 5.38b. Particles outside of the irradiation field are discarded. The right scale in Fig. 5.38b provides an estimate for the efficiency of this approach in terms of the percentage of beam particles used for irradiation at a given homogeneity level I/I_0. A r.m.s. beam size $\sigma = 77$ mm would thus be sufficient to reduce intensity fluctuations across a 5 cm × 5 cm target area to ±5 % ($I/I_0 = 0.9$). However, more than 90 % of beam particles will be discarded in this scenario. For $\epsilon_{\mathrm{rms}} = 4.5\,\pi$ mm mrad assumed here, $\sigma = 77$ mm corresponds to $\beta_{x,y} \approx 1500$ m.

5.4.1.5. Beam Envelopes and Apertures

The Beam Envelope (BE) is approximated by

$$\text{Beam Envelope} = \pm\left(\Delta + \left|\frac{\Delta p}{p_0} D\right|\right) \,, \tag{5.65}$$

where the beam half width Δ in the vertical plane is computed as $\Delta_y = 2.5\,\sigma = 2.5\sqrt{\beta_y\,\epsilon_{\mathrm{rms,\,y}}}$, using the maximum vertical emittance $\epsilon_{\mathrm{rms,\,y}} = 4\,\pi$ mm mrad at low energy extraction. Horizontal beam size before scattering is computed as $\Delta_x = \sqrt{\beta\,\epsilon_{\mathrm{unfilled}}}$, using the 'unfilled' emittance $\epsilon_{\mathrm{unfilled}}$ from Table 5.17 as geometric emittance. This overestimates the actual horizontal beam size at most locations.

Thickness of scattering foil and ratio of horizontal and vertical betatron amplitude functions are assumed adjustable, allowing compensation of the momentum dependence of the vertical emittance and fulfilling Eq. (5.63), so that the same emittance $\epsilon'_{\mathrm{rms,\,x}} = \epsilon'_{\mathrm{rms,\,x}} = 4.5\,\pi$ mm mrad can be achieved in both planes after scattering, regardless of beam energy.

The momentum spread $\Delta p/p_0$ of the extracted beam is given by the maximum simultaneously extractable momentum spread, and thus depends on the resonance configuration and the extraction mechanism. For extraction by tune selection T, it corresponds to the full momentum spread of the beam. The value used for previous extraction simulations in Section 5.3.3 $\Delta p/p_0 = \pm 2 \cdot 10^{-4}$ is therefore also assumed for this beamline study.

Beamline segment	Constraint	Location
Extraction Line	$x = -0.42\,\mathrm{m}$, $x' = 140\,\mathrm{mrad}$ [a]	entrance to *KFH3234*
Common horizontal Bend	$d_x = d'_x = 0$ [b] $\beta_x \gg \beta_y$ [c]	exit of horizontal bend at scatter foil
Horizontal Line	$d_x = d'_x = 0$ [d] $\alpha_x = \alpha_y = 0$ [e] $\beta_x = \beta_y = 1\,\mathrm{m}$ to $1500\,\mathrm{m}$ [f]	in target plane in target plane in target plane
Vertical Line	$d_x = d'_x = 0$ [d] $d_y = d'_y = 0$ [d] $\alpha_x = \alpha_y = 0$ [e] $\beta_x = \beta_y = 1\,\mathrm{m}$ to $1500\,\mathrm{m}$ [f]	in target plane in target plane in target plane in target plane
General	$\beta_x = \beta_y < 55\,\mathrm{m}$ [g]	throughout transferlines

[a] Inclination of common horizontal bending line, compare Section 5.3.4.3.
[b] Achromatic beam transport for both horizontal and vertical beamline.
[c] Minimum impact of scatter foil on vertical emittance; location of the scatter foil chosen for bar of charge to be approximately horizontally oriented ($x \gg x'$) when traversing it: $\mu_x \approx \pi$.
[d] Position and momentum of particles uncorrelated in 2D-plane ($d = 0$) and in 3D ($d' = 0$).
[e] Parallel beams; not critical for thin samples.
[f] Pencil beams of 5 mm to 10 mm FWHM correspond to $\beta \approx 1\,\mathrm{m}$ to $4\,\mathrm{m}$, broad beams ($I/I_0 = 0.9$) to $\beta = 1500\,\mathrm{m}$ in target plane.
[g] Beam envelope, smaller $\pm 40\,\mathrm{mm}$.

Table 5.18.: Matching constraints for transfer lines. Conditions $d' = 0$ and $\alpha = 0$ are important for samples with finite thickness and were therefore considered less critical for the vertical beamline. All estimates are based on $\epsilon_{\mathrm{rms}} = 4.5\,\pi\,\mathrm{mm\,mrad}$.

5.4.2. Beamlines

The beamline is logically divided into three parts: An *extraction line* from LEIR and subsequent *horizontal bend* towards the adjacent South Hall, Section 5.4.2.1, a *vertical beamline*, Section 5.4.2.2, and a *horizontal beamline*, Section 5.4.2.3. The same lattice structure for extraction line and horizontal bend are shared among both vertical and horizontal beamline. The horizontal beamline consists of additional focusing structures, the vertical beamline of an additional vertical bend and focusing structures.

Estimations from Section 5.4.1, together with the specifications outlined in Table 5.1, pose constraints on the betatron amplitude functions throughout the lattice (aperture limitation) and in the target planes (beam size and uniformity): A maximum aperture of $\pm 40\,\mathrm{mm}$ is targeted in this study. Pencil beams of 5 mm to 10 mm FWHM correspond to $\beta \approx 1\,\mathrm{m}$ to $4\,\mathrm{m}$ in the target plane. To achieve broad beams of homogeneity $I/I_0 = 0.9$, $\beta = 1500\,\mathrm{m}$ is required, Fig. 5.38b. Beam functions in the target plane are further constrained to achieve parallel pencil beams with zero dispersion, as well as zero dispersion broad beams.

All parameter constraints are summarised in Table 5.18.

Figure 5.39 shows survey plots of LEIR together with the proposed beamlines in the $\hat{\mathbf{x}} - \hat{\mathbf{z}}$ (Fig.5.39a), $\hat{\mathbf{z}} - \hat{\mathbf{y}}$ (Fig.5.39b) and $\hat{\mathbf{x}} - \hat{\mathbf{y}}$ (Fig.5.39c) plane. LEIR and beamlines are positioned in CERN coordinates, based on survey measurements from CERN's GEODE

portal[23], and civil infrastructure information from the GIS portal[24].

5.4.2.1. Extraction Line and Common Horizontal Bend

The extraction line starts at the ES and its first part, up to kicker *KFH31*, is identical to the first part of LEIR's SS30. LEIR quadrupole magnets (*QDN31*, *QFN31*) therefore determine the evolution of the initial beam parameters in this part of the extraction line.

Based on the extraction configuration outlined in Section 5.3.4.3, two magnetic septa, *MS1** and *MS2*, are installed downstream of *KFH31* and their strengths adjusted to deflect the extracted beam to $x = -42\,\text{cm}$, $x' = -140\,\text{mrad}$ at the entry to *KFH3234*. These coordinates are chosen as central orbit for the subsequent common horizontal bending line that contains first focusing quadrupoles and bends the extracted beam towards the adjacent storage area.

With these entry coordinates, the extracted beam exits *KFH3234* at $x = -58\,\text{cm}$ and $x' = -140\,\text{mrad}$. LEIR quadrupole and sextupole magnets installed downstream of *KFH3234* extend to at most $\pm 50\,\text{cm}$ horizontally, so that a beam pipe of $\sim 8\,\text{cm}$ diameter can be used to guide the beam past these elements. This study assumes that no more than 50 cm horizontal space to LEIR elements is required for the placement of a first quadrupole downstream of *KFH3234*[25]. The first quadrupole can therefore be placed 3.5 m downstream of the entrance to *KFH3234*, next to a beam monitor that is installed between the last quadrupole in SS30 and the beginning of *ARC30*, compare Fig. 5.39a.

The maximum beam rigidity to be transported in the horizontal bending magnet corresponds to the maximum beam rigidity that can be accelerated in LEIR after upgrade of main magnet power supplies, $B\rho = 6.67\,\text{T m}$. With $B_{\text{max}} = 1.6\,\text{T}$ of conventional bending magnets, the bending radius of the structure amounts to $\rho = 4.17\,\text{m}$. Its total length is proportional to the bending angle which must be sufficiently large for the horizontal beamline not to be restricted by the walls highlighted in Fig. 5.39a. On the other hand, the orientation of the structure must allow the vertical beamline to be installed within the location of maximum space availability. This area is delimited by the PS wall on one side and by the transport crane rails, indicated as dashed orange line in Fig. 5.39a and 5.39c, on the other side. The total bending angle in the setup shown in Fig. 5.39a amounts to 118°. The horizontal bending structure was modelled by four identical *SBEND* segments with half gap of 40mm and flux integral of 0.5[26]. These properties are summarised in Table 5.19.

The common horizontal bending line has to fulfill the constraints listed in Table 5.18. First, it is required to remove the initial negative horizontal dispersion, for both downstream beamlines. Second, for the reasons discussed in Section 5.4.1.3, a thin scatter foil needs to be introduced in the common section, Fig. 5.40. For maximum efficacy, the bar of charge should be horizontally oriented at the location of the scatter foil, which requires the phase advance $\Delta\mu_x$ between ES and the scatter foil to be a multiple of π. Horizontal and vertical betatron functions are required to be adjustable in order to allow regulation

[23] `https://espace.cern.ch/service-geode/geode/default.aspx`
[24] `https://maps.cern.ch/mapsearch/ISP/en/gisportals_en.html`
[25] For comparison, the yokes of LEIR quadrupoles have a half-width of 39cm.
[26] MAD-X parameters: $HGAP = 0.04$, $FINT = 0.5$

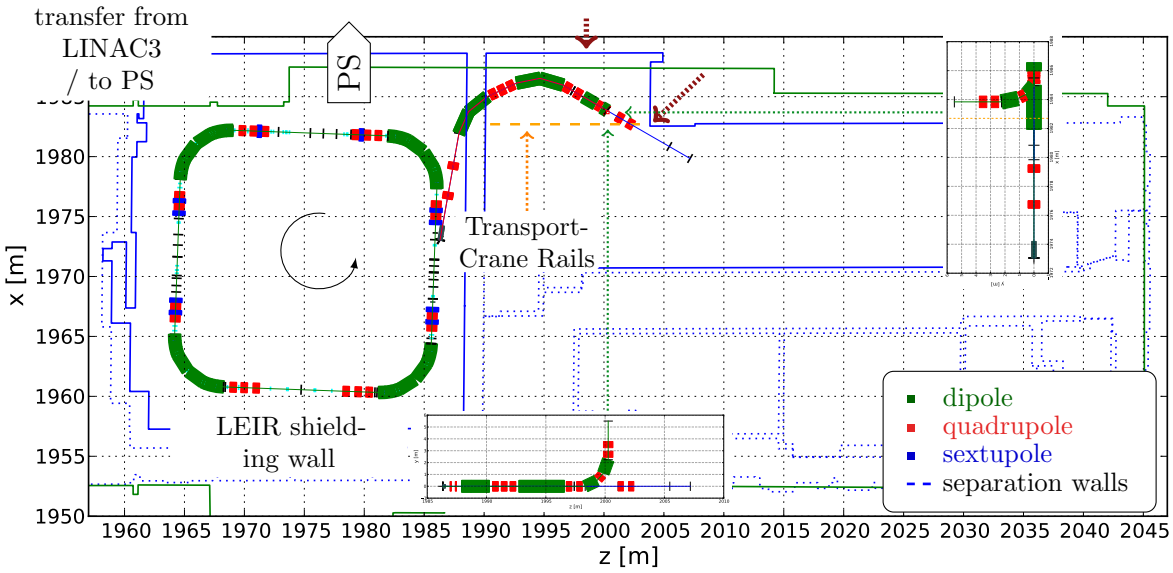

(a) $\hat{\mathbf{x}} - \hat{\mathbf{z}}$-plane.

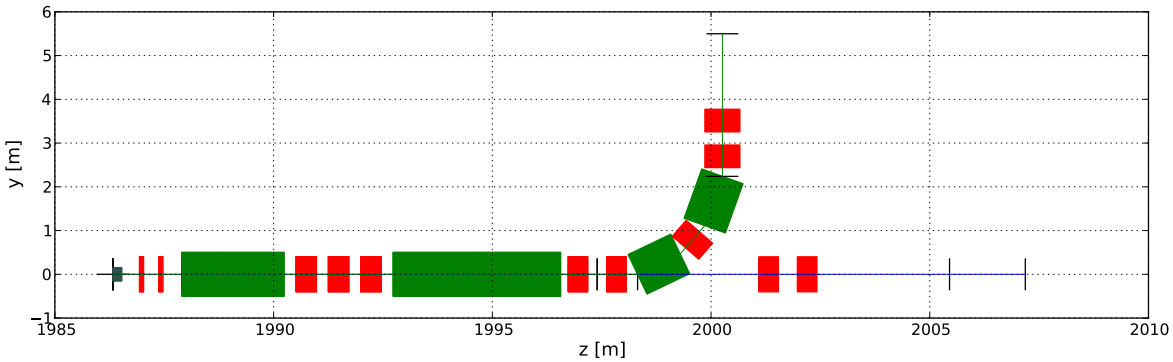

(b) $\hat{\mathbf{z}} - \hat{\mathbf{y}}$- plane.

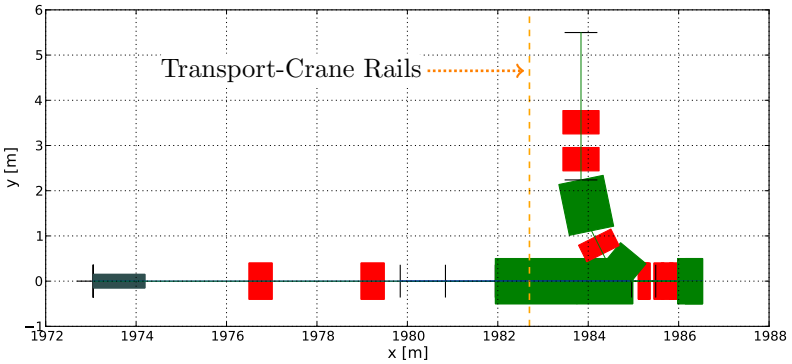

(c) $\hat{\mathbf{x}} - \hat{\mathbf{y}}$-plane.

Figure 5.39.: Survey plot of LEIR and beamlines in $\hat{\mathbf{x}} - \hat{\mathbf{z}}$ plane (a). Vertical and horizontal beamline in (b) $\hat{\mathbf{z}} - \hat{\mathbf{y}}$ and (c) $\hat{\mathbf{x}} - \hat{\mathbf{y}}$ plane. Floor-level building walls are represented in blue, top-level walls in green in (a). The position of transport crane rails is indicated by dashed orange lines in (a) and (c).

	Max $B\rho$ [T m]	**Radius** ρ [a] [m]	**Angle** [°]	**Half Gap** [mm]
Horizontal Bend	6.67	4.17	118 [b]	40
Vertical Bend	2.55	1.59	90	40

[a] Assuming $B_{\max} = 1.6\,\mathrm{T}$.
[b] Inclination of LEIR ($\approx 2°$) is subtracted from 120° bending angle.

Table 5.19.: Properties of beamline dipole magnets. Values for the horizontal bend are based on 430 MeV/n and $Q/A = 1/2$, values for the vertical bend on 75 MeV/n, $Q/A = 1/2$.

of emittance growth in both planes as assumed in Section 5.4.1.3, and $\beta_x \gg \beta_y$ in order to minimise the effect of the scatter foil on the vertical emittance.

Dispersion removal at the end of the bending magnet requires the dispersion function to be focused towards positive values in the horizontal bend. Further focusing is then needed at the centre of the bend in order to compensate the increase in dispersion caused by the second pair of bending magnets. Such focusing could be achieved with only two focusing quadrupoles, upstream of and in the centre of the bending section. However, for better control of the betatron amplitude functions, the upstream focusing quadrupole must be replaced by a quadrupole doublet (*QC01*, *QC02*). A single focusing quadrupole in the centre of the bend would result in strong 'over-focusing' of the horizontal and defocusing of the vertical betatron function when adequately powered to remove dispersion. It would thus increase both β_x and β_y strongly, reaching values $\beta_x \approx 150\,\mathrm{m}$, $\beta_y \approx 100\,\mathrm{m}$ at the exit of the bending segment. Instead, dispersion correction and better control of both horizontal and vertical betatron amplitude functions at the exit of the last bending magnet is accomplished by a quadrupole triplet (*QCB1*, *QCB2*, *QCB3*) installed at the centre of the horizontal bending section.

With phase advance $\Delta\mu_x$ between $1.8\,\pi$ to $2\,\pi$, small divergence spread and large beam width in horizontal phase space are expected at the position of the quadrupole doublet (*QC03*, *QC04*) downstream of the exit of the bending section. Other locations are less suited for the installation of a thin scatter foil due to either $\Delta\mu_x \neq n \cdot \pi$, or $\beta_y \gg \beta_x$.

Extraction line from SS30 and common bending line are shown in Fig. 5.40. The first subplot in this figure illustrates the position of lattice elements, their normalised integrated strengths $k_{1/2}l$ and lengths. The second and third plot show β and α functions in horizontal and vertical phase space, respectively. Dispersion and its derivative along the beam are shown in the fourth subplot. The last subplot illustrates the evolution of the beam envelope along the line, computed according to Eq. (5.65) and the assumptions made in Section 5.4.1.5. Scattering is assumed to result in immediate increase of r.m.s. emittances, leading to the sudden growth of the horizontal beam envelope between *QC03* and *QC04*.

Enforcing constraints $d_x = 0$, $d'_x = 0$ at the exit of the bend and $\beta_y < 50\,\mathrm{m}$ at the position of the quadrupole triplet, *QCB1*, *QCB2*, *QCB3*, determines the coefficients of the first five quadrupoles in this common line segment. Under these constraints, the beta functions at *QC03* assume values around $\beta_x \leq 100\,\mathrm{m}$ and $\beta_y \ll 10\,\mathrm{m}$. The ratio between horizontal and vertical betatron function at the scatter foil can then be adjusted over a wide range of values via the focusing quadrupole *QC03*. Figure 5.40 corresponds to an

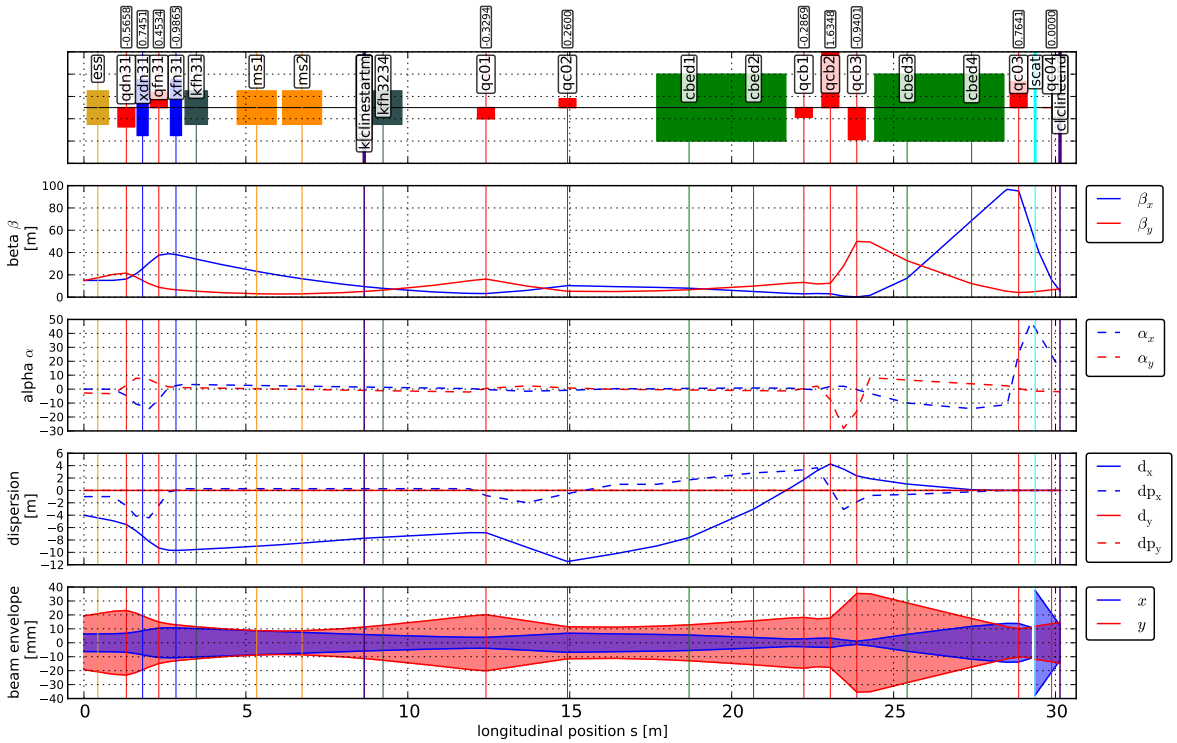

Figure 5.40.: Extraction line from LEIR and common horizontal bending line for vertical and horizontal beamlines. The extraction line includes LEIR quadrupole and sextupole magnets (*QDN31*, *QFN31*, *XDN31*, *XFN31*). ES and magnetic septa (*MS1*, *MS2*) are not seen by the beam circulating in LEIR. The common horizontal bending line starts from the entrance of *KFH3234*.

intermediate setting.

5.4.2.2. Vertical Transfer Line

In order to maximise vertical space availability, the vertical bend needs to be installed directly downstream of the quadrupole doublet *QC03*, *QC04* which focuses the widened horizontal component of the scattered beam into the vertical bending section. This section is designed to bend particles with energies up to 75 MeV/n ($B\rho = 2.55\,\mathrm{T\,m}$, $Q/A = 1/2$) and has a bending radius $\rho = 1.69\,\mathrm{m}$, compare Table 5.19. Like the horizontal bending magnets, it is modelled by two *SBEND* segments with half gap of 40mm and flux integral of 0.5[27]. The bend is designed as an achromatic structure in the vertical plane, with defocusing quadrupole *QVB1* centred between both 45° bending segments. A further quadrupole doublet, *QV01* and *QV02*, allows focusing of the beam onto the target plane.

The height of the target plane is adjusted to 7 m above ground (5.5 m from the level of the accelerator structure, compare Fig. 5.39b), leaving about 0.5 m space for the installation of measurement instrumentation downstream of the target.

In addition to the constraints imposed on the common bending line, dispersion in the vertical plane needs to be suppressed by the achromatic bending structure, and the values

[27]MAD-X parameters: $HGAP = 0.04$, $FINT = 0.5$

of beta functions in the target plane be adjustable over a wide range. Further, a parallel beam in the target plane is desirable. Table 5.18 lists the main matching constraints.

Figure 5.41 shows all elements of the vertical beamline and matching results for pencil, Fig. 5.41a, and broad beams, Fig. 5.41b, respectively. Matching results in Table 5.20 indicate that parallel focusing is possible for $\beta < 30\,\mathrm{m}$, resulting in pencil beams with FWHM spot sizes between 4 mm to 27 mm, *V1* to *V4*. In order to achieve larger beam sizes, the quadrupole doublet *QV01*, *QV02* is converted from a focusing-defocusing arrangement to a focusing-focusing configuration, thus over-focusing the beam in the horizontal and strongly defocusing it in the vertical plane. This rapid increase of betatron amplitude over the short available drift space of approximately 2 m naturally results in very divergent beams, with α of several hundred.

A configuration achieving a r.m.s. beam half-width of 67mm (*V7*), corresponding to approximately $\pm 6\,\%$ intensity variation across an irradiated area of $5\,\mathrm{cm} \times 5\,\mathrm{cm}$, is illustrated in Fig. 5.41b.

Table 5.20 lists the beam parameters for several target values of β. Dispersion and its derivative are matched to zero in both planes. Quadrupole coefficients for *QC01* to *QCB3*, with the exception of *QCB1*, deviate by less than $\pm 5\,\%$ from the values obtained from matching the common bending line alone. Values for *QCB1* are 20 % to 30 % higher in *V6*, *V7* and *V8*.

Variation of $\beta_{\mathrm{scat,\,x}}$ and $\beta_{\mathrm{scat,y}}$ at the scatter foil is restricted by other matching constraints. For example in matching configuration *V2* ($\beta = 10\,\mathrm{m}$), $\beta_{\mathrm{scat,\,x}}$ can be adjusted between approximately 80 m to 40 m ($\beta_{\mathrm{scat,\,y}} = 5\,\mathrm{m}$ to 10 m) without requiring modification of any of the quadrupoles upstream of *QC03*. However, such manipulation may increase the divergence of the beam in the target plane up to $|\alpha_{x,y}| \approx 3$. Including all quadrupoles in the matching process makes a wider range of $\beta_{\mathrm{scat,\,x}}$ accessible and leads to better matching results for $\beta_{\mathrm{scat,\,y}}$ values. Also with this approach, beam divergence tends to increase, $|\alpha_{x,y}| < 4$, and non-zero dispersion in the target plane is obtained, $|d_{x,y}| < 1\,\mathrm{m}$, $\left|d'_{x,y}\right| < 1$. Similarly, in broad beam mode, such as *V7* ($\beta = 1000\,\mathrm{m}$), $\beta_{\mathrm{scat,\,x}}$ can be adjusted between approximately 80 m to 45 m ($\beta_{\mathrm{scat,\,y}} = 5\,\mathrm{m}$ to 8 m), at the cost of non-zero dispersion in the target plane $|d_{x,y}| < 0.5\,\mathrm{m}$, $\left|d'_{x,y}\right| < 0.5$.

5.4.2.3. Horizontal Transfer Line

The horizontal line extends the common horizontal bending component by a further quadrupole doublet (*QH01*, *QH02*), installed downstream of the vertical bend. Sufficient space for the installation of the vertical achromatic bending structure is provisioned in the design by assuming 3.5 m drift space between *QC04* and *QH01*. The location of the target plane was chosen 5.5 m downstream of *QH02*, so that a pencil beam scanning system could be accommodated as part of a future upgrade, without the need for relocating the experimental end-station. Requirements on beam functions in the target plane are listed in Table 5.18. As for the vertical line, enforcement of achromatic beam transfer throughout the line defines the coefficients of quadrupoles up to *QCB3*, Table 5.22a.

The setup shown in Fig. 5.42 achieves minimum beam sizes of 5 mm to 7 mm FWHM in the vertical and horizontal plane respectively, with $|\alpha| < 0.5$ and $d_x = d'_x = 0$ in the target plane. FWHM beam sizes between approximately 11 mm ($\beta = 5\,\mathrm{m}$) and 22 mm ($\beta = 20\,\mathrm{m}$) additionally fulfill $\alpha = 0$, Table 5.21. In order to achieve parallel pencil

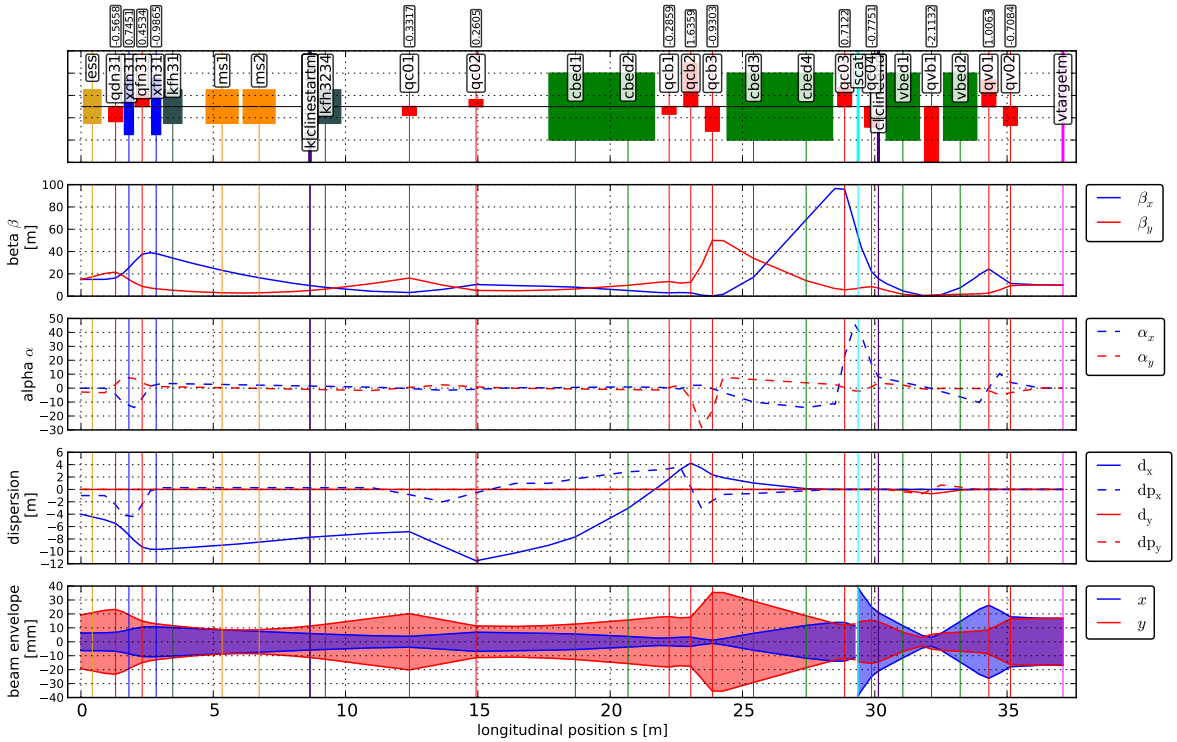

(a) Pencil beam ($\beta_x = \beta_y = 10\,\mathrm{m},\ V3$).

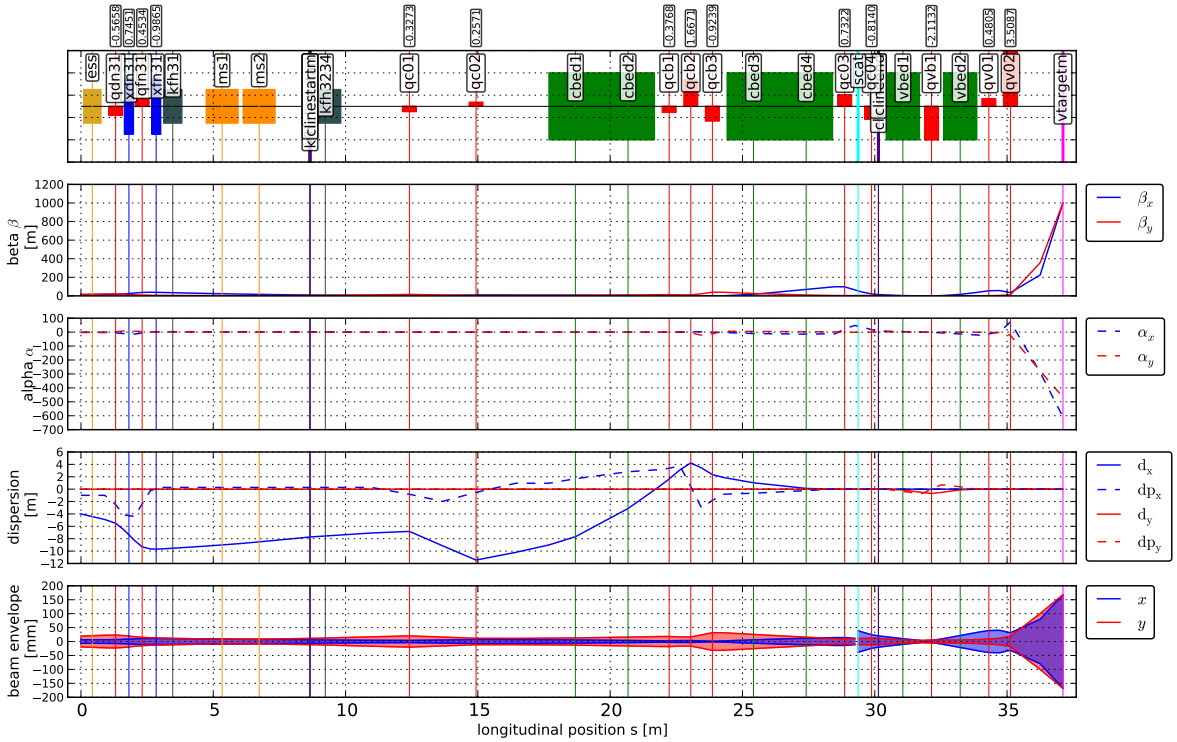

(b) Broad beam ($\beta_x = \beta_y = 1000\,\mathrm{m},\ V7$).

Figure 5.41.: Optical functions in vertical beamline for pencil beam (a) and broad beam (b) matching, corresponding to configurations *V3* and *V7* in Table 5.20.

ID	target $\beta_{x,y}$	β_x [m]	β_y [m]	α_x	α_y	$\Delta_{\mathrm{x,rms}}$ [mm]	$\Delta_{\mathrm{y,rms}}$ [mm]	[mm]
Pencil Beam								FWHM spot size
V1	0.1	0.44	0.11	-0.09	0.01	1.7	0.7	<4
V2	1	1.00	0.90	0.02	0.50	2.1	2.1	4.9
V3	10	10.00	10.00	0.00	0.00	6.7	6.7	15.8
V4	30	29.94	30.00	-0.85	-0.26	11.6	11.6	27.3
Broad Beam								I/I_0
V5	100	99.89	99.82	-13.24	-24.68	21.2	21.2	0.25
V6	500	500.00	500.00	-324.38	-224.37	47.4	47.4	0.76
V7	1000	1000.00	1000.00	-609.36	-466.84	67.1	67.1	0.87
V8	1500	1500.00	1500.00	-875.37	-719.87	82.2	82.2	0.91

Table 5.20.: Beam functions in target plane for vertical beamline. Zero dispersion strictly imposed in both horizontal and vertical phase space: $\mathcal{O}(d_x,\, d'_x) = 10^{-6}$, $\mathcal{O}(d_y,\, d'_y) = 10^{-2}$. Slightly elevated $\mathcal{O}(d_x) = 10^{-2}$ and $\mathcal{O}(d_y) = 10^{-1}$ for *V8* and *V5*, respectively. Small vertical beta function required at scatter foil $\beta_y \ll \beta_x$; for listed matchings $\beta_x = 52\,\mathrm{m}$ to $55\,\mathrm{m}$, $\beta_y = 4\,\mathrm{m}$ to $7\,\mathrm{m}$.

beams with smaller spot sizes, the distance between the last quadrupole doublet and the target plane would need to be shortened, or larger beam envelopes ($|BE| > 40\,\mathrm{mm}$) be permitted at the location of the vertical bending magnets.

Creation of large broad beams, requires one very strongly focusing quadrupole to 'over-focus' the horizontal and defocus the vertical betatron function, either upstream of the vertical bending segment (*QC04*) or downstream (*QH01* or *QH02*). These configurations correspond to *H7*, *H8* and *H7II*, *H8II* in Table 5.21, respectively. In the former configuration, Fig. 5.43a, the maximum attainable broad beam size is limited by the horizontal gap of the vertical bending magnet, and by the maximum strength of this focusing quadrupole. The latter configuration, Fig. 5.43b, results in larger beam divergence in the target plane, but lower aperture and magnet strength requirements. Maximum beam envelopes and required quadrupole gradients are discussed in the following section.

5.4.2.4. Quadrupole Properties

Table 5.22 lists the maximum values for quadrupole gradients and beam envelopes that were observed in matching configurations for vertical and horizontal beamlines. Beam envelopes in most of the quadrupoles used by both horizontal and vertical beamline (*QC01* to *QC03*) stay within $\pm 40\,\mathrm{mm}$, Table 5.22a. This is also the upper limit on beam envelopes observed at the positions of vertical beamline quadrupoles (*QVB1* to *QV02*), as well as at the position of the last common quadrupole *QC04* in matchings for vertical beamline parameters, Table 5.22b.

Maximum quadrupole gradients of about $22\,\mathrm{T\,m^{-1}}$ are observed for the central focusing magnet in the triplet structure of the common horizontal bending magnet (*QCB2*). This magnet is used for correcting the initial dispersion in all configurations. In the vertical beamline segment, strong defocusing is required to achieve sufficiently homogeneous

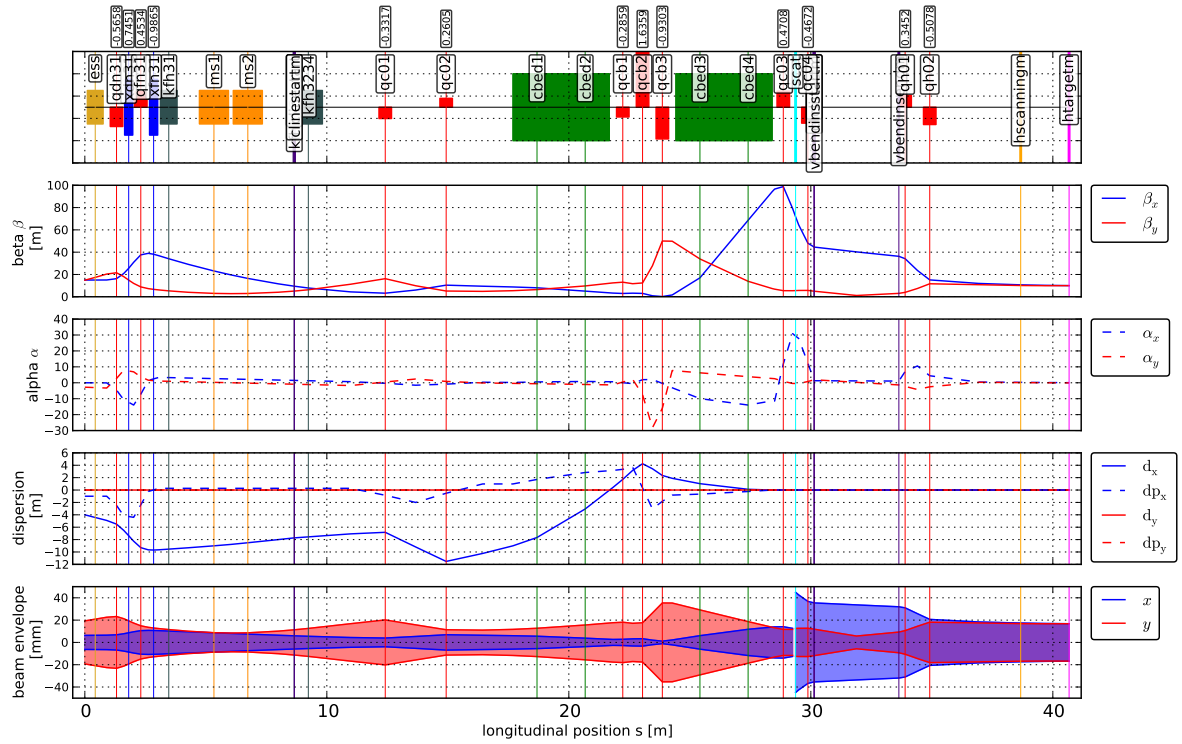

Figure 5.42.: Optical functions in horizontal beamline for pencil beam ($\beta_x = \beta_y = 10\,\mathrm{m}$, *H3*).

ID	target $\beta_{x,y}$	β_x [m]	β_y [m]	α_x	α_y	$\Delta_{\mathrm{x,rms}}$ [mm]	$\Delta_{\mathrm{y,rms}}$ [mm]	[mm]
Pencil Beam								FWHM spot size
H1	0.1	2.22	0.62	-0.34	0.06	3.1	1.7	< 7.5
H2	1	2.12	1.15	-0.32	0.09	3.1	2.3	< 7.5
H3	10	10.00	9.99	0.07	-0.08	6.7	6.7	15.8
H4	30	29.96	30.00	-0.29	-0.03	11.6	11.6	27.3
Broad Beam								I/I_0
H5	100	98.70	99.36	-6.74	-4.04	21.0	21.1	0.25
H6	500	499.13	499.12	-44.56	-45.33	47.4	47.4	0.76
H7	1000	990.64	989.18	-82.28	-91.17	66.8	66.8	0.87
H7II	1000			-185.38	-153.81			
H8	1500	1458.97	1458.57	-133.42	-134.67	81.0	81.0	0.91
H8II	1500			-285.81	-242.39			

Table 5.21.: Beam functions in target plane for horizontal beamline. Zero dispersion strictly imposed in horizontal phase space: $\mathcal{O}(d_x,\, d'_x) = 10^{-6}$. Small vertical beta function required at scatter foil $\beta_y \ll \beta_x$; for listed matchings $\beta_x = 48\,\mathrm{m}$ to $72\,\mathrm{m}$, $\beta_y = 5\,\mathrm{m}$ to $8\,\mathrm{m}$.

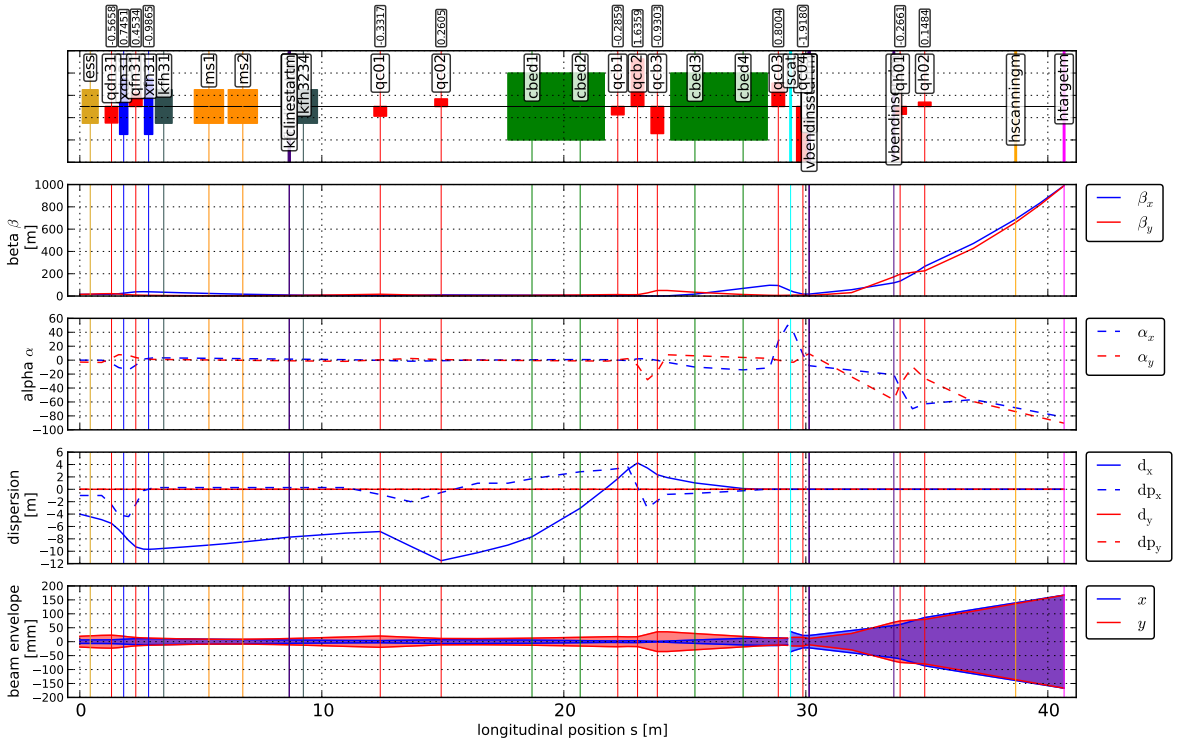

(a) Broad beam ($\beta_x = \beta_y = 1000\,\mathrm{m}$, *H7*).

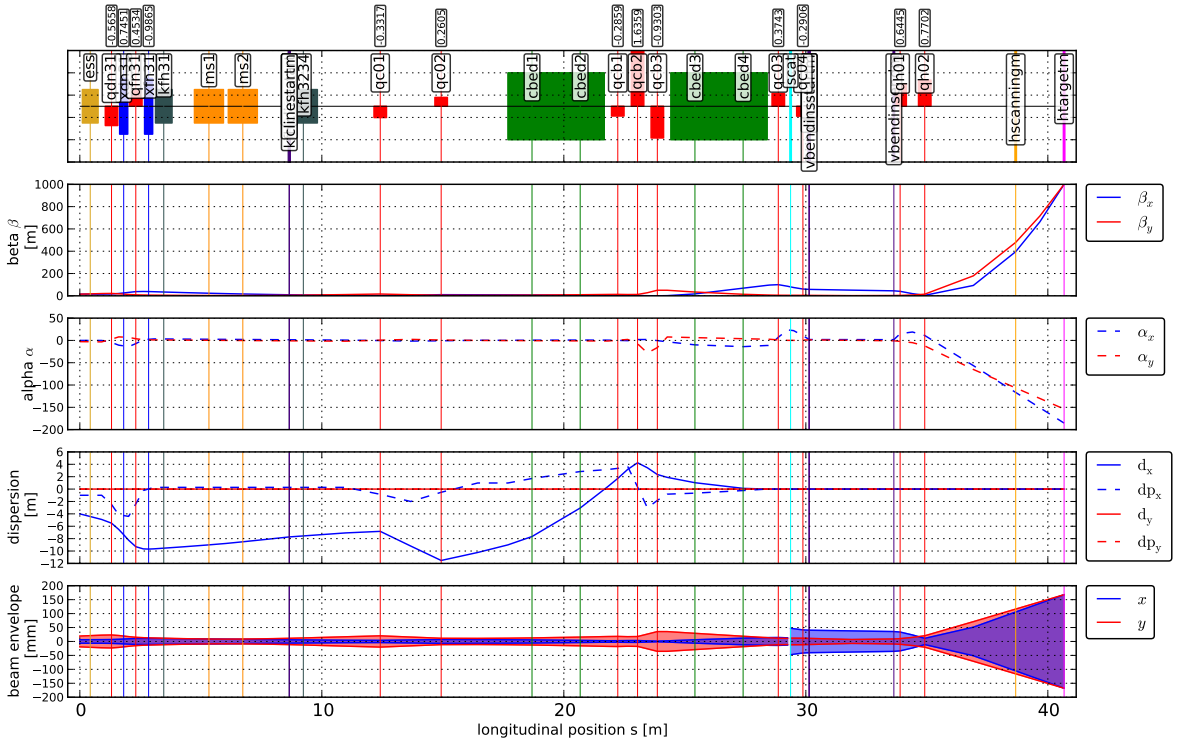

(b) Broad beam ($\beta_x = \beta_y = 1000\,\mathrm{m}$, *H7-II*).

Figure 5.43.: Optical functions in horizontal beamline for broad beam matching: Over-focusing upstream of vertical bending magnet (a) using *QC04* and downstream of vertical bending magnet (b) using *QH01*.

Common Bend		*QC01*	*QC02*	*QCB1*	*QCB2*	*QCB3*	*QC03*
k	[T m^{-1}]	-4.54	3.41	-5.31	21.82	-11.94	9.51
max radius	[mm]	220.3	293.5	188.2	45.8	83.7	105.2
BE_x	[mm]	3.9	6.8	2.8	3.5	3.3	13.5
BE_y	[mm]	20.1	11.6	18.1	17.6	35.4	12.0

(a) Common bending segment, Section 5.4.2.1.

Vline		*QC04*	*QVB1*	*QV01*	*QV02*
k	[T m^{-1}]	-11.41	-10.42	6.54	22.42
max radius	[mm]	87.7	96.0	152.8	44.6
BE_x	[mm]	25.0	4.0	39.7	31.5
BE_y	[mm]	15.9	7.2	9.2	18.8

(b) Vertical beamline, Section 5.4.2.2.

HLine		**I**	*QC04*	*QH01*	*QH02*	**II**	*QC04*	*QH01*	*QH02*
k	[T m^{-1}]		-32.53	7.01	-9.07		-3.73	8.27	20.88
max radius	[mm]		30.7	142.7	110.2		268.0	120.9	47.9
BE_x	[mm]		36.9	77.5	96.2		41.5	33.8	18.7
BE_y	[mm]		15.3	75.9	95.2		11.7	10.3	20.6

(c) Horizontal beamline, Section 5.4.2.3.

Table 5.22.: Maximum quadrupole gradients and largest beam envelopes observed in common part of beam transfer line (a), as well as in vertical (b) and in horizontal (c) beamline extension. Based on matching configurations Table 5.20 and 5.21, respectively. Values k based on $B\rho = 6.64\,\mathrm{T\,m}$ for common parts of transfer line and horizontal beamline, and on $B\rho = 2.55\,\mathrm{T\,m}$ for vertical beamline. Quadrupole lengths were assumed equal to LEIR quadrupoles ($l = 0.52\,\mathrm{m}$).

broad beams over the short drift space available. This leads to high gradients $22\,\mathrm{T\,m^{-1}}$ for the final focusing quadrupole magnet (*QV02*).

The results of two different matching approaches for the horizontal beamline segment are compared in Table 5.22c: Strong over-focusing upstream of the vertical bending structure (*H7*, *H8*) results in maximum beam envelopes up to approximately $\pm 77\,\mathrm{mm}$ (*QH01*) and $\pm 96\,\mathrm{mm}$ (*QH02*) and would require a very strong *QC04* with $k \approx -33\,\mathrm{T\,m^{-1}}$. Comparing the maximum radius of such a quadrupole[28] to its required aperture $>\pm 37\,\mathrm{mm}$ indicates that this configuration will be difficult to achieve and would require a longer quadrupole $l > 0.52\,\mathrm{m}$. A more workable solution is provided by configurations *H7II*, *H8II* where over-focusing takes place downstream of the vertical bending magnet. *QC04* will require a slightly enlarged aperture $>\pm 42\,\mathrm{mm}$, but lower maximum gradients are sufficient. The

[28] Using a maximum field of 1T at the pole tip as estimate for the inner radius r of a quadrupole: $B = k\,r = 1\,\mathrm{T}$

last focusing magnet *QH02* in this configuration requires $k \approx 21\,\mathrm{T\,m^{-1}}$.

5.4.3. Summary & Discussion

This section developed an optical design for beam transferlines from LEIR SS30 to future experimental endstations in the adjacent 'South Hall' area. The design consists of a common transport line and two separate beamlines for horizontal and vertical beam delivery. It is based on horizontal beam parameters in Table 5.16 that were estimated from simulations of quadrupole-driven extraction, Section 5.3.3.3.

The setup consists of 2 bending segments of 118° and 90°, and 12 quadrupoles located at positions with maximum beam envelopes of about ±42 mm (assuming configurations *H7II* and *H8II*) and <25 mm for seven of them (*QC01*, *QC02*, *QCB1*, *QCB2*, *QC03*, *QVB1*, *QH02*). Assuming quadrupoles of length $l = 0.52\,\mathrm{m}$ (as in LEIR), maximum gradients $\approx 22\,\mathrm{T\,m^{-1}}$ are required, however, $<10\,\mathrm{T\,m^{-1}}$ are sufficient for half of the elements (*QC01*, *QC02*, *QCB1*, *QC03*, *QV01*, *QH01*).

Results of a preliminary study of the effect of alignment and magnet errors[29] indicate that the minimum pencil beam sizes (FWHM) of $(5 \pm 1)\,\mathrm{mm}$ can be achieved in the vertical line and $(8 \pm 1)\,\mathrm{mm}$ in the horizontal line, as well as broad beams with irradiation inhomogeneities $\leq \pm 5\,\%$ across a sample area of $5\,\mathrm{cm} \times 5\,\mathrm{cm}$.

5.4.3.1. Design Parameters and Effect of Random Errors

Beam size and beam homogeneity for vertical and horizontal beamlines are within the requirements given in Table 5.1, except for the minimum pencil beam size in the horizontal beamline that exceeds the design value of 5 mm. Smaller beam sizes at low dispersion and divergence can be achieved by decreasing the distance between target plane and the last focusing doublet *QH01*, *QH02*.

Large values of α in broad beam delivery will result in slightly diverging beams. This increase of beam cross-section with depth results in loss of particles from the target volume. The maximum 'effective' divergence in the target plane, however, is limited by the dimensions of the irradiated field and its distance from the focusing element. Assuming a uniform distribution and neglecting the effect of scattering in the medium, a decrease of particle flux by approximately 1 % per cm depth in the target plane was estimated for irradiation in the vertical beamline and by approximately 0.5 % in the horizontal beamline. Also with a more sophisticated delivery mechanism, such as beam scanning, the beam direction will depend on the position on the target.

Preliminary error analysis indicates stable values for dispersion and α in pencil beam configuration and positioning errors around ±1 mm for both beamlines and in both planes. Due to the strong powering of quadrupole magnets, larger deviations are expected in the broad beam configuration. Horizontal dispersion is found to vary by up to ±4 m in both beamlines, and large positioning errors of up to about ±33 mm in the target plane of the vertical beamline and ±24 mm in the target plane of the horizontal beamline were observed. Mispositioning of this magnitude would introduce large uncertainties in

[29] Random alignment errors ($\sim 10^{-4}\,\mathrm{m}$), as well as constant and relative quadrupole coefficient errors (combined error $\mathcal{O}(\Delta k_1 l) = 10^{-2}$) were applied randomly after matching. Parameter statistics were computed on 1 000 runs per configuration.

dose homogeneity across the irradiated sample area. Confirmation of these results and investigation of mitigation strategies will be necessary for further design decisions.

Sensitivity to random errors is expected to decrease towards smaller β in the target plane. Whether the resulting less homogeneous fields are accepted by the user community will influence the further implementation approach. More sophisticated beam delivery mechanisms may have to be considered already in a first implementation stage. Such upgrade options are discussed in the following Section 5.4.3.2.

5.4.3.2. Future Upgrade Options

While broad beams may be used for cell irradiation studies, most experiments that simulate clinical treatment situations prefer pencil beams, as these are becoming the standard for patient treatment. The current design achieves both pencil and broad beams, however it does not include mechanisms for beam steering. Installation of a pencil-beam scanning system in the horizontal beamline will require additional horizontal and vertical scanning magnets. In order to facilitate such a future upgrade, the drift length between the last focusing quadrupole *QFH02* and the target plane of the horizontal beamline was chosen to fit the space requirements of a scanning system [178], scaled to an irradiation field of 5 cm × 5 cm. Small parallel beams $\beta = 1$, $\alpha = 0$ can be achieved approximately 3.5 m downstream of *QFH02*, where such a system could be installed.

Upgrading the vertical beamline for beam scanning, if necessary, will be more challenging: scanning magnets would need to be installed either on the level of the common bend, or downstream of the vertical bend. The former would require vertical bending dipoles with enlarged apertures, and space availability will be a concern for the latter, particularly if the beamline is installed above ground as assumed in this study. Since the vertical beamline is mainly envisaged to be used for cellular experiments, size and weight of samples may allow a moving setup table to be employed as alternative to a scanned beam.

Most difficulties in the beamline design process are linked to the need to achieve a very wide range of beta functions over short drift spaces and in the same setup. This is required due to the delivery method for homogeneous broad beams, Section 5.4.1.4.

A more elegant method uses nonlinear optical elements for 'flattening' an initially Gaussian beam so that homogeneous irradiation fields can be achieved across large sample areas without strong beam defocusing: for example 19 cm × 19 cm and uniformity within ±2.5 % using octupoles in [206]. For implementation in the beamline design, two octupoles need to be placed at positions with $\beta_x \gg \beta_y$ and $\beta_y \gg \beta_x$, respectively, in order to modify the beam distribution in both planes. Additionally, the slow extracted beam needs to be turned into an approximately Gaussian distribution before entering these elements. This may be achieved by a thin scatter foil [206], ideally at a location where $\beta_x \gg \beta_y$, as already foreseen in this study. The linear optics design presented here can be used as starting point for the exploration of such upgrade options.

5.4.3.3. Conclusion

A first design of beam transport lines for biomedical experiments at LEIR was developed, permitting horizontal and vertical delivery of broad and pencil beams with energies of up

to 430 MeV/n and 75 MeV/n, respectively. The design assumes a very simple, but mostly active, broad beam delivery method which exploits the homogeneity of the central part of a strongly defocused Gaussian beam to achieve homogeneous coverage of irradiation fields up to 5 cm × 5 cm with intensity fluctuations $<\pm 5\,\%$. However, the low efficiency of this delivery mode gives rise to radiation protection concerns, particularly for the high-energy horizontal beamline. Also, first error analysis studies indicate that large positioning errors may occur in broad-beam delivery due to the strong beam defocusing.

Radiation protection studies need to be undertaken to estimate the ambient radiation resulting from broad-beam collimation in the current setup. Based on these studies, viability of this delivery method for biomedical experiments in an initial implementation stage can be investigated. Depending on the outcome, mitigation strategies for reducing errors in beam positioning need to be developed, or one of the more advanced delivery mechanisms discussed in the previous Section 5.4.3.2 will need to be implemented already from the outset. Furthermore, underground placement of the vertical beamline should be considered as it may facilitate radiation protection. It would also lift restrictions on the positioning of the vertical beamline, Section 5.4.1.1, and would thus allow a longer common beamline to be envisaged that could provide more space for additional optical elements.

The design proposed here is based on conservative estimates for initial beam functions, and allows dispersion compensation in the common bending magnet for both positive and negative initial dispersion. However, changes in initial beam parameters influence the location where $\beta_x \gg \beta_y$ which is needed for the installation of a thin scatter foil that can transform the extracted 'bar of charge' in horizontal phase space into an approximately Gaussian distribution. Additional well-defined locations where either horizontal or vertical beam size dominate would also be needed for a future upgrade with non-linear optical elements. The degree to which optical beam functions in the common bending element and in other parts of the beamlines can be decoupled from the characteristics of the extracted beam therefore requires further investigation. This might necessitate changes to the common transport and bending segment since space for positioning new quadrupoles between *KFH3234* and the first horizontal bending magnet is limited.

5.5. Conclusion

The results of first feasibility studies towards the creation of an ion beam facility for biomedical experiments at LEIR were presented in this chapter.

A suitable resonance configuration was identified that achieves sufficiently large spiral step sizes to permit slow extraction from the current LEIR for energies up to 240 MeV/n. The study takes into account limitations on apertures, sextupole positioning and strengths, and requires the installation of one electrostatic and one magnetic septum. An upgrade for future high-energy extraction up to 430 MeV/n is proposed which requires a thinner first and installation of a stronger second magnetic septum due to the increased beam rigidity and the resulting reduction in horizontal kick imparted by the septa.

Designs for a common beam transport line from kicker magnet *KFH3234* in LEIR to the adjacent South Hall, as well as for beamlines to vertical and horizontal experimental endstations were developed. The setup consists of 12 quadrupoles and two bending

segments of 118° in the horizontal and 90° in the vertical plane. Based on beam start parameters estimated from single particle tracking, pencil beam sizes (FWHM) of (5 ± 1) mm can be achieved in the vertical line, and (8 ± 1) mm in the horizontal line. Both beamlines allow for broad beam irradiation with intensity inhomogeneities $<\pm 5\,\%$ across a sample area of 5 cm × 5 cm.

The main challenges in the configuration of the extraction process are linked to the constraints imposed by the existing LEIR lattice and its continued use for LHC operation, in particular: limited space for the installation of new extraction elements, and strict constraints on their minimum horizontal position. Additionally, the aperture of kicker element *KFH31* limits the maximum transportable width of the extracted beam segment. Depending on the number and powering levels of sextupoles in LEIR, strong amplitude detuning was observed in some configurations. Available choices for the separatrix angle at the electromagnetic septum and resonance excitation strengths were limited by these effects.

Challenges in the beamline design are mainly related to the requirement to achieve a wide range of beam sizes under tight space constraints in the vertical beamline: The studied design relies on selecting the central part of a large Gaussian beam for the production of homogeneous broad beams, thus requiring betatron amplitude functions to be adjustable over three orders of magnitude. In this delivery mode, more than 90 % of the beam are discarded, which gives rise to radiation protection concerns, particularly for the high-energy horizontal beamline.

In order to gain more flexibility in extraction geometry, amplitude detuning effects related to sextupole configurations need to be further investigated and mitigation strategies be developed. Choice and positioning of magnetic septa in SS30 requires further investigation in order to identify an optimum setup that minimises particle losses for extraction of all beam energies. Such studies are currently underway and will be available as CERN report [205]. Multi-particle simulation studies will be needed to quantify the expected particle losses during extraction.

Detailed study of the variation of initial beam parameters in horizontal phase-space, in dependence of extraction method and configuration, will establish the range of optical parameters that must be matched by the beam transfer lines. In order to yield a robust beamline design, the degree to which optical beam functions in the common bending element and in other parts of the beamlines can be decoupled from the characteristics of the extracted beam requires further investigation.

Radiation due to particle losses in LEIR, activation of extraction elements and the ambient radiation resulting from beam collimation in the current broad beam delivery mechanism must be quantified in detailed radiation protection studies. Based on those results, and a detailed error analysis study, alternative beam delivery methods may be investigated: In particular, an extension for pencil beam scanning in the horizontal beamline and creation of broad beams using non-linear optical elements for the vertical beamline. Both upgrade options can be based on the linear optics design presented here and would address radiation protection issues, as well as difficulties linked to large betatron amplitude functions in this current design. Underground placement of the vertical beamline may also be considered, as it would lift the tight positioning constraints for the vertical beamline assumed in this study.

6. Summary & Conclusion

This thesis investigates two distinct streams of research, with the common goal to contribute towards the creation of evidence in the field of HT:

First, by developing a methodology for form-based data capture and data analysis with the aim to ensure accurate computable documentation of collected data and of data resulting from analysis process, while reducing implementation and maintenance cost of the respective software systems, Chapter 3 and 4. Second, by undertaking first studies towards an ion beam facility at CERN that could provide the necessary beam-time for needed radiobiological experiments, Chapter 5.

Both, the lack of solid clinical evidence despite a large number of treated patients, and large uncertainties in the biological effectiveness of ion beam radiation pose fundamental questions about the viability of HT. This chapter briefly summarises the key findings of this thesis and their contribution towards HT.

6.1. Software Architecture for Capturing Clinical Information

The first part of this thesis proposes a metadata-driven software architecture for clinical data capture and analysis to support the clinical evidence creation process, and develops selected metamodels as its principal components.

Collection of high-quality clinical data is essential for the functioning of this architecture, as it is for the evidence derivation process. Given the importance of data capture forms in clinical data collection and for data documentation, a metamodel for the specification of 'forms' was developed. Two distinctive features distinguish this metamodel from related standards in the domain: Due to its expressiveness, the Forms-Metamodel supports both, user interface generation and data documentation, thus ensuring consistency between the properties of Data Capture Instruments (DCIs), the collected data and their documentation. Generation of software artefacts from implementation-independent form specifications will reduce the cost of form design, as well as of creation and maintenance of data capture services. The ability to compose new forms from existing model fragments allows form components to be shared and reused, regardless of any particular implementation technology. This may increase reporting homogeneity and lead to improved data interoperability.

Similarly to primary data, collected over the course of medical studies, information derived from analysis processes also requires adequate documentation to ensure its correct use and interpretation. In response to the need for better documentation of simulation studies for health-economic assessments, metamodels for Markov model-based simulations were developed. No open standards for computable documentation of such

simulation studies exist, despite their common usage for the synthesis of evidence in health care.

The design of both metamodels is informed by existing domain standards and best practices, and was validated by implementation and comparison to related standards and guidelines.

While the 'historic failure to leverage the collection and sharing of anonymised data' [25] in HT cannot be reverted, the proposed software architecture and the developed metamodels have the potential to improve the documentation of data capture in future studies and may facilitate its coordination. A methodology of application was therefore demonstrated on the example of HT.

Based on the form metamodel, a library of relevant forms and form fragments can be set up, from which the components of form specifications can be drawn and used in future clinical studies. Such a technology-independent repository of forms may facilitate collaboration in the domain: Study sites can maintain system and data sovereignty, while at the same time committing to the collection of interoperable data. Every observation will be documented by the DCIs used and the context in which it was acquired, so that it can be 'queried' in an implementation-independent manner in terms of study context and form properties. As no privacy concerns apply to form and study metadata, specifications of forms and studies can be published and discovery of relevant data sources for analyses projects will thus be facilitated.

With the existence of analysis models, such as the Markov model, future analysis goals in the community can be made explicit. Interoperability of existing and currently collected data with regard to these analysis procedures can be verified (semi-)automatically, allowing timely intervention to align ongoing data capture towards common analysis goals, if needed. Computable documentation of the assumptions and processes involved in analysis procedures simplifies their verification and the reproduction of their results.

While illustrated on the example of HT, the demonstrated principles apply similarly to other heterogeneous data capture and analysis scenarios in and beyond medicine.

6.2. Design of Ion Beam for Radiobiology

Despite the need for research to reduce radiobiological uncertainties in HT treatment, beam-time for pre-clinical radiation biology studies at existing treatment and research facilities is limited. A dedicated facility could provide this needed beamtime and would permit large systematic measuring campaigns in a controlled setting: for example for microdosimetry studies, or for studies of RBE for different LET conditions and on a large number of human cell lines.

Part of the rationale for creating such a facility at CERN is based on the potential for infrastructure savings by making use of the existing LEIR synchrotron. The studies performed in the second part of the thesis confirm this rationale by showing that slow extraction from LEIR is possible with moderate effort:

A suitable resonance configuration for quadrupole-driven extraction was identified that achieves sufficiently large spiral step sizes to permit slow extraction from the current LEIR for beam energies up to 240 MeV/n. The study takes into account limitations

on apertures, sextupole positioning and strengths, and requires the installation of one electrostatic and one magnetic septum in the LEIR lattice. An upgrade for future high-energy extraction up to 430 MeV/n is proposed which requires a thinner first magnetic septum and installation of a strong second magnetic septum due to the increased beam rigidity. Investigations towards optimising septum properties and positioning are currently undergoing to allow low and high energy extraction with a single septum configuration.

Designs for a common beam transport line from SS30 in LEIR to the adjacent South Hall area, as well as for beamlines to vertical and horizontal experimental endstations, were developed. The setup consists of 12 quadrupoles and two bending segments, one for the horizontal and one for the vertical plane. Based on start parameters estimated from single particle tracking of the extraction process, the design achieves pencil beam sizes (FWHM) of (5 ± 1) mm in the vertical beamline, and (8 ± 1) mm in the horizontal beamline. Both beamlines allow for broad beam irradiation with intensity inhomogeneities $<\pm 5\,\%$ across a sample area of 5 cm $\times$ 5 cm.

Broad beam delivery is based on a simple, mostly active, delivery method that exploits the homogeneity of the central part of a strongly defocused Gaussian beam. Since the majority of beam particles is discarded in this delivery mode, radiation protection studies must be carried out before concluding on its viability for biomedical experiments in a first implementation stage. Depending on these results, the beamline should be further optimised for robustness, or alternative delivery methods be investigated based on this initial linear-optics design.

Both studies identify areas of research that needs to be adressed for the further planning of a biomedical ion beam research facility based on LEIR. The proposed transferline design provides first estimates for obtainable beam characteristics which will guide negotiations with potential users and inform further design decision.

A. Appendix Software Architecture

A.1. Forms-Metamodel Definition and Model Mappings

Table A.1 defines the Forms-Metamodel metaclasses, their attributes and relations. Enumeration types used by the Forms-Metamodel are listed in Table A.2. Table A.3 indicates mapping relations between ISO/IEC 11179 and Forms-Metamodel metaclasses. Mapping relations between Forms-Metamodel metaclasses and Forms-Metamodel-Template are listed in Table A.4. Mappings from the Forms-Metamodel-Template into the OpenClinica are detailed in Table A.5 and mappings into ISO/IEC 19763-13:2013 in Table A.6.

All model mappings focus exclusively on *non-abstract* metaclasses and their attributes and relations. Inherited metaclass properties are indicated by ' *'. Transformations between mappable metamodel features without direct correspondence in the other metamodel are represented by '→' which specifies the involved target metaclass and attribute or relation. Metamodel features without mapping correspondence in the other metamodel cannot be translated.

Table A.7 proposes modifications and extensions to the Forms-Metamodel, resulting from its validation in Section 4.1.5. Likewise, suggestions for improving ISO/IEC 19763-13:2013 are made in Table A.8.

Table A.1.: Forms-Metamodel metaclasses.

Class	Attribute/Reference	DataType/Class	Card.	Prec.	Comments
		Identification			
IdentifiedItem					
attributes	globalID	`String`	1		identifier that must be *unique in global scope*
NamedItem					
attributes	definition	`String`	1		textual definition
	language	`LanguageCode`	1		language in and for which the item is designed, represented by e.g. ISO/IEC 639-3:2007
	name	`String`	1		name of the item
		Administration			
additional metaclasses for registration and administration of *IdentifiedItem* elements may be included in inheritance hierarchy, such as *Registered_Item* (ISO/IEC 11179-3:2012, 8.1.2.1) and *Administered_Item* (ISO/IEC 11179-3:2012, 8.1.2.2)					
		Logical Structure			
FormElement		⇒ *NamedItem*			
top-level element for form design					
		Structural Components			
Structure		⇒ *FormElement*			
references	externalAnnotation	ExternalAnnotation	0..*	Y	relation between current *Structure* and objects that are not *Structure* elements, such as concepts from externally maintained domain ontology
	structureAnnotation	StructureAnnotation	0..*	Y	relation between current *Structure* and other *Structure* elements
	generalInformation	*InteractionElement*	0..*	Y	information that is provided with a *Structure* element but not used to explain the purpose of the element or how to use it correctly, example: copyright information, institution logo, general disclaimers
	instruction	*InteractionElement*	0..*	Y	information explaining the correct use of a *Structure* element or communicating form completion logic to the user, example: 'go-to' statements
ComposedStructure		⇒ *Structure*			
references	title	*InteractionElement*	0..1	Y	contextual information about other elements included in the *ComposedStructure*, represented as form or section title, example: 'Adverse Events after treatment' vs. '5y Follow-up - Adverse Events', 'Applicant personal details - Contact Details' vs. 'Dependents - Contact Details'
	localAnnotation	LocalAnnotation	0..*	Y	relation across substructures in the scope of current *ComposedStructure* element, *scope limited to ComposedStructure* [a]
	localPrepopulation-Assignment	LocalPrepopulation-Assignment	0..*	Y	definition of default values for substructures, possibly computed from other substructures in the scope of current *ComposedStructure*, *scope limited to ComposedStructure* [b]
	consistencyConstraint	ConsistencyConstraint	0..*	Y	constraints across substructures in scope of current *ComposedStructure*, *scope limited to current ComposedStructure* [c]
	containsComposition	StructureComposition	1	Y	composition mechanism for grouping of *Structure* elements
Group		⇒ *ComposedStructure*			
					instantiable version of *ComposedStructure*
Form		⇒ *ComposedStructure*			
attributes	preferredAccessMode	`AcessModeType`	1		specification of `AcessModeType` for which the current Form is designed
references	submissionProperties	SubmissionProperties	1	Y	specification of how strictly validation rules shall be enforced upon form submission
	logicalHierarchy	LogicalHierarchy	0..*	Y	mark-up for substructures (*ComposedStructure*) to indicate their role in form structuring
	presentation	*Presentation*	1	Y	presentation mark-up for substructures
SimpleStructure		⇒ *Structure*			

Class	Attribute/Reference	DataType/Class	Card.	Prec.	Comments
references	question	*InteractionElement*	0..1	Y	the question that the user is asked to respond to
	responseType	*SimpleResponseType*	1	N	defines characteristics of the 'kind of' data accepted as response, similar to Value_Domain (ISO/IEC 11179-3:2012, 11.3.2.5)
	entryConstraint	*EntryConstraint*	0..*	Y	additional constraints on *responseType* of *SimpleStructure*, *not all combinations SimpleResponseType - EntryConstraint are permitted* [b]
Field		⇒ *SimpleStructure*			
					instantiable version of *SimpleStructure*
Composition & Process Constraints					
CompositionComponent					
references	precondition	*BooleanExpression*	0..1	Y	if specified, the *precondition* defines conditions under which the current *CompositionComponent* becomes *active* at form run-time, otherwise, the *CompositionComponent* is *active* by default
StructureComposition		⇒ *CompositionComponent*			
attributes	compositionType	`CompositionType`	1		defines completion order and validation logic of *StructureComposition*
references	composes	*CompositionComponent*	2..*		allows nesting of *CompositionComponent*s
StructureInComposition		⇒ *CompositionComponent*			
attributes	localID	`String`	1		identifier that must be *unique within scope of ComposedStructure that contains the element*
	isAccessible	`Boolean`	1		specifies whether the user can access the form component, or if it is 'hidden'
	minRequiredResponses	`NonNegInteger`	1		minimum number of occurrences of current form component that *must* be completed, *minRequiredResponses = 0* corresponds to an 'optional' form component, *minRequiredResponses > 0* corresponds to a 'mandatory' form component
	maxResponses	`NonNegInteger`	1		maximum number of occurrences of current form component that *may* be completed, *minRequiredResponses* $\leq$ *maxResponses*
references	generalInformation	*InteractionElement*	0..*	Y	context-specific extension to *generalInformation* provided by included *Structure* element
	instruction	*InteractionElement*	0..*	Y	context-specific extension to *instruction* provided by included *Structure* element
	number	*InteractionElement*	0..1	Y	context-specific identifier of form component, indicates form completion order and may be used in *instruction* texts to refer to the respective form component
	structure	*Structure*	1	N	reference to the *Structure* element that is to be placed in the context of the current *StructureComposition*, *structure reference may only refer to Field or Group, not to Form*
	externalAnnotation	ExternalAnnotation	0..*	Y	context-specific extension to *externalAnnotation* provided by included *Structure* element
	localAnnotation	LocalAnnotation	0..*	Y	context-specific extension to *localAnnotation* provided by included *Structure* element, *only applies to Group elements, scope limited to included ComposedStructure* [a]
	localPrepopulation-Assignment	LocalPrepopulation-Assignment	0..*	Y	context-specific extension to *localPrepopulationAssignment* provided by included *Structure* element, *only applies to Group elements, scope limited to included ComposedStructure* [b]
	consistencyConstraint	ConsistencyConstraint	0..*	Y	context-specific extension to *consistencyConstraint* provided by included *Structure* element, *only applies to Group elements, scope limited to included ComposedStructure* [c]
	entryConstraint	*EntryConstraint*	0..*	Y	context-specific extension to *entryConstraint* provided by included *Structure* element, *only applies to Field elements, permitted EntryConstraints depend on responseType of referenced Field* [d]
SubmissionProperties					
attributes	enforceHardConstraints	`Boolean`	1		all 'mandatory' form components required to be *completed* and *valid*
	allowPartialSubmission	`Boolean`	1		all *completed* form components required to be *valid*, but *empty* 'mandatory' form components permitted
LogicalHierarchy					
attributes	hierarchyLevel	`NonNegInteger`	1		indicates level in tree structure, '0' corresponds to top-level

Class	Attribute/Reference	DataType/Class	Card.	Prec.	Comments
references	structureInComposition-Reference	StructureInComposition	1		reference to *StructureInComposition* element, *scope limited to current Form*
		Prepopulation			
LocalPrepopulationAssignment					
attributes	label	`String`	0..1		descriptive name
	valueLocked	`Boolean`	1		indicates that prepopulation value cannot be modified by user
references	assignmentTarget	StructureInComposition	1	N	reference to the form component that is to be prepopulated, *referenced StructureInComposition must correspond to a Field, otherwise the assignment is ambigious*
	assignmentExpression	*Expression*	1	Y	*Expression* that defines the prepopulation value
	prepopulationPrecondition	*BooloeanExpression*	0..1	Y	if specified, the *prepopulationPrecondition* defines a condition that has to hold for the *assignmentTarget* to be prepopulated
		Constraints			
		Response Types			
SimpleResponseType		⇒ *FormElement*			
attributes	dataType	`DATATYPE`	1		expected data type of response, represented by e.g. Datatype (ISO/IEC 11179-3:2012, 11.3.2.9)
references	unitOfMeasure	UnitOfMeasure	0..1	N	optional unit for the response, represented by e.g. Unit_Of_Measure (ISO/IEC 11179-3:2012, 11.4.3.1)
	instruction	*InteractionElement*	0..*	Y	information that serves for explaining correct use of the *SimpleResponseType*, independent of its association to a particular Field
NonEnumeratedResponseType		⇒ *SimpleResponseType*			
					instantiable version of *SimpleResponseType*
EnumeratedResponseType		⇒ *SimpleResponseType*			
attributes	ordered	`Boolean`	1		indicates whether the order of EnumeratedResponseTypeComponents is significant for the interpretation and use of the EnumeratedResponseType
references	component	EnumeratedResponseType-Component	2..*	Y	sequence of predefined answer choices
EnumeratedResponseTypeComponent					
attributes	valueCode	`String`	1		the response value that is going to be used by the system, has to conform to *dataType*
	valueDefinition	`String`	1		textual definition of the answer choice
references	valueDisplay	*InteractionElement*	1..*	Y	representations of *valueCode* to user, example: *valueCode* = 0, display: 'Yes'; or *valueCode* = 'happy', display: 'happy' & image:
BlobResponseType		⇒ *SimpleResponseType*			
attributes	mimeType	`MIMETYPE`	1		*SimpleResponseType* with binary *dataType*
UnitOfMeasure		⇒ *FormElement*			
references	unitOfMeasureDisplay	*InteractionElement*	0..*	Y	representation of UnitOfMeasure to user
		Constraints			
Constraint					
attributes	label	`String`	0..1		descriptive name
references	constraintPrecondition	*BooleanExpression*	0..1	Y	defines condition under which the *Constraint* has to hold; if unspecified, *Constraint* must always be fulfilled
EntryConstraint					

Class	Attribute/Reference	DataType/Class	Card.	Prec.	Comments
ValueRangeConstraint		⇒ *EntryConstraint*			*requires NonEnumeratedResponseType with numeric dataType*
attributes	min	`String`	0..1		smallest permissible response value
	max	`String`	0..1		highest permissible response value, $min \leq max$
PatternConstraint		⇒ *EntryConstraint*			*requires NonEnumeratedResponseType*
attributes	regExp	`String`	1		regular expression defining the permissible format of a response value
SelectionMultiplicityConstraint		⇒ *EntryConstraint*			*requires EnumeratedResponseType*
attributes	min	`String`	1		minimum number of answer choices *required* to be selected from EnumeratedResponseType, default = 1
	max	`String`	1		maximum number of answer choices *permitted* to be selected from EnumeratedResponseType, default = 1, $min \leq max$
BlobSizeConstraint		⇒ *EntryConstraint*			*requires BlobResponseType*
attributes	maxSize	`String`	1		maximum file size of BlobResponseType
ConsistencyConstraint					
	constraint	*BooleanExpression*	1	Y	*BooleanExpression* that specifies constraints across substructures in scope of *ComposedStructure*
		Expression Language			
BooleanExpression					
attributes	negated	`Boolean`	1		if TRUE then ¬ *BooleanExpression*
SimpleBooleanExpression		⇒ *BooleanExpression*			
attributes	value	`Boolean`	1		TRUE or FALSE
BooleanCombination		⇒ *BooleanExpression*			
attributes	booleanExpressionCombinator	`BooleanCombinatorType`	1		boolean operator to combine sequence of *BooleanExpression*s
references	combines	*BooleanExpression*	2..*	Y	defines sequence of *BooleanExpression*s to be combined
Relation		⇒ *BooleanExpression*			
attributes	comparator	`ComparatorType`	1		operator comparing *lhsExpression* and *rhsExpression*
references	lhsExpression	*Expression*	1	Y	one of two *Expression*s to be compared
	rhsExpression	*Expression*	1	Y	one of two *Expression*s to be compared
Expression					
ExpressionCombination		⇒ *Expression*			
attributes	expressionCombinator	`ExpressionCombinatorType`	1		arithmetic operator for combining a sequence of Expressions
references	combines	*Expression*	2..*	Y	defines sequence of *Expression*s to be combined
SimpleExpression		⇒ *Expression*			
ExternalValue		⇒ *SimpleExpression*			
attributes	valueReference	`AnyURI`	1		*SimpleExpression* value obtained from e.g. a webservice at run-time
Constant		⇒ *SimpleExpression*			
attributes	value	`String`	1		*SimpleExpression* value specified at design-time
Variable		⇒ *SimpleExpression*			
references	structureInCompositionReference	StructureInComposition	1	N	*SimpleExpression* value specified by reference to a form component; value is available at run-time, once the form component has been completed; *variable must be guaranteed to exist and be unambigious.* [e]

Class	Attribute/Reference	DataType/Class	Card.	Prec.	Comments
		Presentation			
		User-Form Interaction			
InteractionElement					
attributes	label	String	0..1		descriptive name
TextElement		⇒ *InteractionElement*			
attributes	text	String	1		text that is displayed to the user
MediaElement		⇒ *InteractionElement*			
attributes	explanationText	String	1		textual definition of the MediaElement
	fileReference	AnyURI	1		reference address to the binary object that is used as MediaElement
	mimeType	MIMEType	1		specification of the MIMEType of the binary object
		Form Element Presentation			
Presentation					
SimplePresentation		⇒ *Presentation*			
attributes	inactiveStructureAs	InactivePresentation	1		specifies presentation of StructureInComposition elements whose *precondition* evaluates to FALSE
	repeating-SimpleStructureAs	RepeatingPresentation	1		specifies presentation of StructureInComposition (Field) elements with $maxResponses > 1$
	repeating-ComposedStructureAs	RepeatingPresentation	1		specifies presentation of StructureInComposition (Group or Form) elements with $maxResponses > 1$
references	inputFieldPresentation	InputFieldPresentation	0..*		specifies presentation of 'input field' of Field elements and their *SimpleResponseType*
Stylesheet Presentation		⇒ *Presentation*			
attributes	stylesheet	String	1		presentation by means of *stylesheet*
InputFieldPresentation					
attributes	selectorType	SelectorType	1		specifies type of 'input field' used to represent the *SimpleResponseType* of a given Field
references	structureInComposition-Reference	StructureInComposition	1		reference to *StructureInComposition* element, *scope limited to current Form*
		Annotation			
Annotation					
attributes	predicate	AnnotationPredicate	1		specifies the type of relation that the *Annotation* asserts between 'annotation subject' and 'annotation object'
StructureAnnotation		⇒ *Annotation*			
references	structureObject	*Structure*	1	N	reference to another *Structure* element that serves as 'annotation object' in this *Annotation*
LocalAnnotation		⇒ *Annotation*			
references	localAnnotationSubject	StructureInComposition	1	N	reference to *StructureInComposition* element that serves as 'annotation subject', *scope limited to current ComposedStructure*
	localAnnotationObject	StructureInComposition	1	N	reference to *StructureInComposition* element that serves as 'annotation object', *scope limited to current ComposedStructure*
ExternalAnnotation		⇒ *Annotation*			
attributes	externalAnnotationObject	AnyURI	1		reference to external object that serves as 'annotation object' in this *Annotation*

[a] Scope of LocalAnnotation:*annotationSubject* and LocalAnnotation:*annotationObject* limited to StructureInComposition elements in scope of *ComposedStructure*.

[b] Scope of LocalPrepopulationAssignment:*assignmentTarget* and variable in LocalPrepopulationAssignment:-

assignmentExpression limited to StructureInComposition elements (Field) in scope of *ComposedStructure*.

[c] Scope of variables in ConsistencyConstraint:*constraintPrecondition* limited to StructureInComposition elements (Field) in scope of *ComposedStructure*.

[d] SelectionMultiplicityConstraint requires EnumeratedResponseType, PatternConstraint or RangeConstraint require NonEnumeratedResponseType, FileSizeConstraint or MIMETypeConstraint require MIMEresponseType; context-specific *EntryConstraint* on StructureInComposition may only narrow meaning of included *Structure*.

[e] Reference only to 'mandatory' (minRequiredResponse = 1) and 'non-repeating' (maxResponse = 1) StructureInComposition:*structure* Field.

Table A.2.: Forms-Metamodel ENUMERATION types.

Type	Value	Description
`CompositionType`		
	sequential	strict ordering of composition siblings, 'cascading relevance', see Table 4.2 for more properties
	parallel	no ordering of composition siblings, siblings independent, see Table 4.2 for more properties
	choice	no ordering of composition siblings, completion of exactly one sibling required, see Table 4.2 for more properties
`BooleanCombinatorType`		
	and	all *BooleanExpression*s in sequence are to be combined by boolean AND
	or	all *BooleanExpression*s in sequence are to be combined by boolean OR
	xor	all *BooleanExpression*s in sequence are to be combined by boolean XOR
`ComparatorType`		
	$=$	*lhs* and *rhs* *Expression*s are 'equal'
	$\neq$	*lhs* and *rhs* *Expression*s are *not* 'equal'
	$\leq$	*lhs* *Expression* is smaller than or 'equal' to *rhs* *Expression*
	$\geq$	*lhs* *Expression* is greater than or 'equal' to *rhs* *Expression*
	$>$	*lhs* *Expression* is greater than *rhs* *Expression*
	$<$	*lhs* *Expression* is smaller than *rhs* *Expression*
`ExpressionCombinatorType`		
	$+$	all *Expression*s in sequence are to be 'added'
	$-$	all *Expression*s in (ordered) sequence are to be 'subtracted'
	$\times$	all *Expression*s in sequence are to be 'multiplied'
	$/$	all *Expression*s in (ordered) sequence are to be 'divided'
`AccessmodeType`		
	visualDigital	indicates that the form specification was created for 'visually' accessible forms in digital media, such as normal web form
	visualPrint	indicates that the form specification was created for 'visually' accessible forms in print media, such as normal paper form
	braille	indicates that the form specification was created for 'Braille' access
`MIME Type`		
	audio	audio file
	image	image file
	video	video file
	...	other
`SelectorType`		
	textfield	text input field, for NonEnumeratedResponseTypes of most *dataType*s
	dateSelector	calender pop-up from which date can be selected, NonEnumeratedResponseTypes with 'date' *dataType*
	locationSelector	map where location can be chosen, NonEnumeratedResponseTypes with 'coordinate' *dataType*
	fileSelector	pop-up field that allows browsing file system and selecting file, BlobResponseType
	slider	input field for range values, for NonEnumeratedResponseTypes with numeric *dataType* and RangeConstraint
	checkbox	answer choices rendered as checkboxes, for EnumeratedResponseType, single or multiple selections
	dropdown	answer choices rendered as checkboxes, for EnumeratedResponseType, typically for single selection
`Inactive Presentation`		
	hide	inactive form elements are hidden from user (requires *accessmodeType*=`visualDigital`)
	crossOutFade	inactive form elements are crossed-out or faded (requires *accessmodeType*=`visualDigital`)
	gotoStatements	the presentation of inactive form elements remains unchanged but instructions are created to indicate when form elements can be skipped (any *accessmodeType*)
`Repeating Presentation`		

Type	Value	Description
	table	repeating form elements (*maxResponses*>1) are represented in tabular structure
	individualStructures	repeating form elements (*maxResponses*>1) are represented as individual (repeating) questions
`AnnotationPredicate`		
for all ***Annotation*** *types*	sameAs	asserts believe of semantic *equivalence* between annotation subject and object (OWL:*sameAs*) StructureAnnotation: e.g. equivalence of two Fields: *What is your age?*, *How old are you?* LocalAnnotation: e.g. equivalence of two Fields in particular usage context (as StructureInComposition elements): *Do you mind that your partner smokes?*, *Does this bother you?*
	narrowerThan	indicates that annotation subject has *narrower* meaning than annotation object (SKOS:*narrower*); *Your Name:*, *Your Last Name*
	broaderThan	the inverse of `narrowerThan`
	relatedTo	indicates a *generic relationship* between annotation subject and object (SKOS:*related*); *Where were you born?*, hidden *Correct response:* as in Fig. 4.31
for ***StructureAnnotation***	derivedFrom	asserts that the annotation subject, a ***Structure*** element, has been *derived* from the annotation object, another ***Structure*** element
for ***ExternalAnnotation***	implements	asserts that annotation subject represents a *truthfull implementation* of the annotation object, such as the implementation of a Field *How old are you?* from a ISO11179:Data_Element *Age of Person*
for ***LocalAnnotation***	semantically-DependentOn	indicates that annotation subject has *semantic dependency* on annotation object, *Choose your favourite colour.*, *Why have you chosen . . . as your favourite colour?*

Table A.3.: Mapping relations between selected elements of ISO/IEC 11179-3:2012 and Forms-Metamodel

ISO/IEC 11179-3:2012					Forms-Metamodel				
Class	**Attribute/Reference**	**DataType/Class**	**Card.**	**Prec.**	**Class**	**Attribute/Reference**	**DataType/Class**	**Card**	**Prec.**
Data_Element					**Field**				
attributes	data_element_precision	Integer	0..1						
references	data_element_meaning	Data_Element_Concept	1						
	data_element_domain	Value_Domain	1	N	*references*	responseType	*SimpleResponseType*	1	N
Value_Domain					**SimpleResponseType**				
attributes	datatype	DATATYPE	1		*attributes*	dataType	DATATYPE	1	
	maximum_character_-quantity	Integer	0..1		→	PatternConstraint			
	format	String	0..1		→	PatternConstraint			
references	unit_of_measure	Unit_Of_Measure	0..1	N	*references*	unitOfMeasure	UnitOfMeasure	0..1	N
	value_domain_meaning	Conceptual_Domain	1	N					
						instruction	InteractionElement	0..*	Y
Described_Value_Domain					**NonEnumeratedResponseType**				
attributes	datatype *	DATATYPE	1		*attributes*	dataType *	DATATYPE	1	
	maximum_character_-quantity *	Integer	0..1		→	PatternConstraint			
	format *	String	0..1		→	PatternConstraint			
	description	Text	1		*references*	instruction *	InteractionElement	0..*	Y
references	unit_of_measure *	Unit_Of_Measure	0..1	N		unitOfMeasure *	UnitOfMeasure	0..1	N
	value_domain_meaning	Conceptual_Domain	1	N					
Enumerated_Value_Domain					**EnumeratedResponseType**				
attributes	datatype *	DATATYPE	1		*attributes*	dataType *	DATATYPE	1	
	maximum_character_-quantity *	Integer	0..1		→	PatternConstraint			
	format *	String	0..1		→	PatternConstraint			
						ordered	Boolean	1	
					references	instruction *	InteractionElement	0..*	Y
references	unit_of_measure *	Unit_Of_Measure	0..1	N		unitOfMeasure *	UnitOfMeasure	0..1	N
	value_domain_meaning	Conceptual_Domain	1	N					
	permissible_value_set	Permissible_Value	1..*	Y		component	EnumeratedResponseType-Component	2..*	Y
Permissible_Value					**EnumeratedResponseTypeComponent**				
attributes	permitted_value	VALUE	1		*attributes*	valueCode	String	1	
	begin_date	DATE	1						
	end_date	DATE	0..1						
references	permissible_value_meaning	Value_Meaning	1	N		valueDefinition	String	1	
						valueDisplay	*InteractionElement*	1..*	Y
Unit_Of_Measure					**UnitOfMeasure**				
as ISO11179:Designatable_Item									
references	item_designation	Designation	0..*						
	item_definition	Definition	0..*		*references*	unitOfMeasureDisplay	*InteractionElement*	1..*	

Table A.4.: Mapping relations between Forms-Metamodel and Forms-Metamodel-Template for main differences between both metamodels.

Forms-Metamodel					Form-Metamodel-Template				
Class	**Attribute/Reference**	**DataType/Class**	**Card.**	**Prec.**	**Class**	**Attribute/Reference**	**DataType/Class**	**Card**	**Prec.**
IdentifiedItem					**DerivedItem**				
attributes	globalID	`String`	1		*attributes*	derivedFrom	`String`	1	
Structure		⇒ *FormElement*							
references	externalAnnotation	ExternalAnnotation	0..*	Y					
	structureAnnotation	StructureAnnotation	0..*	Y					
	generalInformation	*InteractionElement*	0..*	Y					
	instruction	*InteractionElement*	0..*	Y					
ComposedStructure		⇒ *Structure*							
references	title	*InteractionElement*	0..1	Y					
	localAnnotation	LocalAnnotation	0..*	Y					
	localPrepopulation-Assignment	LocalPrepopulation-Assignment	0..*	Y					
	consistencyConstraint	ConsistencyConstraint	0..*	Y					
	containsComposition	StructureComposition	1	Y					
StructureInComposition		⇒ *CompositionComponent*			**StructureInComposition**		⇒ *CompositionComponent*		
attributes	localID	`String`	1		*attributes*	localID	`String`	1	
	isAccessible	`Boolean`	1			isAccessible	`Boolean`	1	
	minRequiredResponses	`NonNegInteger`	1			minRequiredResponses	`NonNegInteger`	1	
	maxResponses	`NonNegInteger`	1			maxResponses	`NonNegInteger`	1	
references	generalInformation	*InteractionElement*	0..*	Y	*references*	generalInformation	*InteractionElement*	0..*	Y
	instruction	*InteractionElement*	0..*	Y		instruction	*InteractionElement*	0..*	Y
	number	*InteractionElement*	0..1	Y		number	*InteractionElement*	0..1	Y
	structure	*Structure*	1	N					
	externalAnnotation	ExternalAnnotation	0..*	Y		externalAnnotation	ExternalAnnotation	0..*	Y
	localAnnotation	LocalAnnotation	0..*	Y					
	localPrepopulation-Assignment	LocalPrepopulation-Assignment	0..*	Y					
	consistencyConstraint	ConsistencyConstraint	0..*	Y					
	entryConstraint	*EntryConstraint*	0..*	Y					
						structureAnnotation	StructureAnnotation	0..*	Y
Group		⇒ *ComposedStructure*			**Group**		⇒ *StructureInComposition*		
					references	title	*InteractionElement*	0..1	Y
						localAnnotation	LocalAnnotation	0..*	Y
						localPrepopulation-Assignment	LocalPrepopulation-Assignment	0..*	Y
						consistencyConstraint	ConsistencyConstraint	0..*	Y
						containsComposition	StructureComposition	1	Y
Form		⇒ *ComposedStructure*			**FormTemplate**		⇒ *FormElement*		
attributes	preferredAccessMode	`AcessModelType`	1		*attributes*	preferredAccessMode	`AcessModelType`	1	
references	submissionProperties	SubmissionProperties	1	Y	*references*	submissionProperties	SubmissionProperties	1	Y
	logicalHierarchy	LogicalHierarchy	0..*	Y		logicalHierarchy	LogicalHierarchy	0..*	Y

Forms-Metamodel					Forms-Metamodel-Template				
Class	**Attribute/Reference**	**DataType/Class**	**Card.**	**Prec.**	**Class**	**Attribute/Reference**	**DataType/Class**	**Card.**	**Prec.**
	presentation	*Presentation*	1	Y		presentation	*Presentation*	1	Y
						title	*InteractionElement*	0..1	Y
						generalInformation	*InteractionElement*	0..*	Y
						instruction	*InteractionElement*	0..*	Y
						localAnnotation	LocalAnnotation	0..*	Y
						externalAnnotation	ExternalAnnotation	0..*	Y
						structureAnnotation	StructureAnnotation	0..*	Y
						localPrepopulation-Assignment	LocalPrepopulation-Assignment	0..*	Y
						consistencyConstraint	ConsistencyConstraint	0..*	Y
						containsComposition	StructureComposition	1	Y
SimpleStructure		⇒ *Structure*							
references	question	*InteractionElement*	1	Y					
	responseType	*SimpleResponseType*	1	N					
	entryConstraint	*EntryConstraint*	0..*	Y					
Field		⇒ *SimpleStructure*			**Field**		⇒ *StructureInComposition*		
					references	question	*InteractionElement*	1	Y
						responseType	*SimpleResponseType*	1	**Y** [a]
						entryConstraint	*EntryConstraint*	0..*	Y
SimpleResponseType		⇒ *FormElement*			**SimpleResponseType**		⇒ *FormElement*		
attributes	dataType	DATATYPE	1		*attributes*	dataType	DATATYPE	1	
references	unitOfMeasure	UnitOfMeasure	0..1	N	*references*	unitOfMeasure	UnitOfMeasure	0..1	**Y** [a]
	instruction	*InteractionElement*	0..*	Y		instruction	*InteractionElement*	0..*	Y

[a] *SimpleResponseType* and UnitOfMeasure included via 'composition' relation, not via reference as in Forms-Metamodel.

Table A.5.: Mapping relations between Forms-Metamodel-Template and main components of the OpenClinica forms metamodel.

Forms-Metamodel-Template					OpenClinica Metamodel				
Class	**Attribute/Reference**	**DataType/Class**	**Card.**	**Prec.**	**Class**	**Attribute/Reference**	**DataType/Class**	**Card**	**Prec.**
Logical Structure									
Structural Components									
FormTemplate		⇒ *DerivedItem*			**CRF**				
attributes	derivedFrom *	`String`	1						
	definition *	`String`	1						
	language *	`LanguageCode`	1						
	name *	`String`	1		*attributes*	crf_name	`String`	1	
	preferredAccessMode	`AcessModeType`	1						
						version	`String`	1	
						version_description	`String`	1	
						revision_notes	`String`	1	
references	submissionProperties	SubmissionProperties	1	Y					
	logicalHierarchy	LogicalHierarchy	0..*	Y					
	presentation	*Presentation*	1	Y	→	Item:*response_type*			
	title	*InteractionElement*	0..1	Y	→	Section:*section_title*			
	generalInformation	*InteractionElement*	0..*	Y					
	instruction	*InteractionElement*	0..*	Y	→	Section:*instructions*			
	localAnnotation	LocalAnnotation	0..*	Y					
	externalAnnotation	ExternalAnnotation	0..*	Y					
	structureAnnotation	StructureAnnotation	0..*	Y					
	localPrepopulation-Assignment	LocalPrepopulation-Assignment	0..*	Y	→	Item:*default_value* or Item:*response_values_or_calculations*[a]			
	consistencyConstraint	ConsistencyConstraint	0..*	Y	→	Item:*validation*			
	containsComposition	StructureComposition	1	Y	→	Item:*section_label*			
Group		⇒ *StructureInComposition*							
attributes	derivedFrom *	`String`	1						
	definition *	`String`	1						
	language *	`LanguageCode`	1						
	name *	`String`	1						
	localID *	`String`	1		→	Section:*section_label* or Group:*group_label*			
	isAccessible *	`Boolean`	1						
	minRequiredResponses *	`NonNegInteger`	1		→	Group:*group_repeat_number*			
	maxResponses *	`NonNegInteger`	1		→	Group:*group_repeat_max*			
references	title	*InteractionElement*	0..1	Y	→	Section:*section_title* or Group:*group_header*			
	generalInformation *	*InteractionElement*	0..*	Y					
	instruction *	*InteractionElement*	0..*	Y	→	Section:*instructions*			
	number *	*InteractionElement*	0..1	Y					
	structureAnnotation *	StructureAnnotation	0..*	Y					
	externalAnnotation *	External Annotation	0..*	Y					
	localAnnotation	LocalAnnotation	0..*	Y					
	precondition *	*BooleanExpression*	0..1	Y	→	Group:*group_display_status*			

Forms-Metamodel-Template					OpenClinica Metamodel				
Class	**Attribute/Reference**	**DataType/Class**	**Card.**	**Prec.**	**Class**	**Attribute/Reference**	**DataType/Class**	**Card**	**Prec.**
	localPrepopulation-Assignment	LocalPrepopulation-Assignment	0..*	Y	→	Item:*default_value* or Item:*response_values_or_calculations*			
	consistencyConstraint	ConsistencyConstraint	0..*	Y	→	Item:*validation*			
	containsComposition	StructureComposition	1	Y	→	Item:*section_label*, Section:*parent_label*			
Group[b]		⇒ *StructureInComposition*			**Section**				
			Group:*localID*	←	*attributes*	section_label	`String`	1	
			Group:*title*	←		section_title	`String`	1	
						subtitle	`String`	0..1	
			Group:*instruction*	←		instructions	`String`	0..1	
						page_number	`Integer`	0..1	
		Group:*containsComposition* (parent), LogicalHierarchy		←		parent_section	`String`	0..1	
						borders	`Boolean`	0..1	
Group[c]		⇒ *StructureInComposition*			**Group**				
			Group:*localID*	←	*attributes*	group_label	`String`	1	
						group_layout	`GROUP_LAYOUT_TYPE`	1	
			Group:*title*	←		group_header	`String`	0..1	
			Group:*minRequiredResponses*	←		group_repeat_number	`Integer`	0..1	
			Group:*maxResponses*	←		group_repeat_max	`Integer`	0..1	
			Group:*precondition*	←		group_display_status	`DISPLAY_STATUS_TYPE`	0..1	
Field		⇒ *StructureInComposition*			**Item**				
attributes	derivedFrom *	`String`	1						
	definition *	`String`	1						
	language *	`LANGUAGECODE`	1						
	name *	`String`	1						
	localID *	`String`	1		*attributes*	item_name	`String`	1	
	isAccessible *	`Boolean`	1						
	minRequiredResponses *	`NonNegInteger`	1						
	maxResponses *	`NonNegInteger`	1						
			UnitOfMeasure	←		units	`String`	0..1	
						right_item_text	`String`	0..1	
		Group:structureComposition, Form:logicalHierarchy		←		section_label	`String`	1	
		Group:structureComposition, Form:logicalHierarchy		←		group_label	`String`	1	
			Field:*generalInformation*	←		header	`String`	0..1	
			Field:*generalInformation*	←		subheader	`String`	0..1	
			Form:*presentation*	←		parent_item	`String`	0..1	
			Form:*presentation*	←		column_number	`String`	0..1	
						page_number	`String`	0..1	
	SimpleResponseType & *EntryConstraint*, Presentation:*inputFieldPresentation*			←		response_type	`RESPONSE_TYPE`	1	
			SimpleResponseType:*globalID*	←		response_label	`String`	1	
			EnumeratedResponseType:*component*	←		response_options_text	`String`	0..1	
			Group:*localPrepopulationAssignment*	←		response_values_or_calculations	`String`	0..1	
			EnumeratedResponseType:*component*	←		response_layout	`RESPONSE_LAYOUT_TYPE`	0..1	

Forms-Metamodel-Template					OpenClinica Metamodel				
Class	**Attribute/Reference**	**DataType/Class**	**Card.**	**Prec.**	**Class**	**Attribute/Reference**	**DataType/Class**	**Card**	**Prec.**
		Group:*localPrepopulationAssignment*		←		default_value	`String`	0..1	
		Group:*responseType*		←		data_type	`DATA_TYPE`	1	
		ValueRangeConstraint, PatternConstraint		←		validation	`String`	0..1	
		validation_error_message	`String`	0..1					
		protected_health_information	`Boolean`	1					
		Field:*minRequiredResponses*, Field:*maxResponses*		←		required	`Boolean`	1	
		Field:*precondition*		←		item_display_status	`Display_Status_Type`	0..1	
references	question	*InteractionElement*	0..1	Y		description_label	`String`	1	
	generalInformation *	*InteractionElement*	0..*	Y					
	instruction *	*InteractionElement*	0..*	Y		left_item_text	`String`	0..1	
	number *	*InteractionElement*	0..1	Y		question_number	`String`	0..1	
	structureAnnotation *	StructureAnnotation	0..*	Y					
	externalAnnotation *	External Annotation	0..*	Y					
	precondition *	*BooleanExpression*	0..1	**Y**	→	*simple_conditional_display*			
	responseType	*SimpleResponseType*	1	Y	→	*response_type*, *data_type*			
	entryConstraint	*EntryConstraint*	0..*	Y	→	*width_decimal*, *validation*			
ResponseTypes									
ResponseTypes can be converted between the Forms-Metamodel and the OpenClinica forms metamodel: A single OC:ResponseType typically corresponds to a combination of FMT:SimpleResponseType, FMT:InputFieldPresentation and FMT:*Constraint*, examples are given in Section 4.1.5.3.									

[a] In combination with ResponseTypeItem:`CALCULATION`.
[b] Group with LogicalHierarchy markup, indicating role as 'Section'.
[c] Group without LogicalHierarchy markup.

Table A.6.: Mapping relations between Forms-Metamodel-Template and ISO/IEC 19763-13:2013.

Forms-Metamodel-Template					ISO/IEC 19763-13:2013				
Class	**Attribute/Reference**	**DataType/Class**	**Card.**	**Prec.**	**Class**	**Attribute/Reference**	**DataType/Class**	**Card**	**Prec.**
Logical Structure									
Structural Components									
FormTemplate		⇒ *FormElement*			**FormDesign**		⇒ MODEL		
attributes	derivedFrom *	`String`	1						
	definition *	`String`	1						
	language *	`LanguageCode`	1						
	name *	`String`	1						
	preferredAccessMode	`AcessModeType`	1						
references	submissionProperties	SubmissionProperties	1	Y					
	logicalHierarchy	LogicalHierarchy	0..*	Y					
	presentation	*Presentation*	1	Y	→	*Form_Design_Element*:*style*			
	title	*InteractionElement*	0..1	Y	→	Section_Element:*section_title*			
	generalInformation	*InteractionElement*	0..*	Y	→	*contained_element* *Presentation_Element*			
	instruction	*InteractionElement*	0..*	Y	→	Section_Element:*section_instruction*			
	localAnnotation	LocalAnnotation	0..*	Y	→	MFI:Model_Element_Set_Mapping			
	externalAnnotation	ExternalAnnotation	0..*	Y	→	MDR_Mapping			
	structureAnnotation	StructureAnnotation	0..*	Y	→	MFI:Model_Element_Set_Mapping			
	localPrepopulation-Assignment	LocalPrepopulation-Assignment	0..*	Y	→	Section_Element:*rule* or Input_Field:*default_value*			
	consistencyConstraint	ConsistencyConstraint	0..*	Y	→	Section_Element:*rule*			
	containsComposition	StructureComposition	1	Y	→	Section_Element:*contained_element*			
					→	Section_Element:*rule* or List_Item:*guarded_element*			
		containsComposition StructureComposition		←		contained_element	*Form_Design_Element*	1..*	Y
						describing_language	Form_Language	1	Y
						header	Section_Element	0..1	Y
						footer	Section_Element	0..1	Y
StructureComposition		⇒ *CompositionComponent*							
attributes	compositionType	`CompositionType`	1		→	Section_Element:*ordered*			
references	compositionComponent	*CompositionComponent*	2..*		→	*Form_Design_Element*:*contained_element*			
	precondition *	*BooleanExpression*	0..1		→	*Form_Design_Element*:*rule*			
Group		⇒ *ComposedStructure*			**Section_Element**		⇒ *Form_Design_Element*		
attributes	derivedFrom *	`String`	1						
	definition *	`String`	1						
	language *	`LanguageCode`	1						
	name *	`String`	1						
	localID *	`String`	1		*attributes*	label *	`String`	0..1	
	precondition, *localPrepopulationAssignment*, *consistencyConstraint*			←		rule *	Local_Definition	0..*	
		FormTemplate:*presentation*		←		style *	`String`	0..*	
	isAccessible *	`Boolean`	1						
	minRequiredResponses *	`NonNegInteger`	1			cardinality *	`Natural_Range` [a]	1	
	maxResponses *	`NonNegInteger`	1						

Forms-Metamodel-Template					ISO/IEC 19763-13:2013				
Class	**Attribute/Reference**	**DataType/Class**	**Card.**	**Prec.**	**Class**	**Attribute/Reference**	**DataType/Class**	**Card**	**Prec.**
		StructureComposition:*compositionType*		←		ordered	Boolean	1	
references	title	*InteractionElement*	0..1	Y	*references*	section_title	Prompt	0..1	Y
	generalInformation *	*InteractionElement*	0..*	Y		contained_element *	*Presentation_Element*	0..*	Y
	instruction *	*InteractionElement*	0..*	Y		section_instruction	Additional_Text	0..1	Y
			instruction	←		additional_instruction	Additional_Text	0..*	Y
	number *	*InteractionElement*	0..1	Y		section_number	Number	0..1	Y
	structureAnnotation *	StructureAnnotation	0..*	Y					
	externalAnnotation *	External Annotation	0..*	Y					
	localAnnotation	LocalAnnotation	0..*	Y					
	precondition *	*BooleanExpression*	0..1	Y	→	*rule* on containing *Form_Design_Element*			
	localPrepopulation-Assignment	LocalPrepopulation-Assignment	0..*	Y	→	*rule* or Input_Field:*default_value*			
	consistencyConstraint	ConsistencyConstraint	0..*	Y	→	*rule*			
	containsComposition	StructureComposition	1	Y	→	*contained_element*, *contained_section*			
		StructureComposition:*compositionComponent*		←		contained_element *	Question_Element	0..*	Y
		StructureComposition:*compositionComponent*		←		contained_element *	Section_Element	0..*	Y
		StructureComposition:*compositionComponent*		←		contained_section *	Section_Element	0..*	Y
Field		⇒ *SimpleStructure*			**Question_Element**		⇒ *Form_Design_Element*		
attributes	derivedFrom *	`String`	1						
	definition *	`String`	1						
	language *	`LanguageCode`	1						
	name *	`String`	1						
	localID *	`String`	1		*attributes*	label *	`String`	0..1	
		precondition, *entryConstraint*		←		rule *	Local_Definition	0..*	
		FormTemplate:*presentation*		←		style *	`String`	0..*	
	isAccessible *	`Boolean`	1						
	minRequiredResponses *	`NonNegInteger`	1			cardinality *	`Natural_Range` [a]	1	
	maxResponses *	`NonNegInteger`	1						
references	question	*InteractionElement*	0..1	Y	*references*	question_prompt	Prompt	0..1	Y
	generalInformation *	*InteractionElement*	0..*	Y					
	instruction *	*InteractionElement*	0..*	Y		question_instruction	Additional_Text	0..*	Y
	number *	*InteractionElement*	0..1	Y		question_number	Number	0..1	Y
	structureAnnotation *	StructureAnnotation	0..*	Y					
	externalAnnotation *	External Annotation	0..*	Y					
	precondition *	*BooleanExpression*	0..1	**Y**	→	*rule*			
	responseType	*SimpleResponseType*	1	Y	→	*entry_field*			
			responseType	←		entry_field	*Input_Field*	1	Y
	entryConstraint	*EntryConstraint*	0..*	Y	→	*rule*, Input_Field			
						contained_section *	Section_Element	0..*	Y
Response Types									
NonEnumeratedResponseType		⇒ *SimpleResponseType*			**Text_Field**		⇒ *Input_Field*		
attributes	derivedFrom *	`String`	1						
	definition *	`String`	1						

Forms-Metamodel-Template					ISO/IEC 19763-13:2013				
Class	**Attribute/Reference**	**DataType/Class**	**Card.**	**Prec.**	**Class**	**Attribute/Reference**	**DataType/Class**	**Card**	**Prec.**
	language *	LanguageCode	1						
	name *	String	1						
	dataType *	DataType	1		*attributes*	datatype *	Datatype	0..1	
references	unitOfMeasure *	UnitOfMeasure	0..1	Y		unit_of_measure *	Unit_Of_Measure	0..1	
	LocalPrepopulationAssignment:*assignmentExpression* in Group or From			←		default_value *	String	0..1	
	LocalPrepopulationAssignment:*valueLocked* in Group or From			←		default_value_read_only *	Boolean	0..1	
	PatternConstraint:*regExp* in Field:*entryConstraint*			←		maximum_character_-quantity *	Integer	0..1	
	PatternConstraint:*regExp* in Field:*entryConstraint*			←		format *	String	0..1	
	RangeConstraint:*min* in Field:*entryConstraint*			←		minimum_value	String	0..1	
	RangeConstraint:*max* in Field:*entryConstraint*			←		maximum_value	String	0..1	
	instruction *	*InteractionElement*	0..*	Y	*references*	input_field_instruction *	AdditionalText	0..*	Y
EnumeratedResponseType		⇒ *SimpleResponseType*			**List_Field**		⇒ *Input_Field*		
attributes	derivedFrom *	String	1						
	definition *	String	1						
	language *	LanguageCode	1						
	name *	String	1						
	dataType *	DataType	1		*attributes*	datatype *	Datatype	0..1	
	ordered	Boolean	1			ordered	Boolean	1	
references	unitOfMeasure *	UnitOfMeasure	0..1	Y		unit_of_measure *	Unit_Of_Measure	0..1	
	LocalPrepopulationAssignment:*assignmentExpression* in Group or From			←		default_value *	String	0..1	
	LocalPrepopulationAssignment:*valueLocked* in Group or From			←		default_value_read_only *	Boolean	0..1	
	PatternConstraint:*regExp* in Field:*entryConstraint*			←		maximum_character_-quantity *	Integer	0..1	
	PatternConstraint:*regExp* in Field:*entryConstraint*			←		format *	String	0..1	
	SelectionMultiplicityConstraint in Field:*entryConstraint*			←		multiselect	Boolean	1	
						fill_in	String	0..1	
	instruction *	*InteractionElement*	0..*	Y	*references*	input_field_instruction *	AdditionalText	0..*	Y
	component	EnumeratedResponseType-Component	2..*	Y		list_item	List_Item	2..*	Y
EnumeratedResponseTypeComponent					**List_Item**				
attributes	valueCode	String	1		*attributes*	value	String	1	
CompositionComponent:*precondition* referring to List_Item:*guarded_element*				←		guard	Guard_State_Type	0..1	
	valueDefinition	String	1		*references*	value_meaning	AdditionalText	0..1	Y
references	valueDisplay	*InteractionElement*	1..*	Y		item_prompt	Prompt	0..1	Y
						item_number	Number	0..1	Y
		CompositionComponent with *precondition*		←		guarded_element	*Form_Design_Element*	0..*	Y
BlobResponseType		⇒ *SimpleResponseType*							
attributes	derivedFrom *	String	1						
	definition *	String	1						
	language *	LanguageCode	1						
	name *	String	1						
	dataType *	DataType	1						

Forms-Metamodel-Template					ISO/IEC 19763-13:2013				
Class	**Attribute/Reference**	**DataType/Class**	**Card.**	**Prec.**	**Class**	**Attribute/Reference**	**DataType/Class**	**Card**	**Prec.**
	mimeType	MIMEType	1						
references	unitOfMeasure *	UnitOfMeasure	0..1	Y					
	instruction *	*InteractionElement*	0..*	Y					
LookUp_Field		⇒ *Input_Field*							
						datatype *	DATATYPE	0..1	
						unit_of_measure *	UNIT_OF_MEASURE	0..1	
						default_value *	String	0..1	
						default_value_read_only *	Boolean	0..1	
						maximum_character_-quantity *	Integer	0..1	
						format *	String	0..1	
						end_point	ANYURI	0..1	
						input_field_instruction *	AdditionalText	0..*	Y
Entry Constraints									
LocalPrepopulationAssignment									
attributes	label	String	0..*						
	valueLocked	Boolean	1		→	Entry_Field:*default_value_read_only*			
references	assignmentTarget	StructureInComposition	1	N	→	Entry_Field or LocalDefinition			
	assignmentExpression	*Expression*	1	Y	→	Entry_Field:*default_value* or LocalDefinition:*consequence*			
	prepopulationPrecondition	*BooloeanExpression*	0..1	Y	→	Local_Definition:*predicate*			
Constraints									
EntryConstraint									
ValueRangeConstraint		⇒ *EntryConstraint*							
attributes	min	String	0..1		→	Text_Field:*minimum_value*			
	max	String	0..1		→	Text_Field:*maximum_value*			
PatternConstraint		⇒ *EntryConstraint*							
attributes	regExp	String	1		→	*Input_Field*:*format*, *Input_Field*:*maximum_character_quantity*			
SelectionMultiplicityConstraint		⇒ *EntryConstraint*							
attributes	min	String	1						
	max	String	1		→	List_Field:*multiselect*			
BlobSizeConstraint		⇒ *EntryConstraint*							
attributes	maxSize	String	1						
ConsistencyConstraint		⇒ ConsistencyConstraint							
attributes	label	String	0..1						
references	constraintPrecondition	*BooleanExpression*	0..1	Y	→	Local_Definition:*predicate*			
	constraint	*BooleanExpression*	1	Y	→	Local_Definition:*consequence*			
Expression Language									
BooleanExpression					**Expression**				

There is no grammar definition for the expression language in ISO/IEC 19763-13:2013 (yet). Its elements Constant, for constant values defined at design-time, and Variable, for values that become available at run-time, correspond to identically named metaclasses in the Forms-Metamodel. The draft specification does not indicate the availability of a metaclass corresponding to ExternalValue. Its *Binary_Operation* metaclass foresees set operators, which are not provided by *BooleanExpression*s in the Forms-Metamodel.

Forms-Metamodel-Template					ISO/IEC 19763-13:2013				
Class	**Attribute/Reference**	**DataType/Class**	**Card.**	**Prec.**	**Class**	**Attribute/Reference**	**DataType/Class**	**Card**	**Prec.**
Presentation									
User-Form Interaction									
InteractionElement					**Presentation_Element**				
attributes	label	`String`	0..1		*attributes*	label	`text`	0..1	
						style	`text`	0..1	
						cardinality	`NATURAL_RANGE`	1	
						rule *	Local_Definition	0..*	
					references	contained_section *	Section_Element	0..*	Y
TextElement		⇒ *InteractionElement*			**Text_Element**		⇒ *Presentation_Element*		
attributes	label	`String`	0..1		*attributes*	label	`text`	0..1	
						style	`text`	0..1	
						cardinality	`NATURAL_RANGE`	1	
	text	`String`	1						
						rule *	Local_Definition	0..*	
					references	representation	Media_Element	0..*	Y
						contained_section *	Section_Element	0..*	Y
MediaElement		⇒ *InteractionElement*			**Media_Element**		⇒ *Presentation_Element*		
attributes	label	`String`	0..1		*attributes*	label	`text`	0..1	
						style	`text`	0..1	
						cardinality	`NATURAL_RANGE`	1	
						rule *	Local_Definition	0..*	
	explanationText	`String`	1						
	fileReference	`ANYURI`	1						
	mimeType	`MIMETYPE`	1						
					references	contained_section *	Section_Element	0..*	Y
Form Element Presentation									
Presentation									
style attribute on every ISO:*Form_Design_Element*									
Annotation - Mapping									
StructureAnnotation and LocalAnnotation are mapped into MFI:Model_Element_Set_Mapping; LocalAnnotation into MDR_Mapping									

[a] *cardinality* = 'unbounded' cannot be expressed in the Forms-Metamodel

Table A.7.: Proposed changes to Forms-Metamodel metaclasses.

Class	Attribute/Reference	DataType/Class	Card.	Prec.	Comments
Form					
references	header	StructureInComposition	0..1	N	specification of optional form header, *StructureInComposition required to be in direct scope of Form:mainGroup*
	footer	StructureInComposition	0..1	N	specification of optional form footer, *StructureInComposition required to be in direct scope of Form:mainGroup*
	mainGroup	Group	1	N	'main' Group that contains all other *FormElement*s
Change in inheritance hierarchy: Form independent of *FormElement*, compare Fig. 4.27					
InteractionElement		⇒ *FormElement*			
references	complements	*InteractionElement*	0..*	Y	optional *InteractionElement*s that complement information content of another *InteractionElement*
Change in inheritance hierarchy: InteractionElement *specialises* *FormElement*, compare Fig. 4.27					
EnumeratedResponseType					
references	fillInComponent	FillInComponent	0..1	Y	optional FillInComponent
FillInComponent		⇒ EnumeratedResponseType			
attributes	valueCode	`String`	1		
	exclusiveChoice	`Boolean`	1		
references	valueDisplay	*InteractionElement*	0..*	Y	
EnumeratedResponseTypeComponent					
attributes	exclusiveChoice	`Boolean`	1		

Table A.8.: Proposed changes to ISO/IEC 19763-13:2013 metaclasses.

Class	Attribute/Reference	DataType/Class	Card.	Prec.	Comments
Form_Design					
attributes	containedElement	*Form_Design_Element*	1	N	change cardinaltiy from 0..* to 1
Presentation_Element		⇒ *Form_Design_Element*			
references	complements	*Presentation_Element*	0..*	Y	optional *Presentation_Element*s that complement information content of another *Presentation_Element*
Replacement of all associations to Text_Element by associations to *Presentation_Element*, removal of Text_Element:*representation*.					
Form_Design_Element					
attributes	isAccessible	BOOLEAN	1	N	indicates whether a *Form_Design_Element* is accessible at form run-time
Blob_Input_Field		⇒ *Input_Field*			
attributes	MIMEtype	MIMEType	1		indicates MIMEType of binary object submitted as question response
List_Field		⇒ *Input_Field*			
attributes	cardinality	NATURAL_RANGE	1		indicates minimum required number of selections and maximum permissible number of selections, default 1..1
references	fill_in_item	Fill-in_Item	0..1		optional 'fill-in' field
Removal of current *fill-in* attribute, removal of current *multiselect* attribute					
List_Item					
attributes	exclusiveChoice	Boolean	1		indicates whether current List_Item may overwrite *cardinality* of List_Field to 1..1
Fill-In_Item		⇒ Text_Field			
attributes	exclusiveChoice	Boolean	1		indicates whether Fill-in_Item may overwrite *cardinality* of List_Field to 1..1
	value	String	1		value code
references	fill-in_prompt	*Presentation_Element*	0..1	Y	label for user interaction

A.2. Markov-Metamodel Definition

Table A.9 lists Markov model and Markov model simulation metaclasses, attributes and relations.

Table A.9.: Markov model and Markov model simulation metaclasses.

Class	Attribute/Reference	DataType/Class	Card.	Prec.	Comments
		Identification			
IdentifiedItem					
attributes	globalID	`String`	1		identifier that must be *unique in global scope*
NamedItem		⇒ *IdentifiedItem*			
attributes	definition	`String`	1		textual definition
	name	`String`	1		name for the item
		Administration			
additional metaclasses for registration and administration of *IdentifiedItem* elements may be included in inheritance hierarchy, such as *Registered_Item* (ISO/IEC 11179-3:2012, 8.1.2.1) and *Administered_Item* (ISO/IEC 11179-3:2012, 8.1.2.2)					
		MarkovModel			
MarkovModel		⇒ *NamedItem*			
references	state	State	2..*	Y	represents 'markov state', here 'health state'
	transition	Transition	1..*	Y	represents a transition between two States, modelling the likelihood of different disease progress scenarios
	cohort	Cohort	1..*	Y	identifies a subgroup of the population for which *CohortSpecificValue*s are defined
	cohortSpecificValue	*CohortSpecificValue*	1..*	Y	the measures attributed to Transitions and States depend on population Cohort
MarkovModelComponent					
attributes	localID	`String`	1		local identifier, unique within the scope of MarkovModel
s	definition	`String`	0..1		textual definition of component
State		⇒ *MarkovModelComponent*			
attributes	stateType	`StateType`	1		specification of type of 'markov state', can be used for model consistency checks
references	payOff	*PayOff*	0..*	N	abstract metaclass representing different types of measures that may be associated to 'health states' and transitions between them
Transition		⇒ *MarkovModelComponent*			
references	sourceState	State	1	N	instance of metaclass State that represents the source of a Transition
	targetState	State	1	N	instance of metaclass State that represents the target of a Transition
	payOff	*PayOff*	0..*	N	abstract metaclass representing different types of measures that may be associated to 'health states' and transitions between them
	probability	TransitionProbability	1	N	probability for the transition from *sourceState* to *targetState* to occur
Cohort		⇒ *MarkovModelComponent*			
textual definition of patient and treatment groups considered for this MarkovModel					
CohortSpecificValue		⇒ *MarkovModelComponent*			
references	cohortValueSet	CohortValueSet	1..*	Y	mapping between a Value and Cohorts of the MarkovModel for which this value applies
CohortValueSet					
references	cohort	Cohort	1..*	N	reference to Cohorts defined in the MarkovModel
	value	*Value*	1	N	reference to a single Value, see Fig. 4.33
TransitionProbability		⇒ *CohortSpecificValue*			
Type of *CohortSpecificValue* that represents a cohort-specific probability for a Transition.					
PayOff		⇒ *CohortSpecificValue*			
Abstract type of *CohortSpecificValue* representing any measure that can be associated to States and Transition.					
Cost		⇒ *PayOff*			
Type of *PayOff* that represents the monetary *cost* of being in a State, or of a Transition to occur.					

Class	Attribute/Reference	DataType/Class	Card.	Prec.	Comments
Utility		⇒ *PayOff*			
Type of *PayOff* that represents the subjective *benefit* of being in a State.					
		MarkovModelSimulation			
MarkovModelSimulation		⇒ *NamedItem*			
attributes	halfCycleCorrection	`Boolean`	1		indicates whether 'half-cycle correction' is used for computation
	evaluationType	`EvaluationType`	1		indicates whether computation should be based on point estimates for Values, or their distribution function
	discountRateUtility	`Decimal`	1		specifies discount rate for utility values
	discountRateCost	`Decimal`	1		specifies discount rate for cost values
references	simulationCohort	Cohort	1..*	Y	identifies a subgroup of the population for which simulation is to be performed
	markovModelReference	MarkovModelReference	1..*	Y	inclusion mechanism for existing MarkovModels to be used in this simulation
MarkovModelSimulationComponent					
attributes	localID	`String`	1		local identifier, unique within the scope of MarkovModelSimulation
attributes	definition	`String`	0..1		textual definition of component
MarkovModelReference					
attributes	numberOfCycles	`Integer`	1		indicates the number of cycles for which the referenced MarkovModel instance is used
references	markovModelRef	MarkovModel	1	N	references an instance of MarkovModel metaclass
	cohortMapping	CohortMapping	1..*	Y	mapping between Cohort in referenced MarkovModel and SimulationCohort in MarkovModelSimulation
	stateStartPopulation	StateStartPopulation	1..*	Y	assignment of initial population to States in referenced MarkovModel
CohortMapping					
attributes	cohortIdRef	`String`	1		reference to *localID* of Cohort metaclass defined in referenced MarkovModel
references	simulationCohortRef	SimulationCohort	1		reference to SimulationCohort defined in MarkovModelSimulation
StateStartPopulation					
references	targetStateRef	StateReference	1	Y	reference to State in some MarkovModel included as MarkovModelReference in the MarkovModelSimulation
	startPopulation	*Population*	1	Y	specifies start value for population in that state
StateReference					
attributes	stateIdRef	`String`	1		reference to *localID* of State included in MarkovModelReference
references	modelRef	MarkovModelReference	1		references MarkovModelReference
Population					
Abstract type representing the start population assigned to a particular State in a referenced MarkovModel					
PopulationValueFromSimulation		⇒ *Population*			
references	sourceStateRef	StateReference	1	Y	population value taken from simulation result (state population)
PopulationValue		⇒ *Population*			
attributes	value	`Integer`	1		population value specified at design-time

B. Appendix Accelerator Study

B.1. Detailed Tracking Results

Table B.1 summarises tracking results from Section 5.3.3.3.

Config.	δp [10^{-3}]	$\widetilde{\delta Q}$ [10^{-3}]	ϵ	$\Delta x_{\max}$ [mm]		Extr. innermost x[mm]	Extr. innermost x'[mrad]	Extr. outermost x[mm]	Extr. outermost x'[mrad]
C4-AB-BR-1	-0.200	-6.869	37.513	-1.765	ES	-45.000	4.328	-46.765	4.698
					MS[a]	-59.276	5.732	-60.481	6.114
					MS[b]	-65.965	4.931	-67.168	5.319
	0.000	-4.817	18.568	-3.120	ES	-45.000	4.308	-48.120	4.961
					MS[a]	-59.349	5.724	-61.483	6.399
					MS[b]	-66.037	4.923	-68.167	5.610
	0.200	-2.765	6.264	-3.777	ES	-45.000	4.288	-48.777	5.078
					MS[a]	-59.422	5.716	-62.007	6.534
					MS[b]	-66.109	4.916	-68.690	5.746
C4-AB-BR-2	0.000	-6.869	37.218	-1.520	ES	-45.000	3.947	-46.520	4.264
					MS[a]	-60.657	5.612	-61.699	5.941
C4-AB-BR-3	0.200	-6.869	36.643	-1.289	ES	-45.000	3.564	-46.289	3.833
					MS[a]	-62.044	5.493	-62.926	5.772
C4-AE-BR-1	-0.200	-4.104	13.706	-3.747	ES	-45.000	4.825	-48.747	5.610
					MS[a]	-57.473	5.887	-60.034	6.695
					MS[b]	-64.166	5.080	-66.723	5.902
	0.000	-2.052	3.562	-4.137	ES	-45.000	4.812	-49.137	5.678
					MS[a]	-57.520	5.882	-60.351	6.774
					MS[b]	-64.213	5.074	-67.039	5.981
	0.150	-0.513	0.266	-3.982	ES	-45.000	4.802	-48.982	5.634
					MS[a]	-57.556	5.877	-60.287	6.736
					MS[b]	-64.247	5.070	-66.974	5.942
C4-AE-AR-2	0.0	0.513	0.267	-4.140	ES	-45.000	5.101	-49.140	6.967
					MS[a]	-56.471	5.972	-69.308	6.863
C4-AB-AR-1	0.200	6.869	40.346	-0.089	ES	-45.000	4.330	-45.089	4.351
					MS[a]	-59.517	5.553	-59.570	5.573
					MS[b]	-66.224	4.742	-66.276	4.762
	0.000	4.817	19.481	-2.640	ES	-45.000	4.326	-47.640	4.876
					MS[a]	-59.533	5.554	-61.358	6.118
					MS[b]	-66.241	4.743	-68.063	5.317
	-0.200	2.765	6.274	-4.634	ES	-45.000	4.310	-49.634	5.277
					MS[a]	-59.592	5.550	-62.789	6.544

continued

Config.	δp [10^{-3}]	$\widetilde{\delta Q}$ [10^{-3}]	ϵ	$\Delta x_{\max}$ [mm]		Extr. innermost x[mm]	Extr. innermost x'[mrad]	Extr. outermost x[mm]	Extr. outermost x'[mrad]
					MS[b]	-66.301	4.740	-69.493	5.751
C4-AE-AR-1	0.200	4.104	13.546	-3.174	ES	-45.000	3.767	-48.174	4.428
					MS[a]	-61.570	5.377	-63.761	6.059
					MS[b]	-68.272	4.573	-70.459	5.267
	0.000	2.052	3.204	-4.903	ES	-45.000	3.760	-49.903	4.782
					MS[a]	-61.596	5.376	-64.978	6.432
					MS[b]	-68.298	4.573	-71.675	5.647
	-0.150	0.513	0.145	-5.758	ES	-45.000	3.756	-50.758	4.958
					MS[a]	-61.612	5.377	-65.578	6.619
					MS[b]	-68.315	4.574	-72.275	5.837
C5-AB-BR-1	-0.200	-15.427	35.543	-3.422	ES	-45.000	4.573	-48.422	5.323
					MS[a]	-58.265	5.814	-60.477	6.561
					MS[b]	-64.956	4.999	-67.164	5.757
	0.000	-13.427	27.063	-5.116	ES	-45.000	4.318	-50.116	5.438
					MS[a]	-59.200	5.733	-62.510	6.852
					MS[b]	-65.887	4.921	-69.192	6.057
	0.200	-11.427	19.638	-6.408	ES	-45.000	4.059	-51.408	5.461
					MS[a]	-60.149	5.651	-64.301	7.057
					MS[b]	-66.833	4.843	-70.979	6.270
C5-AB-BR-2	0.000	-15.427	35.600	-2.737	ES	-45.000	4.180	-47.737	4.777
					MS[a]	-59.691	5.688	-61.468	6.286
C5-AE-BR-1	-0.200	-5.750	5.184	-11.232	ES	-45.000	5.278	-56.232	7.749
					MS[a]	-55.753	6.042	-63.000	8.499
					MS[b]	-62.449	5.222	-69.687	7.714
	0.000	-3.750	2.252	-10.894	ES	-45.000	5.027	-55.894	7.418
					MS[a]	-56.674	5.962	-63.726	8.347
					MS[b]	-63.367	5.144	-70.410	7.564
	0.200	-1.750	0.523	-10.191	ES	-45.000	4.778	-55.191	7.007
					MS[a]	-57.588	5.882	-64.212	8.114
					MS[b]	-64.279	5.068	-70.893	7.333
C5-AE-BR-2	0.000	-1.750	0.519	-10.855	ES	-45.000	5.184	-55.855	7.563
					MS[a]	-56.113	6.012	-63.153	8.385

[a] Based on kick $\phi = 3.2\,\text{mrad}$ at ES.
[b] Based on kick $\phi = 5.4\,\text{mrad}$ at ES.

Table B.1.: Particle tracking results for extraction configurations from Table 5.13, Section 5.3.3.3.

Bibliography

[1] M. R. Raju. 'Particle Radiotherapy: Historical Developments and Current Status'. English. In: *Radiation Research* 145.4 (1996), pages.

[2] G. Kraft. 'Tumor therapy with heavy charged particles'. In: *Progress in Particle and Nuclear Physics* 45, Supplement 2 (2000), S473–S544.

[3] A. R. Smith. 'Proton therapy'. In: *Physics in Medicine and Biology* 51.13 (2006), R491.

[4] R. Levy et al. 'The current status and future directions of heavy charged particle therapy in medicine'. In: vol. 1099. 2009, pp. 410–425.

[5] H. Giap and B. Giap. 'Historical perspective and evolution of charged particle beam therapy'. In: *Translational Cancer Research* 1.3 (2012).

[6] R. Wilson. 'Radiological use of fast protons'. In: *Radiology* 47 (1946), p. 487.

[7] E. O. Lawrence and M. S. Livingston. 'The Production of High Speed Light Ions Without the Use of High Voltages'. In: *Phys. Rev.* 40 (1 Apr. 1932), pp. 19–35.

[8] *The 184-inch Synchrocyclotron*. Tech. rep. California: University of California, Berkeley, June 1964.

[9] M. Tubiana. *Introduction to radiobiology*. Taylor & Francis, 1990.

[10] E. J. Hall and A. J. Giaccia. *Radiobiology for the Radiologist*. Wolters Kluwer Health, 2006.

[11] T. F. Delaney and H. M. Kooy. *Proton and charged particle radiotherapy*. Lippincott Williams & Wilkins, 2008.

[12] D. Hanahan and R. A. Weinberg. 'The Hallmarks of Cancer'. In: *Cell* 100.1 (2000), pp. 57–70.

[13] D. Hanahan and R. A. Weinberg. 'Hallmarks of Cancer: The Next Generation'. In: *Cell* 144.5 (2011), pp. 646–674.

[14] J. Ferlay et al. 'Estimates of worldwide burden of cancer in 2008: GLOBOCAN 2008'. In: *International Journal of Cancer* 127.12 (2010), pp. 2893–2917.

[15] *Fact sheet 297: Cancer*. Jan. 2013. URL: `http://www.who.int/mediacentre/factsheets/fs297/en/index.html` (visited on 15/09/2013).

[16] OECD. *Health at a Glance: Europe 2012*. OECD Publishing, 2012.

[17] 'Swedish Cancer Society Radiation Therapy Research Investigation'. In: *Acta Oncologica* 41.7 (2002), pp. 596–603.

[18] European Society for Medical Oncology. *The true costs of cancer in Europe revealed*. ESMO 2012 Press Release. Sept. 2012.

[19] W. Levin et al. 'Proton beam therapy'. In: *Br J Cancer* 93 (2005), pp. 849–854.

[20] Particle Therapy Co-Operative Group (PTCOG). *Particle therapy facilities in operation*. PTCOG. URL: `http://ptcog.web.psi.ch/ptcentres.html` (visited on 21/09/2013).

[21] M. Durante and J. S. Loeffler. 'Charged particles in radiation oncology'. In: *Nat Rev Clin Oncol* 7.1 (2010). Journal Article, pp. 37–43.

[22] U. Amaldi and S. Braccini. 'Present challenges in hadrontherapy techniques'. In: *European Physical journaltitle Plus* 126.7 (2011), p. 70.

[23] A. Brahme et al. 'Design of a centre for biologically optimised light ion therapy in Stockholm'. In: *Nuclear Instruments and Methods in Physics Research Section B: Beam Interactions with Materials and Atoms* 184.4 (2001), pp. 569–588.

[24] E. A. Blakely and P. Y. Chang. 'Biology of charged particles'. In: *The Cancer Journal* 15.4 (2009), pp. 271–284.

[25] D. De Ruysscher et al. 'Charged particles in radiotherapy: A 5-year update of a systematic review'. In: *Radiotherapy and Oncology* 103.1 (Apr. 2012), pp. 5–7.

[26] T. van de Water et al. 'The potential benefit of radiotherapy with protons in head and neck cancer with respect to normal tissue sparing: A systematic review of literature'. In: *Oncologist* 16.3 (2011), pp. 366–377.

[27] B. L. Ramaekers et al. 'Systematic review and meta-analysis of radiotherapy in various head and neck cancers: Comparing photons, carbon-ions and protons'. In: *Cancer Treatment Reviews* 37.3 (May 2011), pp. 185–201.

[28] J. P. Grutters et al. 'Comparison of the effectiveness of radiotherapy with photons, protons and carbon-ions for non-small cell lung cancer: A meta-analysis'. In: *Radiotherapy and Oncology* 95.1 (Apr. 2010), pp. 32–40.

[29] T. Terasawa et al. 'Systematic Review: Charged-Particle Radiation Therapy for Cancer'. In: *Annals of Internal Medicine* 151.8 (Oct. 2009), pp. 556–565.

[30] M. Brada, M. Pijls-Johannesma and D. De Ruysscher. 'Proton Therapy in Clinical Practice: Current Clinical Evidence'. In: *Journal of Clinical Oncology* 25.8 (2007), pp. 965–970.

[31] M. Pijls-Johannesma, P. Pommier and Y. Lievens. 'Cost-effectiveness of particle therapy: Current evidence and future needs'. In: *Radiotherapy and Oncology* 89.2 (Nov. 2008), pp. 127–134.

[32] D. R. Olsen et al. 'Proton therapy - A systematic review of clinical effectiveness'. In: *Radiotherapy and Oncology* 83.2 (May 2007), pp. 123–132.

[33] M. Lodge et al. 'A systematic literature review of the clinical and cost-effectiveness of hadron therapy in cancer'. In: *Radiotherapy and Oncology* 83.2 (May 2007), pp. 110–122.

[34] M. Brada, M. Pijls-Johannesma and D. De Ruysscher. 'Proton Therapy in Clinical Practice: Current Clinical Evidence'. In: *Journal of Clinical Oncology* 25.8 (Mar. 2007), pp. 965–970.

[35] A. M. Allen et al. 'An evidence based review of proton beam therapy: The report of ASTRO's emerging technology committee'. In: *Radiotherapy and Oncology* 103.1 (Apr. 2012), pp. 8–11.

[36] D. Schulz-Ertner and H. Tsujii. 'Particle radiation therapy using proton and heavier ion beams'. In: *Journal of clinical oncology: official Journal of the American Society of Clinical Oncology* 25.8 (Mar. 2007). PMID: 17350944, pp. 953–964.

[37] D. L. Sackett et al. 'Evidence based medicine: what it is and what it isn't'. In: *BMJ* 312.7023 (Jan. 1996), pp. 71–72.

[38] M. F. Drummond. *Methods for the economic evaluation of health care programmes*. English. Oxford; New York: Oxford University Press, 1997.

[39] A. L. Cochrane. *Effectiveness And Efficiency: Random Reflections on Health Services*. Royal Society of Medicine Press Limited, 1999.

[40] D. Atkins et al. 'Systems for grading the quality of evidence and the strength of recommendations I: Critical appraisal of existing approaches The GRADE Working Group'. In: *BMC Health Services Research* 4.1 (Dec. 2004), p. 38.

[41] A. B. Hill. 'The Clinical Trial'. In: *New England Journal of Medicine* 247.4 (1952). PMID: 14941297, pp. 113–119.

[42] H. O. Stolberg, G. Norman and I. Trop. 'Randomized Controlled Trials'. In: *American Journal of Roentgenology* 183.6 (Dec. 2004), pp. 1539–1544. (Visited on 12/09/2013).

[43] B. Freedman. 'Equipoise and the Ethics of Clinical Research'. In: *New England Journal of Medicine* 317.3 (July 1987), pp. 141–145.

[44] G. Smith and J. Pell. 'Parachute use to prevent death and major trauma related to gravitational challenge: Systematic review of randomised controlled trials'. In: *British Medical Journal* 327.7429 (2003), pp. 1459–1461.

[45] S. M. Bentzen. 'Randomized controlled trials in health technology assessment: Overkill or overdue?' In: *Radiotherapy and Oncology* 86.2 (Feb. 2008), pp. 142–147.

[46] P. M. Rothwell. 'External validity of randomised controlled trials: "To whom do the results of this trial apply?"' In: *The Lancet* 365.9453 (Jan. 2005), pp. 82–93.

[47] N. Black. 'Why we need observational studies to evaluate the effectiveness of health care'. In: *BMJ* 312.7040 (1996), pp. 1215–1218.

[48] M. Goitein and J. D. Cox. 'Should randomized clinical trials be required for proton radiotherapy?' In: *Journal of clinical oncology: official Journal of the American Society of Clinical Oncology* 26.2 (Jan. 2008). PMID: 18182658, pp. 175–176.

[49] M. Goitein and J. D. Cox. 'In Reply'. In: *Journal of Clinical Oncology* 26.15 (May 2008), pp. 2593–2595.

[50] E. Glatstein et al. 'Should Randomized Clinical Trials Be Required for Proton Radiotherapy? An Alternative View'. In: *Journal of Clinical Oncology* 26.15 (May 2008), pp. 2438–2439.

[51] F. R. Macbeth and M. V. Williams. 'Proton Therapy Should Be Tested in Randomized Trials'. In: *Journal of Clinical Oncology* 26.15 (May 2008), pp. 2590–2591.

[52] J. E. Tepper. 'Protons and Parachutes'. In: *Journal of Clinical Oncology* 26.15 (May 2008), pp. 2436–2437.

[53] B. E. Lewis. 'On Equipoise and Emerging Technologies'. In: *Journal of Clinical Oncology* 26.15 (May 2008), pp. 2590–2590.

[54] J. P. C. Grutters et al. 'When to Wait for More Evidence? Real Options Analysis in Proton Therapy'. en. In: *The Oncologist* 16.12 (Dec. 2011). PMID: 22147003, pp. 1752–1761. (Visited on 13/09/2013).

[55] J. van Loon, J. Grutters and F. Macbeth. 'Evaluation of novel radiotherapy technologies: what evidence is needed to assess their clinical and cost effectiveness, and how should we get it?' In: *The Lancet Oncology* 13.4 (Apr. 2012), e169–e177.

[56] G. V. Glass. 'Primary, Secondary, and Meta-Analysis of Research'. English. In: *Educational Researcher* 5.10 (1976), pages.

[57] The Cochrane Collaboration. *Cochrane Handbook for Systematic Reviews of Interventions Version 5.1.0*. Ed. by J. Higgins and S. Green. Mar. 2011. URL: `www.cochrane-handbook.org`.

[58] L. A. Stewart and J. F. Tierney. 'To IPD or not to IPD?: Advantages and Disadvantages of Systematic Reviews Using Individual Patient Data'. In: *Evaluation & the Health Professions* 25.1 (2002), pp. 76–97.

[59] L. A. Stewart. 'Practical methodology of meta-analyses (overviews) using updated individual patient data'. In: *Statistics in Medicine* 14.19 (1995), pp. 2057–2079.

[60] M. Clarke et al. 'Individual patient data meta-analysis in cancer.' In: *British jounal of cancer* 77.11 (June 1998), pp. 2036–2044.

[61] Early Breast Cancer Trialists' Collaborative Group. 'Tamoxifen for early breast cancer: an overview of the randomised trials'. In: *The Lancet* 351.9114 (May 1998), pp. 1451–1467.

[62] M. J. Clarke and L. A. Stewart. 'Obtaining data from randomised controlled trials: how much do we need for reliable and informative meta-analyses?' In: *BMJ (Clinical research ed.)* 309.6960 (Oct. 1994). PMID: 7950694, pp. 1007–1010.

[63] C. Goble and R. Stevens. 'State of the nation in data integration for bioinformatics'. In: *Journal of Biomedical Informatics* 41.5 (Oct. 2008), pp. 687–693.

[64] O. Brazhnik and J. F. Jones. 'Anatomy of data integration'. In: *Journal of Biomedical Informatics* 40.3 (June 2007), pp. 252–269.

[65] M. Berg and E. Goorman. 'The contextual nature of medical information'. In: *International journaltitle of Medical Informatics* 56.1-3 (1999), pp. 51–60.

[66] D. M. Strong, Y. W. Lee and R. Y. Wang. 'Data quality in context'. In: *Commun. ACM* 40.5 (May 1997), pp. 103–110.

[67] J. Wyatt. 'Acquisition and use of clinical data for audit and research'. In: *Journal of Evaluation in Clinical Practice* 1.1 (1995), pp. 15–27.

[68] R. G. Marks. 'Validating electronic source data in clinical trials'. In: *Controlled Clinical Trials* 25.5 (Oct. 2004), pp. 437–446.

[69] J. A. Welker. 'Implementation of electronic data capture systems: Barriers and solutions'. In: *Contemporary Clinical Trials* 28.3 (May 2007), pp. 329–336.

[70] R. L. Richesson and J. Krischer. 'Data standards in clinical research: Gaps, overlaps, challenges and future directions'. In: *Journal of the American Medical Informatics Association* 14 (2007). Journal Article, pp. 687–696.

[71] T. Souza, R. Kush and J. P. Evans. 'Global clinical data interchange standards are here!' In: *Drug discovery today* 12.3-4 (Feb. 2007). Journal Article, pp. 174–181.

[72] M. Nahm et al. 'Design and implementation of an institutional case report form library'. In: *Clinical Trials* 8.1 (Feb. 2011), pp. 94–102.

[73] R. L. Richesson and P. Nadkarni. 'Data standards for clinical research data collection forms: current status and challenges'. In: *Journal of the American Medical Informatics Association* 18 (May 2011). Journal Article, pp. 341–346.

[74] M. C. Weinstein and W. B. Stason. 'Foundations of Cost-Effectiveness Analysis for Health and Medical Practices'. In: *New England Journal of Medicine* 296.13 (1977), pp. 716–721.

[75] B. O'Brien. 'Economic Evaluation of Pharmaceuticals: Frankenstein's Monster or Vampire of Trials?' English. In: *Medical Care* 34.12 (1996), pages.

[76] M. J. Buxton et al. 'Modelling in Ecomomic Evaluation: An Unavoidable Fact of Life'. In: *Health Economics* 6.3 (1997), pp. 217–227.

[77] K. Claxton, M. Sculpher and M. Drummond. 'A rational framework for decision making by the National Institute For Clinical Excellence (NICE)'. In: *The Lancet* 360.9334 (2002), pp. 711–715.

[78] National Institute for Health and Clinical Excellence. *Hormonal therapies for the adjuvant treatment of early oestrogen-receptor-positive breast cancer*. TA112. NICE, 2006. (Visited on 24/02/2014).

[79] National Institute for Health and Clinical Excellence. *Familial breast cancer*. CG164. NICE, 2013. (Visited on 24/02/2014).

[80] J. Lundkvist et al. 'Cost-effectiveness of proton radiation in the treatment of childhood medulloblastoma'. In: *Cancer* 103.4 (2005), pp. 793–801.

[81] J. Lundkvist et al. 'Economic evaluation of proton radiation therapy in the treatment of breast cancer'. In: *Radiotherapy and Oncology* 75.2 (May 2005), pp. 179–185.

[82] J. Lundkvist et al. 'Proton therapy of cancer: Potential clinical advantages and cost-effectiveness'. In: *Acta Oncologica* 44.8 (Jan. 2005), pp. 850–861.

[83] A. Konski et al. 'Is Proton Beam Therapy Cost Effective in the Treatment of Adenocarcinoma of the Prostate?' In: *Journal of Clinical Oncology* 25.24 (Aug. 2007), pp. 3603–3608.

[84] J. P. Grutters et al. 'The cost-effectiveness of particle therapy in non-small cell lung cancer: Exploring decision uncertainty and areas for future research'. In: *Cancer Treatment Reviews* 36.6 (Oct. 2010), pp. 468–476.

[85] A. Mobaraki et al. 'Cost-effectiveness of carbon ion radiation therapy for locally recurrent rectal cancer'. In: *Cancer Science* 101.8 (2010), pp. 1834–1839.

[86] R. Welte et al. 'A Decision Chart for Assessing and Improving the Transferability of Economic Evaluation Results Between Countries'. In: *PharmacoEconomics* 22.13 (2004), pp. 857–876.

[87] M. F. Drummond et al. 'Issues in the Cross-National Assessment of Health Technology'. In: *International Journal of Technology Assessment in Health Care* 8 (04 Sept. 1992), pp. 670–682.

[88] M. Drummond et al. 'Transferability of Economic Evaluations Across Jurisdictions: {ISPOR} Good Research Practices Task Force Report'. In: *Value in Health* 12.4 (2009), pp. 409–418.

[89] M. C. Weinstein et al. 'Principles of Good Practice for Decision Analytic Modeling in Health-Care Evaluation: Report of the ISPOR Task Force on Good Research Practices—Modeling Studies'. In: *Value in Health* 6.1 (Jan. 2003), pp. 9–17.

[90] M. Drummond, A. Manca and M. Sculpher. 'Increasing the generalizability of economic evaluations: Recommendations for the design, analysis, and reporting of studies'. In: *International Journal of Technology Assessment in Health Care* 21 (02 Apr. 2005), pp. 165–171.

[91] D. Rennie and H. Luft. 'Pharmacoeconomic analyses: Making them transparent, making them credible'. In: *JAMA* 283.16 (2000), pp. 2158–2160.

[92] P. J. Neumann et al. 'The Quality of Reporting in Published Cost-Utility Analyses, 1976-1997'. In: *Annals of Internal Medicine* 132.12 (2000), pp. 964–972.

[93] A. B. Rosen et al. 'Quality of Abstracts of Papers Reporting Original Cost-Effectiveness Analyses'. In: *Medical Decision Making* 25.4 (2005), pp. 424–428.

[94] D. Husereau et al. 'Consolidated Health Economic Evaluation Reporting Standards (CHEERS) statement'. In: *Cost Effectiveness and Resource Allocation* 11.1 (2013), p. 6.

[95] *MFI: Part 13 - Metamodel for Forms Registrations*. Commitee Draft. ISO/IEC 19763:13. International Organization for Standardisation, Aug. 2013. URL: `http://jtc1sc32.org/doc/N2401-2450/32N2417T-text_for_ballot-CD_19763-13.pdf` (visited on 28/09/2013).

[96] D. Abler. 'Extending LEIR to provide ion beams for bio-medical experiments'. In: *Radiotherapy and Oncology* 102, Supplement 1 (2012), S91–S92.

[97] CERN. *Workshop on Physics for Health in Europe: Executive Summary of the Position Paper*. Organizing Committee: SergioBertolucci, Manjit Dosanjh, Steve Myers, Emmanuel Tsesmelis. Geneva, 2010. URL: `http://cds.cern.ch/record/1269323?ln=en`.

[98] LifeSciencesCERN. *Meeting - Possible Biomedical Facility at CERN*. June 2012. URL: https://indico.cern.ch/conferenceTimeTable.py?confId=193910#20120625.

[99] M. H. Holzscheiter et al. 'A community call for a dedicated radiobiological research facility to support particle beam cancer therapy'. In: *Radiotherapy and Oncology* 105.1 (Oct. 2012), pp. 1–3.

[100] M. Dosanjh, B. Jones and S. Myers. 'A possible biomedical facility at the European Organization for Nuclear Research (CERN)'. In: *British Journal of Radiology* 86.1025 (2013).

[101] M. Chanel. *Experiments on adiobiological Effects of Ions on Cells*. Tech. rep. AB-Note-2003-045-ABP. Geneva: CERN, July 2003.

[102] M. Chanel. *Sur l'Utilisation de LEIR pour le Traitement des Cancers avec Faisceaux d'Ions ou de Protons*. Tech. rep. AB-Note-2004-074. CERN-AB-Note-2004-074. CERN, Jan. 2007.

[103] Oxford University Press, ed. *The Oxford English Dictionary - OED online*.

[104] T. G. Pickering et al. 'Recommendations for Blood Pressure Measurement in Humans and Experimental Animals: Part 1: Blood Pressure Measurement in Humans: A Statement for Professionals From the Subcommittee of Professional and Public Education of the American Heart Association Council on High Blood Pressure Research'. In: *Hypertension* 45.1 (2005), pp. 142–161.

[105] A. Olivé. *Conceptual modeling of information systems*. Springer, Oct. 2007.

[106] *Unified Modeling Language (UML)*. Version 2.4.1. Object Management Group (OMG), Aug. 2011. URL: http://www.omg.org/spec/UML/2.4.1/ (visited on 28/09/2013).

[107] *Meta Object Facility (MOF)*. Version 1.4. Object Management Group (OMG), Apr. 2002. URL: http://www.omg.org/spec/MOF/1.4/ (visited on 28/09/2013).

[108] B. Haslhofer and W. Klas. 'A survey of techniques for achieving metadata interoperability'. In: *ACM Comput. Surv.* 42.2 (Mar. 2010), 7:1–7:37.

[109] M. Brochhausen et al. 'The ACGT Master Ontology and its applications - Towards an ontology-driven cancer research and management system'. In: *Journal of Biomedical Informatics* 44.1 (2011), pp. 8–25.

[110] *Metadata Registries (MDR)*. ISO/IEC Standard. ISO/IEC 11179. International Organization for Standardisation, 2013. URL: http://metadata-standards.org/11179 (visited on 28/09/2013).

[111] *Metadata Registries (MDR)*. ISO/IEC Standard. ISO/IEC 11179-3:2013. International Organization for Standardisation, 2013. URL: http://standards.iso.org/ittf/PubliclyAvailableStandards/c050340_ISO_IEC_11179-3_2013.zip (visited on 28/09/2013).

[112] J. Brenton et al. 'CancerGrid: developing open standards for clinical cancer informatics'. In: *Proceedings of the UK escience All Hands Meeting*. Citeseer. 2005, pp. 678–681.

[113] D. Fenstermacher et al. 'The Cancer Biomedical Informatics Grid (caBIGTM)'. In: *Engineering in Medicine and Biology Society, 2005. IEEE-EMBS 2005. 27th Annual International Conference of the*. 2005, pp. 743–746.

[114] J. Davies et al. 'Metadata standards for semantic interoperability in electronic government'. In: *Proceedings of the 2nd international conference on Theory and practice of electronic governance*. ICEGOV '08. New York, NY, USA: ACM, 2008, 67–75.

[115] *Metamodel Framework for Interoperability (MFI)*. Committee Draft. ISO/IEC 19763. International Organization for Standardisation, 2013. URL: `http://metadata-standards.org/19763/` (visited on 28/09/2013).

[116] *Model Driven Architecture (MDA)*. Object Management Group (OMG), July 2001. URL: `http://www.omg.org/cgi-bin/doc?ormsc/01-07-01.pdf` (visited on 28/09/2013).

[117] J. Miller and J. Mukerji, eds. *MDA Guide Version 1.0.1*. 2003. URL: `http://www.omg.org/cgi-bin/doc?omg/03-06-01.pdf` (visited on 28/09/2013).

[118] A. G. Kleppe, J. Warmer and W. Bast. *MDA Explained: The Model Driven Architecture: Practice and Promise*. Boston, MA, USA: Addison-Wesley Longman Publishing Co., Inc., 2003.

[119] K. Czarnecki and S. Helsen. 'Feature-based survey of model transformation approaches'. In: *IBM Systems Journal* 45.3 (2006), pp. 621–645.

[120] D. Moher, K. Schulz and D. Altman. 'The CONSORT statement: revised recommendations for improving the quality of reports of parallel group randomized trials'. In: *BMC Medical Research Methodology* 1.1 (2001), p. 2.

[121] K. Schulz et al. 'CONSORT 2010 Statement: updated guidelines for reporting parallel group randomised trials'. In: *BMC Medicine* 8.1 (2010), p. 18.

[122] D. Husereau et al. 'Consolidated Health Economic Evaluation Reporting Standards (CHEERS) Explanation and Elaboration: A Report of the {ISPOR} Health Economic Evaluation Publication Guidelines Good Reporting Practices Task Force'. In: *Value in Health* 16.2 (2013), pp. 231–250.

[123] R. Calinescu et al. 'Model-driven architecture for cancer research'. In: *Fifth IEEE International Conference on Software Engineering and Formal Methods*. 2007, pp. 59–68.

[124] J. Davies et al. 'Model-driven support for a vaccine study in Kathmandu'. In: *Microsoft eScience Workshop*. 2009.

[125] J. Davies et al. 'The CancerGrid experience: Metadata-based model-driven engineering for clinical trials'. In: *Science of Computer Programming* (2013), pages.

[126] D. Abler et al. 'Models for forms'. In: *Proceedings of the compilation of the co-located workshops on DSM'11, TMC'11, AGERE!'11, AOOPES'11, NEAT'11, & VMIL'11*. SPLASH '11 Workshops. ACM. New York, NY, USA, 2011, pp. 13–18.

[127] *Specification for the Operational Data Model (ODM)*. Version 1.3.1. Clinical Data Interchange Standards Consortium (CDISC), 2010. URL: `http://www.cdisc.org/odm` (visited on 20/09/2013).

[128] *Data Documentation Initiative (DDI): Technical Specification Version 3.1*. DDI Alliance, Oct. 2009. URL: http://www.ddialliance.org/Specification/DDI-Lifecycle/3.1/ (visited on 20/09/2013).

[129] queXML. *queXML, Version 1.3.9*. Feb. 2012. URL: http://quexml.sourceforge.net/ (visited on 28/09/2013).

[130] *Electronic Data Capture Instrument (eDCI)*. Health Level 7 (HL7), 2006.

[131] OpenClinica. *OpenClinica - Open Source for Clinical Research*. Generic. 2012. URL: https://community.openclinica.com/ (visited on 28/09/2013).

[132] Research Electronic Data Capture (REDCap). *REDCap Software*. URL: http://project-redcap.org/ (visited on 28/09/2013).

[133] National Cancer Institute. *Form Builder - caDSR*. URL: https://wiki.nci.nih.gov/display/caDSR/Form+Builder (visited on 28/09/2013).

[134] IBM-SPSS. *SPSS Data Collection*. URL: http://www-01.ibm.com/software/analytics/spss/products/data-collection/ (visited on 28/09/2013).

[135] *SurveyGizmo*. URL: http://www.surveygizmo.com/ (visited on 28/09/2013).

[136] C. Schmitz and LimeSurvey Project Team. *LimeSurvey: An Open Source survey tool*. Hamburg, Germany, 2012.

[137] *SurveyMonkey*. URL: http://www.surveymonkey.com/ (visited on 28/09/2013).

[138] Google. *Google Drive - Forms*. URL: http://www.google.com/drive/start/apps.html#forms (visited on 28/09/2013).

[139] GroupComplete. *Group Complete - Mobile Forms and Mobile Data Collection Software for Smartphones & Tablets*. URL: http://www.groupcomplete.com/ (visited on 28/09/2013).

[140] *XForms 1.1*. W3C Recommendation. World Wide Web Consortium (W3C), Oct. 2009.

[141] Django Software Foundation. *Django*. URL: https://www.djangoproject.com/ (visited on 28/09/2013).

[142] *HTML5*. W3C Candidate Recommendation. World Wide Web Consortium (W3C), Dec. 2012. URL: http://www.w3.org/TR/html5/.

[143] Pivotal. *Spring Framework*. URL: http://www.springsource.org/ (visited on 28/09/2013).

[144] OpenXava. *AJAX Java Web Framework for Rapid Application Development of Enterprise Applications - OpenXava*. URL: http://www.openxava.org/web/guest/home (visited on 28/09/2013).

[145] Apache Software Foundation. *Apache Struts Web Framework*. URL: http://struts.apache.org/ (visited on 28/09/2013).

[146] Oracle. *Oracle Forms*. 2011.

[147] Microsoft. *InfoPath*. 2010.

[148] P. A. Harris et al. 'Research electronic data capture (REDCap)–A metadata-driven methodology and workflow process for providing translational research informatics support'. In: *Journal of Biomedical Informatics* 42.2 (2009), pp. 377–381.

[149] M. Vardigan, P. Heus and W. Thomas. 'Data Documentation Initiative: Toward a Standard for the Social Sciences'. In: *International journaltitle of Digital Curation* 3 (2008), pp. 107–113.

[150] A. Brennan, S. E. Chick and R. Davies. 'A taxonomy of model structures for economic evaluation of health technologies'. In: *Health Economics* 15.12 (Dec. 2006), pp. 1295–1310.

[151] J. E. Stahl. 'Modelling Methods for Pharmacoeconomics and Health Technology Assessment: An Overview and Guide'. In: *PharmacoEconomics* 26.2 (Jan. 2008), pp. 131–148.

[152] F. A. Sonnenberg and J. R. Beck. 'Markov Models in Medical Decision Making'. In: *Medical Decision Making* 13.4 (Dec. 1993), pp. 322–338.

[153] A. Briggs and M. Sculpher. 'An Introduction to Markov Modelling for Economic Evaluation'. In: *PharmacoEconomics* 13.4 (Apr. 1998), pp. 397–409.

[154] I. Taoufik, H. Kabaili and D. Kettani. 'Designing an e-government portal accessible to illiterate citizens'. In: *Proceedings of the 1st international conference on Theory and practice of electronic governance*. ICEGOV '07. New York, NY, USA: ACM, 2007, 327–336.

[155] D. Steinberg et al. *EMF: Eclipse Modeling Framework, 2nd Edition*. 2nd. Addison-Wesley Professional. Part of the Eclipse Series series., Dec. 2008.

[156] *Object Constraint Language (OCL)*. Version 2.3.1. Object Management Group (OMG), Jan. 2012. URL: `http://www.omg.org/spec/OCL/2.3.1/` (visited on 28/09/2013).

[157] F. Jouault et al. 'ATL: A model transformation tool'. In: *Science of Computer Programming* 72.1-2 (2008), pp. 31–39.

[158] A. Briggs et al. 'Probabilistic Analysis of Cost-Effectiveness Models: Choosing between Treatment Strategies for Gastroesophageal Reflux Disease'. In: *Medical Decision Making* 22.4 (2002), pp. 290–308.

[159] W. C. Black. 'The CE Plane: A Graphic Representation of Cost-Effectiveness'. In: *Medical Decision Making* 10.3 (1990), pp. 212–214.

[160] A. Briggs, M. Sculpher and M. Buxton. 'Uncertainty in the economic evaluation of health care technologies: The role of sensitivity analysis'. In: *Health Economics* 3.2 (1994), pp. 95–104.

[161] A. Briggs et al. 'Model Parameter Estimation and Uncertainty: A Report of the ISPOR-SMDM Modeling Good Research Practices Task Force-6'. In: *Value in Health* 15.6 (2012), pp. 835–842.

[162] B. A. Van Hout et al. 'Costs, effects and C/E-ratios alongside a clinical trial'. In: *Health Economics* 3.5 (1994), pp. 309–319.

[163] A. Briggs, B. J. O'Brien and G. Blackhouse. 'THINKING OUTSIDE THE BOX: Recent Advances in the Analysis and Presentation of Uncertainty in Cost-Effectiveness Studies'. In: *Annual Review of Public Health* 23.1 (2002). PMID: 11910068, pp. 377–401.

[164] A. A. Stinnett and J. Mullahy. 'Net Health Benefits: A New Framework for the Analysis of Uncertainty in Cost-Effectiveness Analysis'. In: *Medical Decision Making* 18.2 (1998), S68–S80.

[165] K. Claxton and J. Posnett. 'An economic approach to clinical trial design and research priority-setting'. In: *Health Economics* 5.6 (1996), pp. 513–524.

[166] D. Abler et al. 'Data-driven Markov models and their application in the evaluation of adverse events in radiotherapy'. In: *Journal of Radiation Research* 54.suppl 1 (2013), pp. i49–i55.

[167] C. Weng et al. 'Formal representation of eligibility criteria: A literature review'. In: *Journal of Biomedical Informatics* 43.3 (2010), pp. 451–467.

[168] R Development Core Team. *R: A Language and Environment for Statistical Computing*. ISBN 3-900051-07-0. R Foundation for Statistical Computing. Vienna, Austria, 2011. URL: `http://www.R-project.org/`.

[169] *Stata Statistical Software: Release 13*. College Station, TX: StataCorp LP, 2013.

[170] N. J. Welton and A. E. Ades. 'Estimation of Markov Chain Transition Probabilities and Rates from Fully and Partially Observed Data: Uncertainty Propagation, Evidence Synthesis, and Model Calibration'. In: *Medical Decision Making* 25.6 (2005), pp. 633–645.

[171] C. Sherlaw-Johnson, S. Gallivan and J. Burridge. 'Estimating a Markov Transition Matrix from Observational Data'. English. In: *The Journal of the Operational Research Society* 46.3 (1995), pages.

[172] Particle Therapy Cancer Research Institute (PTCRi). *Desiderata for BioMedical Facility at LEIR*. May 2010.

[173] D. Abler, H. Steve and J. Davies. 'Meta-modelling Markov Model Simulations for cost effectiveness analyses'. In: *Radiotherapy and Oncology* 102, Supplement 1 (2012), S91.

[174] M. Durante et al. 'Preparatory study of a ground-based space radiobiology program in Europe'. In: *Advances in Space Research* 39.6 (2007), pp. 1082–1086.

[175] M. Durante, G. Reitz and O. Angerer. 'Space radiation research in Europe: flight experiments and ground-based studies'. In: *Radiation and environmental biophysics* 49.3 (2010), pp. 295–302.

[176] L. Badano et al. *Proton-Ion Medical Machine Study (PIMMS), 1*. CERN-PS-99-010-DI. Mar. 1999, 232 p.

[177] P. J. Bryant et al. *Proton-Ion Medical Machine Study (PIMMS), 2*. CERN-PS-2000-007-DR. Aug. 2000, 340 p.

[178] U. Amaldi and G. Magrin, eds. *The Path to the Itialian National Centre for Ion Therapy*. Novara, Italy: Edizioni Mercurio, 2006.

[179] P. Andreo et al. *Absorbed Dose Determination in External Beam Radiotherapy An International Code of Practice for Dosimetry Based on Standards of Absorbed Dose to Water*. Tech. rep. 398. IAEA, Dec. 2000.

[180] P. Lefèvre and D. Möhl. *A low energy accumulation ring of ions for LHC (a feasibility study)*. 1993.

[181] G. Fraser. 'CERN's Low Energy Antiproton Ring LEAR'. In: *Beam Line (Stanford linear accelerator center)* 29.3 (1999), pp. 22–27.

[182] D. Möhl. *LEAR, history and early achievements*. PS Note CERN-PS-99-034-DI. Geneva: CERN, 1999.

[183] P. Belochitskii et al. *LEIR Commissioning*. LHC-PROJECT-Report-923. CERN-LHC-Project-Report-923. revised version submitted on 2006-09-15 14:40:46. July 2006, 4 p.

[184] M. Benedikt et al. *LHC Design Report*. Geneva: CERN, 2004.

[185] D. Küchler and J. T. Stafford-Haworth. 'The light ion front end for Linac3'. 2012.

[186] P. Lefèvre, D. Möhl and D. Simon. *Future Machine Improvements in LEAR*. Tech. rep. CERN, 1986.

[187] S. Y. Lee. *Accelerator Physics*. 2nd ed. World Scientific Publishing Company, Dec. 2004.

[188] H. Wiedemann. *Particle Accelerator Physics*. 3rd ed. Springer, May 2007.

[189] E. Wilson. *An Introduction to Particle Accelerators*. Clarendon Press, May 2001.

[190] A. Chao, ed. *Handbook of Accelerator Physics and Engineering*. World Scientific Pub Co Inc, Mar. 1999.

[191] H. Grote and F. Schmidt. *MAD-X: An Upgrade from MAD8*. 2003.

[192] Y. Kobayashi and H. Takahashi. *Improvement of the Emittance in the resonant beam ejection*. 1968.

[193] G. Feldbauer, M. Benedikt and U. Dorda. *Simulations of Various Driving Mechanisms for the 3rd Order Resonant Extraction from the MedAustron Medical Synchrotron*. CERN-ATS-2011-077. Sept. 2011, 3 p.

[194] D. Ondreka and U. Weinrich. 'The Heidelberg ion therapy (HIT) accelerator coming into operation'. In: *Proceedings of EPAC08* (2008), pp. 979–81.

[195] W. Hardt. *Ultraslow Extraction out of LEAR (transverse aspects)*. PS / DL / LEAR Note 81-6. CERN, Apr. 1981.

[196] G. Feldbauer. 'Extraction methods for the MedAustron Synchrotron'. Master thesis. Vienna: TU Vienna, May 2011.

[197] G. Guignard. 'A general treatment of resonances in accelerators.' In: CERN, Geneva, 1977 - 1978. Geneva: CERN, 1978, 72 p.

[198] C. Carli, S. Maury and D. Möhl. *Combined longitudinal and transverse multiturn injection in a heavy ion accumulator*. CERN-PS-97-027-HP. June 1997, 3 p.

[199] J. Bosser, C. Dimopoulou and G. Tranquille. *LEIR Electron Cooler Conceptual Study*. Tech. rep. 2001-017. CERN, 2001.

[200] J. Borburgh. *Septa for LEIR, private communication*. 2012.

[201] F. Galluccio et al. *Simulation of the PS slow extraction 62 with the MAD program*. CERN-PS-88-77-OP-PA. 1988.

[202] F. Schmidt, E. Forest and E. McIntosh. *Introduction to the polymorphic tracking code: Fibre bundles, polymorphic Taylor types and*. Tech. rep. CERN-SL-2002-044-AP. KEK-REPORT-2002-3. Geneva: CERN, July 2002.

[203] M. Chanel et al. 'Sextupolar and dipolar pole face windings at LEAR'. In: *Conf.Proc.* C900612 (1990), pp. 1133–1135.

[204] U. Dorda. *PyAccel & TrackIt!* Geneva, 2011.

[205] A. Garonna, D. Abler and C. Carli. *Proposal for a new LEIR Slow Extraction Scheme dedicated to Biomedical Research*. in preparation. Geneva: CERN, 2014.

[206] N. Tsoupas et al. 'Uniform beam distributions at the target of the NASA Space Radiation Laboratory's beam line'. In: *Phys. Rev. ST Accel. Beams* 10.2 (Feb. 2007), p. 024701.

[207] S. Yonai et al. 'Evaluation of beam wobbling methods for heavy-ion radiotherapy'. In: *Medical Physics* 35 (2008), p. 927.

[208] W. T. Chu, B. A. Ludewigt and T. R. Renner. 'Instrumentation for treatment of cancer using proton and light-ion beams'. In: *Review of Scientific Instruments* 64.8 (Aug. 1993), pp. 2055–2122.

[209] E. Pedroni et al. 'The 200-MeV proton therapy project at the Paul Scherrer Institute: Conceptual design and practical realization'. In: *Medical Physics* 22.1 (1995), pp. 37–53.

[210] T. Haberer et al. 'Magnetic scanning system for heavy ion therapy'. In: *Nucl. Instrum. Meth.* A330 (1993), pp. 296–305.

[211] M. Benedikt, P. J. Bryant and M. Pullia. 'A New Concept for the Control of a Slow-Extracted Beam in a Line with Rotational Optics, 2, rev. Version'. In: *Nucl. Instrum. Methods Phys. Res., A* 430.CERN-PS-99-008-OP. 2/3 (Jan. 1999), 523. 13 p.

[212] Particle Data Group et al. 'Review of Particle Physics'. In: *Physical Review D* 86.1 (July 2012).

[213] D. Möhl. *Sources of emittance growth*. In CERN Accelerator School and KVI: Specialised CAS Course on Small Accelerators. Geneva: CERN, 2006.

[214] T. Furukawa et al. 'Study of Scatterer Method to Compensate Asymmetric Distribution of Slowly Extracted Beam at HIMAC Synchrotron'. In: *EPAC 2006 Proceedings*. Ed. by C. Biscari et al. 2006, 3 p.